Journal of the

ENGINEERING MECHANICS DIVISION

Proceedings of the American Society of Civil Engineers

ENGINEERING MECHANICS DIVISION
EXECUTIVE COMMITTEE
Dan H. Pletta, Chairman; Egor P. Popov, Vice-Chairman; Bruce G. Johnston; Merit P. White; Edward Wenk, Jr., Secretary

COMMITTEE ON PUBLICATIONS
Egor P. Popov, Chairman; Hans H. Bleich; Jack E. Cermack; Albert G. H. Deitz; William J. Hall; John D. Haltiwanger; Ernest F. Masur; Herbert S. Suer

CONTENTS

April, 1960

Papers

	Page
White Noise Representation of Earthquakes by G. N. Bycroft	1
Strength and Efficiency Aspects of Plate Structures by George Gerard	17
Dynamic Analysis of Elasto-Plastic Structures by Glen V. Berg and Donald A. DaDeppo	35
Behavior of Buckled Rectangular Plates by Manuel Stein	59
Waves and Shocks in Locking and Dissipative Media by Mario G. Salvadori, Richard Skalak and Paul Weidlinger	77
Commentary on Plastic Design in Steel: Connections Progress Report No. 6 of the Joint WRC-ASCE Committee on Plasticity Related to Design	107

(Over)

Copyright 1960 by the American Society of Civil Engineers.

Page

Commentary on Plastic Design in Steel: Deflections
Progress Report No. 7 of the Joint WRC-ASCE Committee on
Plasticity Related to Design 141

Preliminary Analysis of Continuous Gable Frames
by James W. Gillespie and Jan J. Tuma 161

Journal of the
ENGINEERING MECHANICS DIVISION
Proceedings of the American Society of Civil Engineers

WHITE NOISE REPRESENTATION OF EARTHQUAKES

By G. N. Bycroft[1]

SYNOPSIS

This investigation is intended to show that white noise is a suitable representation of earthquake motion. It appears that a white-noise source used in conjunction with an analog computer is a convenient method of analyzing structures subjected to complex ground motions and of assigning probabilities to the deformations arising. Until more statistical information is available about earthquakes, it is suggested that a "standard large earthquake" be represented by "white" ground accelerations having a flat spectral density of 0.75 $ft^2/sec^4/cps$ and a duration of 1/2 min.

INTRODUCTION

One of the major difficulties in determining suitable aseismic designs lies in the lack of knowledge of destructive earthquakes. Accelograms of a few large earthquakes are available and these records show very complex ground motions entirely different from each other. They are different in energy content or "size" and different in duration and shape. Earthquakes of the future

Note.—Discussion open until September 1, 1960. To extend the closing date one month, a written request must be filed with the Executive Secretary, ASCE. This paper is part of the copyrighted Journal of the Engineering Mechanics Division, Proceedings of the American Society of Civil Engineers, Vol. 86, No. EM 2, April, 1960.

[1] Research Officer, Bldg. Physics Sect., Div. of Bldg. Research, Natl. Research Council, Ottawa, Can.

will not necessarily bear any relation to those in the past and no prediction of the severity and character of future earthquakes can be made. Two earthquakes having the same energy content will have different effects on any particular structure. Each individual earthquake, of course, has a specific character and a specific effect on a particular structure, but this character is not predictable.

Many investigations of structural vibration due to ground motion have been made on a deterministic basis, using actual records of earthquakes and determining the deformations that would occur in various types of structures. This approach would be satisfactory if a large enough number of records were available and the results displayed on a probability basis. Until this is possible recourse to another mode of attack must be made.

Earthquakes originate as ill-defined slip-faults followed by innumerable reflections, refractions, and attenuations by the complex terrain through which it travels. Intuitively, one feels that the essential characteristic of the earthquake is its irregularity. Many writers[2,3,4] have suggested simulating earthquakes by a random assemblage of impulses. In order that white noise should simulate an earthquake it must have the same effect on the kinds of dynamic systems that arise in structures. A linearly-elastic and elasto-plastic structure are considered herein.

LINEAR ELASTIC STRUCTURE

The response of a linear structure of many degrees of freedom to ground motion may be written in terms of the spectrum of that ground motion. Let

$\alpha(t)$ = the ground acceleration;

$v(x, t)$ = velocity of some point of the structure;

T_n = period of the n^{th} harmonic;

$K(x, T_n)$ = harmonic "weighting" factor and is a function of the structure only;

p = number of degrees of freedom; and

λ_n = fraction of critical damping of the n^{th} harmonic.

then,

$$v(x,t) = \sum_{n=1}^{p} K(x,T_n) \int_0^t \alpha(\tau)\, e^{\frac{-2\pi\lambda_n}{T_n}(t-\tau)} \sin \frac{2\pi}{T_n}(t-\tau)\, d\tau \quad \cdots \quad (1)$$

Eq. 1 states that the response of a multi-degree-of-freedom structure is the sum of the responses of the various modes or harmonics. The earthquake excitation occurs only in the integral factor and consequently this is the only factor we need consider.

---

[2] "Response Spectrum Techniques in Engineering Seismology," by D. E. Hudson, Proceedings, World Conf. on Earthquake Engrg., San Francisco, Calif., June, 1956.

[3] "Some Applications of Probability Theory in Aseismic Design," by E. Rosenblueth, Proceedings, World Conf. on Earthquake Engrg., San Francisco, Calif., June, 1956.

[4] "Response of Tall Buildings to Random Shakes," by A. Cemal Eringen, Tech. Report No. 12, Office Naval Research, Div. of Engrg. Sciences, Purdue Univ., December, 1957.

The velocity spectrum of the ground motion is defined as the maximum value of this integral, that is,

$$V(\lambda,T) = \text{Max} \int_0^t \alpha(\tau) e^{\frac{-2\pi\lambda}{T}(t-\tau)} \sin \frac{2\pi}{T}(t-\tau)\, d\tau \quad \ldots\ldots \quad (2)$$

and is a function of period and damping only.

Spectra of several large earthquakes have been calculated and are well known.[5] The spectra are all different in detail but have the feature in common that they fluctuate rapidly, with respect to period T, about a mean line which starts at the origin and rises asymptotically to a constant value. G. W. Housner drew[6] smooth mean curves through these oscillatory spectra and found that these smooth curves have almost the same shape for different earthquakes. The actual scale of the spectra varies according to the size of the earthquake. The full lines in Fig. 1 are taken from Housner's work[6] and show the shape of these common average spectra, and the particular scale of V shown is that of the largest earthquake recorded, viz., El Centro, Calif., 1940.

The writer used an analog computer to construct mean spectra of bursts of "white noise" for comparison with the mean spectra of Fig. 1. "White noise" is defined as a random signal having a gaussian probability of amplitude distribution and a spectral density which is constant for all frequencies. The spectral density at any particular frequency may be regarded as the average power passing when the signal is filtered by a narrow band pass filter centered at the particular frequency. In practice, of course, one encounters "band-limited white noise," that is, the spectral density is only constant up to a certain frequency and is then rapidly cut off. As long as this frequency is large compared with the frequencies of the system being considered, the response of the system is unaffected by the value of the cut-off point. The computer used provides a band-limited white noise having a spectral density flat from 0 to 35 cycles.

The equation of motion of the mechanical oscillator subjected to an acceleration $\alpha(t)$ is simply,

$$\ddot{x} + 2\omega\lambda x + \omega^2 x = \alpha(t) \quad \ldots\ldots\ldots\ldots \quad (3)$$

in which x is the displacement of the mass relative to its zero position and ω is the angular frequency of the oscillator. Variables in the computer are represented by voltages having an allowable maximum of 100 volts. If $\dot{x}$ is to have an expected maximum of V ft per sec the mechanical equation is scaled to

$$\left[\frac{100\ \ddot{x}}{V\ \omega}\right] + 2\lambda \left[\frac{100\ \dot{x}}{V}\right] + \left[\frac{100\ \omega\ x}{V}\right] = \frac{100}{V\ \omega}[\alpha(t)] \quad \ldots\ldots \quad (4)$$

where the terms in square brackets are the respective computer voltages.

---

[5] "Spectra Analyses of Strong Motion Earthquakes," by J. C. Alford, G. W. Housner and R. R. Martel, Earthquake Research Lab., Tech. Report to Office of Naval Research, Calif. Inst. of Tech., Pasadena, August, 1951.

[6] "Limit Design of Structures to Resist Earthquakes," by G. W. Housner, Proceedings, First World Conf. on Earthquake Engrg., San Francisco, Calif., June, 1956.

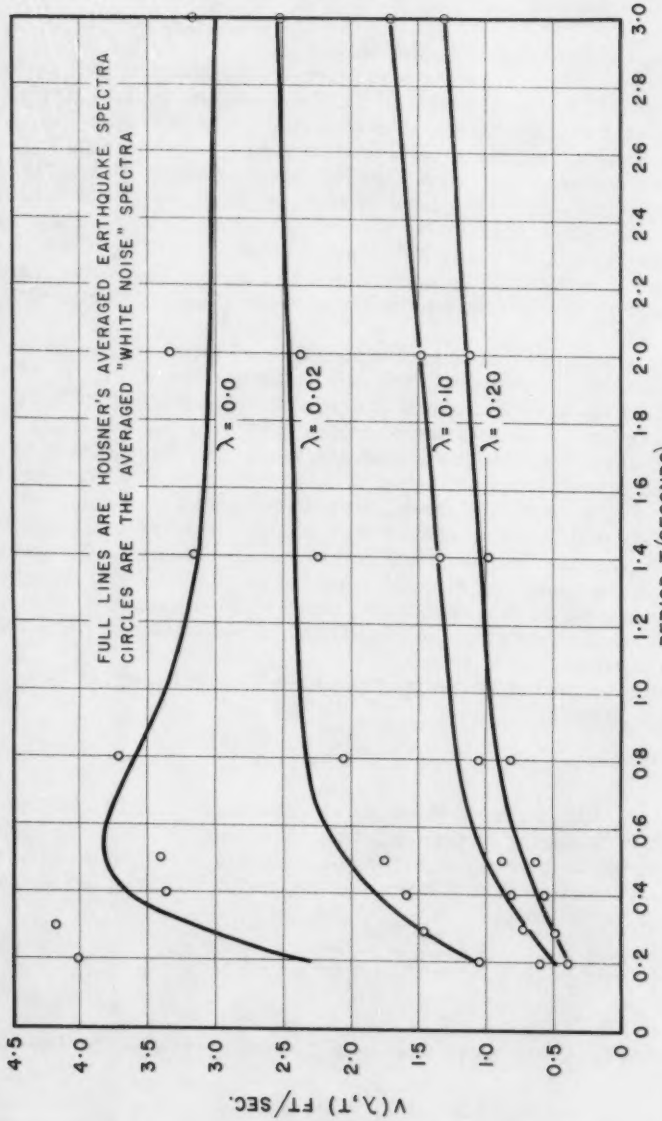

FIG. 1.—EARTHQUAKE AND NOISE SPECTRA.

If W(t) is the actual voltage of the noise source and X the computer variable in volts corresponding to x, we may write the equation as

$$\ddot{X} + 2\lambda\dot{X} + X = \frac{100\ k}{V\ \omega} W(t) \quad \ldots\ldots\ldots\ldots \quad (5)$$

where the factor k will be chosen so that k W(t) in volts is numerically equal to some representative ground acceleration $\alpha(t)$ in ft per sec^2.

The actual velocity $\dot{x}$ in feet per second is given by the computer volts $\dot{X}$ multiplied by V/100, the acceleration by $\ddot{X}$ $V\omega/100$ and the displacement by $X\ V/100\omega$.

Ideally, a probability distribution should be given to the size and duration of the earthquake as well as to its configuration. However, with the available information, this cannot be done satisfactorily. The available records of large earthquakes show that their duration was generally of the order of 20 sec to 30 sec. A duration of 25 sec has been selected here as representative of large earthquakes.

For various values of period T and damping λ, twenty separate bursts of white noise of 25 sec duration were fed into the circuit. The system was reset to zero after every burst. Each burst of noise gives a different value of the maximum velocity acquired by the oscillator.

The maximum value of $\dot{x}$ during each burst of noise is the required spectrum for that particular burst of noise. The mean of the maximum velocity of the twenty runs was taken in each case. This gives the variation of the mean maximum velocity for bursts of white noise as a function of period and damping. However, this mean still contains the scaling factor k, and the value given to k will determine the size of the earthquake being represented. This variation is shown by the circles in Fig. 1. The factor k was chosen so that the scales matched at an arbitrary point viz., T = 3.0 and λ = 0.20. With this value of k the position of the other points was determined. It is seen that the variation of the mean spectra of the noise with both period and damping is very similar to Housner's common average earthquake spectra. The scales could have been matched at any other point but the value of k would not be very different.

From this it appears that "white" ground accelerations are a suitable representation of earthquakes. Further, by choosing the scales so that the mean-noise results fit the averaged spectra of the largest earthquake recorded, we arrive at some kind of a definition of a standard large earthquake. Individual bursts of noise will give results above or below the average just as the actual spectrum of El Centro fluctuates above and below the smooth curves of Fig. 1.

The spectral density of the noise source used was approximately 2.90 $volt^2$/cps and the factor k came to 0.51. Thus a large earthquake may be represented by ground accelerations which are "white" in character and have a spectral density of 0.75 ft^2/sec^4/cps.

Fig. 2 shows a schematic diagram of the computer, where circles are potentiometers, triangles are summers, and double-based triangles are integrators.

ELASTO-PLASTIC STRUCTURE

It is interesting to compare the effect of white noise and an actual earthquake on a non-linear system. The most important type of non-linearity that

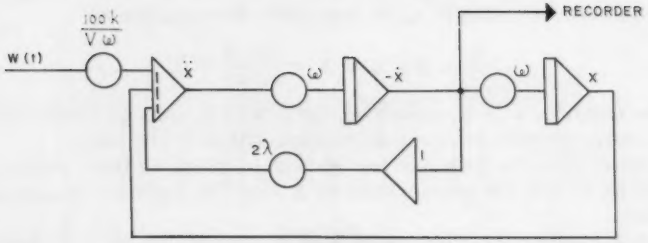

FIG. 2.—COMPUTER DIAGRAM FOR LINEAR DAMPENED OSCILLATOR.

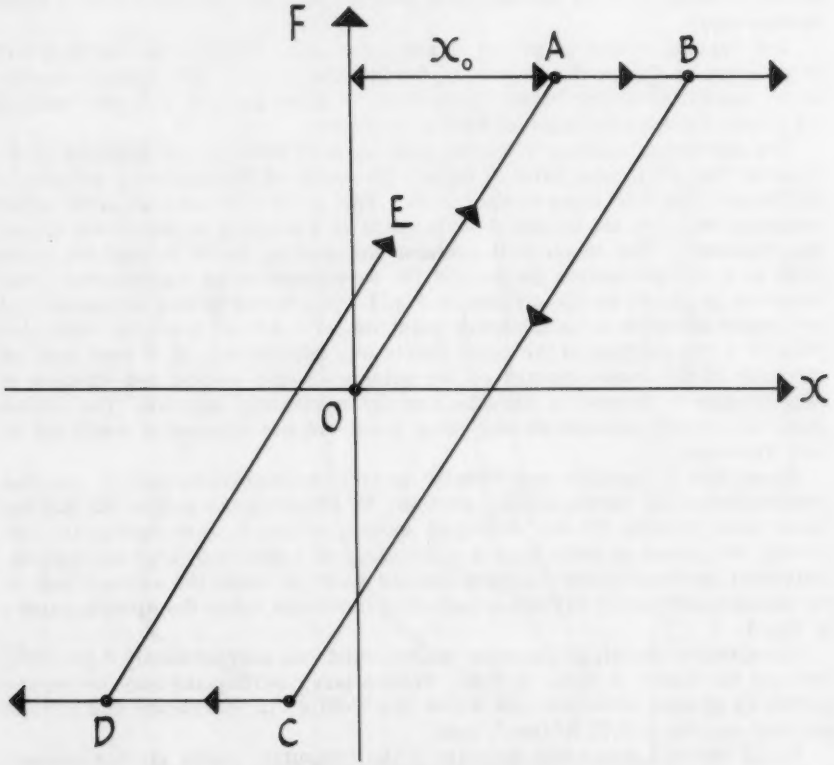

FIG. 3.—ELASTO-PLASTIC CHARACTERISTIC.

will occur in a structure during severe ground motion will be plastic yielding. Fig. 3 shows the assumed relation between restoring force F and displacement x. Starting from zero with positive velocity, the restoring force is proportional to displacement until the yield point A corresponding to a displacement x_0 is reached. The restoring force remains constant at this value until a change in sign of the velocity occurs at some point B. The displacement A B will be called a yield displacement. The force F now decreases along a line parallel to the elastic part of the characteristic and stays on this line until C or perhaps B again is reached. If the velocity stays negative the reverse yield point C is reached and the force stays constant at this opposite value until the velocity becomes positive again and the characteristic proceeds from D to E. Areas enclosed by loops represent hysteretic energy loss.

In a recent paper[7] the writer considers the yield displacements that occur when an oscillator with this yielding stiffness characteristic is subject to the 1940 El Centro earthquake. These yield displacements determined for this specific earthquake are now compared with the yields arising when the same system is subjected to bursts of "white" ground acceleration of spectral density 0.75 $ft^2/sec^4/cps$ simulating the standard large earthquake.

The equations of motion may be derived from a consideration of the elasto-plastic characteristic shown in Fig. 3. There are separate equations depending on whether the motion is taking place in the elastic or the plastic part of the characteristic. On the plastic part of the characteristic the retarding force is constant and has the sign of the velocity shown by sgn $\dot{x}$. On the elastic part of the characteristic the restoring force must be referred to the changing zero position caused by the yielding. The equations of motion are:

$$\ddot{x} + 2\,\omega\lambda\,\dot{x} + \omega^2(x - \mu) = \alpha(t),\ |x - \mu| \leq x_0 \quad \ldots\ldots\ldots \text{(6a)}$$

and

$$\ddot{x} + 2\,\omega\lambda\,\dot{x} + \omega^2\,x_0\ \text{sgn}\ \dot{x} = \alpha(t),\ |x - \mu| \geq x_0 \quad \ldots\ldots\ldots \text{(6b)}$$

where μ is the algebraic sum of all previous yield displacements up to the time considered and the sign of the yield displacement taken as that of $\dot{x}$ at the time. Thus, in Fig. 3, when working on the linear portion D E, the value of μ is A B - C D.

It will be more convenient now if the yield point is specified in terms of equivalent acceleration rather than the displacement x_0. Let G be the equivalent fraction of gravity and then

$$\omega^2\,x_0 = G\,g \quad \ldots\ldots\ldots\ldots\ldots\ldots \text{(7)}$$

If S is the expected maximum value of x, and X is the scaled computer variable corresponding to x, then the scaled equations become:

$$\ddot{X} + 2\,\lambda\,\dot{X} + (X - U) = \frac{0.51\ W(t)\ 100}{\omega^2\ S},\ |X - U| \leq X_0 \quad \ldots\ldots \text{(8a)}$$

$$\ddot{X} + 2\,\lambda\,\dot{X} + \frac{100\ G\ g}{\omega^2\ S}\ \text{sgn}\ \dot{X} = \frac{0.51\ W(t)\ 100}{\omega^2\ S},\ |X - U| \geq X_0 \quad \ldots \text{(8b)}$$

---

[7] "Earthquake Yield Spectra," by G. N. Bycroft, M. J. Murphy and K. E. Brown, Proceedings, ASCE, October, 1959.

where the ground acceleration has been replaced by the representative noise voltage 0.51 W(t).

These equations were simulated on the computer by the circuit diagram shown in Fig. 4. The stiffness characteristic is provided by the diode-limited integrator. As $\dot{X}$ increases initially the output of the integrator is -X until limited by the diode. If $\dot{X}$ continues positive the voltage output stays at this constant value. However, if $\dot{X}$ changes sign, the integrator starts subtracting a linearly-increasing quantity and thus provides the term (X-U) until limited in the opposite direction.

The output to the recorder is the total displacement of the oscillator from its initial zero at any time. This displacement consists of the elastic displacement x_0 added to the algebraic sum of all previous yield displacements. The maximum value of the algebraic sum of the yield displacements will be called the maximum yield displacement and is the maximum recorder output minus x_0. For various values of linear period T, damping factor λ, and yield

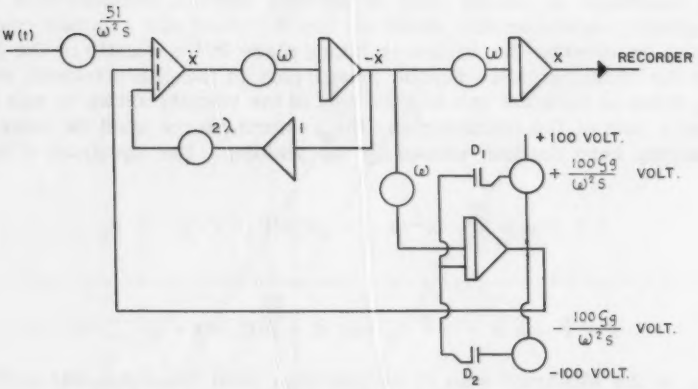

FIG. 4.—COMPUTER DIAGRAM FOR ELASTO-PLASTIC OSCILLATOR.

value G, the mean of the maximum yield displacements arising was determined when the system was subjected to ten runs of 25 sec duration. Fig. 5 to 13 show this mean maximum yield displacement together with the elastic displacement x_0. An addition of the two gives the mean maximum total displacement. The full lines are from the paper mentioned earlier and refer to the 1940 El Centro earthquake. The results from the white noise are shown as circles.

These results show a remarkable similarity. It is to be remembered that the representative level of the noise was determined from the linear case, and using this value, it is seen that the noise gives similar results as an actual earthquake in this non-linear system.

The double-peaked shape appearing in the cases shown in Figs. 8 and 9 is also reproduced by the noise and thus must be an essential function of the system and not merely of the particular character of the earthquake considered.

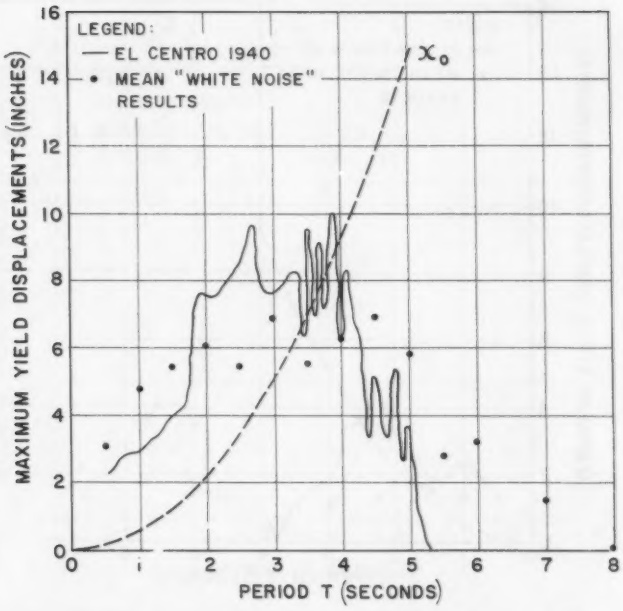

FIG. 5.—MAXIMUM YIELD DISPLACEMENTS G = 0.06, λ = 0.03.

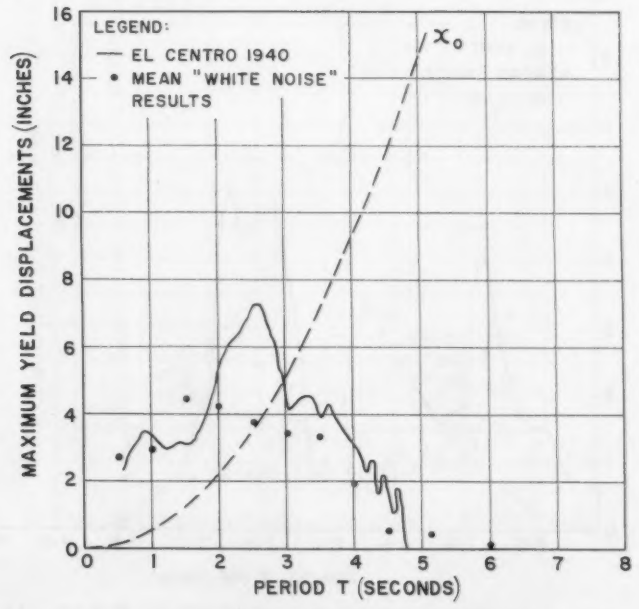

FIG. 6.—MAXIMUM YIELD DISPLACEMENTS G = 0.06, λ = 0.10.

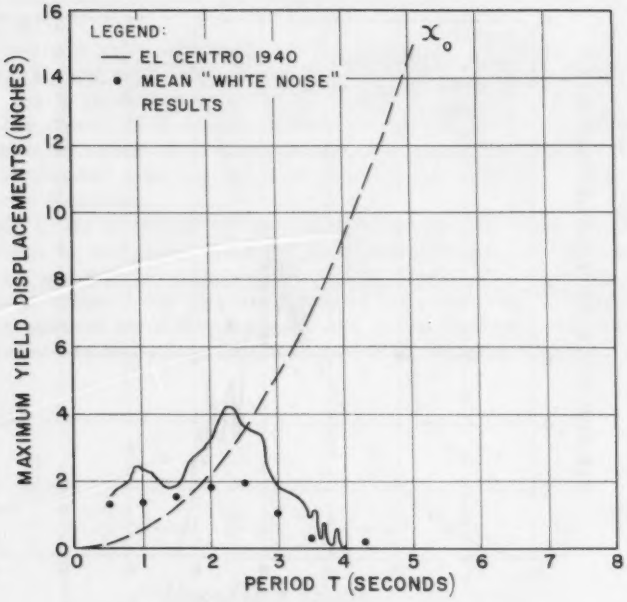

FIG. 7.—MAXIMUM YIELD DISPLACEMENTS G = 0.06, λ = 0.20.

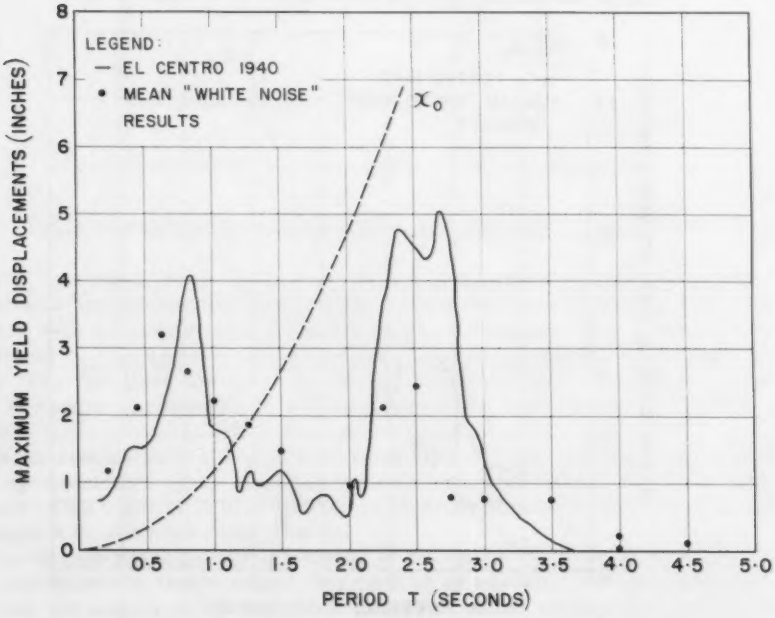

FIG. 8.—MAXIMUM YIELD DISPLACEMENTS G = 0.12, λ = 0.10.

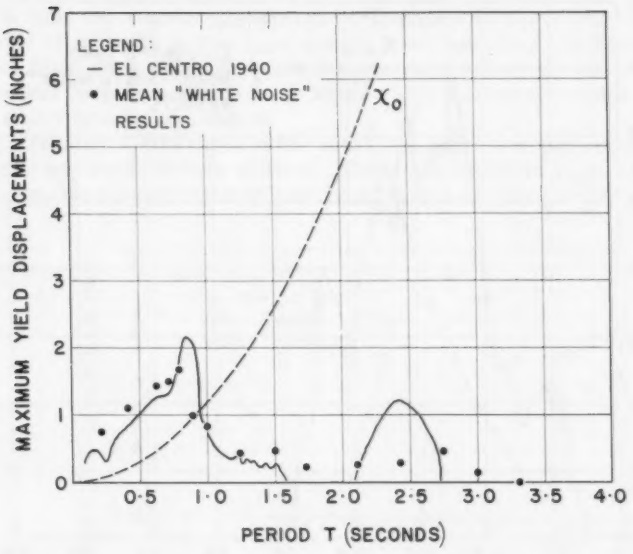
LEGEND:
— EL CENTRO 1940
• MEAN "WHITE NOISE" RESULTS
χ_0
MAXIMUM YIELD DISPLACEMENTS (INCHES)
0 1 2 3 4 5 6 7
0·5 1·0 1·5 2·0 2·5 3·0 3·5 4·0
PERIOD T (SECONDS)

FIG. 9.—MAXIMUM YIELD DISPLACEMENTS G = 0.12, λ = 0.10.

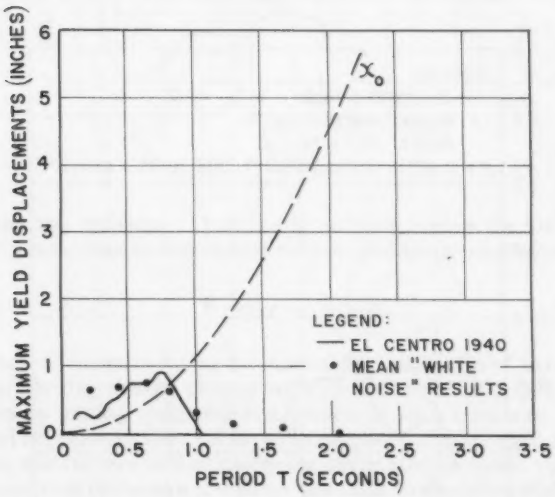
χ_0
LEGEND:
— EL CENTRO 1940
• MEAN "WHITE NOISE" RESULTS
MAXIMUM YIELD DISPLACEMENTS (INCHES)
0 1 2 3 4 5 6
0 0·5 1·0 1·5 2·0 2·5 3·0 3·5
PERIOD T (SECONDS)

FIG. 10.—MAXIMUM YIELD DISPLACEMENTS G = 0.12, λ = 0.20.

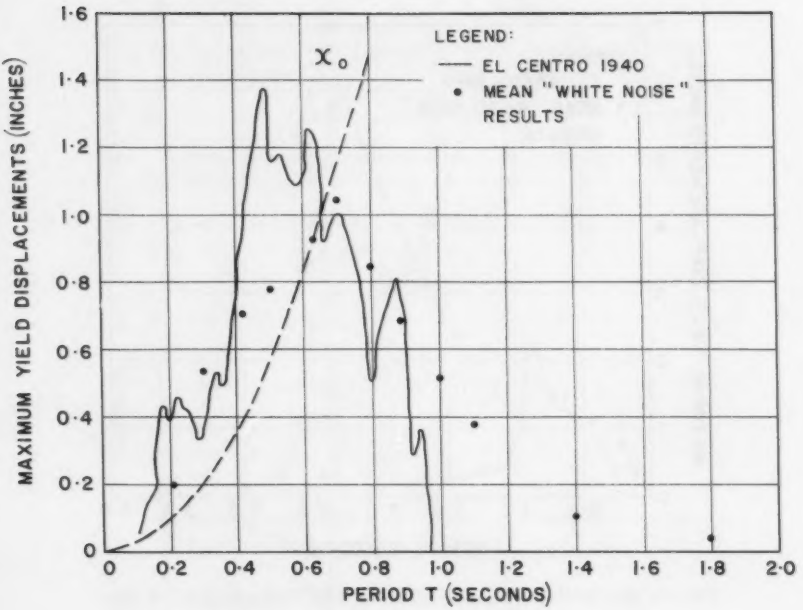

FIG. 11.—MAXIMUM YIELD DISPLACEMENTS G = 0.24, λ = 0.03.

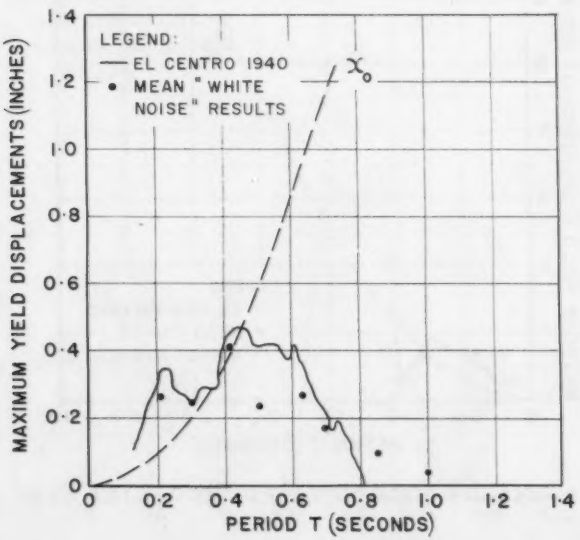

FIG. 12.—MAXIMUM YIELD DISPLACEMENTS G = 0.24, λ = 0.10.

These figures, of course, compare the mean of the maxima of ten runs of noise with the maximum of one specific earthquake. Ideally, the comparison should be with the average of several earthquakes of equal spectral density. Each burst of noise is of the same energy level but gives a different value of maximum yield lying above or below the averaged values shown. Presumably one individual burst of noise could be found which would correspond to this one particular earthquake considered.

The probability distribution of the maximum yield was determined in three cases from one hundred runs of noise. These are shown in Figs. 14 to 16, and show reasonable probabilities of individual bursts of noise giving values of up

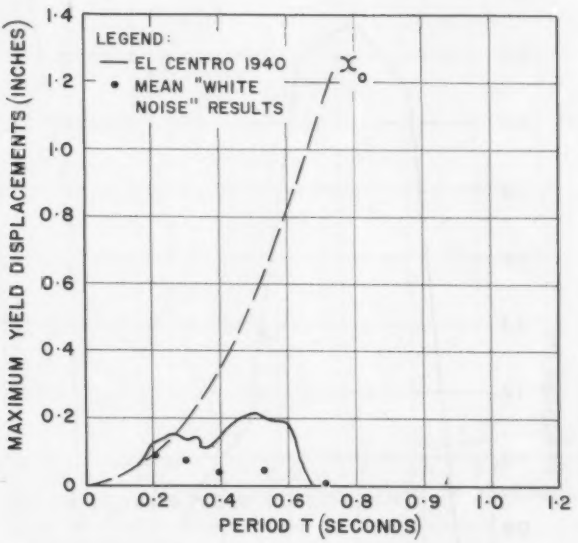

FIG. 13.—MAXIMUM YIELD DISPLACEMENTS G = 0.24, λ = 0.20.

to four times the average. This easily accommodates the differences shown between the average noise values and the one particular earthquake considered.

CONCLUSIONS

"White noise" appears to be a reasonable simulation of earthquake excitation for engineering design purposes. The technique of simulating a complex structure on an analog computer and feeding it with bursts of noise having an energy level representative of a large earthquake is a straight forward method of analyzing a structure and of assigning probabilities to the various displacements. Using this technique it will be possible to simulate multi-story structures deflecting in bending and shear and incorporating yield characteristics.

The probability values given in Figs. 14 to 16 illustrate an important point. Each burst of noise is of the same energy level but the resulting displacements for individual shots can differ by factors of 10 and more. Thus two earthquakes of the same content energy or magnitude but of different configurations may have vastly different effects on any particular structure. Also,

one particular earthquake may seriously affect a structure with a certain set of parameters but have little effect on another one. This may well be part of the explanation of the inconsistencies noted in seismic damage.

ACKNOWLEDGMENTS

The writer is indebted to the Engineering Analysis and Computation Group of the Division of Mechanical Engineering, N.R.C., Ottawa, for the use of their P.A.C.E. analog computer and to J. B. Milsum for guidance in its application. This paper is a contribution from the Division of Building Research, National Research Council of Canada and is published with the approval of the Director of the Division.

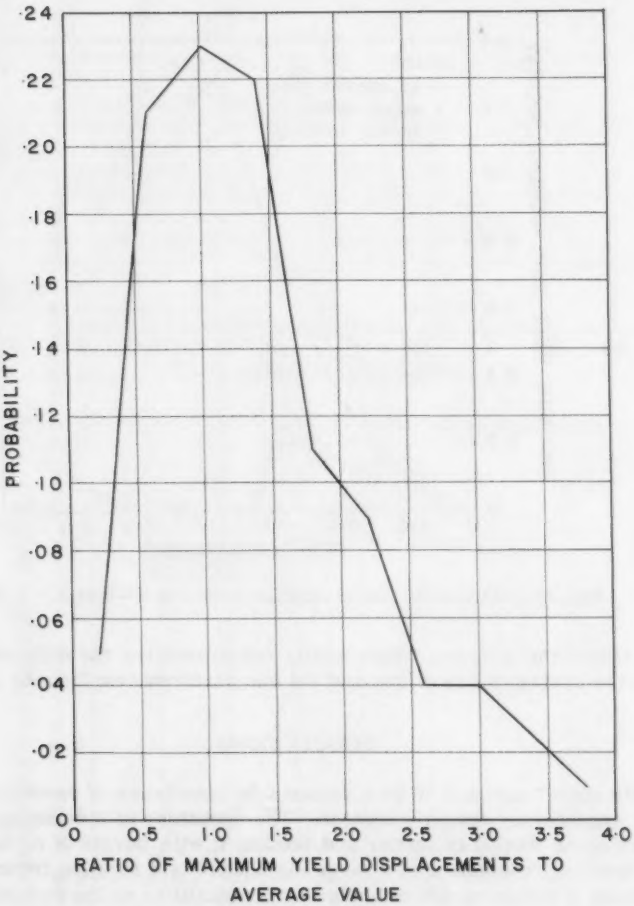

FIG. 14.—PROBABILITY DISTRIBUTION OF MAXIMUM YIELD DISPLACEMENTS G 0.12, 0.10, T 0.75.

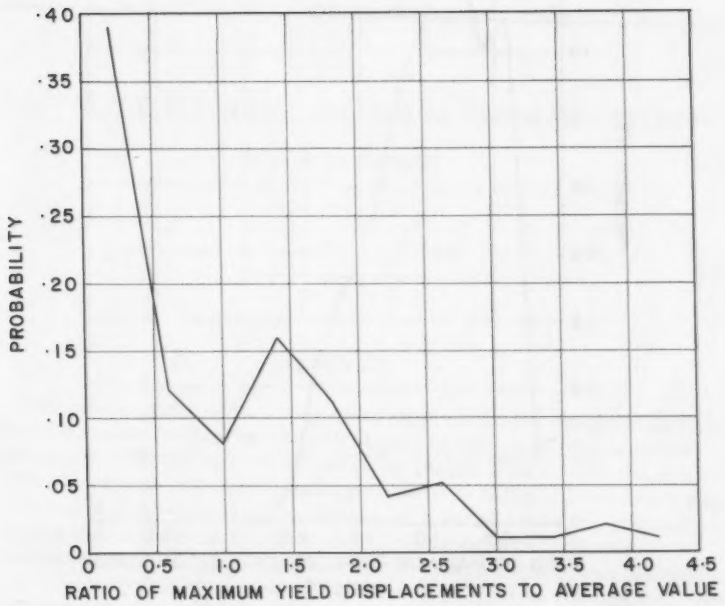

FIG. 15.—PROBABILITY DISTRIBUTION OF MAXIMUM YIELD DISPLACEMENTS
G 0.12, 0.03, T 2.5.

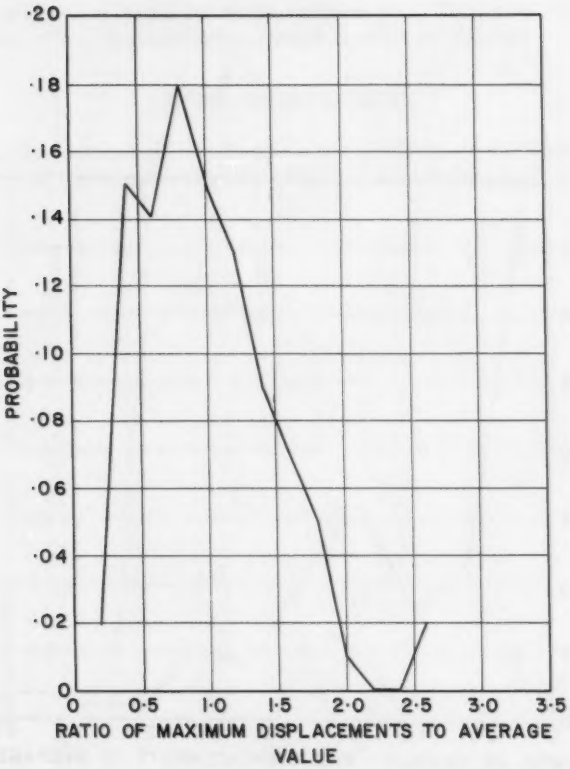

FIG. 16.—PROBABILITY DISTRIBUTION OF MAXIMUM YIELD DISPLACEMENTS G 0.24, 0.10, T 0.20.

Journal of the
ENGINEERING MECHANICS DIVISION
Proceedings of the American Society of Civil Engineers

STRENGTH AND EFFICIENCY ASPECTS OF PLATE STRUCTURES[a]

By George Gerard[1]

SYNOPSIS

Two recent developments that may be of interest in the design of thin-gage metal structures are presented. The first part of the paper is concerned with the compressive-strength analysis of long flat plates after elastic buckling occurs. The plates have various boundary conditions along the unloaded edges. The results of a semi-empirical analysis of a large mass of test data are shown to apply to various forms of composite box-beam structures.

The second part of the paper considers the design rather than the analysis aspects of composite stiffened plate structures subject to instability. Some principles of minimum-weight design are presented for transversely supported, longitudinally stiffened plating. It is indicated that designs based on these principles constitute efficient forms of limit-design structures.

INTRODUCTION

The field of structural mechanics concerned with elastic and plastic stability has reached a high level of development as a result of important contributions from various engineering disciplines. The literature of this field through the years provides ample evidence that civil, aeronautical, and naval structural engineers have contributed significantly to its advancement.

Note.—Discussion open until September 1, 1960. To extend the closing date one month, a written request must be filed with the Executive Secretary, ASCE. This paper is part of the copyrighted Journal of the Engineering Mechanics Division, Proceedings of the American Society of Civil Engineers, Vol. 86, No. EM 2, April, 1960.

[a] Presented at the October, 1959 ASCE Convention in Washington, D. C.

[1] Assoc. Dir. of Research, College of Engrg., New York Univ., New York, N. Y.

The importance of minimum-weight considerations in the design of air vehicles has focussed particular attention on the stability of thin-gage metal structures. Consider that approximately two-thirds of the structural weight of an airplane is designed by stability criteria and its importance becomes readily apparent. This has naturally provided a powerful impetus for a concentrated research effort in this area.

In the spirit of continuing to share knowledge in this field, some recent developments are presented which are taken mostly from research in the aeronautical field during the past decade (the 1950's). It is hoped that these results may be of value in the design of other types of thin-gage metal structures.

COMPRESSIVE STRENGTH OF PLATE STRUCTURES

It is rather well known that the compressive strength of flat plates at failure can significantly exceed the buckling stress when the latter occurs elastically. In the plastic region, however, the buckling stress and failure strength are essentially coincident. The theory of plastic stability is now in a satisfactory state of development and the advances during the past decade have been rather completely summarized.[2]

The compressive or crippling strength of flat plates is of particular importance in the economical design of thin-gage metal structures. Some rather recent developments in this area, which are based on the analysis of a large mass of test data,[3,4] are presented.

Approximate Strength Analysis.—Exact analysis of the crippling strength of flat plates presents a complex mathematical problem. This is a result of the non-linear, large deflection behavior of the plate after buckling, in addition to the nonlinear plastic behavior which ultimately results in failure.

It is noteworthy that E. Z. Stowell[5] and J. Mayers and B. Budiansky[6] have performed theoretical analyses of failures of flanges and plates, respectively. In both analyses, the plates were assumed to have supported unloaded edges that do not warp but remain straight in the plane of the plate after buckling, as shown in Fig. 1(a).

The significant physical fact which is evident from these analyses is that the stress along the supported, unloaded edge is intimately associated with failure. Apparently failure occurs when the stress intensity at the edge reaches a value approximately equal to the compressive-yield strength of the material.

Because of the complexities of the crippling-strength problem, it is convenient to resort to a "strength of materials" approach which is semi-empirical in nature. Both theory and tests indicate that after elastic buckling occurs,

---

[2] "Handbook of Structural Stability, Part I - Buckling of Flat Plates," by G. Gerard, and H. Becker, NACA TN 3781, July, 1957.

[3] "Handbook of Structural Stability, Part IV - Failure of Plates and Composite Elements," by G. Gerard, NACA TN 3784, August, 1957.

[4] "Handbook of Structural Stability, Part V - Compressive Strength of Flat Stiffened Panels," by G. Gerard, NACA TN 3785, August, 1957.

[5] "Compressive Strength of Flanges," by E. Z. Stowell, NACA TN 2020, January, 1950.

[6] "Analysis of Behavior of Simply Supported Flat Plates Compressed Beyond the Buckling Load into the Plastic Range," by J. Mayers and B. Budiansky, NACA TN 3368, February, 1955.

the following relation between the average compressive stress, $\bar{\sigma}$, in the plate and the supported unloaded edge stress, σ_e, is valid:

$$\bar{\sigma}/\sigma_{cr} = \alpha_1(\sigma_e/\sigma_{cr})^n \quad \ldots\ldots\ldots\ldots\ldots \quad (1)$$

where

$$\sigma_{cr} = \frac{\pi^2 \, k \, E}{12(1-\nu^2)} \left(\frac{t}{b}\right)^2 \quad \ldots\ldots\ldots\ldots\ldots \quad (2)$$

If it is now assumed that failure occurs when the edge stress reaches the compressive-yield strength, then Eq. 1 can be transformed into

$$\bar{\sigma}_f/\sigma_{cy} = \alpha_1(\sigma_{cr}/\sigma_{cy})^{1-n} \quad \ldots\ldots\ldots\ldots\ldots \quad (3)$$

By substituting Eq. 2 into 3

$$\bar{\sigma}_f/\sigma_{cy} = \alpha \, k^{1-n} \left[\frac{t}{b}\left(\frac{E}{\sigma_{cy}}\right)^{1/2}\right]^{2(1-n)} \quad \ldots\ldots\ldots \quad (4)$$

In a simplified form

$$\bar{\sigma}_f/\sigma_{cy} = \beta\left[\frac{t}{b}\left(\frac{E}{\sigma_{cy}}\right)^{1/2}\right]^m \quad \ldots\ldots\ldots\ldots\ldots \quad (5)$$

where

$$\beta = \alpha \, k^{m/2} \quad \ldots\ldots\ldots\ldots\ldots\ldots \quad (6)$$

Eq. 5 contains the non-dimensional parameters $\bar{\sigma}_f/\sigma_{cy}$ and $(t/b)(E/\sigma_{cy})^{1/2}$, which can be used to synthesize test data on the crippling of flat plates of various types of materials. The constants m and β are determined by a best fit of Eq. 5 to the test data.

Flat Plates.—There is a considerable mass of test data from many investigators on the crippling strength of long, simply supported flat plates. These data have been summarized[3,4] and include plates tested in V-groove supporting fixtures at the unloaded edges as well as square tubes which act as an assembly of four, simply supported plates.

In both of these cases, the unloaded edges are free to warp after buckling and thus the stress distribution resembles that shown in Fig. 1(b). This difference in edge conditions between the tested plates and those assumed in the theoretical analyses of Stowell[5] and Mayers and Budiansky,[6] and shown in Fig. 1(a), results in a significant difference in crippling strength. The plates with warped edges generally have a lower strength.

Available data on V-groove plates and square tubes, of various aluminum and magnesium alloys and steel, are presented in terms of the parameters of Eq. 5. It can be observed that relatively good correlation is obtained among the various materials which differ significantly in E and σ_{cy}. Also Eq. 5 fits the data within $\pm$ 10% limits up to the yield strength when the following values of the constants are used:

$$m = 0.85, \quad \beta = 1.42 \quad \ldots\ldots\ldots\ldots\ldots \quad (7)$$

In addition to the data on simply supported plates, there are some test data on long, clamped flat plates that can be used to check Eq. 6. These data were obtained[7] by K. B. Jackson and A. H. Hall who used a special test fixture that provided clamping along the supported unloaded edges and also permitted in-plane warping.

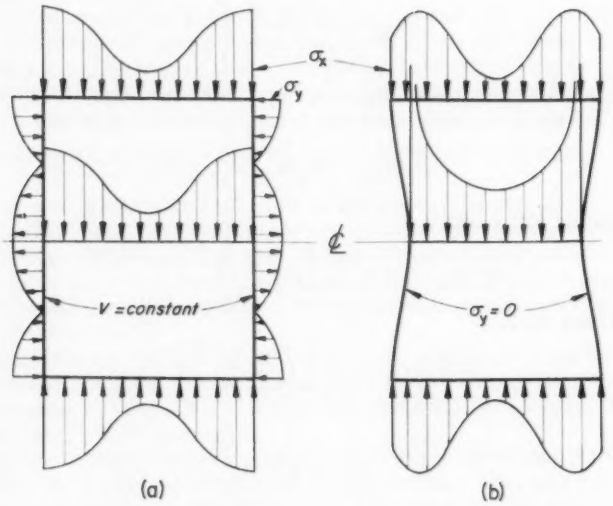

FIG. 1.—STRESSES IN FLAT PLATES AFTER BUCKLING UNDER CONDITIONS OF UNIFORM END SHORTENING. (a) STRAIGHT UNLOADED EDGES. (b) STRESS-FREE UNLOADED EDGES.

The data in terms of the parameters of Eq. 5 are shown in Fig. 3. It can be observed that the value of m = 0.85 fits the data well. The value of β was predicted by using Eq. 6 in the form

$$\beta_2 = \beta \left(k_2/k\right)^{0.425} \quad \ldots\ldots\ldots\ldots\ldots \quad (8)$$

Since for the simply supported case k = 4 and β = 1.42, and for the clamped case k_2 = 6.98, it is predicted by Eq. 8 that for the clamped plates

$$\beta_2 = 1.80 \quad \ldots\ldots\ldots\ldots\ldots \quad (9)$$

It can be observed in Fig. 3 that this value of β_2 does, indeed, provide a good fit to the test data.

Actually, the data presented in Figs. 2 and 3 are a sample of the much larger mass of test data.[2,3,8] The excellent correlation obtained therein, for many

[7] "Curved Plates in Compression," by K. B. Jackson and A. H. Hall, National Research Council (Canada), Report AR-L, 1947.

[8] "The Crippling Strength of Compression Elements," by G. Gerard, Journal Aeronautical Sciences, Vol. 25, No. 1, January, 1958, pp. 37-52.

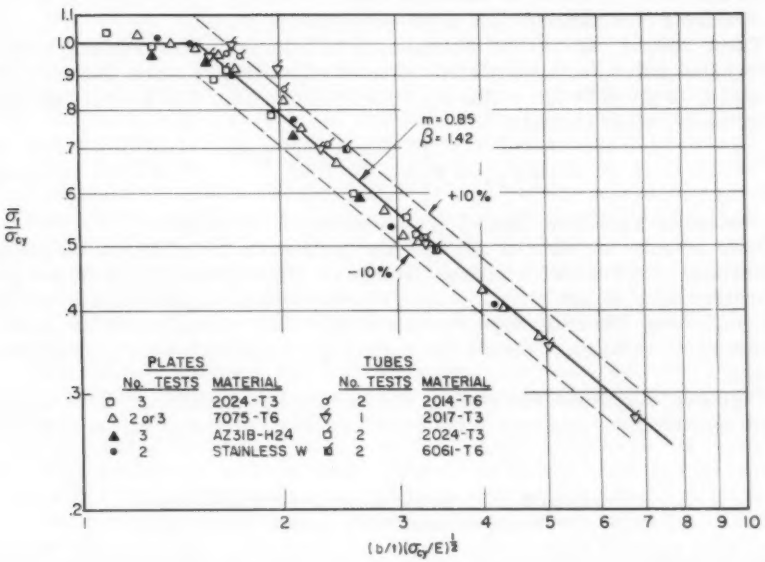

FIG. 2.—CRIPPLING DATA ON SIMPLY SUPPORTED PLATE ELEMENTS IN COMPRESSION.

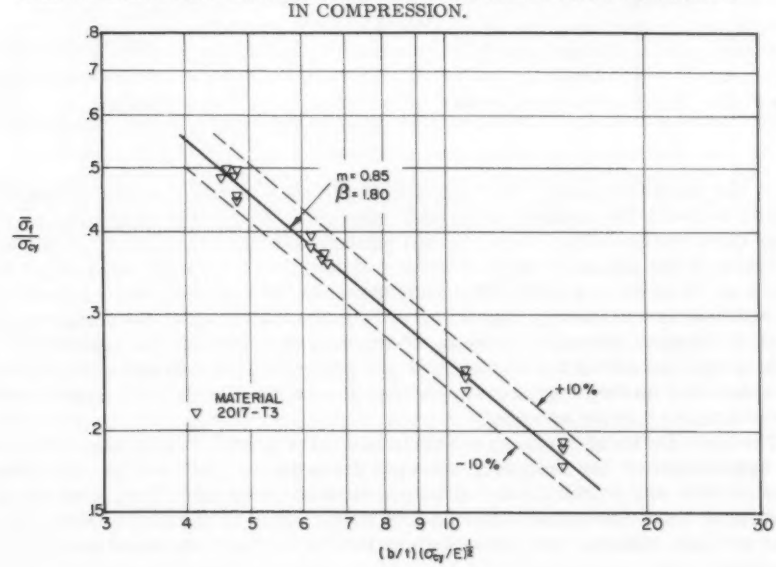

FIG. 3.—CRIPPLING DATA ON CLAMPED PLATE ELEMENTS IN COMPRESSION.

materials, configurations of plate elements, and temperature conditions, lends considerable confidence to this semi-empirical approach.

These results can now be summarized as follows: The crippling strength of long flat plates, with supported unloaded edges free to warp in the plane of the plate, is given by the following relationship within ± 10% limits up to the compressive yield strength:

$$\bar{\sigma}_f/\sigma_{cy} = \beta\left[\frac{t}{b}\left(\frac{E}{\sigma_{cy}}\right)^{1/2}\right]^{0.85} \quad \ldots\ldots\ldots\ldots\ldots (10)$$

The values of β given in Table 1 are based on Eqs. 7 and 8.

Plate Structures.—It is of interest now to consider the application of the data concerning compressive crippling strength on plate elements to stiffened plate structures such as box beams in bending. It can be anticipated that under certain conditions, the crippling formulas presented previously may be useful in predicting the strength of relatively complex plate structures in a rather simple manner.

V-groove supported flat plates, and tubular assemblies of plates achieve crippling strengths in excess of the elastic buckling stress by virtue of support

TABLE 1.—CRIPPLING COEFFICIENTS FOR VARIOUS BOUNDARY CONDITIONS

k	β	Unloaded edge support
4	1.42	simple support
5	1.56	rotational restraint
6	1.69	rotational restraint
6.98	1.80	clamped

along the unloaded edges. This support effectively permits the edge-stress intensity to reach the compressive-yield strength. In a plate structure, on the other hand, various types of stiffening elements are used to support the unloaded edges. If the unloaded edge-stiffening elements are strongly attached to the plates so as to form a monolithic structure, and the deflectional restraint of the stiffener is sufficiently high so as to remain straight up to the compressive yield of the plate, then the crippling strength of the plate can be achieved. In such cases, the stiffening elements of the plate structure effectively perform the same role as the V-groove supporting fixture for the plate elements or the corners of the tubular assembly.

The bases for these remarks are contained in the work[8,9] which demonstrates the application of the crippling-strength formulas to stiffened panels under compression and multicellular box beams under bending. Test data on the latter may be of particular interest and, thus, some of the test results taken from various sources and presented by the writer[9] are summarized in the following.

9 "Handbook of Structural Stability," Part VII - Strength of Thin-Wing Construction," by G. Gerard and H. Becker, NACA TN (to be published).

The tests under consideration were conducted on aluminum alloy box beams in bending. Some of the beams were single-cell tubes while most were fabricated boxes of 1, 2, or 3 cells with various angle attachments at the web-cover joint. Depending on the web geometry relative to that of the plate elements of the compression cover, as well as the joint details, the cover-plate elements received elastic restraint along the unloaded edges in some cases. Thus, the test data presented in Fig. 4 are divided according to values of buckling coefficient, k = 4, 5.35, and 6.35 pertinent to the test. In Fig. 4, b is the width of the cover plate between web stiffeners, E and σ_{cy} are the mechanical properties of the plate material, and the crippling strength is computed from $\bar{\sigma}_f = M\,c/I$, where the cover material is assumed to be fully effective.

It can be observed from Fig. 4 that for the k = 4 case which corresponds to simple support, Eq. 10 fits the data very well when using the value of $\beta = 1.42$ given in Table 1. The lines for the other two values of k shown in Fig. 4 were computed by use of Eq. 8: for k = 5.35, $\beta = 1.60$ and for k = 6.35, $\beta = 1.75$. In all cases, the use of Eqs. 10 and 8, based on plate elements under compression, predicted the behavior of the multicell box beams under bending with acceptable accuracy.

Another test of the predictive value of Eq. 10 is afforded by the data summarized[10] by J. Vasta on tests of steel ship hulls to failure. One hull was tested in the sagging condition and experienced a compressive failure of the deck. This is shown as point 1 in Fig. 5 where the lines correspond to Eq. 10 for the various values of k given in Table 1. The relatively light framing used in the region of the deck failure did not provide any significant elastic restraint beyond simple support.

The other two hull tests were conducted for the hogging condition and resulted in compressive failure of the bottom plating adjacent to the keel. In both cases, the plating was bounded by relatively deep longitudinals which apparently provided significant elastic restraint along the unloaded edges of the plate. Thus, points 2 and 3 in Fig. 5 correspond to k of approximately 6, which appears to be entirely reasonable in this case.

From Figs. 4 and 5, there appear to be some positive indications that Eq. 10 can be applied to plate structures. It must be remembered, however, that the method is semi-empirical in nature and requires verification in cases which may depart significantly from the tests on which it is based.

MINIMUM-WEIGHT DESIGN

In the design of thin-gage metal structures under compressive loading, stability rather than yield considerations generally constitute the limiting strength conditions. Therefore, in such cases, economy of design must be based on minimum-weight stability concepts rather than on the more conventional limit-design principles, which require simultaneous yielding of the structural elements. Alternately, minimum-weight designs, according to stability concepts, often constitute the most economical form of limit design.

There is, of course, a long history of civil engineering interest and developments in economy of design. Particularly in recent years, modern developments in plasticity theory have resulted in renewed interest in the economical design

---

[10] "Lessons Learned from Full-Scale Ship Structural Tests," by J. Vasta, Soc. of Naval Archts. and Marine Engrs., Preprint No. 1, November, 1958.

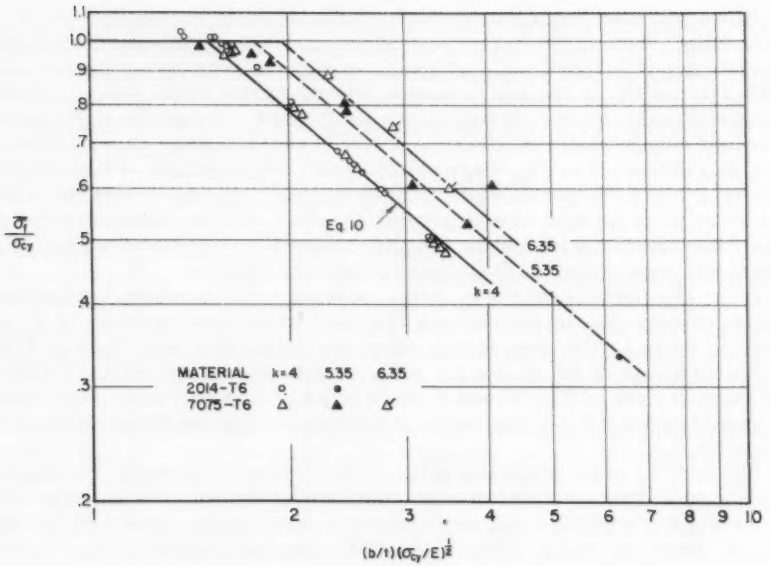

FIG. 4.—DATA ON BOX BEAMS UNDER BENDING WHICH FAIL BY CRIPPLING OF THE COMPRESSION SURFACE.

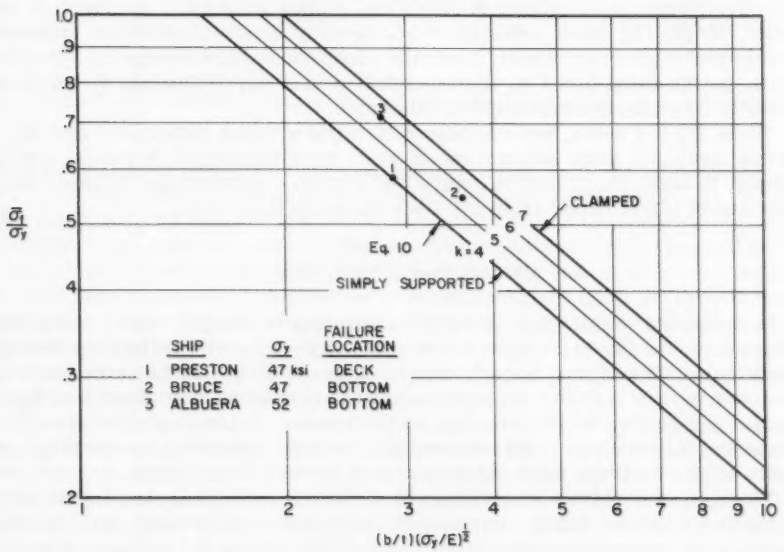

FIG. 5.—DATA ON SHIP HULLS UNDER BENDING WHICH FAIL BY CRIPPLING OF THE COMPRESSION SURFACE.

of beam and shell structural elements. Such analyses, however, exclude stability as a mode of failure and, consequently, apply only to relative thick-walled structures. Because of the interest in thin-gage structures, it is pertinent to turn now to some of the developments in the aeronautical field concerned with the minimum-weight design of such structures.

Design Conditions.—In the design of a structure, certain of the overall dimensions are, generally, fixed by considerations over which little choice can be exercised, such as span or panel width. However, as the structure is divided into components by the introduction of longitudinal and transverse stiffening elements, it is then possible to influence the weight of the structure by the spacing of the stiffening system.

In addition to these geometrical considerations, the overall loading features are, also, generally fixed by design conditions over which the structural designer has little control. These factors are governed primarily by the performance requirements of the structure. Thus, in approaching the structural design, the overall geometrical and loading features are essentially prescribed within rather narrow limits.

By combining the loading and geometric parameters into a suitable loading index, it is possible to conduct minimum-weight analyses of various types of compression elements. A relatively wide variety of such cases is available,[11,12] based on appropriate indices. For the purpose of presenting a review of some of the essential aspects of minimum-weight design, the analysis of a wide, longitudinally stiffened panel is developed in the following. These results are then combined with those for a lateral-stiffening system in order that the structural efficiency of composite compression surfaces can be considered.

Wide Longitudinally Stiffened Panels.—In view of the large possible number of buckling and failure modes of a wide longitudinally stiffened panel, it appears that any analysis aimed at predicting the strength might be limited in scope. It is remarkable, however, that such analyses are in substantially good agreement with test data. In an attempt to arrive at conclusions concerning the major factors to be considered in the design of efficient, wide, longitudinally stiffened panels, a simplified analysis first presented[13] by A. Zahorski leads to useful results.

The assumed conditions for minimum-weight design of a compression structure are that the applied stress and allowable stress be equal and that the possible forms of buckling occur simultaneously. Thus, the applied stress,

$$\sigma_a = N/\bar{t} \quad \ldots\ldots\ldots\ldots\ldots\ldots (11)$$

where

$$\bar{t} = \left(A_{st}/b_s\right) + t_s \quad \ldots\ldots\ldots\ldots\ldots\ldots (12)$$

It is to be noted that the loading N may contain appropriate safety factors.

For the wide, stiffened panel, it is assumed that the flexural type of instability predominates which is given by

---

11 "Weight-Strength Analysis of Aircraft Structures," by F. R. Shanley, McGraw-Hill Book Co., 1st Edition, 1952.

12 "Minimum-Weight Analysis of Compression Structures," by G. Gerard, New York Univ. Press, New York, 1956.

13 "Effects of Material Distribution on Strength of Panels," by A. Zahorski, Journal Aeronautical Sciences, Vol. 11, No. 3, July, 1944, pp. 247-253.

$$\sigma_{co} = c\,\pi^2\,\tau\,E/(L/\rho)^2 \quad \ldots\ldots\ldots\ldots\ldots\ldots (13)$$

The stiffened panel is then considered as an assembly of plate elements and a second type of instability involving local buckling of these elements is given by

$$\sigma_{cr} = \frac{\pi^2\,k\,\eta\,E}{12(1-\nu^2)}\left(\frac{t_s}{b_s}\right)^2 \quad \ldots\ldots\ldots\ldots\ldots\ldots (14)$$

Eqs. 11, 13, and 14 can then be combined into

$$\sigma_{co}\,\sigma_{cr}\,\sigma_a^2 = \left(\frac{c\,\pi^2\,\tau\,E\,\rho^2}{L^2}\right)\left[\frac{\pi^2\,k\,\eta\,E\,t_s^2}{12(1-\nu^2)\,b_s^2}\right]\frac{N^2}{\bar{t}^2} \quad \ldots\ldots (15)$$

On the condition that the applied stress and various buckling stresses are equal,

$$\sigma_{co} = \sigma_{cr} = \sigma_a \quad \ldots\ldots\ldots\ldots\ldots\ldots (16)$$

and denoting the stress under the conditions of Eqs. 16 as $\bar{\sigma}$, Eq. 15 can be reduced to

$$\bar{\sigma} = \pi\left[\frac{c\,k}{12(1-\nu^2)}\right]^{1/4}\left(\frac{\rho}{b_s}\,\frac{t_s}{\bar{t}}\right)^{1/2}(\tau\,\eta)^{1/4}\left(\frac{N\,E}{L}\right)^{1/2} \quad \ldots\ldots (17)$$

It is convenient to rewrite Eq. 17 in the following form:

$$\bar{\sigma} = \alpha_p(N\,\bar{\tau}\,E/L')^{1/2} \quad \ldots\ldots\ldots\ldots\ldots\ldots (18)$$

where

$$\alpha_p = \pi\left[\frac{k}{12(1-\nu^2)}\right]^{1/4}\left(\frac{\rho}{b_s}\,\frac{t_s}{\bar{t}}\right)^{1/2}$$

and

$$\bar{\tau} = (\eta\,\tau)^{1/2}$$

Panel Efficiency.—The panel-efficiency coefficient, α_p, contains terms, representing the geometric properties of the panel cross section, which are not generally fixed by those considerations which govern the structural loading index N/L. Consequently, it is possible to arrange the material in the cross section to arrive at an optimum distribution that results in the maximum value of α_p for the configuration and, therefore, optimum stress according to Eq. 18.

A commonly used longitudinal stiffening arrangement is shown in Fig. 6. For $b_f/b_w = 0.3$ and $t_f/t_w = 1.0$, the following are the geometric properties of a unit average cross section of periodicity b_s:

$$\bar{t}/t_s = 1 + 1.6\,r_b\,r_t \quad \ldots\ldots\ldots\ldots\ldots\ldots (19)$$

and

$$\frac{\rho}{b_s} = r_b \frac{\left[r_b\, r_t \left(0.633 + 0.37\, r_b\, r_t\right)\right]^{1/2}}{1 + 1.6\, r_b\, r_t} \quad \ldots\ldots\ldots (20)$$

In Eqs. 19 and 20, r_b denotes b_w/b_s and r_t represents t_w/t_s. By combining Eqs. 19 and 20 with 18, the panel-efficiency coefficient for the stiffened wide panel becomes

$$\alpha_p = \frac{\pi}{\left[12(1-\nu^2)\right]^{1/4}} \frac{\left[k\, r_b^3\, r_t \left(0.633 + 0.37\, r_b\, r_t\right)\right]^{1/4}}{1 + 1.6\, r_b\, r_t} \quad \ldots\ldots (21)$$

An approximate method of analysis, which yields excellent results for the Z-stiffened wide panel, is based on the assumption that the various elements in the cross section are pin-jointed. The approximation results in equal buckling stresses for the skin and stiffener web. Hence,

$$t_w/b_w = t_s/b_s \quad \ldots\ldots\ldots\ldots\ldots\ldots (22)$$

Therefore,

$$r_b = r_t \quad \ldots\ldots\ldots\ldots\ldots\ldots (23)$$

By substituting Eq. 23 into 21 and taking $k = 4$ for pin-jointed webs and $\nu = 0.3$,

$$\alpha_p = \frac{\pi}{\left[3(1-\nu^2)\right]^{1/4}} \frac{\left[r_b^4 \left(0.633 + 0.37\, r_b^2\right)\right]^{1/4}}{1 + 1.6\, r_b^2} \quad \ldots\ldots (24)$$

Upon maximizing Eq. 24, $\partial\alpha_p/\partial r_b = 0$, the following results are obtained:

$$\left(\alpha_p\right)_o = 0.945 \quad \ldots\ldots\ldots\ldots\ldots\ldots (25)$$

$$\left(r_b\right)_o = \left(r_t\right)_o = 0.94 \quad \ldots\ldots\ldots\ldots\ldots\ldots (26)$$

In Fig. 7, a comparison between the results of the theory, Eqs. 8 and 25, and the results of an extensive test program conducted by the National Advisory Committee for Aeronautics[12] is presented. In observing Fig. 7 it must be remembered that an idealized stress-strain curve was used for the theory. The discrepancy in the region of $N/L' = 0.2$ ksi is virtually eliminated when the proper value of the plasticity reduction factor, $\bar{\eta}$ in Eq. 8, is used in the region between the proportional limit and the yield strength.

By substituting the values given by Eq. 26 into Eq. 19, we can deduce that the optimum distribution of material in the longitudinally stiffened panel is $0.415\,\bar{t}$ in the plating, and $0.585\,\bar{t}$ in the longitudinal stiffeners.

It is interesting to note that this method of analysis can be extended to other cross-sectional configurations. D. J. Farrar has given[14] results based on a

---

14 "The Design of Compression Structures for Minimum Weight," by D. J. Farrar, Journal Royal Aeronautical Soc., Vol. 53, November, 1949, pp. 1041-1052.

somewhat more exact method of analysis for Z, hat, and Y stiffened wide panels. In practically all cases, the results for common stiffening elements indicate that $\alpha_p \cong 1$. Again, as shown by the writer,[12] excellent agreement is obtained between theory and test data for the other stiffener shapes.

Transversely Supported Stiffened Panels - Optimum Design.—In the preceding analysis of wide, longitudinally stiffened panels, the results are based on

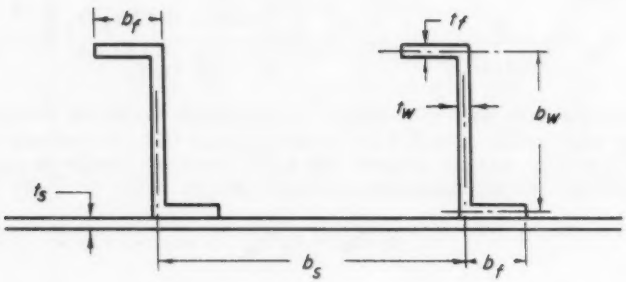

FIG. 6.—LONGITUDINALLY STIFFENED WIDE PANEL CONFIGURATION.

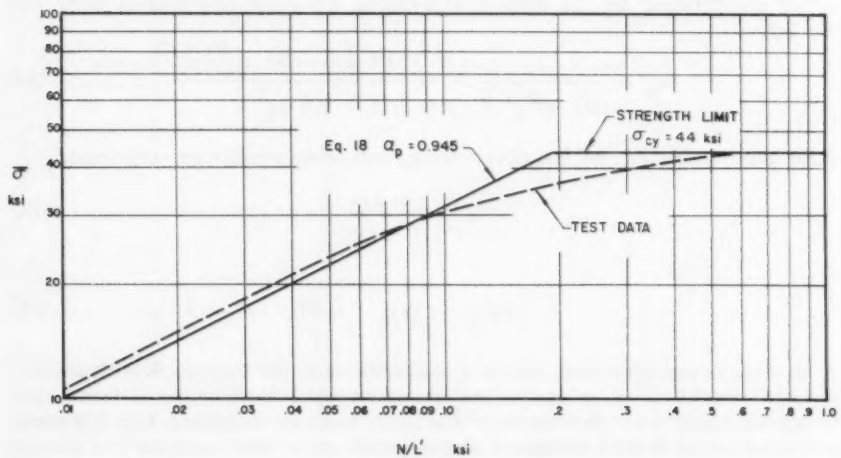

FIG. 7.—COMPARISON BETWEEN TEST DATA AND THEORY FOR WIDE, LONGITUDINALLY Z-STIFFENED PANELS OF MINIMUM WEIGHT FOR 2024-T3 ALUMINUM ALLOY (E = 10.5 x 10^3 ksi).

the loading index, N/L. Since L is the length of the panel between transverse supports, as shown in Fig. 8, there is usually some degree of freedom available to the structural designer in choosing the spacing of the transversals. Thus, the remaining part of this problem is to determine the optimum spacing L which results in minimum weight of the composite compression system, consisting of the wide longitudinally stiffened panel and the transverse stiffeners.

This type of analysis has been presented in rather complete detail.[12] For purposes of illustration of the method, some of the essential results are presented in the following.

The minimum deflectional rigidity of the simply supported transverse stiffener that is required to enforce nodes in the stiffened panel and, thus, avoid general instability, is given[12] as

$$(E\ I)_r = 4\ w^4\ N/\left(\pi^4\ L\right) \quad \ldots\ldots\ldots\ldots\ldots (27)$$

The moment of inertia of a transverse stiffener, with concentrated flanges at a distance h apart, can be approximated by

$$I_r = h^3\ \bar{t}_r/4 \quad \ldots\ldots\ldots\ldots\ldots\ldots (28)$$

By combining Eqs. 27 and 28, the effective thickness of the transverse stiffener becomes

$$\bar{t}_r = 16\ w^4\ N/\left(\pi^4\ h^3\ E\ L\right) \quad \ldots\ldots\ldots\ldots\ldots (29)$$

For the long, transversely supported stiffened panel shown in Fig. 8, the volume of material in a length L equal to the transverse spacing is given by

$$V = \bar{t}\ w\ L + \bar{t}_r\ h\ w \quad \ldots\ldots\ldots\ldots\ldots\ldots (30)$$

Since $\bar{t} = N/\bar{\sigma}$, from Eq. 11, and by substituting Eq. 18 for $\bar{\sigma}$ and Eq. 29 for $\bar{t}_r$, Eq. 30 can be transformed into the following non-dimensional form for $\bar{\tau} = 1$ and c = 1:

$$\frac{\bar{t}_c}{w} = \frac{1}{\alpha_p}\left(\frac{L}{w}\right)^{1/2}\left(\frac{N}{E\ w}\right)^{1/2} + \frac{16}{\pi^4}\left(\frac{w}{h}\right)^2\left(\frac{w}{L}\right)^2\frac{N}{E\ w} \quad \ldots\ldots (31)$$

where $\bar{t}_c$ is the effective thickness of the composite structure.

Since the minimum-weight design is of interest, Eq. 31 can be minimized in terms of the transverse, stiffener spacing L by performing the operation $\partial\bar{t}_c/\partial L = 0$ with the following results. The optimum spacing is

$$\left(\frac{L}{w}\right)_o = \left(\frac{64\ \alpha_p}{\pi^4}\right)^{2/5}\left(\frac{w}{h}\right)^{4/5}\left(\frac{N}{E\ w}\right)^{1/5} \quad \ldots\ldots\ldots (32)$$

The resulting effective, composite, structural thickness for minimum weight is found to be

$$\left(\frac{\bar{t}_c}{w}\right)_o = \left(\frac{64}{\pi^4\ \alpha_p^4}\right)^{1/5}\left(\frac{w}{h}\right)^{2/5}\left(\frac{N}{E\ w}\right)^{3/5}\left(1 + \frac{1}{4}\right) \quad \ldots\ldots (33)$$

It can be observed from Eqs. 32 and 33, that the optimum spacing $(L/w)_o$ and optimum effective thickness (t_c/w_o) are in terms of the geometric proportions of the transverse stiffeners (w/h) and the loading index (N/w). Thus, the original objective of determining the solution in terms of the prescribed loading (N) and geometric quantity (w) has been achieved.

In Eq. 33 the terms in the last bracket represent the effective thickness of the stiffened panel and that of the lateral stiffeners, respectively. Thus, the total effective thickness is distributed as follows:

Element	Fraction of $\bar{t}_c$
Plating	0.33
Longitudinal stiffeners	0.47
Transverse stiffeners	0.20

Transversely Stiffened Panels - Yield-Strength Design.—Having completed the analysis for transversely stiffened panels of optimum design, it is of some interest to consider how such panels may be designed for the compressive yield strength. This is of importance in two respects: It provides the analysis of

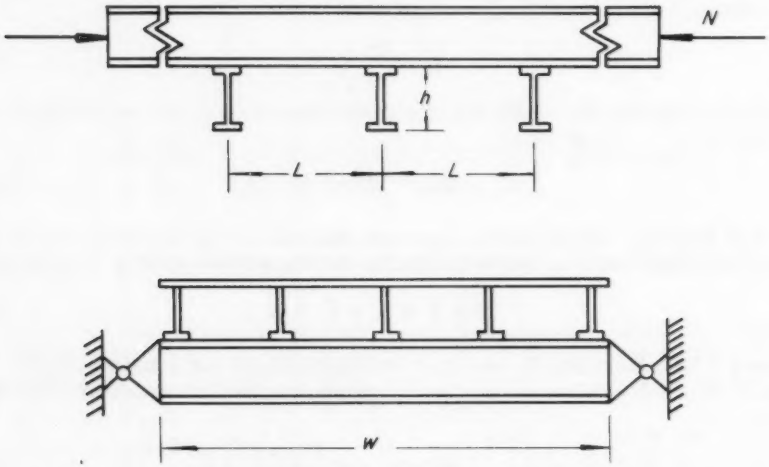

FIG. 8.—TRANSVERSELY SUPPORTED LONGITUDINALLY STIFFENED PANEL CONFIGURATION.

panels designed for a yield limit rather than a stability limit, and, also, serves to illustrate the difference in weight between these two design conditions.

For a wide longitudinally stiffened panel with $\bar{\sigma} = \sigma_{cy}$, the effective thickness, from Eq. 11, is

$$\bar{t} = N/\sigma_{cy} \quad \ldots\ldots\ldots\ldots\ldots\ldots (34)$$

Since the stress level is fixed at the yield strength, the transverse stiffener spacing is fixed by Eq. 18. For $c = 1$ and $\bar{\tau} = 1$,

$$L = \alpha_p^2 \, N \, E/\sigma_{cy}^2 \quad \ldots\ldots\ldots\ldots\ldots\ldots (35)$$

By substituting Eqs. 34, 35, and 29 into Eq. 30 and rearranging terms, the effective thickness of the composite, transversely supported stiffened panel becomes

$$\frac{\bar{t}_c}{w} = \left(\frac{E}{\sigma_{cy}}\right)\left(\frac{N}{E\,w}\right)\left[1 + \left(\frac{2}{\pi\,\alpha_p}\right)^4\left(\frac{w}{h}\right)^2\left(\frac{E\,w}{N}\right)^2\left(\frac{\sigma_{cy}}{E}\right)^5\right] \quad \ldots (36)$$

The last complete term in the brackets represents the effective thickness of the transverse supports. As compared to Eq. 33, it is not a fixed fraction of the total effective thickness, but varies with the loading index and characteristics of the material used.

Typical results for the composite, compression structures designed according to stability, Eq. 33, and according to yield strength, Eq. 36, are illustrated in Fig. 9. In the computations, an idealized stress-strain curve was used which was composed of an elastic portion and a horizontal yield strength limit of $\sigma_{cy} = E/300$.

It can be observed from Fig. 9 that at the lower values of N/E w, the optimum design according to stability does, indeed, provide a structure of con-

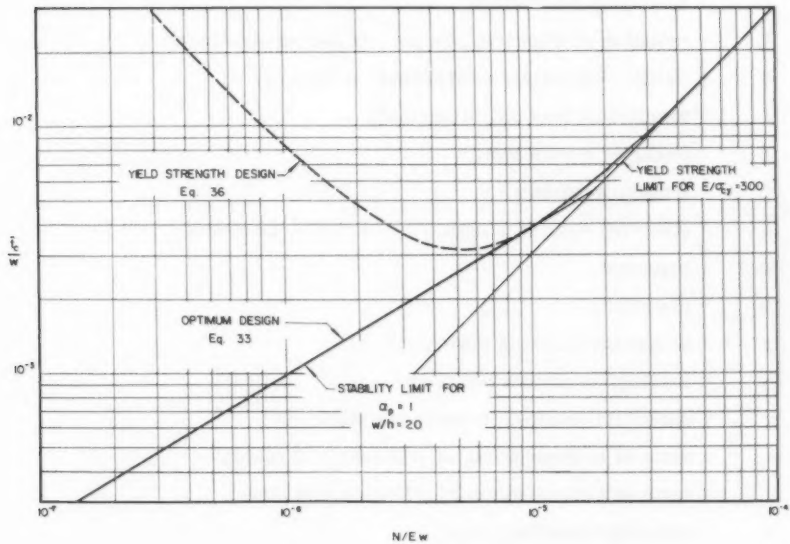

FIG. 9.—STRUCTURAL EFFICIENCY OF TRANSVERSELY SUPPORTED, LONGITUDINALLY STIFFENED PANELS, FOR $\alpha_p = 1$, w/h = 20.

siderably less weight than the yield-strength design. This difference is primarily a result of the fact that a relatively large weight of transverse structure is required to support the stiffened panels at the yield strength.

At values of N/E w equal to 10^{-5}, the yield strength and optimum designs are equal. Beyond this value of N/E w, the yield-strength design must be followed in recognition of the strength limitations of the material used in this example.

CONCLUSIONS

The examples which have been presented serve to illustrate the significant types of design information that can be determined from minimum weight analy-

ses. This approach can be applied to many other types of compression structures.[12] Not only can the minimum-weight configurations of a particular form of construction be determined, but the comparative efficiencies of various types of construction can also be investigated. Finally, such analyses are of considerable value in studying the comparative efficiencies of materials of different elastic moduli and strength levels.

LIST OF SYMBOLS

A_{st} = stiffener area, in square inches;

b = longitudinal stiffener spacing, in inches;

c = end fixity coefficient;

E = modulus of elasticity, in pounds per square inch;

h = height of transverse stiffener, in inches;

I = moment of inertia, in inches^4;

k = buckling coefficient;

L = length, in inches;

L' = effective column length, $L' = L/c^{1/2}$, in inches;

m = exponent;

n = exponent;

o = subscript denoting optimum;

N = loading, in pounds per inch;

r = subscript denoting transverse stiffener;

r_b = ratio of b-dimensions of stiffener and plate;

r_t = ratio of t-dimensions of stiffener and plate;

s = subscript denoting skin;

t = thickness, in inches;

$\bar{t}$ = effective thickness of stiffened panel, in inches;

$\bar{t}_c$ = effective thickness of panel and transverse stiffener, in inches;

V = volume, in cubic inches;

w = panel width, in inches;

w = subscript denoting longitudinal stiffener;

α = crippling coefficient;

α_p = efficiency coefficient of stiffened panel;

β = crippling coefficient;

η = plasticity reduction factor for plates;

ν = Poisson's ratio;

ρ = radius of gyration, in inches;

σ_a = applied stress, in pounds per square inch;

σ_{co} = column stress, in pounds per square inch;

σ_{cr} = buckling stress, in pounds per square inch;

σ_{cy} = compressive yield strength, in pounds per square inch;

σ_e = edge stress, in pounds per square inch;

$\bar{\sigma}$ = average or effective stress, in pounds per square inch;

$\bar{\sigma}_f$ = crippling strength, in pounds per square inch; and

τ = plasticity reduction factor for columns.

Journal of the
ENGINEERING MECHANICS DIVISION
Proceedings of the American Society of Civil Engineers

DYNAMIC ANALYSIS OF ELASTO-PLASTIC STRUCTURES

By Glen V. Berg,[1] F. ASCE and Donald A. DaDeppo,[2] A. M. ASCE

SYNOPSIS

A numerical method is presented for determining the response of an elasto-plastic structure of a finite number of degrees of freedom to dynamic loads by a high-speed digital computer. Damping, either linear or non-linear, may exist. The method consists of numerical integration combined with a matrix solution for the elasto-plastic constraints. Uniqueness of the elasto-plastic solution is proved. A numerical example illustrates the process.

INTRODUCTION

In recent years the problem of analyzing the response of a non-linear system to dynamic forces has received increasing attention. To the structural engineer the elasto-plastic response problem is perhaps the most important case, and recent contributions in that area have been numerous.

The present paper looks into a special case of the elasto-plastic response problem, namely, the multi-story elasto-plastic structure responding to lateral dynamic forces. A complete and practicable machine method of solution is presented.

Note.—Discussion open until September 1, 1960. To extend the closing date one month, a written request must be filed with the Executive Secretary, ASCE. This paper is part of the copyrighted Journal of the Engineering Mechanics Division, Proceedings of the American Society of Civil Engineers, Vol. 86, No. EM 2, April, 1960.

[1] Assoc. Prof. of Civil Engrg., Univ. of Michigan, Ann Arbor.
[2] Ass't. Prof. of Civil Engrg., Univ. of Arizona, Tucson.

SOLVING THE EQUATIONS OF MOTION FOR NON-LINEAR DYNAMIC SYSTEMS

The dynamic system considered in this paper is a lumped mass system of n degrees of freedom, subjected to external forces and/or motion of the base. Such a system of order two is shown symbolically in Fig. 1, in which the springs and dampers may be non-linear.

Let

m_i = mass of the i^{th} body;

x_i = displacement of the i^{th} body, relative to a coordinate system fixed in the base;

$y(t)$ = displacement of the base, relative to a "fixed" frame of reference;

$F_i(t)$ = external force applied to the i^{th} body;

$R_i(x,\dot{x},t)$ = resistance force exerted on the i-th body by the spring and damper system;

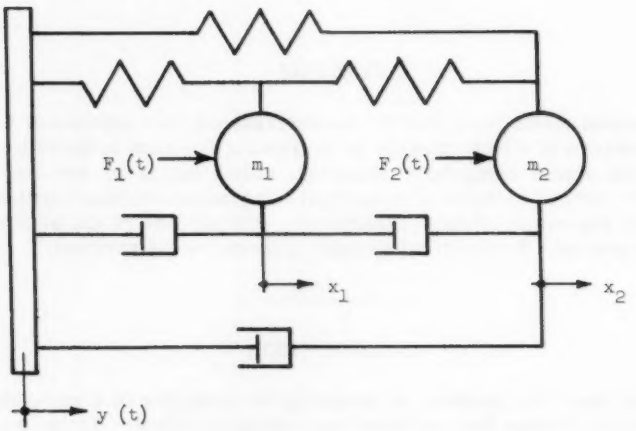

x_1 and x_2 are displacements relative to base

y is displacement of base

FIG. 1.—DAMPED DYNAMIC SYSTEM.

and dots denote differentiation with respect to time. The equations of motion for the system are then

$$m_i \ddot{x}_i + R_i(x_1,x_2,\ldots x_n, \dot{x}_1,\dot{x}_2,\ldots \dot{x}_n, t) = f_i(t) \qquad (i=1,2,\ldots n) \ldots (1)$$

where

$$f_i(t) = F_i(t) = m_i \ddot{y}(t) \ldots\ldots\ldots\ldots\ldots (2)$$

There are many methods of approximating the solution to Eq. 1 numerically, and no one method can be claimed to be the best for all cases.

The Milne Predictor-Corrector method[3] is well suited to problems in which (a) damping forces are absent or negligible, and therefore the resistance functions R_i do not involve the velocities $\dot{x}$; and (b) the driving forces f_i can be approximated by smooth curves through sets of discrete points equally spaced in time. Blast problems, for example, often meet these requirements.

The steps of the method are:

Predictor

$$x_i^*(t+h) = x_i(t) + \dot{x}_i(t-2h) - x_i(t-3h) + \frac{h^2}{4}\left[5\ddot{x}_i(t) + 2\ddot{x}_i(t-h) + 5\ddot{x}_i(t-2h)\right] \quad \ldots\ldots\ldots (3)$$

Corrector

$$x_i(t+h) = 2x_i(t) - x_i(t-h) + \frac{h^2}{12}\left[\ddot{x}_i^*(t+h) + 10\ddot{x}_i(t) + \ddot{x}_i(t-h)\right] \quad \ldots (4)$$

By recursive use of these two formulas one advances step by step through the solution.

For problems which involve very irregular driving forces, such as the earthquake response problem, it is advantageous to use a single-step method—that is, one which projects to time t + h from the values of x_i, $\dot{x}_i$ and $\ddot{x}_i$ at time t, and the functions f_i, without using the values of the variables at earlier times. The Runge-Kutta procedure[4] is a single-step method well suited to high-speed computers.

For the equations

$$\dot{y}_i = \dot{y}_i(y_1, y_2, \ldots y_n, t) \qquad (i = 1,2,..n) \quad \ldots\ldots\ldots (5)$$

the formulas for the Runge-Kutta third order procedure are

$$\kappa_{i0} = h\,\dot{y}_i(y_1, y_2, \ldots y_n, t) \quad \ldots\ldots\ldots (6a)$$

$$\kappa_{i1} = h\,\dot{y}_i(y_1 + p\,\kappa_{10},\ y_2 + p\,\kappa_{20}, \ldots y_n + p\,\kappa_{n0},\ t + p\,h) \quad \ldots\ldots\ldots (6b)$$

$$\kappa_{i2} = h\,\dot{y}_i(y_1 + [q-r]\,\kappa_{10} + r\,\kappa_{11}, \ldots y_n + [q-r]\,\kappa_{n0} + r\,\kappa_{n1},\ t + q\,h) \quad (6c)$$

and

$$y_i(t+h) = y_i(t) + l\,\kappa_{i0} + m\,\kappa_{i1} + n\,\kappa_{i2} \quad \ldots\ldots\ldots (7)$$

The relations governing the constants l, m, n, p, q, and r are

$$\left.\begin{aligned} l + m + n &= 1 \\ m\,p + n\,q &= 1/2 \\ m\,p^2 + n\,q^2 &= 1/3 \\ n\,p\,r &= 1/6\ , \end{aligned}\right\} \quad \ldots\ldots\ldots\ldots (8)$$

---

[3] "Numerical Calculus," by W. E. Milne, Princeton Univ. Press, Princeton, N. J., 1949.

[4] "Numerical Solutions of Differential Equations," by H. Levy and E. A. Baggott, Dover Publications, Inc., New York, 1950.

to which there are infinitely many solutions. One of the more useful solutions is

$$\left.\begin{aligned} l &= 1/4 \\ m &= 0 \\ n &= 3/4 \\ p &= 1/3 \\ q &= 2/3 \\ r &= 2/3 \end{aligned}\right\} \quad \ldots\ldots\ldots\ldots\ldots\ldots \quad (9)$$

This makes $m = (q-r) = 0$ and thus reduces the number of arithmetic operations required. A second solution, due to S. Conte and R. Reeves,[5] is

$$\left.\begin{aligned} l &= 0.62653829327 \\ m &= 0.85614352807 \\ n &= -0.48268182134 \\ p &= 0.62653829327 \\ q &= 0.07542588774 \\ r &= -0.55111240553 \end{aligned}\right\} \quad \ldots\ldots\ldots\ldots\ldots\ldots (10)$$

In this solution, $\ell = p = (q-r)$, which leads to a reduced storage requirement for the computer.

To adapt Eqs. 1 to the Runge-Kutta process, one can write them in the form

$$\left.\begin{aligned} \dot{x}_i &= z_i \\ \text{and} \\ \dot{z}_i &= \frac{1}{m_i}\left[f_i(t) - R_i\left(x_1, x_2, \ldots x_n, z_1, z_2, \ldots z_n, t\right)\right] \end{aligned}\right\} \quad \ldots\ldots (11)$$

The solution is then straight forward.

The foregoing numerical methods are applicable to any system, subject only to the restrictions that the number of degrees of freedom must be finite and the resistance functions R_i must be single-valued and piece-wise continuous.

THE RESISTANCE FORCES FOR AN ELASTO-PLASTIC BENT

The specific problem considered herein is the response of a multi-story bent to lateral dynamic forces. The bent is a rectangular plane framework of elasto-plastic members, loaded by lateral dynamic forces applied at the joints and in the plane of the bent. Connections may be either pinned or fully restrained. The mass of the structure is assumed to be concentrated at the joints. Damping is assumed to be viscous. Deformations due to axial forces and shear forces in the members are neglected, and the effect of axial forces upon the

[5] "A Kutta Third-Order Procedure for Solving Differential Equations Requiring Minimum Storage," by S. Conte and R. Reeves, Technical Note No. 1037, Ballistics Research Labs., Aberdeen, Md., January, 1956.

stiffnesses and plastic hinge moments of the members is neglected. These assumptions yield a dynamic system having degrees of freedom equal to the number of stories in the bent. The principles used can be extended to more general problems, but such extension is not considered herein.

Consistent with the assumption of viscous damping, the resistance functions R_i are separable into damping forces D_i, which are linear functions of the velocities, and restoring forces Q_i. The damping forces are

$$D_i = \sum_{j=1}^{n} c_{ij} \dot{x}_j \quad \ldots\ldots\ldots\ldots\ldots\ldots (12)$$

The coefficient c_{ij} is the damping force that would exist at the i^{th} floor if the structure were passing through the equilibrium configuration with unit velocity at the j^{th} floor and zero velocity at all other floors.

The restoring forces for an elastic frame can be expressed in terms of a matrix of stiffness coefficients k such that

$$Q_i = \sum_{j=1}^{n} k_{ij} x_j \quad \ldots\ldots\ldots\ldots\ldots\ldots (13)$$

The forces Q_i ($i = 1,2,\ldots n$) are the forces necessary to hold the frame in static equilibrium in the configuration defined by the lateral deflections x_j ($j = 1,2,\ldots n$). The j^{th} column of the matrix k represents the set of static lateral forces that would be required to hold the frame in equilibrium with unit lateral deflection at the j^{th} floor and zero lateral deflection at all other floors. A conventional static analysis is sufficient to evaluate the stiffness matrix. The effect of eccentricity of dead load can be taken into account in evaluating the matrix if desired.

Let the subscripts k and ℓ denote locations in the frame, such that each value of the subscript denotes the end of a specific structural member at a specific joint; and let M_k be the moment at location k, considered positive when it tends to rotate the end of the member clockwise. Then the end moments in the members of an elastic frame can be expressed in terms of a matrix of influence coefficients μ such that

$$M_k = \sum_{j=1}^{n} \mu_{kj} x_j \quad \ldots\ldots\ldots\ldots\ldots\ldots (14)$$

The j^{th} column of the matrix μ is the set of end moments that would exist in the members if the frame had unit lateral deflection at the j^{th} floor and zero lateral deflection at all other floors. The matrix μ can be evaluated by conventional static analysis.

If the lateral deflections become sufficiently large, the elastic limit may be exceeded at one or more locations in the frame. This occurrence will, of course, affect the restoring forces and moments.

For this paper it is assumed that the connections are either pinned or fully restrained, and that all members in the frame, columns and girders alike, have ideal elasto-plastic moment-rotation characteristics. The typical moment-rotation curve follows a linear elastic branch until the moment reaches the plastic hinge moment. Upon further deformation, the moment remains constant and a plastic hinge forms, making a "kink" in the member. Upon reversal of

strain after reaching plasticity, the moment-rotation curve follows a path parallel to the original elastic branch. It remains on the second elastic branch until the plastic hinge moment, either positive or negative, is reached, and then follows a plastic branch as before. Extreme reversals cause the moment-rotation curve to follow a hysteresis loop. This idealized behavior is illustrated in Fig. 2.

As soon as plasticity is reached at any location, the frame behaves just as though the member were hinged at that location, with a constant moment applied to the hinge. This condition prevails until the next hinge forms or until a decrease in strain occurs at an existing plastic hinge location, causing the hinge to disappear.

E. Cohen, L. S. Levy and L. E. Smollen developed[6] a procedure for adapting the method of normal modes to an elasto-plastic frame with infinitely rigid girders, and Leo Schenker, M. ASCE,[7] indicated a method of extending this to include the frame with flexible girders. In both procedures, an elastic solution

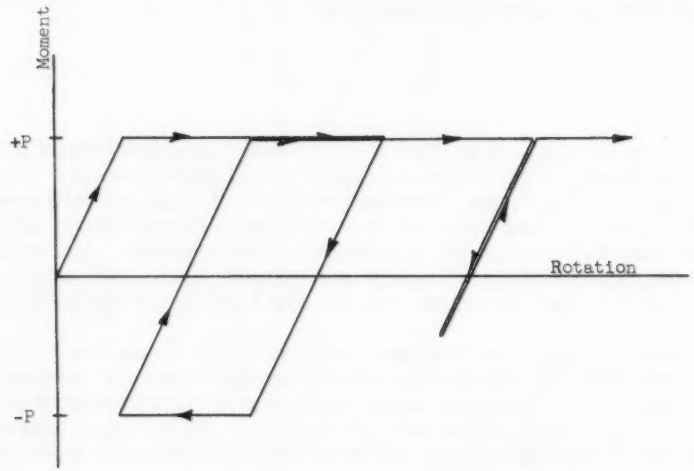

FIG. 2.—IDEALIZED MOMENT - ROTATION DIAGRAM

is carried out by the method of normal modes to the point where plasticity is reached at some location. The frame is then modified by inserting a real hinge at the plastic hinge location, the new normal modes and frequencies are computed, and the solution is continued as a superposition of the conditions at the instant of transition and the changes found by solving the modified frame. Each time a new hinge forms or an old one disappears, the frame is modified accordingly. In this way a continuous solution can be found.

For a step-by-step numerical solution, an analogous and somewhat simpler procedure can be devised. The conditions at the end of a time step can be found as a superposition of the conditions at the beginning of the step and the changes during the step. To find the changes during the time step, one first computes the "elastic increments"; that is, the changes which would be caused

6 "Impulsive Motion of Elasto-Plastic Shear Buildings," by E. Cohen, L. S. Levy and L. E. Smollen, Transactions, ASCE, Vol. 122, 1957.

7 "The Dynamic Analysis of Tall Structures in the Elastic and Inelastic Ranges," by Leo Schenker, Doctoral dissertation, University of Michigan, 1954.

by the motion during the time step if plastic hinge rotations did not occur. The resulting moments may exceed the plastic hinge moments at one or more locations in the frame. To remedy this, "corrector" solutions are superimposed in which the frame has hinges at these locations, and these hinges are rotated in such a way that the total moments, obtained from superposition of the elastic and corrector solutions, nowhere exceed the plastic hinge moments. The superposition of elastic and corrector solutions is illustrated in Fig. 3.

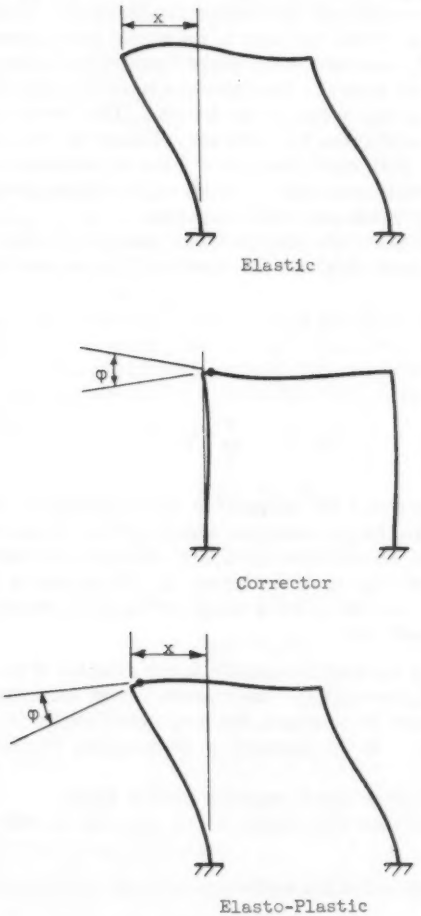

FIG. 3.—ELASTO-PLASTIC SOLUTION BY SUPERPOSITION.

This is an adaptation of the incremental theory of plasticity to a framed structure.[8] W. T. Thomson was perhaps the first to apply the concept to the type of problem considered here,[9] and H. H. Bleich recently formulated a

[8] "Theory of Perfectly-Plastic Solids," by W. Prager and P. G. Hodge, John Wiley & Sons, Inc., New York, 1951.

[9] "Impulsive Response of Beams in the Elastic and Plastic Regions," by W. T. Thomson, Journal of Applied Mechanics, Vol. 21, No. 3, September, 1954, pp. 271-278.

method of analysis employing the same concept in a somewhat broader problem.[10] However, no method of solving the resulting inequalities was given in the Bleich paper, and the existence and uniqueness of the solution were assumed intuitively.

The effects of plastic hinge rotations upon the forces at the floors and the bending moments in the frame members can be expressed in terms of two matrices of influence coefficients b and ν, evaluated as described below.

Let ϕ_ℓ be the plastic hinge rotation at location ℓ, taken as positive when it corresponds to clockwise rotation of the end of the member. (The hinge rotation in Fig. 3 is positive.) Take the bent in its initial (unstrained) position, insert a hinge at location ℓ, and rotate the hinge through an angle $\phi_\ell = 1$, with zero lateral deflection at all joints. Evaluate the lateral forces at all floors and the end moments for the members in the frame. The lateral force at the i^{th} floor is the influence coefficient $b_{i\ell}$, and the moment at location k is the influence coefficient $\nu_{k\ell}$. Both matrices b and ν can be evaluated by conventional static analysis. It will be seen that only those locations at which plastic hinges form are significant to the dynamic response.

If the lateral deflections x and the plastic hinge rotations ϕ were known for some instant of time, one could evaluate the restoring forces and moments as

$$Q_i = \sum_j k_{ij}\, x_j + \sum_l b_{il}\, \phi_l \quad \ldots\ldots\ldots\ldots\ldots (15)$$

and

$$M_k = \sum_j \mu_{kj}\, x_j + \sum_l \nu_{kl}\, \phi_l \quad \ldots\ldots\ldots\ldots\ldots (16)$$

The deflections x can be found by integrating the equations of motion, but one must also find the plastic hinge rotations which satisfy all the constraints of the elasto-plastic system. An iterative method of solution is developed below.

Consider the time rates of change of the forces Q_i, the moments M_k, and the plastic hinge rotations ϕ_k. Let the plastic hinge moment at location k be P_k. The elasto-plastic constraints are:

1. The moment M cannot exceed the plastic hinge moment P in magnitude.
2. If a positive plastic hinge exists, the moment must be either constant or decreasing. If the moment is constant, the hinge may rotate in a direction consistent with the moment. If the moment is decreasing, the hinge cannot rotate.
3. Equivalent conditions exist for a negative plastic hinge.
4. If the moment is less than the plastic hinge moment in magnitude, the hinge cannot rotate.

These conditions may be expressed mathematically as the following set of constraints:

---

[10] "Response of Elastoplastic Structures to Transient Loads," by H. H. Bleich, Transactions, New York Academy of Sciences, Ser. II, Vol. 18, No. 2, December, 1955, pp. 135-143.

$$\left.\begin{array}{l} 1.\ -P_k \le M_k \le P_k \\ 2.\ \text{If } M_k = P_k, \text{ then } \dot{M}_k \le 0,\ \dot{\phi}_k \le 0, \text{ and } \dot{M}_k \dot{\phi}_k = 0 \\ 3.\ \text{If } M_k = -P_k, \text{ then } \dot{M}_k \ge 0,\ \dot{\phi}_k \ge 0, \text{ and } \dot{M}_k \dot{\phi}_k = 0 \\ 4.\ \text{If } -P_k < M_k < P_k, \text{ then } \dot{\phi}_k = 0 \end{array}\right\} \quad \ldots (17)$$

Differentiating Eq. 16, one gets

$$\dot{M}_k = \sum_j \mu_{kj} \dot{x}_j + \sum_l \nu_{kl} \dot{\phi}_l \quad \ldots (18)$$

The following uniqueness theorem can be established: Given any rigid-jointed rectangular plane framework of ideal elasto-plastic flexural members, and given any $\dot{x}$'s whatever, and any M's not exceeding the plastic hinge moments,* there exists one and only one set of $\dot{M}$'s and $\dot{\phi}$'s which satisfies Eq. 18 and Constraints 17. The proof follows.

First, observe that if for one or more values of k, $-P_k < M_k < P_k$, then $\dot{\phi}_k = 0$ and there is no constraint on $\dot{M}_k$. Thus the solution for $\dot{\phi}_k$ is unique, it does not affect other locations, and the effect of conditions at other locations upon $\dot{M}_k$ is immaterial. Hence it is sufficient to consider only those locations for which $|M_k| = P_k$.

Define

$$\left.\begin{array}{l} y_k = -(\text{sgn } M_k)\dot{M}_k \\ a_k = (\text{sgn } M_k) \sum_j \mu_{kj} \dot{x}_j \\ \xi_{kl} = (\text{sgn } M_k)(\text{sgn } M_l)\, \nu_{kl} \\ z_l = (\text{sgn } M_l)\dot{\phi}_l \end{array}\right\} \quad \ldots (19)$$

Eq. 18 then can be written

$$\sum_l \xi_{kl} z_l - \sum_l \delta_{kl} y_l = a_k \quad \ldots (20)$$

where $\delta_{k\ell}$ is the Kronecker delta,

$$\delta_{kl} = 1, \quad k = l$$

$$\delta_{kl} = 0, \quad k \neq l$$

* The case in which all members at a joint become hinges simultaneously is excluded.

Constraints 17 become

$$\left.\begin{aligned} y_k &\geq 0 \\ z_k &\geq 0 \\ y_k\, z_k &= 0 \end{aligned}\right\} \quad \ldots\ldots\ldots\ldots\ldots\ldots (21)$$

The vector a is unrestricted. To establish uniqueness, it must be shown that the matrix ξ has properties which guarantee that, corresponding to any vector a, there exists one and only one pair of vectors y and z that satisfies Eq. 20 and Constraints 21. This amounts to a partition problem in n-dimensional Euclidean space.

Consider the columns of the matrices $-\delta$ and ξ as vectors $\eta_1, \eta_2, \ldots \eta_n$; $\xi_1, \xi_2, \ldots \xi_n$. That is, let $\{\eta_i\} = \{-\delta_{ji}\}$ and $\{\zeta_i\} = \{\xi_{ji}\}$. Then let $\alpha_1, \alpha_2, \ldots \alpha_n$ be a set of vectors such that every α_i is either η_i or ζ_i. There are 2^n such sets. If the η's and ξ's partition the space, every vector a in the space can be formed by linear combination of one and only one set of α_i's with nonnegative coefficients.* In other words, for any given vector a there is one and only one set of α_i's for which

$$\{a\} = \sum_i q_i \{\alpha_i\} \quad \ldots\ldots\ldots\ldots\ldots\ldots (22)$$

where every q_i is nonnegative. If this is so, then for those i for which $\alpha_i = \eta_i$, one has $y_i = q_i$ and $z_i = 0$; and for those i for which $\alpha_i = \xi_i$, one has $y_i = 0$ and $z_i = q_i$. Thus the vectors y and z corresponding to any given vector a are unique and satisfy the constraints.

To illustrate this concept, consider the two-dimensional case. Suppose positive plastic hinges exist at locations 1 and 2, and all other locations are elastic. Further, suppose that the matrix ν is

$$\nu_{k1} = \begin{bmatrix} 69{,}700 & -16{,}580 \\ -16{,}580 & 105{,}560 \end{bmatrix} \text{ in.-kips/radian}$$

In this case, $\nu_{k\ell} = \xi_{k\ell}$, and Eq. 20 becomes

$$\begin{bmatrix} 69{,}700 & -16{,}580 \\ -16{,}580 & 105{,}560 \end{bmatrix} \{z\} + \begin{bmatrix} -1 & 0 \\ 0 & -1 \end{bmatrix} \{y\} = \{a\}$$

The columns of the matrices in this equation are plotted as the vectors ζ_1, ζ_2, η_1, and η_2 in Fig. 4. The four vectors partition the plane so that any vector {a} in the entire plane can be formed by linear combination of one and only one set of α_i's with nonnegative coefficients.

By virtue of a recent theorem due to H. Samelson, R. M. Thrall and O. Wesler,[11] necessary and sufficient conditions for the columns of ξ and $-\delta$ to partition the space are that every principal minor of the matrix ξ be positive.

Consider now the frame with real hinges at one or more locations, in the equilibrium configuration. This is the frame used for the "corrector" solutions,

---

* If any coefficient is zero, say $q_m = 0$, obviously one can have either $\alpha_m = \eta_m$ or $\alpha_m = \eta_m$. However, in the case $y_m = z_m = 0$ and uniqueness is preserved.

11 "A Partition Theorem for Euclidean n-Space," by H. Samelson, R. M. Thrall and O. Wesler, Proceedings, AMS, Vol. 9, No. 5, October, 1958, pp. 805-807.

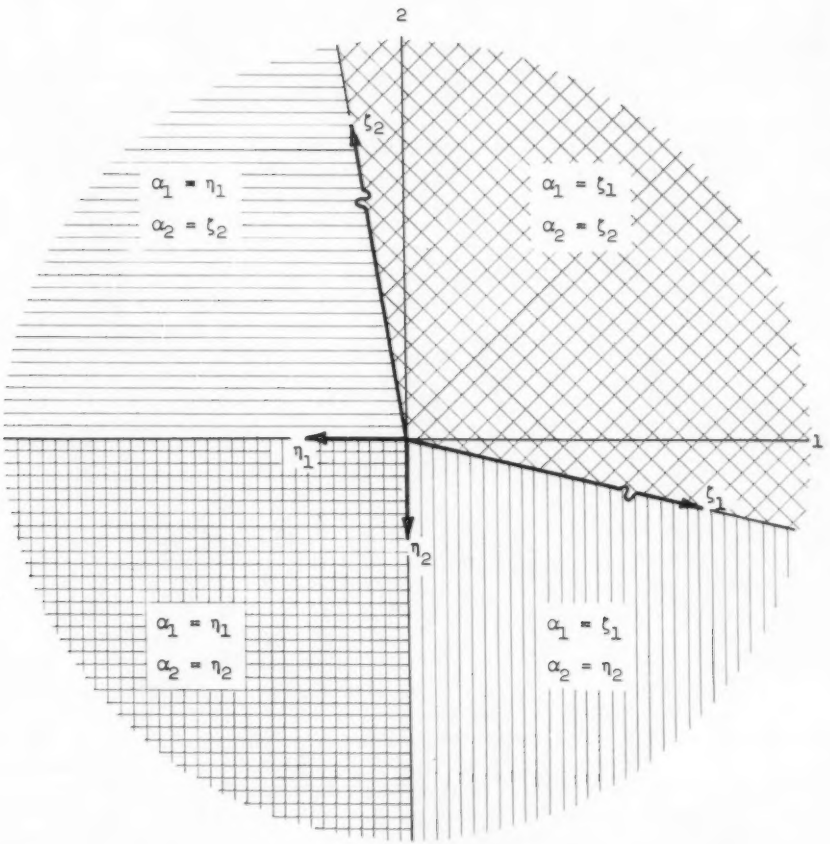

FIG. 4.—PARTITIONING VECTORS.

above. Let the hinged joints in this frame undergo hinge rotations ϕ, with lateral deflection of the floors prevented. The resulting strain energy in the frame is

$$E = \frac{1}{2} \sum_k \phi_k M_k \quad \ldots\ldots\ldots\ldots\ldots\ldots (23)$$

The moments are

$$M_k = \sum \nu_{kl} \phi_l \quad \ldots\ldots\ldots\ldots\ldots\ldots (24)$$

Combining Eqs. 23 and 24, one gets

$$E = \frac{1}{2} \sum_k \sum_l \nu_{kl} \phi_k \phi_l \quad \ldots\ldots\ldots\ldots\ldots\ldots (25)$$

Because Eq. 25 is a strain-energy equation, it is a positive definite quadratic form. The principal minors of ν are therefore positive. Finally, since ζ was obtained from ν simply by changing the signs of the off-diagonal elements of certain rows and the corresponding columns (see Eqs. 19), the principal minors of ζ are positive. It follows from the Samelson-Thrall-Wesler theorem that a unique solution exists.

The solution can be found by the following iterative scheme: Let z^p be the p^{th} approximation to the vector z, with all elements of z^p nonnegative. (Zero is a convenient and satisfactory first approximation.) For convenience in notation, define

$$\xi_{k0} = \xi_{kn+1} = z_0 = z_{n+1} = 0$$

Starting with k = 1, let

$$u_k^{p+1} = a_k - \sum_{l=0}^{k-1} \xi_{kl}\, z_l^{p+1} - \sum_{l=k+1}^{n+1} \xi_{kl}\, z_l^{p} \quad \ldots\ldots (26)$$

Then,

$$\text{if} \qquad u_k^{p+1} > 0, \text{ let } z_k^{p+1} = \frac{u_k^{p+1}}{\xi_{kk}} \quad \ldots\ldots\ldots\ldots (27)$$

$$\text{and if} \qquad u_k^{p+1} \leq 0, \text{ let } z_k^{p+1} = 0.$$

Repeat this for k = 2, k = 3, . . . k = n. Then let

$$y_k^{p+1} = \sum_{l=1}^{n} \xi_{kl}\, z_l^{p+1} - a_k \qquad (k = 1,2,..n) \ldots\ldots (28)$$

The $(p+1)^{st}$ approximation to the vectors y and z is then complete. It satisfies Eq. 20 and the constraint $z_k \geq 0$, but may fail to satisfy the other constraints in Constraints 21. The process is repeated until the amount by which the approximation fails to satisfy all the constraints is insignificant.

Once the vector z is determined (and therefore the $\dot{\phi}$'s) the rates of change of the restoring forces are found by the equation

$$\dot{Q}_i = \sum_j k_{ij}\, \dot{x}_j + \sum_l b_{il}\, \dot{\phi}_l \quad \ldots\ldots\ldots\ldots (29)$$

The foregoing procedure is, in essence, an adaptation of the Gauss-Seidel iterative method of solving linear equations. Eq. 20 and Constraints 21 reduce finally to a system of linear equations, since at least one of z_k, y_k must be zero for each value of k. The nonzero elements form a system of n (or fewer) linear equations in the same number of unknowns. In this application, the Gauss-Seidel procedure is used to set up the equations as well as to solve them. The procedure lends itself well to machine computation, and it turns out that convergence is quite rapid.

Using this procedure, at each step one must perform three matrix multiplications and solve a system of equations equal in number to the number of plastic hinges. An obvious alternate is moment distribution, whereby at each step one must solve a set of equations equal in number to twice the number of members in the structure.

In developing the above procedure, rates of change of deflection, hinge rotation, and moment have been used. As soon as one introduces finite time intervals in place of differentials, one loses the claim to uniqueness, since it cannot be claimed that reversals in strain do not occur within the time interval. However, by taking the intervals sufficiently small and considering the strain rates as everywhere monotonic within any one time interval, the exact, unique solution of the differential system can be approximated to any desired degree of accuracy by the finite difference system.

To set up the finite difference system, let the subscripts s and s+1 denote a condition at the end of the s^{th} and $(s+1)^{st}$ time step; for example, $x_{i,s+1}$ is the value of the variable x_i at the end of the $(s+1)^{st}$ time step. Also, let

$$\left.\begin{aligned} \Delta x_i &= x_{i,s+1} - x_{i,s} \\ \Delta Q_i &= Q_{i,s+1} - Q_{i,s} \\ \Delta M_i &= M_{k,s+1} - M_{k,s} \\ \Delta \phi_k &= \phi_{k,s+1} - \phi_{k,s} \end{aligned}\right\} \quad \ldots\ldots\ldots\ldots\ldots (30)$$

Then the finite-difference equations are

$$\Delta Q_i = \sum_j k_{ij}\, \Delta x_j + \sum_l b_{il} \Delta \phi_l \quad \ldots\ldots\ldots\ldots (31)$$

and

$$\Delta M_k = \sum_j \mu_{kj}\, \Delta x_j + \sum_l \nu_{kl} \Delta \phi_l \quad \ldots\ldots\ldots\ldots (32)$$

which correspond to Eqs. 29 and 18.
The elasto-plastic constraints are:

$$\left.\begin{aligned} &1.\ \text{If } 0 \leq M_{k,s} \leq P_k, \\ &\text{then either } \Delta M_k = P_k - M_{k,s} \text{ and } \Delta \phi_k \leq 0 \\ &\text{or } -P_k - M_{k,s} < \Delta M_k < P_k - M_{k,s} \text{ and } \Delta \phi_k = 0 \end{aligned}\right\} \quad \ldots\ldots (33)$$

and

$$\left.\begin{aligned} &2.\ \text{If } -P \leq M_{k,s} \leq 0, \\ &\text{then either } \Delta M_k = -P_k - M_{k,s} \text{ and } \Delta \phi_k \geq 0 \\ &\text{or } -P_k - M_{k,s} < \Delta M_k < P_k - M_{k,s} \text{ and } \Delta \phi_k = 0 \end{aligned}\right\} \quad \ldots\ldots (34)$$

ADAPTATION FOR THE COMPUTER

In using the computer, both storage requirements and computation time can be reduced by expressing the moments in nondimensional form. To do this, one can define

$$\left.\begin{aligned} \rho_k &= \frac{M_k}{P_k} \\ \psi_k &= \frac{\nu_{kk}\,\phi_k}{P_k} \\ \beta_{il} &= \frac{b_{il}\,P_l}{\nu_{ll}} \\ \lambda_{kj} &= \frac{\mu_{kj}}{P_k} \\ \sigma_{kl} &= \frac{\nu_{kl}}{\nu_{ll}}\,\frac{P_l}{P_k} \end{aligned}\right\} \quad \ldots\ldots\ldots\ldots\ldots\ldots (35)$$

These transformations do not affect the uniqueness of the solution. In this notation, Eqs. 31 and 32 become

$$\Delta Q_i = \sum_j k_{ij}\,\Delta x_j + \sum_l \beta_{il}\,\Delta\psi_l \quad \ldots\ldots\ldots\ldots (36)$$

$$\Delta\rho_k = \sum_j \lambda_{kj}\,\Delta x_j + \sum_l \sigma_{kl}\,\Delta\psi_l \quad \ldots\ldots\ldots\ldots (37)$$

and the elasto-plastic constraints (33) and (34) become

$$\left.\begin{aligned} &1.\ \text{If } 0 \le \rho_{k,s} \le 1, \text{ then} \\ &\text{either } \Delta\rho_k = \left(1 - \rho_{k,s}\right) \text{ and } \Delta\psi_k \le 0 \\ &\text{or } \left(-1 - \rho_{k,s}\right) < \Delta\rho_k < \left(1 - \rho_{k,s}\right) \text{ and } \Delta\psi_k = 0 \end{aligned}\right\} \quad \ldots\ldots (38)$$

$$\left.\begin{aligned} &2.\ \text{If } -1 \le \rho_{k,s} \le 0, \text{ then} \\ &\text{either } \Delta\rho_k = \left(-1 - \rho_{k,s}\right) \text{ and } \Delta\psi_k \ge 0 \\ &\text{or } \left(-1 - \rho_{k,s}\right) < \Delta\rho_k < \left(1 - \rho_{k,s}\right) \text{ and } \Delta\psi_k = 0. \end{aligned}\right\} \quad \ldots\ldots (39)$$

The iterative procedure of Eqs. 26, 27, and 28 is readily adapted to this formulation of the problem. Let

r = number of moment locations (the order of the matrix σ)

and

$\Delta\psi_k^p$ = p^{-th} approximation to $\Delta\psi_k$.

Define

$$\Delta\psi_k^0 = 0 \text{ for all } k,$$

$$\sigma_{k0} = \sigma_{kr+1} = 0 \text{ for all } k,$$

$$\Delta\psi_0^p = \Delta\psi_{r+1}^p = 0 \text{ for all } p.$$

Then, starting with k = 1 and p = 1, compute

$$u_k^p = \sum_j \lambda_{kj}\,\Delta x_j + \sum_{l=0}^{k-1} \sigma_{kl}\,\Delta\psi_l^p + \sum_{l=k+1}^{r+1} \sigma_{kl}\,\Delta\psi_l^{p-1} \quad \ldots\ldots(40)$$

$$\left.\begin{aligned} &\text{If } \left(\rho_{k,s} + u_k^p\right) > 1, && \text{let } \Delta\psi_k^p = \left(1 - \rho_{k,s} - u_k^p\right) \\ &\text{if } -1 \leq \left(\rho_{k,s} + u_k^p\right) \leq 1, && \text{let } \Delta\psi_k^p = 0 \text{ ; and} \\ &\text{if } \left(\rho_{k,s} + u_k^p\right) < -1, && \text{let } \Delta\psi_k^p = \left(-1 - \rho_{k,s} - u_k^p\right) \end{aligned}\right\} \ldots(41)$$

Repeat this for k = 2, k = 3, . . . k = r. This completes the p^{th} approximation. Then let

$$e^p = \sum_{k=1}^{r} \left| \Delta\psi_k^p - \Delta\psi_k^{p-1} \right| \quad \ldots\ldots\ldots\ldots\ldots(42)$$

which is an indicator of the amount by which the solution fails to satisfy the Constraints 38 and 39. If e^p is larger than some predetermined error test δ, one returns to k=1 and computes the $(p+1)^{st}$ approximation. When the convergence test is satisfied, one accepts the last approximation as the correct solution for the $\Delta\psi_k$ and computes ΔQ_i and $\Delta\rho_k$ from Eqs. 36 and 37.

NUMERICAL EXAMPLE

The following numerical example illustrates the foregoing processes. Consider the undamped bent shown in Fig. 5. Taking f_y = 36,000 psi, one gets for plastic hinge moments

$$P_1 = P_2 = P_3 = 1398 \text{ in.-kips}$$

$$P_4 = 2072 \text{ in.-kips}$$

$$P_5 = 1583 \text{ in.-kips}$$

Because the bent is symmetrical and the effects of axial forces on the member stiffnesses are ignored, the stress distribution will also be symmetrical. Hence only half the moments need be recorded. Moreover, the moment at location 5 cannot reach plasticity and therefore does not need to be recorded.

The matrices of influence coefficients k_{ij}, $b_{i\ell}$, μ_{kj}, and $\nu_{k\ell}$ which describe the elasto-plastic properties of the system are the forces and moments shown

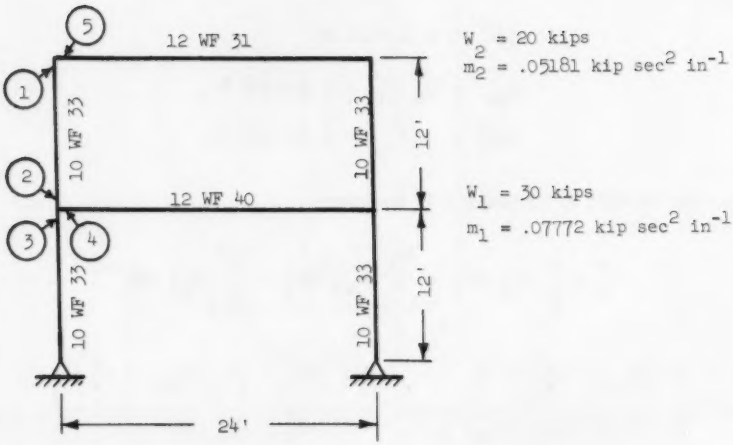

FIG. 5.—BENT FOR NUMERICAL EXAMPLE.

in Figs. 6 and 7. The effect of eccentricity of the dead load on the moments may be taken into account if desired. It is neglected in this example. The complete matrices are

$$k_{ij} = \begin{bmatrix} 35.73 & -24.11 \\ -24.11 & 20.20 \end{bmatrix} \text{ kip in.}^{-1}$$

$$b_{i1} = \begin{bmatrix} 1425 & 2019 & -1674 & -345 \\ -1325 & -1584 & 563 & 1021 \end{bmatrix} \text{ kips/radian}$$

$$\mu_{kj} = \begin{bmatrix} 726.1 & -662.6 \\ 1009.6 & -791.8 \\ -836.9 & 281.3 \\ -172.7 & 510.5 \end{bmatrix} \text{ in.-kips/in.}$$

$$\nu_{k1} = \begin{bmatrix} 69,709 & 25,720 & -9,140 & -16,580 \\ 25,720 & 88,300 & -31,370 & -56,930 \\ -9,140 & -31,370 & 80,010 & -48,640 \\ -16,580 & -56,930 & -48,640 & 105,560 \end{bmatrix} \text{ in.-kips/radian}$$

Converting the moments to nondimensional form according to Eqs. 35, one obtains

$$\beta_{i1} = \begin{bmatrix} 29.12 & 31.97 & -29.25 & -6.78 \\ -26.58 & -25.08 & 9.83 & 20.04 \end{bmatrix} \text{ kip}$$

$$\lambda_{kj} = \begin{bmatrix} .5194 & -.4740 \\ .7222 & -.5664 \\ -.5987 & .2012 \\ -.0833 & .2464 \end{bmatrix} \text{ in.}^{-1}$$

$$\sigma_{k1} = \begin{bmatrix} 1.0000 & .2913 & -.1142 & -.2328 \\ .3690 & 1.0000 & -.3921 & -.7993 \\ -.1311 & -.3553 & 1.0000 & -.6829 \\ -.1605 & -.4350 & -.4102 & 1.0000 \end{bmatrix}$$

Suppose that at time t_0 the system is in the configuration

$$x_1 = 2.600 \text{ in.} \qquad \dot{x}_1 = 10.00 \text{ in./sec}$$
$$x_2 = 4.900 \text{ in.} \qquad \dot{x}_2 = 25.00 \text{ in./sec}$$

and that plasticity has not yet been encountered at any location. Suppose also that the driving forces at time t_0 are

$$f_1 = f_2 = 10.00 \text{ kips},$$

and that these forces decay linearly to zero at time $t_0 + 0.1$ sec. The complete process for determining inelastic behavior and executing one time step of Runge-Kutta integration is given below.

The Runge-Kutta constants for this example are those given in Eq. 9, and a time interval of $h = 0.02$ sec is used. These initial conditions and time interval have been chosen for illustrative purposes, and are not necessarily typical or optimum.

Because plasticity has not yet been reached, the restoring forces at time t_0 are given by Eq. 13,

$$Q_i = \sum_j k_{ij} x_j = \begin{bmatrix} 35.73 & -24.11 \\ -24.11 & 20.20 \end{bmatrix} \begin{bmatrix} 2.600 \\ 4.900 \end{bmatrix} = \begin{bmatrix} -25.24 \\ 36.29 \end{bmatrix} \text{ kips}$$

and the nondimensional moments at time t_0 are

$$\rho_k = \sum_j \lambda_{kj} x_j = \begin{bmatrix} 0.5194 & -0.4740 \\ 0.7222 & -0.5664 \\ -0.5987 & 0.2012 \\ -0.0833 & 0.2464 \end{bmatrix} \begin{bmatrix} 2.600 \\ 4.900 \end{bmatrix} = \begin{bmatrix} -0.9722 \\ -0.8976 \\ -0.5707 \\ 0.9908 \end{bmatrix}.$$

From Eqs. 11 and the initial conditions,

$$\dot{x}_1\ (t_0) = 10.00 \text{ in./sec}$$

$$\dot{x}_2\ (t_0) = 25.00 \text{ in./sec}$$

$$\dot{z}_1\ (t_0) = \frac{1}{0.07772}\ (10 + 25.24) = +453.4 \text{ in./sec}^2$$

$$\dot{z}_2\ (t_0) = \frac{1}{0.05181}\ (10 - 36.29) = -507.4 \text{ in./sec}^2$$

The first of Eqs. 6 yields

$$\kappa^x_{10} = h\ \dot{x}_1\ (t_0) = (0.02)(10.00) = 0.200 \text{ in.}$$

$$\kappa^x_{20} = h\ \dot{x}_2\ (t_0) = (0.02)(25.00) = 0.500 \text{ in.}$$

$$\kappa^z_{10} = h\ \dot{z}_1\ (t_0) = (0.02)(453.4) = 9.068 \text{ in./sec}$$

$$\kappa^z_{20} = h\ \dot{z}_2\ (t_0) = (0.02)(-507.4) = -10.148 \text{ in./sec}$$

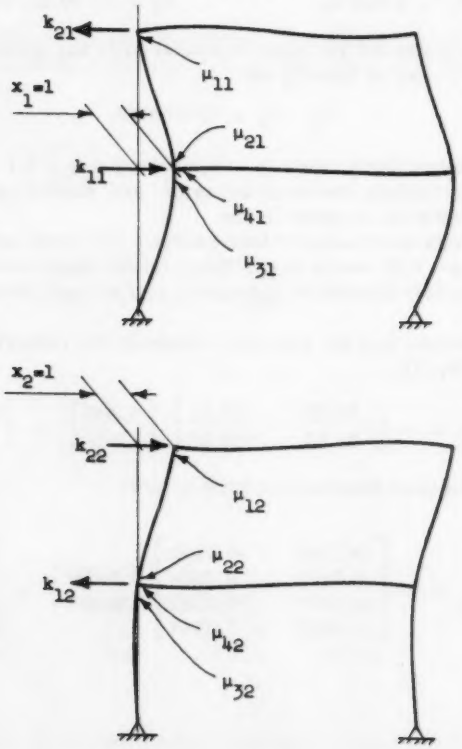

FIG. 6.—MATRIX ELEMENTS k_{ij} and μ_{kj}

The superscripts x and z identify the variable associated with κ. Before proceeding to the second of Eqs. 6, one must evaluate the functions $Q(x_i + \frac{1}{3}\kappa^x_{i0})$, which, in turn, require the evaluation of the $\Delta\psi$'s. The first terms in Eqs. 40 are

$$\sum_j \lambda_{kj}\,\Delta x_j = \sum_j \lambda_{kj}\left(\frac{1}{3}\,\kappa_{j0}\right)$$

$$= \frac{1}{3}\begin{bmatrix} 0.5194 & -0.4740 \\ 0.7222 & -0.5664 \\ -0.5987 & 0.2012 \\ -0.0833 & 0.2464 \end{bmatrix}\begin{bmatrix} 0.200 \\ 0.500 \end{bmatrix} = \begin{bmatrix} -0.0444 \\ -0.0462 \\ -0.0064 \\ 0.0355 \end{bmatrix}$$

The iteration of Eqs. 40 and 41 yields, for p = 1,

$$u_1^1 = -0.0444$$

$$\rho_1 + u_1^1 = -0.9722 - 0.0444 = -1.0166$$

$$\Delta\psi_1^1 = +0.0166$$

$$u_2^1 = -0.0462 + (0.3690)(0.0166) = -0.0401$$

$$\rho_2 + u_2^1 = -0.8976 - 0.0401 = -0.9377$$

$$\Delta\psi_2^1 = 0$$

$$u_3^1 = -0.0064 + (-0.1311)(0.0166) = -0.0086$$

$$\rho_3 + u_3^1 = -0.5707 - 0.0086 = -0.5793$$

$$\Delta\psi_3^1 = 0$$

$$u_4^1 = +0.0355 + (-0.1605)(0.0166) = +0.0328$$

$$\rho_4 + u_4^1 = 0.9908 + 0.0328 = 1.0236$$

$$\Delta\psi_4^1 = -0.0236$$

From Eq. 42,

$$e^1 = \sum_i \left| \Delta\psi_i^1 - \Delta\psi_i^0 \right| = 0.0402$$

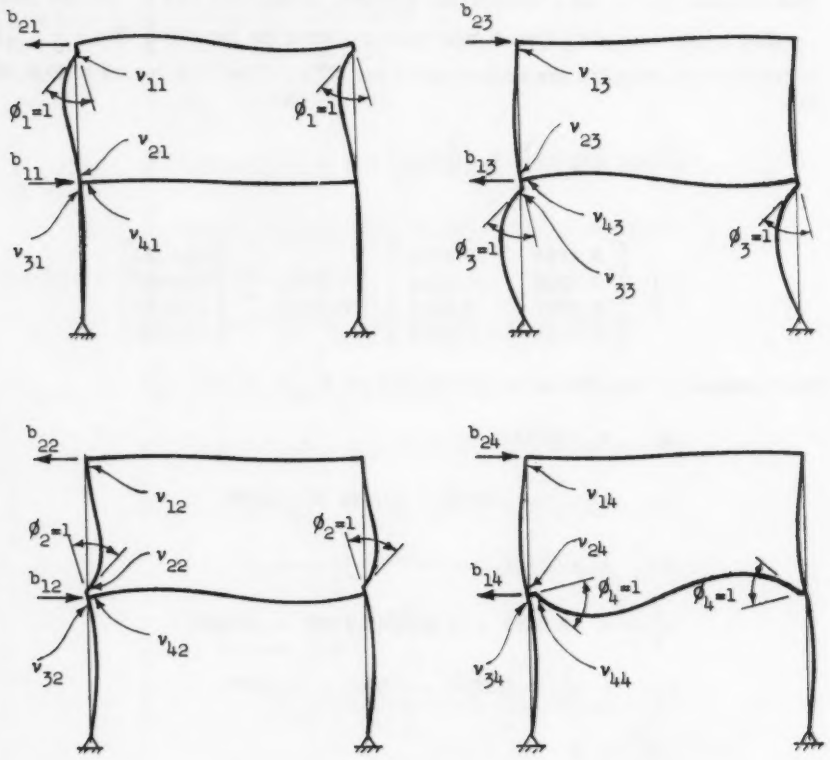

FIG. 7.—MATRIX ELEMENTS b_{il} and ν_{kl}

As the process is repeated, eP approaches zero and the iteration converges to

$$\Delta\psi_1 = 0.0109 \qquad \rho_1 + \Delta\rho_1 = -1.0000$$

$$\Delta\psi_2 = 0 \qquad \rho_2 + \Delta\rho_2 = -0.9201$$

$$\Delta\psi_3 = 0 \qquad \rho_3 + \Delta\rho_3 = -0.5617$$

$$\Delta\psi_4 = -0.0246 \qquad \rho_4 + \Delta\rho_4 = 1.0000$$

Eq. 36 then yields

$$\Delta Q_i = \sum_j k_{ij} \left(\frac{1}{3} \kappa^{x}_{j0} \right) + \sum_l \beta_{il} \Delta\psi_l$$

or

$$\Delta Q_1 = -1.15 \text{ kips}$$

$$\Delta Q_2 = 0.98 \text{ kips}$$

One can now return to the second of Eqs. 6 and compute

$$\kappa^{x}_{11} = 0.260 \text{ in.}$$

$$\kappa^{x}_{21} = 0.432 \text{ in.}$$

$$\kappa^{z}_{11} = 9.193 \text{ in./sec}$$

$$\kappa^{z}_{21} = -10.784 \text{ in./sec.}$$

Before going to the last of Eqs. 6 one must evaluate $Q\left(x_i + \frac{2}{3}\kappa^{x}_{i1}\right)$. Using Eqs. 36, 37, 40, 41, and 42 again, just as illustrated earlier, one gets

$$\Delta\psi_1 = 0.0080 \qquad \rho_1 + \Delta\rho_1 = -1.0000$$

$$\Delta\psi_2 = 0 \qquad \rho_2 + \Delta\rho_2 = -0.8958$$

$$\Delta\psi_3 = 0 \qquad \rho_3 + \Delta\rho_3 = -0.5861$$

$$\Delta\psi_4 = -0.0460 \qquad \rho_4 + \Delta\rho_4 = 1.0000$$

$$\Delta Q_1 = -0.21 \text{ kips}$$

$$\Delta Q_2 = 0.50 \text{ kips}$$

The last of Eqs. 6 is now executed, yielding

$$\kappa^{x}_{12} = 0.323 \text{ in.}$$

$$\kappa^{x}_{22} = 0.356 \text{ in.}$$

$$\kappa^{z}_{12} = 8.779 \text{ in./sec}$$

$$\kappa^{z}_{22} = -10.856 \text{ in./sec.}$$

Eq. 7 now yields the displacements and velocities for the end of the time step.

$$x_1 (t_0+h) = 2.892 \text{ in.}$$

$$x_2 (t_0+h) = 5.292 \text{ in.}$$

$$\dot{x}_1 (t_0+h) = 18.85 \text{ in./sec}$$

$$\dot{x}_2 (t_0+h) = 14.32 \text{ in./sec}$$

The terminal values of Q and ρ for this time step must now be computed from Eqs. 36, 37, 40, 41, and 42, as before. The results are

$$\Delta\psi_1 = 0 \qquad \rho_1\ (t_0+h) = -0.9916$$

$$\Delta\psi_2 = 0 \qquad \rho_2\ (t_0+h) = -0.8584$$

$$\Delta\psi_3 = 0 \qquad \rho_3\ (t_0+h) = -0.6236$$

$$\Delta\psi_4 = -0.0630 \qquad \rho_4\ (t_0+h) = 1.0000$$

$$Q_1\ (t_0+h) = -23.83 \text{ kips}$$

$$Q_2\ (t_0+h) = 35.91 \text{ kips}$$

One now advances to the next time step, taking these terminal values as the initial values for the next step.

APPLICATION

The multi-degree elasto-plastic response problem has been programmed for solution on an IBM Type 650 computer at the University of Michigan. Both the Milne Predictor-Corrector Method and the Runge-Kutta Method have been used. The programs were written for the basic IBM 650, without index registers, automatic address modification, or floating point hardware. If the programs were to be rewritten today, they could be simplified a great deal by taking advantage of these improvements.

The 2,000-word memory was able to accommodate a system with as many as 16 degrees of freedom and 16 plastic hinges using the Milne method, and with the Runge-Kutta method the system could go to 12 degrees of freedom and 16 plastic hinges. The more severe limitation for Runge-Kutta occurred partly because viscous damping and a form of inelastic deformation not considered in this paper were taken into account in that program.

The four matrices, k_{ij}, $\beta_{i\ell}$, λ_{kj}, and $\sigma_{k\ell}$, were stored in the memory initially as part of the data for the main program. A separate program was written to evaluate all of these matrices. Input for the matrix evaluation program comprised the number of stories, number of bays, story weights, member stiffnesses, plastic hinge locations, and plastic hinge moments. Acting on this information, the machine wrote the slope deflection equations, solved them by iteration, evaluated the matrix elements, and printed the matrices on load cards ready for use with the main program.

For the matrices $\beta_{i\ell}$, λ_{kj} and $\sigma_{k\ell}$, one need consider only those locations at which plastic hinges form during the response. There is no need to calculate or record the moments at locations that remain elastic. Thus the limitation of 16 plastic hinges is not as severe as it might seem. Intuition and experience with smaller systems may enable one to predict which locations are most likely to become plastic during the response. The unlikely locations can be omitted from the matrices. One can process the output data after the run is complete to check whether or not all of the unrecorded locations did, in fact, remain elastic.

The programs were applied to the problems of structural response to blast and earthquake. In each case the driving forces were put in punched cards which were read by the computer as the solution progressed. For the blast problem, the equations governing the dynamic pressures were given to the machine in a separate program and the machine calculated the driving forces and converted them to punched cards ready for input for the main program. For the earthquake problem, recorded accelerograms were approximated by piecewise linear functions, and the time-acceleration coordinates of the intersection points of successive line segments were put in punched card form. The machine accepted this input data and interpolated where necessary to find the desired driving forces.

CONCLUSIONS

Experience with both the blast and earthquake problems shows that the methods of analysis presented herein are practical and can be carried out on equipment that exists today. Tomorrow's equipment, or even a late version of today's equipment, greatly facilitates programming and permits many of the restrictions to be relaxed.

ACKNOWLEDGMENT

This paper is based in part upon research conducted for the University of Michigan Research Institute under contract with Air Force Special Weapons Center, Albuquerque, N. M., and in part upon research conducted by the senior author for his doctoral dissertation at the University of Michigan under a doctoral committee of which Bruce G. Johnston was chairman. Computation was performed at the Statistical and Computation Laboratory of the University of Michigan. The authors wish especially to thank Bruce Arden and Mrs. Sarah Brando, of the Computation Laboratory staff, for their unlimited cooperation.

NOTATION

Symbols are defined where they first appear in the text. Those used frequently are summarized here for reference.

$b_{i\ell}$ = rotation-force coefficient;

c_{ij} = damping coefficient;

D_i = damping force;

f_i = driving force;

h = time interval in numerical integration;

i, j = subscripts associated with mass or force;

k, ℓ = subscripts associated with bending moment or plastic hinge;

k_{ij} = stiffness coefficient;

ℓ, m, n, p, q, r = constants in Runge-Kutta method of integration;

m_i = mass;

M_k = bending moment;

P_k = plastic hinge moment;

Q_i = restoring force;

R_i = resistance force;

x_i = displacement;

$\beta_{i\ell}$ = rotation-force coefficient (with dimensionless moments);

δ_{kl} = Kronecker delta;

λ_{kj} = displacement - moment coefficient (dimensionless moments);

μ_{kj} = displacement - moment coefficient;

$\nu_{k\ell}$ = rotation - moment coefficient;

ρ_k = dimensionless bending moment; and

$\sigma_{k\ell}$ = rotation - moment coefficient (dimensionless moments);

ϕ_k = plastic hinge rotation; and

ψ_k = plastic hinge rotation (with dimensionless bending moment).

Journal of the
ENGINEERING MECHANICS DIVISION
Proceedings of the American Society of Civil Engineers

BEHAVIOR OF BUCKLED RECTANGULAR PLATES[a]

By Manuel Stein[1]

SYNOPSIS

A review is presented of recent work done by the writer on the post-buckling of rectangular plates. Theoretical and experimental results which indicate possible changes in buckle pattern are given for simply supported plates in longitudinal compression. Results of a separate analysis of the phenomenon of change in buckle pattern are presented and interpreted. A detailed analysis is presented of the stiffness in shear of a plate buckled in compression.

INTRODUCTION

Unlike simple columns, rectangular plates which are supported on all edges may carry considerable load beyond their buckling load. Under some conditions it may be advantageous to utilize this additional load-carrying

Note.—Discussion open until September 1, 1960. To extend the closing date one month, a written request must be filed with the Executive Secretary, ASCE. This paper is part of the copyrighted Journal of the Engineering Mechanics Division, Proceedings of the American Society of Civil Engineers, Vol. 86, No. EM 2, April, 1960.

[a] Part of the information presented herein was included in a dissertation offered in partial fulfillment of the requirements for the degree of Doctor of Philosophy in Applied Mechanics, Virginia Polytechnic Inst., Blacksburg, Va., June, 1958.

[1] Aeronautical Research Engr., Structures Research Div., Natl. Aeronautics and Space Admin., Langley Field, Va.

capacity. This paper will present a review of the results of several years' work by the writer on the post-buckling behavior of rectangular plates.

In discussing the post-buckling behavior of plates the basic equations will be presented and the method of solution will be indicated. For the problem of a simply supported rectangular plate subject to longitudinal compression, theoretical load-shortening curves will be presented which indicate possible changes in buckle pattern. Results will be presented of a separate study of change in buckle pattern. Comparisons will then be drawn between the results of the plate problem and other theoretical results and with experiment. Inasmuch as the details of these analyses are available elsewhere,[2,3] they will be omitted herein. Finally, a discussion is presented of the stiffness in shear of an infinitely long, simply supported plate already buckled by longitudinal compressive loads. The details of this analysis are presented in the Appendix.

BASIC EQUATIONS AND METHOD OF SOLUTION

T. von Karman has presented the basic nonlinear differential equations for a plate undergoing large deflections. For a plate with no lateral load the basic equations may be written:

$$\left.\begin{aligned} &N_{x,x} + N_{xy,y} = 0 \\ &N_{y,y} + N_{xy,x} = 0 \\ &D\,\nabla^4 w - \left(N_x\, w_{,xx} + N_y\, w_{,yy} + 2\, N_{xy}\, w_{,xy}\right) = 0 \end{aligned}\right\} \quad \ldots\ldots \quad (1)$$

where N_x, N_y, N_{xy} are the resultant forces, w is the lateral deflection, D denotes the plate stiffness $\left[D = \frac{E\,h^3}{12(1 - \mu^2)}\right]$, E is Young's modulus, h represents plate thickness, μ is Poisson ratio,

$$\nabla^4 = \frac{\partial^4}{\partial x^4} + 2\,\frac{\partial^4}{\partial x^2\,\partial y^2} + \frac{\partial^4}{\partial y^4}$$

and x and y when they appear as a subscript following a comma indicate partial differentiation of the main symbol with respect to x and y. Only plates without initial eccentricities subject to in-plane loading are considered. Hooke's law expresses stress in terms of strain for an elastic body. By proper substitution in Hooke's law for a plate the forces can be expressed in terms of displacements as follows:

$$\left.\begin{aligned} N_x &= \frac{E\,h}{1 - \mu^2}\left[u_{,x} + \frac{1}{2}\,w_{,x}^2 + \mu\left(v_{,y} + \frac{1}{2}\,w_{,y}^2\right)\right] \\ N_y &= \frac{E\,h}{1 - \mu^2}\left[v_{,y} + \frac{1}{2}\,w_{,y}^2 + \mu\left(u_{,x} + \frac{1}{2}\,w_{,x}^2\right)\right] \\ N_{xy} &= \frac{E\,h}{2(1 + \mu)}\left(u_{,y} + v_{,x} + w_{,x} w_{,y}\right) \end{aligned}\right\} \quad \ldots\ldots \quad (2)$$

---

[2] "Loads and Deformations of Buckled Rectangular Plates," by Manuel Stein, NASA Technical Report, R40, 1959.

[3] "The Phenomenon of Change in Buckle Pattern in Elastic Structures," by Manuel Stein, NASA Technical Report, R39, 1959.

where u and v are the displacements in the x and y directions, respectively.

Eqs. 1 and 2 together with a complete set of boundary equations determine the problem. Notice that, if the N's from Eq. 2 are substituted into Eqs. 1, the resulting three equations in the three unknowns u, v, and w are nonlinear. All the previous studies of this type[4-15] used either energy methods or Fourier series expansions of these basic equations, except for one study[15] that made use of successive approximations. The present work, however, makes use of a perturbation method whereby[2] the nonlinear equations are converted into a set of linear equations by assuming that u, v, and w may be expanded in a power series in terms of an arbitrary parameter ϵ. For the present purposes u, v, and w are to be expanded about the point of buckling (at buckling $\epsilon = 0$):

$$\left.\begin{aligned} u &= \sum_{n=0,2}^{\infty} u^{(n)} \epsilon^n \\ v &= \sum_{n=0,2}^{\infty} v^{(n)} \epsilon^n \\ w &= \sum_{n=1,3}^{\infty} w^{(n)} \epsilon^n \end{aligned}\right\} \quad \ldots\ldots\ldots\ldots\ldots \quad (3)$$

If Eqs. 2 and 3 are substituted into Eq. 1, equating power of ϵ leads to an infinite set of linear equations. The ones corresponding to the zeroeth and

4 "The Strength of Thin Plates in Compression," by Theodor von Karman, Ernest E. Sechler and L. H. Donnell, Transactions, ASME, AMP-54-5, Vol. 54, No. 2, January 30, 1932, pp. 53-57.

5 "The Buckling of Thin Plates in Compression," by H. L. Cox, R and M No. 1554, British A. R. C., 1933.

6 "Theory of Elastic Stability," by S. Timoshenko, McGraw-Hill Book Co., Inc., 1936, pp. 390-395.

7 "Uber die Tragfahigkeit eines langsbel Plattenstreifens nach Uberschreiten der Beullast," by K. Marguerre and E. Tefftz, Z. f. a. M. M., Bd. 17, Heft 2, April, 1937, pp. 85-100.

8 "Apparent Width of the Plate in Compression," by Karl Marguerre, NACA, TM 833, 1937.

9 "Behavior of a Plate Strip Under Shear and Compressive Stresses Beyond the Buckling Limit," by A. Kromm and K. Marguerre, NACA, TM 870, 1938.

10 "Bending of Rectangular Plates With Large Deifections," NACA, Report 737, 1942.

11 "De meedragende breedte bij groote overschrijding ker knikspanning voor verschillende inklemming der plaatranden," by W. T. Koiter, Report S. 287, National Luchtvaartlaboratorium, Amsterdam, December, 1943.

12 "Effect of Small Deviations from Flatness on Effective Width and Buckling of Plates in Compression," by Pai C. Hu, Eugene E. Lundquist and S. B. Batdorf, NACA, TN 1124, 1946.

13 "Large Deflection Theory for Plates with Small Initial Curvature Loaded in Edge Compression," by J. M. Coan, Journal of Applied Mechanics, Vol. 18, No. 2, June, 1951, pp. 143-151.

14 "Analysis of Behavior of Simply Supported Flat Plates Compressed Beyond the Buckling Load into the Plastic Range," by J. Mayers and Bernard Budiansky, NACA, TN 3368, February, 1955.

15 "A Postcritical Study of Flexible Elastic Plates," by S. A. Alexeev, U.S.S.R., Vol. XX, No. 6, November-December, 1956, pp. 673-679.

first powers of ϵ can be identified as the usual small-deflection equations. The ones corresponding to the second and third powers of ϵ introduce a first approximation to the post-buckling behavior of plates. Solutions of additional equations give a second approximation and then higher approximations. The advantages of the present method are greater accuracy and simpler application.

COMPRESSION PROBLEM

Theoretical Solution.—The post-buckling behavior of simply supported rectangular plates in end compression (the edges are constrained to remain straight) is investigated in detail by solving the first few of the equations. Nondimensional load-shortening curves presenting some of the results of this problem are shown for plates of various length-width ratio in Figs. 1 to 5. For plates of finite length-to-width ratio the curves are also labeled according to m, the number of buckles along the length. Curves are presented which were obtained by using the values of m corresponding to the lowest buckling load. In addition, load-shortening curves are given for other values of m which intersect with these basic curves for the range plotted.

Change in Buckle Pattern.—The intersections of the load-shortening curves indicate possible changes in buckle pattern. In order to discuss the phenomenon of change in buckle pattern on a sound theoretical basis, a simple model was chosen, as shown in Fig. 6, which has the important properties of plates and for which an exact solution could be obtained. This model, which has been analyzed[3] is a simply supported three-element column connected by linear torsional springs and supported laterally by nonlinear extensional springs (the nonlinear springs represent plate membrane stiffness). Each of three elements are of length l, the spring constants are C for the linear torsional springs, and K and K_1 for the nonlinear extensional springs, and this column is subject either to a load or to a shortening.

As shown in the Fig. 7, this idealized structure duplicates the important property of plates in that there is an intersection of the load-shortening curve of one mode (say the symmetric mode which corresponds to the lower buckling load) with the load-shortening curve of another mode (antisymmetric). The analysis also yields a transition curve (which represents a buckle pattern which is neither symmetric nor antisymmetric) from the symmetric to the antisymmetric buckling configuration. Change in buckle pattern starts to occur at a loading corresponding to the intersection of the load-shortening curve for the symmetric buckle pattern and the transition curve. The load at which the first change in buckle pattern starts to occur is called the secondary buckling load. Whether the transition curve is stable is shown to depend on the stiffness of the nonlinear springs and upon the method of loading (controlled load, controlled shortening) which is shown by comparing Figs. 7 and 8. However, the load (and shortening) at which the buckle pattern starts to change (secondary buckling) is independent of the method of loading. Secondary buckling always occurred for loads and shortenings greater than those given by the intersection of the load-shortening curves for the symmetric and antisymmetric equilibrium configurations.

Stability occurs as one might expect intuitively. For example, for controlled load, if the transition path from the curve for symmetric buckling to that for antisymmetric buckling indicates increasing load, then the transition

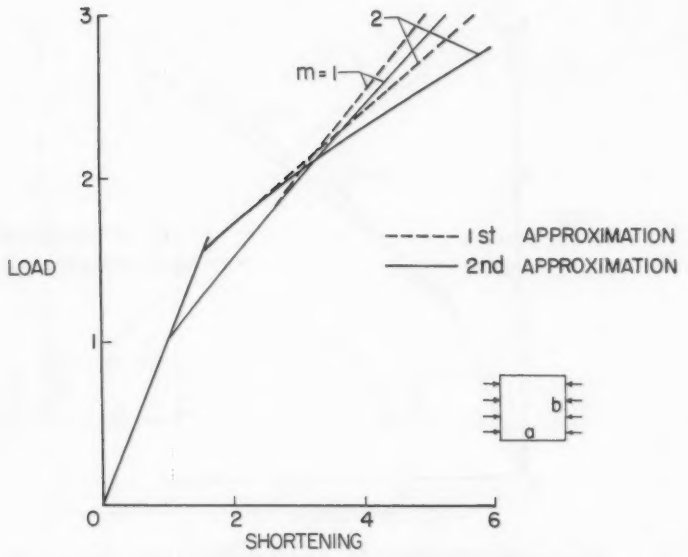

FIG. 1.—NONDIMENSIONAL LOAD-SHORTENING CURVES OF RECTANGULAR SIMPLY SUPPORTED PLATES IN COMPRESSION. a/b = 1.

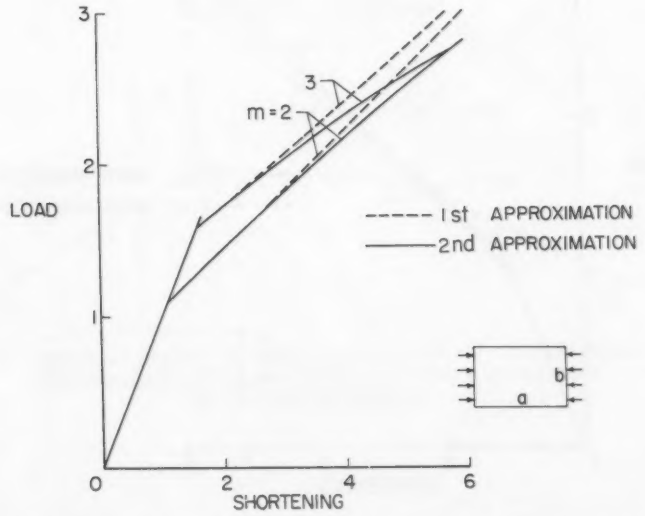

FIG. 2.—NONDIMENSIONAL LOAD-SHORTENING CURVES OF RECTANGULAR SIMPLY SUPPORTED PLATES IN COMPRESSION. a/b = 1.5.

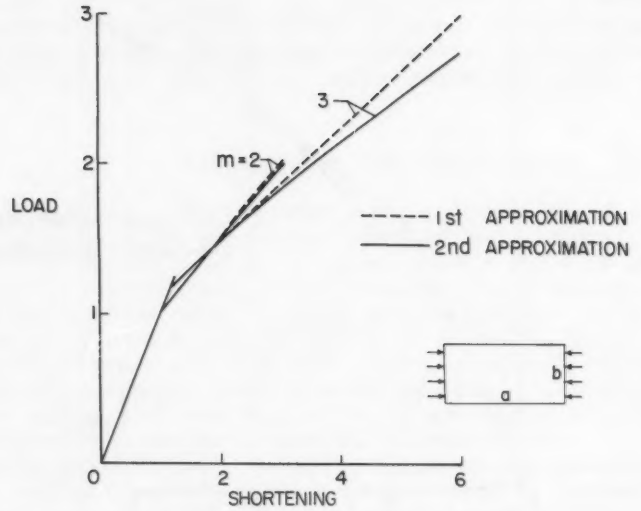

FIG. 3.—NONDIMENSIONAL LOAD-SHORTENING CURVES OF RECTANGULAR SIMPLY SUPPORTED PLATES IN COMPRESSION. a/b = 2.

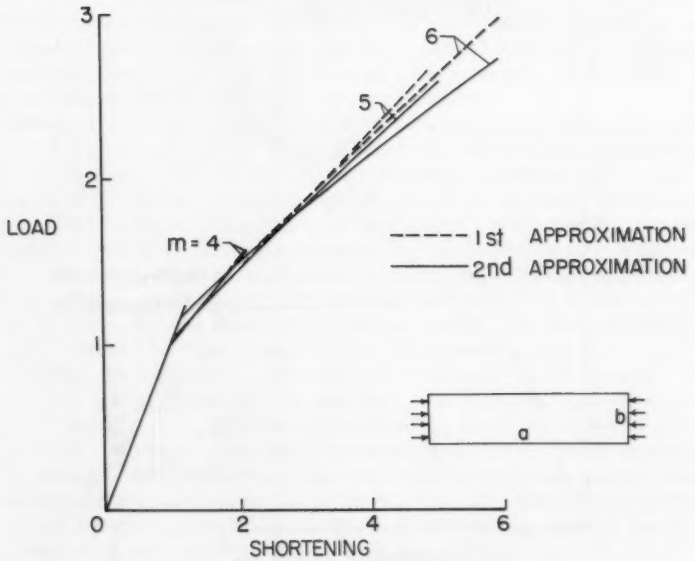

FIG. 4.—NONDIMENSIONAL LOAD-SHORTENING CURVES OF RECTANGULAR SIMPLY SUPPORTED PLATES IN COMPRESSION. a/b = 4.

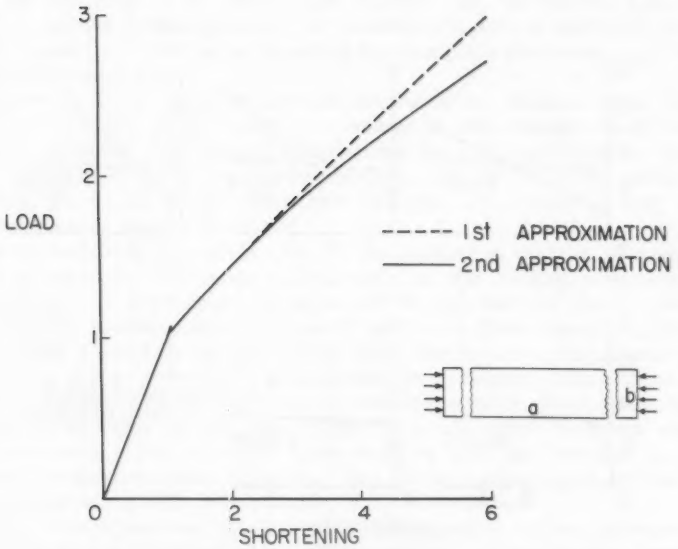

FIG. 5.—NONDIMENSIONAL LOAD-SHORTENING CURVES OF INFINITELY LONG SIMPLE SUPPORTED PLATES IN COMPRESSION.

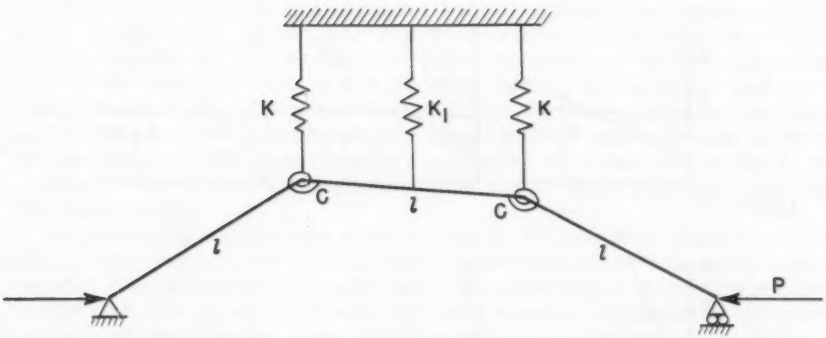

FIG. 6.—THREE-ELEMENT COLUMN CONNECTED BY LINEAR TORSIONAL SPRINGS AND LATERALLY RESTRAINED BY NONLINEAR EXTENSIONAL SPRINGS.

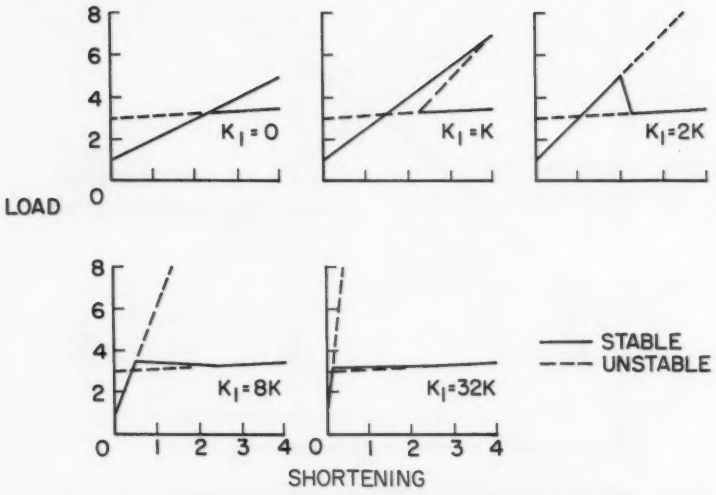

FIG. 7.—NONDIMENSIONAL LOAD-SHORTENING CURVES FOR THE THREE ELEMENT COLUMN. CONTROLLED SHORTENING.

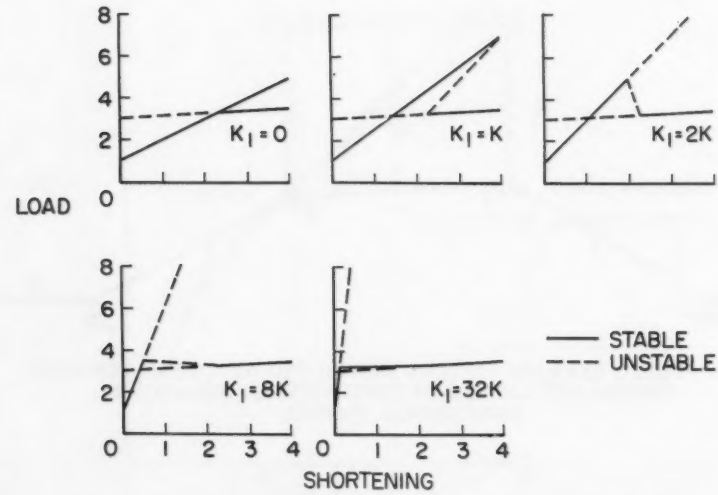

FIG. 8.—NONDIMENSIONAL LOAD-SHORTENING CURVES FOR THE THREE ELEMENT COLUMN. CONTROLLED LOAD.

path is stable; otherwise, the transition path is unstable. In order to determine the stability of an equilibrium position for the column problem in a rigorous fashion it was necessary to examine the second variation of the total potential energy. It would be expected that for plate problems, stability could be decided intuitively.

Changes in buckle patterns are not calculated for plates of finite length-to-width ratio for the present analysis because of the extensive calculations required. However, preliminary calculations have indicated that for length-to-width ratios near unity the change in buckle pattern would be rather abrupt; whereas, for higher length-width ratios, changes in buckle pattern would be continuous or at least less abrupt.

For an infinitely long plate (Fig. 5) the number of buckles along the length would be expected to change continuously as the loading progresses. The buckle length for a given shortening would be such that the load is a minimum. Note that the results giving the lowest load for a given shortening for length-width ratios 2 and 4 do not differ much from the infinite-plate results. Indeed, the infinite-plate curves form an envelope for the finite-plate curves.

Comparisons with other theory.—For the square plate buckling into a square buckle both Samuel Levy[10] and S. A. Alexeev[15] obtained essentially exact solutions. For a square plate buckling into two buckles (m = 2) only Alexeev obtained an exact solution. The present results for the second approximation agree with the results of Levy and Alexeev.

For plates of various other finite length-to-width ratios, previous results are available for the initial slope after buckling. As can be seen from Figs. 1 to 4, for some length-to-width ratios used, straight-line load-shortening curves based on these initial slopes would give unduly higher loads for given shortenings everywhere in the post-buckling range except immediately after buckling.

The best available previous results for the infinitely long plates are those of W. T. Koiter.[11] As shown in Fig. 9, the results of the solution of Koiter and the solution of Karl Marguerre[8] follow the curve of the first approximation in the lower part of the post-buckling range. In the upper part of the range Marguerre's solution continues to follow the first approximation whereas Koiter's solution deviates slightly from the first approximation in the direction of the second approximation as shown by the dotted line in Fig. 9. The results of the second approximation give lower, more accurate loads than previous results.

Experimental Results and Comparisons of Theory With Experiment.—To obtain simply supported loaded edges is impractical in laboratory experiments. The experimental results were therefore obtained for panels subject to flat end loading which results in almost complete clamping of the loaded edges. However, if the panel tested is long compared with its width (say of length-to-width ratio 4 or greater), the size and shape of the buckles near the center are almost unaffected by this clamping. The experimental results which are compared with theory are for panels that have a length-to-width ratio of at least 4. Hence at least certain of the experimental values obtained should be directly comparable to the simply supported theoretical results. As stated previously, the theoretical results for length-to-width ratios 2 and 4 are not very different from the results for the infinite plate. Thus the experimental results may be compared to the theoretical results for the infinite plate. Such comparisons are shown in some of the following figures. Data are

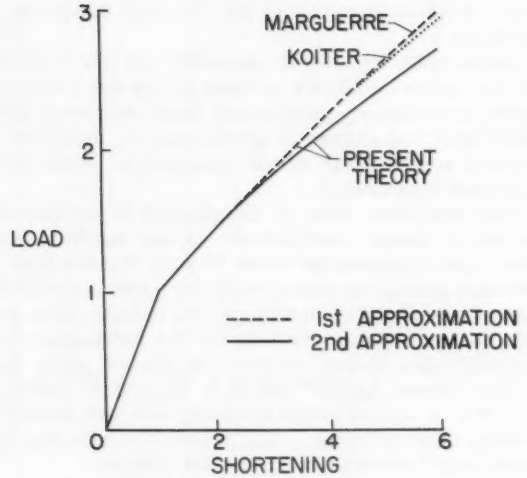

FIG. 9.—COMPARISONS OF THEORETICAL LOAD-SHORTENING CURVES FOR AN INFINITELY LONG SIMPLY SUPPORTED PLATE IN LOGITUDINAL COMPRESSION.

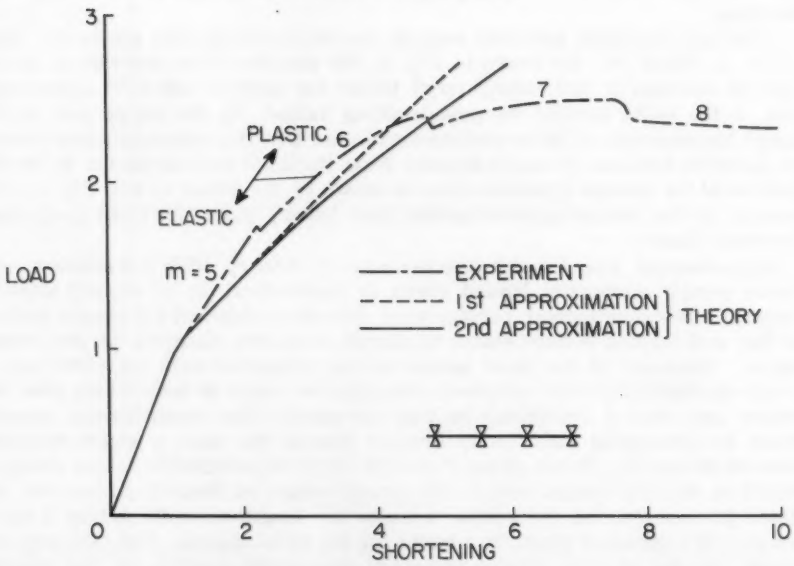

FIG. 10.—COMPARISONS OF LOAD-SHORTENING CURVES AS GIVEN BY (ELASTIC) THEORY AND EXPERIMENT.

presented from three different types of test specimens. In all of the specimens the loaded edges were ground flat and perpendicular to the longitudinal axis of the specimen. They were compressed "flat ended" between the platens of the 1,200,000-lb capacity hydraulic testing machine at the Langley structures research laboratory, which applies load through the use of a hydraulic ram.

Plate Supported by Multiple-Bay Fixture.—In the first test discussed, an attempt was made, by using a fixture having lubricated knife edges free to rotate, to provide the edge conditions usually specified by theory along the unloaded edges of each panel: simply supported straight edges free of in-plane shear.

A comparison with theory is presented in Fig. 10 of the experimental load-shortening curve for this test. The experimental curve shows abrupt changes corresponding to abrupt changes in buckle pattern from 5 to 6 to 7 to 8 buckles while the theoretical curve, which is based on continuous change in buckle pattern, is smooth.

Also shown is the load $\frac{P\,b}{4\,\pi^2\,D} \approx 2$ when strain gages at the crest of a buckle indicated the plate material had been strained into the plastic range. The type of changes of buckle pattern obtained here with a hydraulic-type testing machine is similar to that described in a previous section for a controlled-shortening type of loading. In consideration of the practical difficulties of measuring total shortening, such as how to account for the bending of the testing machine platens, the present agreement between experiment and theory is good.

Bending strains at the crest of a buckle for the same test are plotted against load and compared to the present theoretical results in Fig. 11. Again the abrupt changes in the experimental results do not appear in the theoretical results. The agreement between theory and experiment is good.

Z-Stiffened Panels.—Data on four Z-stiffened panels similar to those used in aircraft-wing construction were obtained in the range from zero strain up to several times the buckling strain. These Z-stiffened panels were part of a large group of panels.[16]

In Fig. 12 the experimentally measured strains at the crest of the buckle are plotted against stiffener strain and compared to the present theory. From the comparison of the results shown, it is evident that, although there is scatter at buckling, the theory for simply supported plates gives strains at the crest of the buckle that agree with practical experiment in the post-buckling range.

Hat-Section Stiffened Panels.—In Fig. 13 buckle depths measured from a series of tests at Langley on panels with hat-section stiffeners are plotted against stiffener strain and are compared to theory. There is a considerable scatter in experimental results. However, it may be stated that in the post-buckling range, theoretical results for the depth of buckle of simply supported plates agree with experimental results on such practical stiffened panels.

SHEAR STIFFNESS OF A BUCKLED PLATE

An extension of the compression problem is presented which treats the problem of the stiffness in shear of a rectangular plate that has been buckled

16 "Compressive Strength of Flat Panels with Z and Hat-Section Stiffeners," by Joseph N. Kotanchik, Robert A. Weinberger, George W. Zender and John Neff, Jr., NACA, Wartime Report L62, 1944.

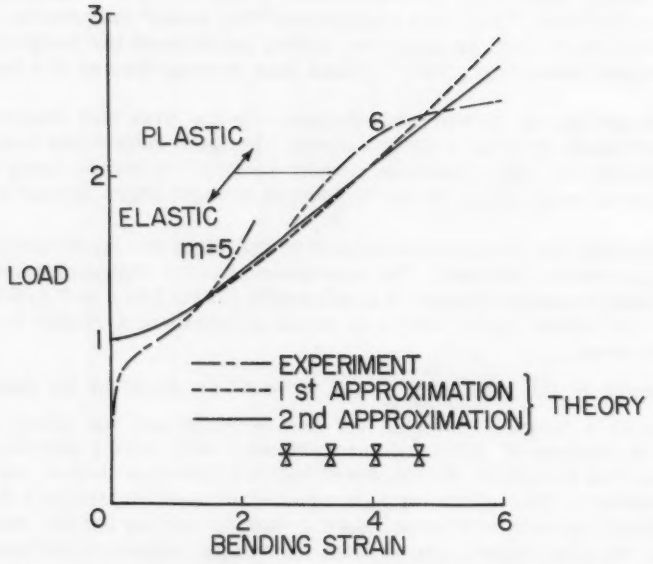

FIG. 11.—COMPARISONS OF BENDING STRAIN AT THE CREST OF A BUCKLE AS GIVEN BY (ELASTIC) THEORY AND EXPERIMENT. ($\mu = 1/3$.)

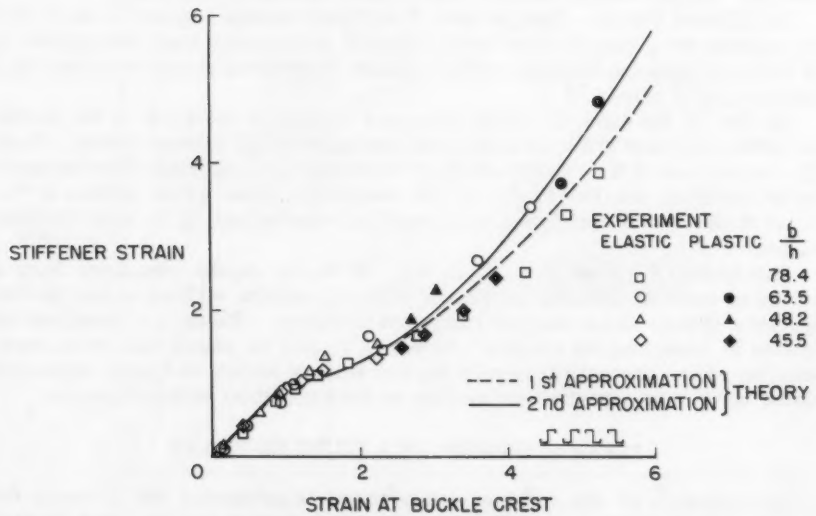

FIG. 12.—COMPARISONS OF EXTREME FIBER STRAIN AT THE CREST OF A BUCKLE AS GIVEN BY (ELASTIC THEORY AND EXPERIMENT. ($\mu = 1/3$.)

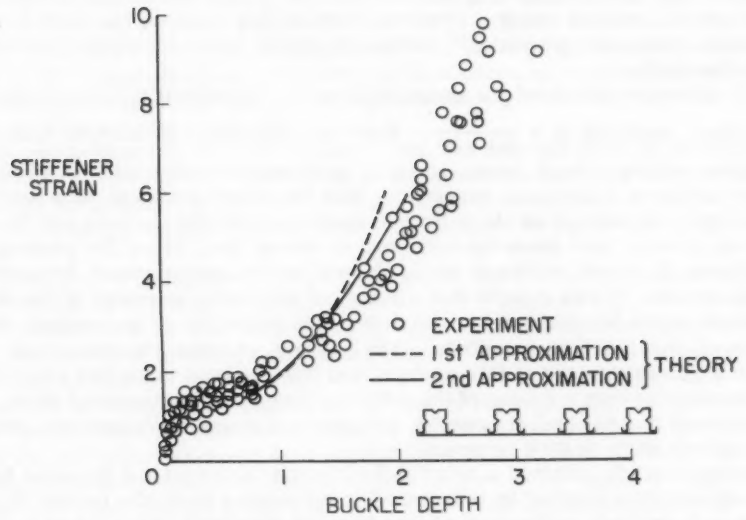

FIG. 13.—COMPARISONS OF BUCKLE DEPTH AS GIVEN BY THEORY AND EXPERIMENT. ($\mu = 1/3$.)

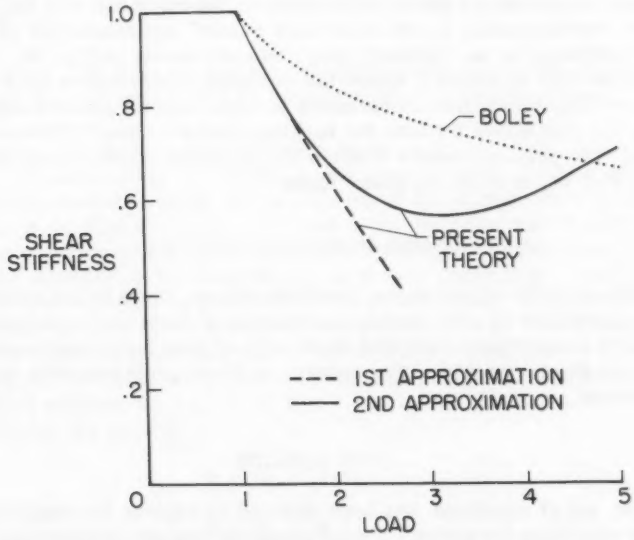

FIG. 14.—COMPARISONS OF NONDIMENSIONAL SHEAR STIFFNESS CURVES FOR AN INFINITELY LONG SIMPLE SUPPORTED PLATE BUCKLED IN LONGITUDINAL COMPRESSION. ($\mu = 1/3$.)

by longitudinal compressive loads. This problem is important in the stress analysis and in the general instability studies of thin-walled structures that have already buckled locally. Previous work on this problem has been done by Bruno A. Boley who presented[17] estimated curves based mainly on theoretical considerations.

If a plate is unbuckled its shear stiffness can be identified immediately as the shear modulus $G = \frac{E}{2(1+\mu)}$. However, if a plate is buckled it is in a rather complex state of stress, and it is necessary to define what is meant by shear stiffness. It seems reasonable that the shear stiffness of a buckled plate could be defined by the ratio of a given applied shear stress and the resulting average unit shearing deformation except that, since the problem is nonlinear, the shear stiffness would depend on the magnitude of the applied shear stress. It was thought that a practical and useful measure of the shear stiffness might be obtained by restricting consideration to an applied shear stress of infinitesimal magnitude. The present analysis considers only the shear stiffness obtained in this manner, and this analysis is further restricted by considering only the case of the infinitely long, simply supported plate. It is expected that the present results will apply to practical rectangular panels of length-to-width ratio 4 or greater.

Having already obtained a solution for the displacement and stresses for a rectangular plate buckled by longitudinal compressive loads the method of solution is to go back to the original von Karman equations (Eqs. 1) and to suppose an initial state of stress and deflection given by the compression solution and to require an additional state of stress and deflection corresponding to a small uniform in-plane shear loading at the edges. Since the additional shear load is considered small (infinitesimal) the equations may be linearized. Solutions corresponding to the first and second approximation of the compression problem for an infinitely long plate are shown in Fig. 14. These solutions show that at about 3 times the buckling compressive load the shear stiffness of the infinite panel decreases to about half its shear stiffness (G) at buckling, but that above 3 times the buckling load the shear stiffness begins to increase. The present results differ with the recommended curve of Boley as shown in Fig. 14, at least for lower loads.

OTHER PROBLEMS SOLVED

In addition to the compression problem solved, there is available[2] the solution by the writer of post-buckling problems of rectangular plates subjected to a uniform temperature rise with three sets of boundary conditions restricting in-plane displacements. The results of these problems will not be discussed herein.

CONCLUSIONS

A linear set of equations has been derived to replace the nonlinear large-deflection equations for plates. The advantage of this set of equations is that it provides a way to obtain accurate results in simple form. The linear equations are subject to the limitation that they cannot be used to solve post-buckling problems for plates with initial eccentricities.

---

17 "The Shearing Rigidity of Buckled Sheet Panels," by Bruno A. Boley, Journal of Aeronautical Science, June, 1950.

For the compression problem, the second approximation of the present theory agrees with exact results for the square plate. Results for plates with finite, as well as infinite, length-to-width ratio indicate that the effects of change in buckle pattern must be considered. For an infinite plate, results obtained in first approximation agree with the best previous results for much of the range, but results for the second approximation give lower and more accurate loads for given shortenings.

The comparisons made here indicate that, for extreme fiber strains and deflections at the crest of a buckle, the present theoretical results for simply supported rectangular plates with straight edges free of shear agree well in the post-buckling range with experimental results on practical stiffened panels.

The results of an analysis of a simple model have been presented, indicating the action of change in buckle pattern for two types of loading. The results indicate that intersections between curves for the various equilibrium configurations lead to change in buckle pattern. The load at which change in buckle pattern occurs is shown to be independent of the type of loading, but the manner of change does depend on the type of loading. Further computations similar to those done for the simple model are necessary to give precisely the secondary buckling load and the transition loading paths for finite rectangular simply supported plates subject to the various types of longitudinal compressive loadings (controlled load, controlled shortening, etc.).

The shear stiffness of an infinite plate buckled by longitudinal compressive load has been investigated in detail indicating that the effective shear stiffness decreases to almost half the shear modulus at 3 times the buckling load, but increases again to about three-quarters the shear modulus at 5 times the buckling load.

APPENDIX.—IN-PLANE SHEAR STIFFNESS OF AN INFINITELY LONG PLATE BUCKLED IN LONGITUDINAL COMPRESSION

An infinitely long plate is considered to be in an initial state of stress and deformation corresponding to a given compression load. Such a state of stress and deformation is given by the solution of the compression problem.[2] The problem is to find the shear stiffness from the additional stresses and deformations corresponding to a small, uniformly applied shearing force at the edge. By considering the shearing force η to be a small perturbation, the equations for the additional stresses and deformation may be made linear by neglecting squares and higher powers of the perturbations. The linear equations obtained in this manner are solved by the Galerkin method.

Equations for the Additional Stresses and Deformations.—Assume that we have the initial solution u_0, v_0, w_0 of Eqs. 1 and let the desired additional solutions be u_1, v_1, w_1 so that

$$\left.\begin{aligned} u &= u_0 + \eta\, u_1 \\ v &= v_0 + \eta\, v_1 \\ w &= w_0 + \eta\, w_1 \end{aligned}\right\} \quad \ldots\ldots\ldots\ldots\ldots \quad (4)$$

Thus

$$\left.\begin{aligned} N_x &= N_{x_0} + \eta\, N_{x_1} \\ N_y &= N_{y_0} + \eta\, N_{y_1} \\ N_{xy} &= N_{xy_0} + \eta\, N_{xy_1} \end{aligned}\right\} \quad \ldots\ldots\ldots\ldots\ldots \quad (5)$$

where the N's with zero subscripts are given by Eqs. 2 if u, v, w in Eqs. 2 are replaced by u_0, v_0, w_0. The N_1's are found to be (neglecting terms in η^2):

$$\left.\begin{aligned} N_{x_1} &= \frac{E\,h}{1 - \mu^2}\left[u_{1,x} + w_{0,x}w_{1,x} + \mu\left(v_{1,y} + w_{0,y}w_{1,y}\right)\right] \\ N_{y_1} &= \frac{E\,h}{1 - \mu^2}\left[v_{1,y} + w_{0,y}w_{1,y} + \mu\left(u_{1,x} + w_{0,x}w_{1,x}\right)\right] \\ N_{xy_1} &= \frac{E\,h}{2(1 + \mu)}\left(u_{1,y} + v_{1,x} + w_{0,x}w_{1,y} + w_{1,x}w_{0,y}\right) \end{aligned}\right\} \quad (6)$$

The zero subscript terms already satisfy Eq. 1; thus there remain the following relations to be satisfied, which were formed by substitution of Eqs. 4 and 5 into Eq. 1 (again neglecting η^2 terms):

$$\left.\begin{aligned} &N_{x_{1,x}} + N_{xy_{1,y}} = 0 \\ &N_{y_{1,y}} + N_{xy_{1,x}} = 0 \\ &D\,\nabla^4 w_1 - \left(N_{x_0} w_{1,xx} + N_{y_0} w_{1,yy} + 2N_{xy_0} w_{1,xy}\right. \\ &\left. + N_{x_1} w_{0,xx} + N_{y_1} w_{0,yy} + 2N_{xy_1} w_{0,xy}\right) = 0 \end{aligned}\right\} \quad \ldots\ldots \quad (7)$$

Eqs. 6 and 7 together with the initial values of the stresses and displacements and the boundary conditions determine the problem.

Boundary Conditions.—The boundary conditions considered are the same as those considered for the compression problem except for the provision of the uniform shearing force η present at all edges. The origin of coordinate is taken along the lower edge of an infinite plate of width b. Zero deflection

$$w(x,0) = w(x,b) = 0 \ldots\ldots\ldots\ldots\ldots\ldots \quad (8)$$

Zero moment

$$w_{yy}(x,0) = w_{yy}(x,b) = 0 \ldots\ldots\ldots\ldots\ldots\ldots \quad (9)$$

Constant displacement

$$v_{,x}(x,0) = v_{,x}(x,b) = 0 \ldots\ldots\ldots\ldots\ldots\ldots \quad (10)$$

Edge shear

$$u_{,y}(x,0) = u_{,y}(x,b) = \frac{2\eta(1+\mu)}{E\,t} \quad \ldots\ldots\ldots\ldots (11)$$

Longitudinal compressive load

$$\int_0^b N_x\,dy = -P \quad \ldots\ldots\ldots\ldots\ldots\ldots (12)$$

No transverse compressive load

$$\int_0^{a/m} N_y\,dx = 0 \quad \ldots\ldots\ldots\ldots\ldots\ldots (13)$$

where a/m is the buckle length. Also, the deformations are considered to be periodic in the x direction.

Solution.—Upon substitution from Eqs. 6 the first and second of Eqs. 7 become

$$u_{1,xx} + \frac{1-\mu}{2}u_{1,yy} + \frac{1+\mu}{2}v_{1,xy} = -\left(w_{0,x}w_{1,x} + \mu\, w_{0,y}w_{1,y}\right),_x - \frac{1-\mu}{2}\left(w_{0,x}w_{1,y} + w_{1,x}w_{0,y}\right),_y$$

$$v_{1,yy} + \frac{1-\mu}{2}v_{1,xx} + \frac{1+\mu}{2}u_{1,xy} = -\left(w_{0,y}w_{1,y} + \mu\, w_{0,x}w_{1,x}\right),_y - \frac{1-\mu}{2}\left(w_{0,x}w_{1,y} + w_{1,x}w_{0,y}\right),_x \quad \ldots\ldots (14)$$

The first step in the Galerkin method of solution used here is to assume a solution for w_1 that satisfies boundary conditions (but not necessarily the differential equations). The simplest w_1 assumed is

$$w_1 = A\cos\frac{m\pi x}{a}\sin\frac{2\pi y}{b} \quad \ldots\ldots\ldots\ldots (15)$$

where the constant A is to be determined by the Galerkin method. Now substitute in the foregoing equations for w_0 and w_1 and solve for u_1 and v_1. (Substitute for the zero subscript terms in these equations corresponding functions from the writer's previous work[2] according to the degree of approximation desired from the compressive problem.)

For the assumption (Eq. 15) the Galerkin method gives the following equation from which A is determined

$$\int_0^{a/m}\int_0^b \left[D\nabla^4 w_1 - \left(N_{x_0}w_{1,xx} + N_{y_0}w_{1,yy} + 2N_{xy_0}w_{1,xy} + N_{x_1}w_{0,xx} + N_{y_1}w_{0,yy} + 2N_{xy_1}w_{0,xy}\right)\right]\cos\frac{m\pi x}{a}\sin\frac{2\pi y}{b}\,dx\,dy = 0 \quad \ldots\ldots (16)$$

Such a procedure as that just outlined using the first approximation[2] for the compression problem and using the assumption of Eq. 15 for the additional deflection w_1 results in

$$\frac{A}{h}\frac{D\pi^2}{b^2} = \frac{\frac{16}{3\pi}\beta\sqrt{\frac{4}{3(1-\mu^2)}\frac{\beta^2 k - (\beta^2+1)^2}{\beta^4+1}}}{(\beta^2+4)^2 k - \beta^2 k + \frac{\beta^2 k - (\beta^2+1)^2}{\beta^4+1}\left[\frac{81\beta^4}{(4\beta^2+1)^2} + \frac{\beta^4}{(4\beta^2+9)^2} - 4\right]} \quad . . (17)$$

where β is the wave length ratio m b/a and $k = Pb^2 / D\pi^2$.

The average unit shearing deformation, Γ, is given by

$$\Gamma = \frac{1}{b}\left[\bar{u}(b) - \bar{u}(0)\right] . . . . . (18)$$

where $\bar{u}$ is the average value of u along the length

$$\bar{u}(y) = \frac{m}{a}\int_0^{a/m} u(x,y)\, dx . . . . . (19)$$

The shearing stiffness is defined as $\eta/(\Gamma h)$ which for an unbuckled plate is equal to the shear modulus $G = \frac{E}{2(1+\mu)}$. Corresponding to the solution (Eq. 17) the following equation is obtained

$$\frac{E h \Gamma}{2(1+\mu)\eta} = 1 + \frac{\frac{512}{9\pi^2(1+\mu)}\beta^2\left[\frac{\beta^2 k - (\beta^2+1)^2}{\beta^4+1}\right]}{(\beta^2+4)^2 - \beta^2 k + \frac{\beta^2 k - (\beta^2+1)^2}{\beta^4+1}\left[\frac{81\beta^4}{(4\beta^2+1)^2} + \frac{\beta^4}{(4\beta^2+9)^2} - 4\right]} \quad . . (20)$$

The curve labeled first approximation in Fig. 17 was obtained by using in Eq. 20 corresponding values of k and β given in Table 1 of the writer's previous work.[2]

No details are presented for the second approximation curve of Fig. 17 which was obtained using the second-approximation results for the compression problem[2] and using Eq. 15 for w_1. The analysis is quite similar but much more tedious.

An extension of this work for the first approximation using more complicated expressions than Eq. 15 for w_1 have indicated that the results for shear stiffness presented in Fig. 17 are about 5% high at two-and-one-half times the buckling load.

Journal of the
ENGINEERING MECHANICS DIVISION
Proceedings of the American Society of Civil Engineers

WAVES AND SHOCKS IN LOCKING AND DISSIPATIVE MEDIA[a]

By Mario G. Salvadori,[1] F. ASCE, Richard Skalak,[2] M. ASCE and Paul Weidlinger,[3] F. ASCE

SYNOPSIS

The propagation of stress waves and shocks in various inelastic media are studied for a semi-infinite body loaded at its free surface.

The first type of material postulated is a locking medium, which responds elasto-plastically at low stress levels but behaves as a rigid body after it is compressed to a certain maximum strain. It is shown that a pressure pulse may generate either a supersonic shock wave, or a subsonic wave with an elastic precursor, or a purely elastic wave. All three phenomena may occur in the foregoing sequence. Criteria for the initiation, existence, and decay of the three types of wave fronts are given.

The second type of medium studied exhibits a constant modulus of elasticity on initial loading and a second larger modulus on unloading. The time history of stress and strain under a pressure pulse is given and it is shown that eventually the medium will reach an unstressed state and remain at rest but with permanent displacements.

Note.—Discussion open until September 1, 1960. To extend the closing date one month, a written request must be filed with the Executive Secretary, ASCE. This paper is part of the copyrighted Journal of the Engineering Mechanics Division, Proceedings of the American Society of Civil Engineers, Vol. 86, No. EM 2, April, 1960.

a This paper is a result of investigations sponsored by the Space Technology Laboratories.

[1] Assoc., Paul Weidlinger, Cons. Engr., New York, and Prof. of Civ. Engrg., Columbia University, New York.

[2] Assoc. Prof. of Civ. Engrg., Columbia University, New York.

[3] Cons. Engr., New York.

INTRODUCTION

This paper is concerned with the behavior of a class of materials which can be compacted (or locked) under certain types of loadings. A compacted layer in such a medium is characterized by a response which can be described as nearly rigid, as compared to the response of the uncompacted or loose portion. In a first type of medium, the compaction is initiated abruptly as a critical strain is reached, as shown by the stress-strain diagram of Fig. 1. Compaction is initiated gradually in a second type of material, which exhibits the stress-strain characteristics shown on Fig. 5 (to be presented subsequently).

The theory for the dispersion of stress waves in media with general stress-strain curves, concave upwards or downwards, has been explored on a mathematical basis,[4] and applied to various problems.[5,6]

For the most part, the assumption of a continuous and smooth stress-strain curve makes it difficult to obtain results in closed form. However, the general types of behavior discussed herein have counterparts in earlier work dealing with such smooth stress-strain curves. M. P. White and L. Griffis used[5] a smooth curve similar to Type I locking media, Fig. 1. They also considered[6] a case which is similar to Type II media, Fig. 5. The idealizations of the present paper permit closed solutions, and comparatively simple computational procedures.

PHYSICAL CHARACTERISTICS OF TYPE I, LOCKING MEDIA

Consider a material which, under a compressive load, has the stress-strain diagram shown in Fig. 1. Let the initial density of the material be ρ_i. On compression up to a stress σ_o, strain ϵ_o and density ρ_o the response is linear and plane stress waves will propagate with the acoustic velocity:

$$c_o = \left(\frac{\sigma_o}{\epsilon_o \rho_i} \right)^{1/2} \quad \ldots\ldots\ldots\ldots\ldots\ldots \quad (1)$$

At the stress σ_o the strain increases from ϵ_o to ϵ_c and the density increases from ρ_o to ρ_c. The values ϵ_c and ρ_c are the maximum possible values of the strain and the density. For stresses above greater than σ_o the stress-strain curve is parallel to the stress axis and the medium, therefore, responds as a rigid body to stresses larger than σ_o. On unloading a permanent strain ϵ_c remains.

Three limiting cases of this stress-strain relation are of interest:

(a) $\epsilon_o = \epsilon_c$; the material is linearly elastic up to the strain ϵ_c.
(b) $\epsilon_o = 0$; the material is rigid-plastic up to the yield stress σ_o.
(c) $\sigma_o = 0$; the material is plastic up to the strain ϵ_c.

---

4 "Propagation of Plastic Deformation in Solids," by Th. Von Karman and P. E. Dawez, Proc. VI, Int. Congr. for Applied Mechanics, Paris, 1946.

5 "The Propagation of Plasticity in Uniaxial Compression," by M. P. White and L. Griffis, Jour. Appl. Mech., Vol. 15, 1948, p. 256.

6 "Permanent Strain in a Uniform Bar due to Longitudinal Impact," by M. P. White and L. Griffis, Jour. Appl. Mech., Vol. 14, 1947, p. A337.

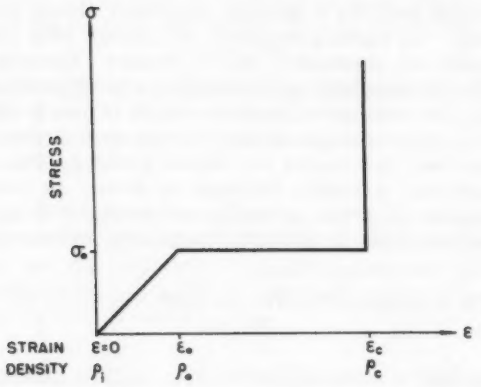

FIG. 1.—STRESS-STRAIN DIAGRAM, TYPE I, LINEAR LOCKING MEDIUM

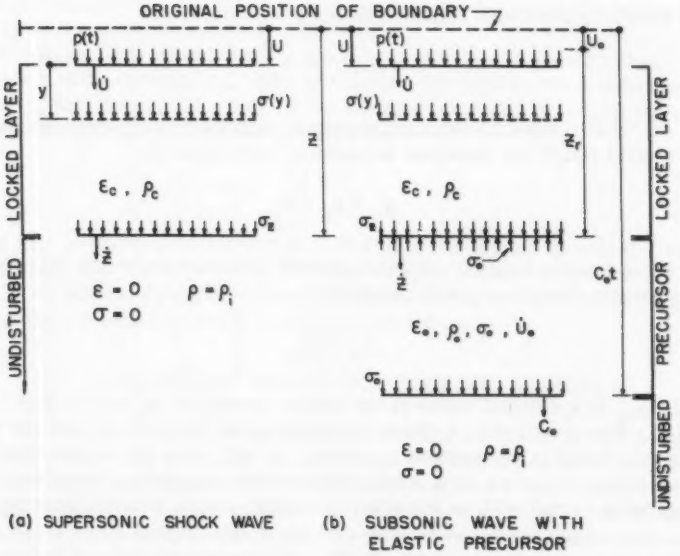

FIG. 2.—COMPACTION WAVES, TYPE I, LOCKING MEDIUM

A medium which exhibits a definite maximum strain has been termed[7] a "locking material." In various practical conditions real materials approximate this behavior, as mentioned[7] by W. Prager. Granular media, such as certain types of soils, also behave like this and are of particular interest. Upon initial loading, the response of such materials is nearly elastic[8] but further increase of the compression produces yielding and breakup of the elastic grains, which are then rearranged in a denser packing. This results in an irreversible compaction; a sudden increase in stress is manifested, beyond which only negligible increase of strain and density will occur. These phenomena are idealized in the behavior of the locking medium postulated.

RESPONSE OF A SEMI-INFINITE LOCKING MEDIUM TO A PRESSURE PULSE

Consider (Fig. 2(a)) a semi-infinite locking medium extending from $y = 0$ to $y = \infty$. If at a time $t = 0$ a decaying pressure $p(t)$ with the initial value p_o is suddenly applied to the boundary $y = 0$, a pressure wave of finite amplitude will propagate with a plane wave front. In what follows, stress, density, and particle velocities are assumed to have finite discontinuities across the wave front, and the analysis of the wave propagation is carried out for finite compressive strains, less than unity.

The response of the medium with the stress-strain characteristics, shown in Fig. 1, may be expected to be influenced by the magnitude of the initial value p_o of the applied pressure. Three distinct types of response are anticipated:

(a) Elastic waves with acoustic velocity will occur if:

$$0 < p_o \leq \sigma_o$$

(b) An elastic wave of constant stress σ_o followed by a subsonic compaction front, behind which the material is located, will occur if:

$$\sigma_o < p_o < p_{cr}$$

(c) A supersonic compaction front, behind which the material is locked without any elastic precursor, will occur if:

$$p_o > p_{cr}$$

in which p_{cr} is a critical value of the initial pressure p_o which separates (b) from (c). The existence of these three types of responses, and the value of p_{cr} is established in subsequent sections. It will also be shown that under a decaying pressure pulse, an initially supersonic compaction front degenerates into a subsonic front with an elastic precursor, which, in turn, is transformed

---

[7] "On Ideal Locking Materials," by W. Prager, Transactions, Soc. of Reheology, Vol. 1, 1957, pp. 169-175.

[8] "On the Theory of Elastic Waves in Granular Substance," by T. Takahashi and Y. Sato, Bulletin, Earthquake Research Inst., Tokyo Univ., Vol. 27, pp. 37-43.

into a purely elastic wave front. An initially subsonic wave front with an elastic precursor will be transformed in time into an elastic wave only.

ELASTIC WAVES IN A LOCKING MEDIUM

If elastic waves are generated by a constant or a decaying pulse, the following phenomena may occur:

(a) If the applied pressure does not excess σ_0 the medium does not lock, but responds elastically. The classical one-dimensional wave equations[9] govern the propagation, and the pulse is transmitted indefinitely without distortion at the acoustic velocity of Eq. 1. Thus, for a decaying or a constant pressure pulse elastic waves only result if

$$0 < p_0 \leq \sigma_0 \quad \ldots\ldots\ldots\ldots\ldots\ldots \quad (2)$$

(b) In the particular case of a constant pressure, $p_0 \leq \sigma_0$, the behavior of the medium in the elastic range is identical to that of a locking material because the medium behind the wave front is at a constant strain ϵ and moves as a rigid body with the constant particle velocity

$$\dot{u} = \epsilon\, c_0 \quad (0 < \epsilon \leq \epsilon_0) \ldots\ldots\ldots\ldots\ldots \quad (3)$$

(c) An elastic wave cannot exist behind a compaction front because the pressure at the compaction front which is greater than σ_0, locks the medium at the strain ϵ_c and compacts it into a rigid body.

(d) If the applied pressure $p_0 > \sigma_0$, and the compaction front velocity is less than the acoustic velocity c_0, then an elastic precursor with a constant stress equal to σ_0 will propagate ahead of the compaction front at a velocity c_0. The elastic precursor generates the particle velocity

$$\dot{u} = \epsilon_0\, c_0 \quad \ldots\ldots\ldots\ldots\ldots\ldots \quad (4)$$

This can be seen by noting that the stress in the elastic precursor cannot be greater than σ_0, since greater stresses would cause compaction, while the stress is an elastic precursor cannot be less than σ_0 since increasing stresses up to σ_0 are propagated at the acoustic velocity c_0.

COMPACTION WAVES IN A LOCKING MEDIUM

Let the location of the compaction wave front be given by z(t) and the displacement of the free boundary by u(t), where z and u are measured from the initial position of the boundary. The velocity of the front is $\dot{z}$ and that of the boundary is $\dot{u}$, where dots indicate derivatives with respect to t. Since the medium is locked behind the front, the particle displacements and velocities are also u and $\dot{u}$, respectively, (Fig. 2).

The state of the locked medium behind the front is characterized by density ρ_c, strain ϵ_c, velocity $\dot{u}(t)$, and stress $\sigma(y, t)$, where y is the distance from the

[9] "A Treatise on the Mathematical Theory of Elasticity," by A. E. Love, Dover Publications, New York.

position of the boundary at time t. The value of $\dot{u}(t)$ is independent of y since the locked medium is a rigid body.

If $\dot{z} > c_o$ the front is supersonic. Then the medium ahead of the front will be at rest, unstressed, and at initial density ρ_i. If $\dot{z} < c_o$ the front is subsonic and there will be an elastic precursor wave. The material just ahead of the compaction front is then at density ρ_o, strain ϵ_o, stress σ_o and velocity $\dot{u}_o = \epsilon_o c_o$. To permit the simultaneous treatment of both subsonic and supersonic cases it is convenient to define $\delta = f(\dot{z}/c_o)$ such that:

$$\left.\begin{aligned} \delta &= 0 \text{ if } \dot{z}/c_o > 1 \\ \delta &= +1 \text{ if } \dot{z}/c_o < 1 \end{aligned}\right\} \quad \ldots\ldots\ldots\ldots\ldots\ldots (5)$$

The state ahead of the front z is given for both cases by:

$$\left.\begin{aligned} &\text{density:} && \rho_i + \delta\left(\rho_o - \rho_i\right) \\ &\text{strain:} && \delta\epsilon_o \\ &\text{stress:} && \delta\sigma_o \\ &\text{velocity:} && \delta\dot{u}_o \end{aligned}\right\} \quad \ldots\ldots\ldots\ldots\ldots\ldots (6)$$

The velocities of the compaction front and of the boundary, relative to the constant velocity $\delta\dot{u}_o$ of the medium ahead of the front, are called $\dot{z}_r$ and $\dot{u}_r$, where

$$\left.\begin{aligned} z_r &= z - \delta\, \dot{u}_o\, t & \qquad u_r &= u - \delta\, \dot{u}_o\, t \\ \dot{z}_r &= \dot{z} - \delta\, \dot{u}_o & \qquad \dot{u}_r &= \dot{u} - \delta\, \dot{u}_o \end{aligned}\right\} \quad \ldots\ldots\ldots\ldots\ldots (7)$$

Conservation of mass requires, that:

$$\rho_i = \rho_c\left(1 - \epsilon_c\right) = \rho_o\left(1 - \epsilon_o\right) \ldots\ldots\ldots\ldots\ldots (8a)$$

or in terms of δ, that:

$$\rho_c\left(1 - \epsilon_c\right) = \left[\rho_i + \delta\left(\rho_o - \rho_i\right)\right]\left(1 - \delta\epsilon_o\right) \ldots\ldots\ldots\ldots (8b)$$

and, since the medium behind the front is compressed from its original length z_r to the length $z_r - u_r$, that:

$$\left(1 - \delta\epsilon_o\right)\left(z_r - u_r\right) = \left(1 - \epsilon_c\right) z_r \quad \ldots\ldots\ldots\ldots (9)$$

The momentum of the mass $\rho_c\,(z_r - u_r)$ between the compaction front and the surface is $\rho_c\,(z_r - u_r)\,\dot{u}_r$. This momentum changes at a rate equal to the net force:

$$\frac{d}{dt}\left[\rho_c\left(z_r - u_r\right)\dot{u}_r\right] = p(t) - \delta\sigma_o \quad \ldots\ldots\ldots\ldots (10)$$

Substituting Eqs. 1, 8b, and 9 into 10, the equation of motion becomes

$$\frac{d}{dt}\left(z_r\,\dot{z}_r\right) = c_o^2\,k^2\left[\frac{p(t)}{\sigma_o} - \delta\right] \quad \ldots\ldots\ldots\ldots (11)$$

where

$$k^2 = \frac{\left(1 - \delta\epsilon_o\right)^2}{\left(\epsilon_c/\epsilon_o\right) - \delta} \quad \ldots\ldots\ldots\ldots (12)$$

The stress $\sigma(y)$ can be obtained from another form of the equation of motion:

$$p(t) - \sigma(y, t) = \rho_c\, y\, \ddot{u}_r \quad \ldots\ldots\ldots\ldots (13)$$

and the stress immediately behind the front at $y = z_r - u_r$ is obtained by substituting Eqs. 8b, 9, and 11 into Eq. 13:

$$\sigma_z = \left[\delta + \left(\frac{\dot{z}_r}{c_c}\right)^2 \frac{1}{k^2}\right]\sigma_o \quad \ldots\ldots\ldots\ldots (14)$$

Differentiating the left-hand side of Eq. 11, and setting $z(0) = 0$, the initial velocity of the front is given by:

$$\dot{z}(0) = k\,c_o\left[\frac{p_o}{\sigma_o} - \delta\right]^{1/2} + \delta\,\dot{u}_o \quad \ldots\ldots\ldots\ldots (15)$$

The critical initial pressure p_{cr}, separating the supersonic from the subsonic motion, is obtained by setting $\dot{z}(0) = c_o$ in Eq. 15, which yields for either value of δ:

$$p_{cr} = \sigma_o\left(\frac{\epsilon_c}{\epsilon_o}\right) \quad \ldots\ldots\ldots\ldots (16)$$

The significance of p_{cr} on the stress-strain diagram is shown in Fig. 3.

SUPERSONIC SHOCK IN A LOCKING MEDIUM

When $p_o > p_{cr}$, $\dot{z}/c_o > 1$, ($\delta = 0$), the equation of motion reduces to:

$$\frac{d(z\,\dot{z})}{dt} = c_o^2\,\frac{\epsilon_o}{\epsilon_c}\,\frac{p(t)}{\sigma_o} \quad \ldots\ldots\ldots\ldots (17)$$

Integrating twice with the initial conditions $z\ \dot{z} = z = 0$ at $t = 0$, the motion of the shockfront is given by:[b]

$$z = c_o\, t \left(\frac{\epsilon_o}{\epsilon_c}\right)^{1/2} \left[\frac{2 \int dt \int p(t)\, dt}{\sigma_o\, t^2}\right]^{1/2} \quad \ldots\ldots\ldots\ldots (18)$$

$$\dot{z} = c_o \left(\frac{\epsilon_o}{\epsilon_c}\right)^{1/2} \frac{\dfrac{\int p(t)\, dt}{\sigma_o\, t}}{\left[\dfrac{2 \int dt \int p(t)\, dt}{\sigma_o\, t^2}\right]^{1/2}} \quad \ldots\ldots\ldots\ldots (19)$$

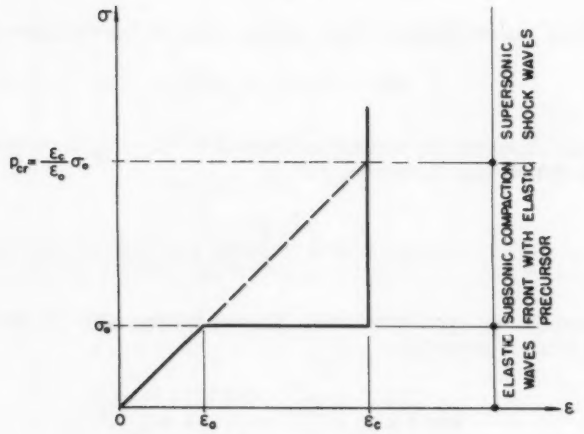

FIG. 3.—WAVE FORMATION CRITERIA, IN TYPE I, LOCKING MEDIUM

The initial velocity by Eqs. 13 or 19 is:

$$\dot{z}(0) = c_o \left[\frac{p_o}{p_{cr}}\right]^{1/2} \quad \ldots\ldots\ldots\ldots\ldots\ldots (20)$$

The stress at the shock front, from Eq. 14 is:

$$\sigma_z = p_{cr} \left(\frac{\dot{z}}{c_o}\right)^2 \quad \ldots\ldots\ldots\ldots\ldots\ldots (21)$$

---

[b] The integrals are taken between the limits: $0 \rightarrow t$ unless otherwise indicated.

The particle velocity is obtained by differentiating Eq. 9:

$$\dot{u} = \epsilon_c \dot{z} \quad \ldots\ldots\ldots\ldots\ldots\ldots (22)$$

As the surface pressure p(t) decays, the front velocity $\dot{z}$ decreases. Let t_s be defined as the time at which:

$$\frac{\dot{z}(t_s)}{c_o} = 1 \quad \ldots\ldots\ldots\ldots\ldots\ldots (23)$$

Using Eq. 23 in 19, the time t_s is found from:

$$\int_0^{t_s} p(t)dt = \left[p_{cr}\ 2 \int_0^{t_s} dt \int_0^{t_s} p(t)\ dt \right]^{1/2} \quad \ldots\ldots\ldots (24)$$

At time t_s the front is at:

$$z_s = z(t_s) = c_o\ t_s \frac{\int_0^{t_s} p(t)\ dt}{p_{cr} t_s} \quad \ldots\ldots\ldots\ldots\ldots (25)$$

and the stress at the shock front has decayed to:

$$\sigma_z(t_s) = p_{cr} \quad \ldots\ldots\ldots\ldots\ldots\ldots (26)$$

Also at t_s the acceleration of the shock front is:

$$\ddot{z}(t_s) = \frac{c_o^2}{z_s} \left[\frac{p(t_s)}{p_{cr}} - 1 \right] \quad \ldots\ldots\ldots\ldots\ldots (27)$$

The particle velocity and acceleration are given at $t = t_s$ by:

$$\dot{u}(t_s) = \epsilon_c\ c_o \quad \ldots\ldots\ldots\ldots\ldots\ldots (28)$$

and

$$\ddot{u}(t_s) = \frac{c_o^2}{z_s} \left[\frac{p(t_s)}{p_{cr}} - 1 \right] \epsilon_c \quad \ldots\ldots\ldots\ldots\ldots (29)$$

At the time t_s the supersonic motion ceases. Since the particle acceleration is negative for a decaying pressure, it follows from Eq. 29 that:

$$p(t_s) < p_{cr}$$

but because of Eq. 28:

$$\dot{u}(t_s) > \dot{u}_o = \epsilon_o c_o$$

and, therefore, the shock front does not degenerate into an elastic wave. The motion must continue with a subsonic compaction preceded by an elastic precursor.

SUBSONIC FRONT IN A LOCKING MEDIUM

When $\sigma_o < p_o < p_{cr}$, $\dot{z}/c_o < 1$, ($\delta = 1$), and the equation of motion (Eq. 11) becomes:

$$\frac{d}{dt}(z_r \dot{z}_r) = c_o^2 \frac{(1-\epsilon_o)^2}{(\epsilon_c/\epsilon_o)-1} \left[\frac{p(t)}{\sigma_o} - 1\right] \quad \ldots\ldots\ldots (30)$$

where from Eq. 7:

$$\left.\begin{aligned} z_r &= z - \dot{u}_o t \\ \dot{z}_r &= \dot{z} - \dot{u}_o \end{aligned}\right\} \ldots\ldots\ldots\ldots\ldots (31)$$

The initial velocity of the compaction front from Eq. 15 is:

$$\dot{z}(0) = \frac{1-\epsilon_o}{\sqrt{(\epsilon_c/\epsilon_o) - 1}} c_o \left[(p_o/\sigma_o) - 1\right]^{1/2} + \dot{u}_o \quad \ldots\ldots (32)$$

If the subsonic front was preceded by a supersonic shock which became sonic at a time $t = t_s$, initial conditions for the subsonic phase are:

$$\dot{z}(t_s) = c_o$$

and

$$z(t_s) = z_s = c_o \frac{\int_0^{t_s} p(t)\, dt}{p_{cr}}$$

Since both the subsonic front, and the precursor start at the time t_s and depth z_s, a new coordinate $\bar{z}_r$ and its derivative can be given in the form:

$$\bar{z}_r = z - \dot{u}_o\left(t - t_s + \frac{z_s}{c_o}\right) \quad \ldots\ldots\ldots\ldots\ldots\ldots (33)$$

$$\dot{\bar{z}}_r = \dot{z} = \dot{u}_o = \dot{z}_r$$

This transformation introduces a new time $\bar{t} = t - t_s + \frac{z_s}{c_o}$ and the equation of motion becomes Eq. 30 with t, z_r, $\dot{z}_r$ replaced by $\bar{t}$, $\bar{z}_r$, $\dot{\bar{z}}_r$.
Eq. 30 when written in terms of $\bar{z}_r$ and $\dot{\bar{z}}_r$, may be integrated twice. (The solution for a pulse which starts a subsonic front at t = 0 is obtained from the general solution by setting $t_s = z_s = 0$.)

The motion of the front is given by:

$$z = \frac{1 - \epsilon_o}{\sqrt{(\epsilon_c/\epsilon_o) - 1}}\, c_o\left(t - t_s\right)\left\{\frac{2\int dt \int p(t)\, dt}{\sigma_o\left(t - t_s\right)^2} - \left[\frac{z_s}{c_o\left(t-t_s\right)} + 1\right]^2\right\}^{1/2} + \epsilon_o\, c_o\left(t-t_s\right) + \epsilon_o\, z_s \quad \ldots\ldots\ldots (34)$$

and

$$\dot{z} = \frac{1 - \epsilon_o}{\sqrt{(\epsilon_c/\epsilon_o) - 1}}\, c_o\, \frac{\frac{\int p(t)\, dt}{\sigma_o\left(t-t_s\right)} - \left[\frac{z_s}{c_o\left(t-t_s\right)} + 1\right]}{\left\{\frac{2\int dt \int p(t)\, dt}{\sigma_o\left(t-t_s\right)^2} - \left[\frac{z_s}{c_o\left(t-t_s\right)} + 1\right]^2\right\}^{1/2}} + \epsilon_o\, c_o \quad \ldots (35)$$

The stress at the front, from Eq. 14, is:

$$\sigma_z = \sigma_o\left[1 + \left(\frac{\dot{z}}{c_o} - \epsilon_o\right)^2 \frac{(\epsilon_c/\epsilon_o) - 1}{\left(1 - \epsilon_o\right)^2}\right] \quad \ldots\ldots\ldots (36)$$

and the particle velocity from Eq. 9 is:

$$\dot{u} = \dot{z}\,\epsilon_o\,\frac{(\epsilon_c/\epsilon_o) - 1}{1 - \epsilon_o} + \epsilon_o\, c_o\,\frac{1 - \epsilon_c}{1 - \epsilon_o} \quad \ldots\ldots\ldots\ldots (37)$$

The particle acceleration is obtained by differentiating Eq. 37:

$$\ddot{u} = \ddot{z}\,\epsilon_o\,\frac{(\epsilon_c/\epsilon_o) - 1}{1 - \epsilon_o} \quad \ldots\ldots\ldots\ldots\ldots (38)$$

At the time $t = t_s$, the stress σ_z at the front, the particle velocity, and the particle acceleration are equal to the values derived for the end of the supersonic motion given by Eqs. 26, 28, and 29. The front acceleration however, becomes discontinuous,

$$\ddot{z}(t_s+) = \ddot{z}(t_s-) \frac{(1-\epsilon_o)}{(\epsilon_c/\epsilon_o)-1} \frac{\epsilon_c}{\epsilon_o} \quad \ldots\ldots\ldots\ldots (39)$$

and the front velocity shows a corresponding change in slope at that time.

Let time $t = t_e$ be the instant when the motion of the compaction front, relative to the medium ahead, ceases:

$$\dot{z}_r(t_e) = 0 \quad \ldots\ldots\ldots\ldots\ldots\ldots (40)$$

then, from Eq. 33:

$$\dot{z}(t_e) - \dot{u}_o = \epsilon_o c_o \quad \ldots\ldots\ldots\ldots\ldots\ldots (41)$$

At the time t_e, by Eq. 37, the particle velocity also has the value:

$$\dot{u}(t_e) = \dot{u}_o = \epsilon_o c_o \quad \ldots\ldots\ldots\ldots\ldots\ldots (42)$$

The entire locked mass, therefore, moves at the particle velocity of the precursor. The time t_e is defined by Eq. 40, that is, by:

$$t_e - t_s = \frac{\int_0^{t_e} p(t)\, dt}{\sigma_o} - \frac{z_s}{c_o} \quad \ldots\ldots\ldots\ldots\ldots\ldots (43)$$

The stress at the front decays to the limiting stress at $t = t_e$:

$$\sigma_z = \sigma_o \quad \ldots\ldots\ldots\ldots\ldots\ldots (44)$$

and the compaction ceases, while the elastic wave continues to propagate indefinitely.

LIMITING CASES

The equations derived in the previous sections are also valid for the limiting cases described under the heading "Physical Characteristics of Type I, Locking Media."

Case (a): $\epsilon_o = \epsilon_c$

Supersonic compaction exists if $p_o > \sigma_o$ and the equation of motion with $k^2 = 1$ is

$$\frac{d}{dt}(z\,\dot{z}) = c_o^2 \frac{p_o(t)}{\sigma_o} \quad \ldots\ldots\ldots\ldots\ldots\ldots (45)$$

If $p_o < \sigma_o$ elastic wave propagation will occur, and therefore subsonic phenomena cannot take place.

Case (b): $\epsilon_o = 0$, $\sigma_o \neq 0$, $\epsilon_c \neq 0$

These conditions imply $k^2 = 0$ and $c_o^2 = \infty$ but

$$k^2 c_o^2 = \frac{\sigma_o}{\rho_i \epsilon_c} \quad \ldots\ldots\ldots\ldots\ldots\ldots (46)$$

If $p_o > \sigma_o$, the motion is "subsonic" with an instantaneous stress precursor of stress σ_o and the compaction front propagation is governed by

$$\frac{d}{dt}(z\,\dot{z}) = \frac{1}{\rho_i \epsilon_c}\, p(t) - \sigma_o \quad \ldots\ldots\ldots\ldots\ldots\ldots (47)$$

If $p_o < \sigma_o$ the pressure is instantaneously propagated to infinity without compaction. No supersonic waves are possible.

Case (c): $\sigma_o = 0$ and $\epsilon_c \neq 0$

These conditions imply $c_o = 0$, therefore the motion is always "supersonic" and governed by

$$\frac{d}{dt}(z\,\dot{z}) = \frac{1}{\rho_i \epsilon_c}\, p(t) \quad \ldots\ldots\ldots\ldots\ldots\ldots (48)$$

Compaction will occur whenever $p_o > 0$; neither subsonic, nor elastic waves can exist.

NUMERICAL EXAMPLE

Consider a pressure pulse defined in the non-dimensional form

$$P = \frac{p(t)}{p_o} = e^{-\tau}$$

where the non-dimensional time τ is given in terms of a time constant t_o:

$$\tau = t/t_o$$

The displacements, velocities, and stresses may be expressed in the non-dimensional forms:

$$Z = \frac{z}{c_o t_o} \quad \sum_z = \frac{\sigma_z}{p_o}$$

$$Z' = \frac{\dot{z}}{c_o} \quad U' = \frac{\dot{u}}{c_o}$$

where primes represent derivatives with respect to τ. Fig. 4 shows the results of a numerical example in terms of the non-dimensional parameters for the following values of the constants:

$$\sum_o = \frac{\sigma_o}{p_o} = 0.4107$$

$$P_{cr} = \frac{\left(\epsilon_c/\epsilon_o\right)_{\sigma_o}}{p_o} = 0.6082$$

$$\epsilon_o = 0.1000$$

Fig. 4 shows the results up to the time $\tau = 2.0$, the time at which compaction ceases. After this time the system behaves as a rigid mass (the compacted layer of the medium) on a semi-infinite elastic medium, with the initial conditions corresponding to those given at $\tau = 2.0$.

PHYSICAL CHARACTERISTICS OF TYPE II MEDIA

A second type of medium is defined by the stress-strain diagram of Fig. 5. The stress-strain curve is a straight line OA on initial loading to A. The slope of this line defines an initial modulus, E_1. Upon unloading the stress-strain curve is another straight line AB which defines a second modulus, E_1. If the material is reloaded, it follows line BA to A and then continues along the initial loading line AC.

This medium will behave as a linear elastic material in the limit when E_1 approaches E_o. If in the limit E_1 approaches infinity, the material becomes one in which there is no recovery.

Throughout the remainder of the paper only small strains are considered and, therefore, density is considered constant.

DIFFERENTIAL EQUATIONS OF WAVE PROPAGATION

Consider a plane compression wave propagating into a virgin material. The distribution of pressure at a given instant is shown in Fig. 6. Point A represents the leading edge of the wave propagating in the positive y direction. In the portion of the wave AB the pressure is continuously rising and, hence, this

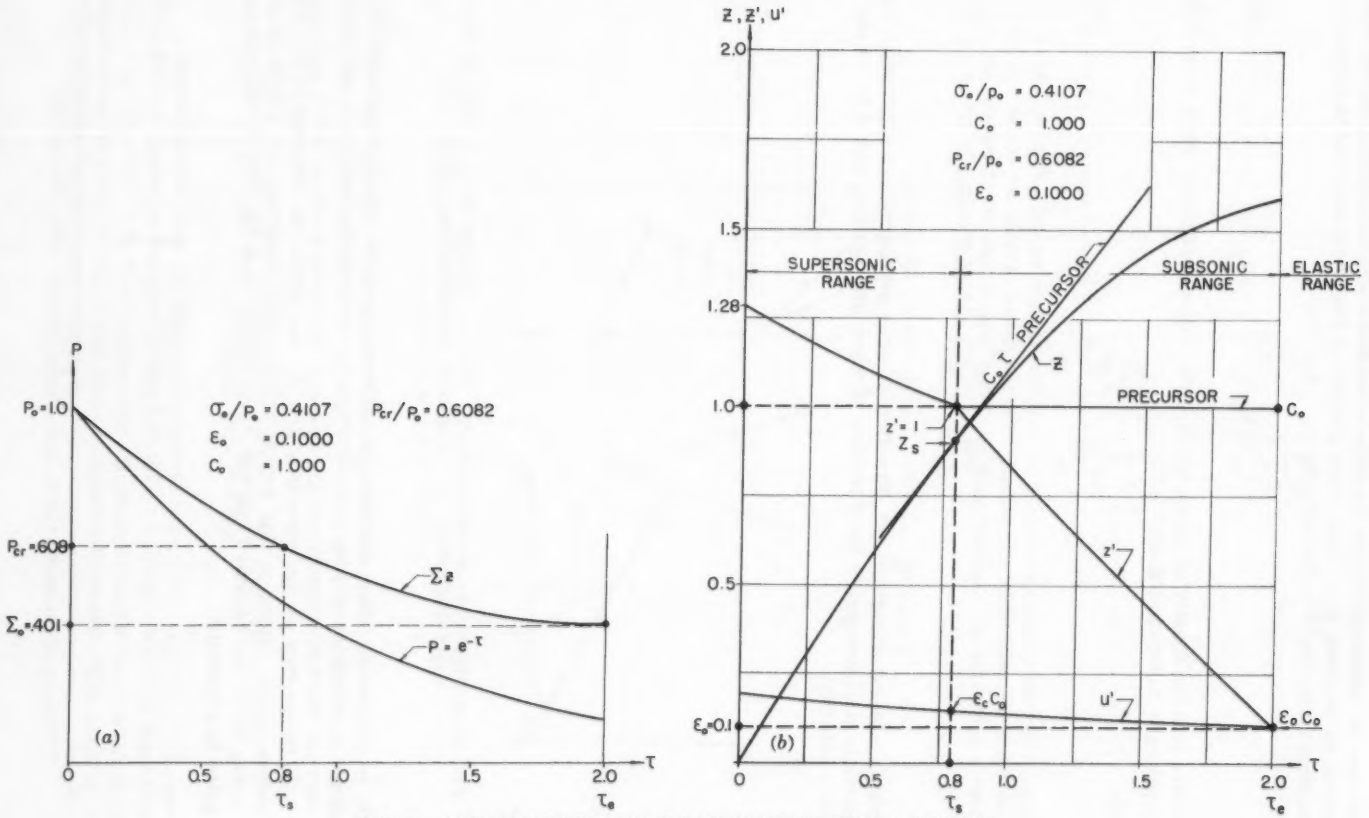

FIG. 4.—DYNAMIC FREE FIELD PARAMETERS, TYPE I MEDIUM

portion is indistinguishable from the wave that would result in an elastic material of modulus E_o. Thus, this portion of the wave will tend to propagate without distortion[10] at the velocity c_o:

$$c_o = \left(E_o/\rho\right)^{1/2} \quad \ldots\ldots\ldots\ldots\ldots\ldots (49)$$

where ρ is the density of the material. The one-dimensional wave equations govern the motion in the zone AB:

$$\frac{\partial^2 \sigma}{\partial y^2} = \frac{1}{c_o^2} \frac{\partial^2 \sigma}{\partial t^2} \quad \ldots\ldots\ldots\ldots\ldots\ldots (50)$$

$$\frac{\partial^2 \dot{u}}{\partial y^2} = \frac{1}{c_o^2} \frac{\partial^2 \dot{u}}{\partial t^2} \quad \ldots\ldots\ldots\ldots\ldots\ldots (51)$$

where σ is the stress in the direction of wave propagation, u represents the particle displacement in the direction of wave propagation, and $\dot{u}$ is the particle velocity.

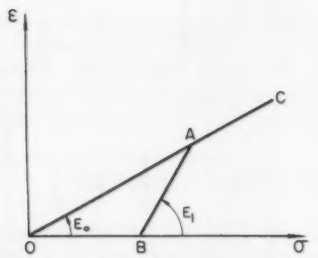

FIG. 5.—STRESS-STRAIN DIAGRAM OF TYPE II MEDIUM

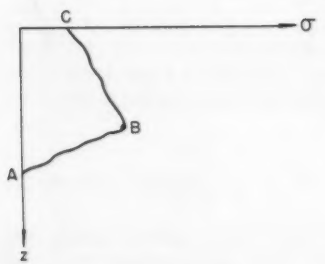

FIG. 6.—STRESS WAVE PROPAGATING VIRGIN MATERIAL INTO

In the loading phase, the behavior is the same as that of a linear elastic material in which the stress, particle velocity, particle displacement, and strain obey the wave equation.[10]

In the portion of the wave BC, Fig. 6, the stress is less than at B. The stress-strain values in this region will lie on an unloading curve such as AB in Fig. 5. It may be shown that the portion of the wave BC, Fig. 6, then propagates at a velocity:

$$c_1 = \left(E_1/\rho\right)^{1/2} \quad \ldots\ldots\ldots\ldots\ldots\ldots (52)$$

10 "Theory of Elasticity," by S. Timoshenko, McGraw-Hill, 1934, p. 381.

and the governing equations in this zone are:

$$\frac{\partial^2 \sigma}{\partial y^2} = \frac{1}{c_1^2} \frac{\partial^2 \sigma}{\partial t^2} \quad \ldots\ldots\ldots\ldots\ldots\ldots (53)$$

and

$$\frac{\partial^2 \dot{u}^2}{\partial y^2} = \frac{1}{c_o^2} \frac{\partial^2 \dot{u}}{\partial t^2} \quad \ldots\ldots\ldots\ldots\ldots\ldots (54)$$

In the unloading phase the particle velocity and stress obey the wave equations 8, 9 since the stress-strain curve is linear. The displacement and strain are not governed by the elastic wave equation because the unloading stress-strain curve is offset from the origin.

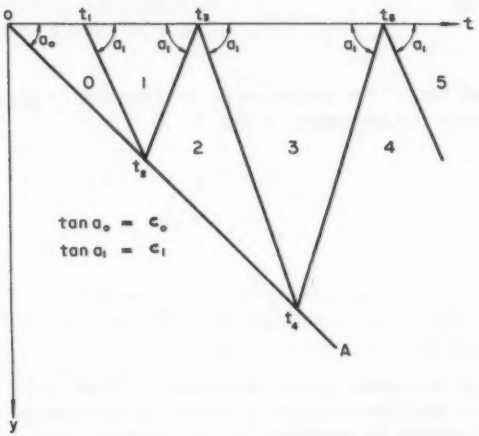

FIG. 7.—SPACE-TIME DIAGRAM FOR DISCONTINUOUS LOADING IN TYPE II MEDIUM

Since the velocity c_1 is greater than c_o, the rear portion of the wave, BC, tends to overtake the forward portion, AB. There is a continuous reflection process at the functure B as will be shown subsequently.

RESPONSE OF A SEMI-INFINITE BODY TO DISCONTINUOUS SURFACE PRESSURES

A semi-infinite body is assumed to extend from $y = 0$ to $y = \infty$. If a pressure $p(t)$ is applied to the surface $y = 0$ at time $t = 0$, there will be a wave front at $y = c_o t$ for all $t > 0$. This implies that the material below the line OA in the space-time diagram of Fig. 7 will be at rest and unstressed. The slope of the line OA is the initial sound velocity c_o.

The particular surface pressure history considered is as follows: At time $t = 0$, the surface pressure $p(t)$ rises abruptly from zero to p_o. The value p_o is maintained until $t = t_1$ at which time the pressure drops to p_1 and remains constant at p_1 indefinitely.

The response for $0 < t < t_1$ is a step wave of pressure p_o propagating at velocity c_o. The conditions in Zone 0 of Fig. 7 are stress $\sigma_o = p_o$ and particle velocity $\dot{u}_o$:

$$\dot{u}_o = \frac{p_o}{\rho c_o} \quad \ldots\ldots\ldots\ldots\ldots\ldots (55)$$

At time t_1 the drop in surface pressure from p_o to p_1 occurs at the surface $y = 0$ and propagates at velocity c_1 which is the slope of the line separating Zones 0 and 1 in Fig. 7. In Zone 1 the stress is $\sigma_1 = p_1$ and the particle velocity is $\dot{u}_1$:

$$\dot{u}_1 = \dot{u}_o - \frac{p_o - p_1}{\rho c_1} \quad \ldots\ldots\ldots\ldots\ldots\ldots (56)$$

The time t_2 at which the pressure p_1 reaches the original wave front may be determined from the geometry of Fig. 7:

$$t_2 = \beta t_1 \quad \ldots\ldots\ldots\ldots\ldots\ldots (57)$$

where

$$\beta = \frac{c_1/c_o}{(c_1/c_o) - 1} \quad \ldots\ldots\ldots\ldots\ldots\ldots (58)$$

At the time t_2 the entire length of material from $y = 0$ to $y = c_o t_2$ is at stress $\sigma_1 = p_1$ and particle velocity $\dot{u}_1$. It may be considered that this material is a body of elasticity E_1 striking the undisturbed mass of elasticity E_o. A wave is propagated into the undisturbed material at velocity c_o and a reflected wave travels upwards[7] at velocity c_1. The reflected wave front is represented by the foundary between zones 1 and 2, Fig. 7.

The stress σ_2 and particle velocity $\dot{u}_2$ throughout zone 2 must be such that for the refracted wave,

$$\dot{u}_2 = \frac{\sigma_2}{\rho c_o} \quad \ldots\ldots\ldots\ldots\ldots\ldots (59)$$

and for the reflected wave,

$$\dot{u}_2 = \dot{u}_1 - \frac{\sigma_2 - \sigma_1}{\rho c_1} \quad \ldots\ldots\ldots\ldots\ldots\ldots (60)$$

From Eqs. 55, 56, 59 and 60 it is found that:

$$\sigma_2 = p_1 + \alpha(p_o - p_1) \quad \ldots\ldots\ldots\ldots\ldots\ldots (61)$$

where

$$\alpha = \frac{(c_1/c_o) - 1}{(c_1/c_o) + 1} = \frac{1}{2\beta - 1} \quad \ldots\ldots\ldots\ldots\ldots\ldots (62)$$

The reflected wave reaches the surface y = 0 at time t_3 which is determined from Fig. 7:

$$t_3 = \frac{1}{\alpha} t_1 \quad \ldots\ldots\ldots\ldots\ldots\ldots (63)$$

Conditions at time t_3 are similar to those at time t_1. The stress and velocity σ_o, $\dot{u}_o$ at time t_1 are replaced by σ_2, $\dot{u}_2$ at time t_3. Hence the values of σ_3, $\dot{u}_3$ may be written down by analogy to σ_1, $\dot{u}_1$:

$$\sigma_3 = p_1 \quad \ldots\ldots\ldots\ldots\ldots\ldots (64)$$

and

$$\dot{u}_3 = \dot{u}_2 - \frac{\sigma_2 - \sigma_3}{\rho c_1} \quad \ldots\ldots\ldots\ldots\ldots\ldots (65)$$

The reflection from the moving wave front which takes place at t_4, Fig. 7, may be analyzed in the same way as the reflection at time t_2. The process may be continued indefinitely and leads to the following general expressions where n is a positive integer:

For n even:

$$t_n = \beta \alpha^{1-n/2} t_1 \quad \ldots\ldots\ldots\ldots\ldots\ldots (66)$$

$$\sigma_n = \sigma_1 + \alpha^{n/2}(p_o - p_1) \quad \ldots\ldots\ldots\ldots\ldots\ldots (67)$$

and

$$\dot{u}_n = \frac{1}{\rho c_o}\left[\sigma_1 + \alpha^{n/2}(\sigma_o - \sigma_1)\right] \quad \ldots\ldots\ldots\ldots\ldots\ldots (68)$$

For n odd:

$$t_n = \alpha^{\frac{1-n}{2}} t_1 \quad \ldots\ldots\ldots\ldots\ldots\ldots (69)$$

$$p_n = p_1 \quad \ldots\ldots\ldots\ldots\ldots\ldots (70)$$

and

$$\dot{u}_n = \frac{1}{\rho c_o}\left[p_1 + \frac{2\alpha^{\frac{n+1}{2}}}{1+\alpha}(p_o - p_1)\right] \quad \ldots\ldots\ldots\ldots (71)$$

where p_o, p_1, t_1, and c_1/c_o are the given parameters of the problem.

The stress at any point oscillates from p_1 for n odd to the value given by Eq. 67 for n even, and approaches p_1 for large values of t_1 since $\alpha < 1$ because $c_1/c_o > 1$. The limiting particle velocity from both Eqs. 68 and 71 is:

$$\dot{u}(y, \infty) = \frac{p_1}{\rho c_o} \quad \ldots\ldots\ldots\ldots\ldots\ldots (72)$$

Thus, the solution for values of t much larger than t_1 corresponds to the final pressure p_1 throughout with no memory of the initial pressure p_o as far as stress and velocity distributions are concerned.

When $c_1 \to c_o$ (purely elastic material) one obtains $c_1/c_o \to 1$, $\alpha \to 0$ and $\beta \to \infty$. The surface pressure reduction from p_o to p_1 never overtakes the original wave front and the boundary between Zones 0 and 1 is parallel to OA in Fig. 7.

When c_1 approaches ∞ while c_o is constant, β approaches 1 from above and α approaches 1 from below. The physical action approaches that of a medium which locks irrecoverably at the maximum strain reached at each point. As the limit $c_1 = \infty$ is approached, the zones in Fig. 7 collapse in the t-direction. Solving Eq. 66 for $\alpha^{n/2}$:

$$\lim_{c_1 \to \infty} \alpha^{n/2} = \lim_{c_1 \to \infty} \frac{t_1}{\beta \alpha t_n} = \frac{t_1}{t_n} \quad \ldots\ldots\ldots\ldots (73)$$

Substituting Eq. 73 in 67 and 68, one obtains for n even:

$$\dot{u}_n = \frac{1}{\rho c_o}\left[p_1 + \frac{t_1}{t_n}(p_o - p_1)\right] = \frac{I}{t_n \rho c_o} \quad \ldots\ldots\ldots\ldots (74)$$

and

$$\sigma_n = p_1 + \frac{t_1}{t_n}(p_o - p_1) \quad \ldots\ldots\ldots\ldots\ldots\ldots (75)$$

where:

$$I = p_1(t_n - t_1) + t_1 p_o \quad \ldots\ldots\ldots\ldots\ldots\ldots (76)$$

is the impulse per unit area exerted by the pressure on the surface. The above results Eqs. 74 and 75 are identical with those which may be derived by a direct analysis of the limiting case, based on the fact that the compacted mass moves

as a rigid body. The stress of Eq. 75 is the value directly behind the wave front as may be seen by reference to the zone pattern in Fig. 7, since at the front, zone numbers are always even.

Manipulating Eqs. 69 through 71 in a similar manner, for n odd:

$$\dot{u}_n = \frac{1}{\rho c_o}\left[p_1 - \frac{t_1}{t_n}(p_o - p_1)\right] \quad \ldots\ldots\ldots\ldots (77)$$

and

$$\sigma_n = p_1 \quad \ldots\ldots\ldots\ldots\ldots\ldots (78)$$

is obtained.

The values of $\dot{u}_n$ given by Eqs. 77 and 74 are identical. The value of σ_n given by Eq. 78 applies to the free surface since here the zone number is always odd.

For points not on the surface nor at the wave front, the value of σ_n is an odd or even zone value depending on the time. The fraction of the time when even values are in effect is equal to the distance from the surface to the point divided by the distance from the surface to the wave front. During the remainder of the time, odd zone values are extant. Thus, in the limit the stress fluctuates with infinite frequency at each intermediate point. By averaging the fluctuating stress at any point, it is seen that the actual value of the stress is:

$$\sigma(y, t) = \sigma_1 + \frac{y}{c_o t}\left[\sigma_1 + \frac{t_1}{t}(\sigma_o - \sigma_1)\right] \quad \ldots\ldots\ldots (79)$$

This result may also be derived by consideration of the equation of motion of the compacted mass.

The wave analysis of this section can be written in the following form:

$$\sigma(y, t) = F_1\left(t - \frac{y}{c_1}\right) + F_2\left(t + \frac{y}{c_1}\right) - F_2\left(t - \frac{y}{c_1}\right) \quad \ldots\ldots\ldots (80)$$

and

$$\dot{u}(y, t) = \frac{1}{\rho c_1}\left[F_1\left(t - \frac{y}{c_1}\right) - F_2\left(t + \frac{y}{c_1}\right) - F_2\left(t - \frac{y}{c_1}\right)\right] + p_o\left[\frac{1}{\rho c_o} - \frac{1}{\rho c_1}\right] \quad \ldots (81)$$

where

$$F_1(t) = p(t) \quad \ldots\ldots\ldots\ldots\ldots\ldots (82)$$

$$F_2(t) = \sum_{n=1}^{\infty} f_n(t) \quad \ldots\ldots\ldots\ldots\ldots\ldots (83)$$

and

$$f_n(t) = \begin{cases} 0 & t < t_1/\alpha^n \\ \alpha^n(p_o - p_1) & t > t_1/\alpha^n \end{cases} \quad \ldots\ldots\ldots\ldots (84)$$

as can be checked by direct substitution. Eqs. 80 and 81 are valid in the zone $0 < y < c_o\, t$. This form of the solution may be constructed by considering the stress and velocity in each new zone of Fig. 7 to be made up of values from the previous zone plus a contribution f_n due to the wave traveling upwards or downwards at velocity c_1. The term $F_2\left(t + \frac{y}{c_1}\right)$ represents the sum of all waves traveling upwards. The term $F_2\left(t - \frac{y}{c_1}\right)$ represents contributions of all waves traveling downwards. The term $F_1\left(t - \frac{y}{c_1}\right)$ contributes the original wave of pressure p_o and the reduction starting at t_1, Fig. 7.

RESPONSE TO CONTINUOUSLY VARIABLE SURFACE PRESSURE

Consider a decreasing surface pressure such as shown in Fig. 8. The pressure p(t) rises from zero to p_o at t = 0. For $t > 0$, the pressure decays continuously to zero. This surface pressure may be regarded as a step wave of amplitude p_o plus a series of infinitesimal, negative steps, $dp = \frac{dp}{dt}\, dt$. Each pressure change, dp, may therefore be treated in the manner of the single pressure change from p_o to p_1 of the previous section. Superimposing all the effects will yield the complete solution for the variable pressure p.

When the surface pressure shown in Fig. 8 is applied to the boundary of a semi-infinite type II locking medium, there will result first a term like F_1 in Eq. 80 of the form:

$$G_1\left(t - \frac{z}{c_1}\right) = p\left(t - \frac{z}{c_1}\right) \quad \ldots\ldots\ldots\ldots\ldots\ldots (85)$$

There will also be a series of contributions life F_2 in Eq. 80. Each term of this series will be again a series like Eq. 83. For a given time, t, the sum of contributions of the form $f_1(t)$, Eq. 84, will be

$$g_1(t) = \alpha \int_0^{\alpha t} \left(-\frac{dp}{dt}\right) dt \quad \ldots\ldots\ldots\ldots\ldots\ldots (86)$$

Eq. 86 represents the integration over all times for which contributions of the form $f_1(t)$ are different from zero. Eq. 86 may be written as:

$$g_1(t) = \alpha\, p_d(\alpha\, t) \quad \ldots\ldots\ldots\ldots\ldots\ldots (87)$$

where $p_d(t)$ is a pressure reduction function defined by

$$p_d(t) = p_o - p(t) \quad \ldots\ldots\ldots\ldots\ldots\ldots (88)$$

The value of p_d is shown graphically in Fig. 8.

In a similar manner, contributions of the form $f_n(t)$, Eq. 84, may be integrated in the present case to yield

$$g_n(t) = \alpha^n p_d(\alpha^n t) \quad \ldots\ldots\ldots\ldots\ldots\ldots (89)$$

A reflected pressure function $p_r(t)$ may now be defined which corresponds to $F_2(t)$, Eq. 83:

$$p_r(t) = \sum_{n=1}^{\infty} g_n(t) \quad \ldots\ldots\ldots\ldots\ldots\ldots (90)$$

The typical form of p_r(tP is shown in Fig. 9.

The complete solution for the stress in the present case has a form similar to Eq. 80:

$$\sigma(y, t) = p\left(t - \frac{y}{c_1}\right) + p_r\left(t + \frac{y}{c_1}\right) - p_r\left(t - \frac{y}{c_1}\right) \quad \ldots\ldots\ldots\ldots (91)$$

The velocity, in the present case, is given by an equation of the form of Eq. 81:

$$\dot{u}(y, t) = \frac{1}{\rho c_1}\left[p\left(t - \frac{y}{c_1}\right) - p_r\left(t + \frac{y}{c_1}\right) - p_r\left(t - \frac{y}{c_1}\right)\right]$$

$$+ p_o\left[\frac{1}{\rho c_o} - \frac{1}{\rho c_1}\right] \quad \ldots\ldots\ldots\ldots\ldots\ldots (92)$$

Eqs. 91 and 92 give the stress and velocity for any y and t in the range $0 < y < c_o t$. The strains at any y and t may be derived from the stress history at the point in question.

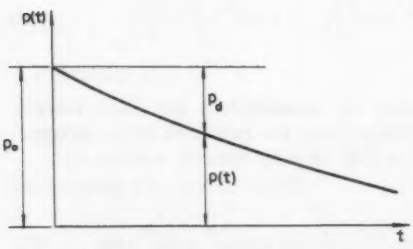

FIG. 8.—CONTINUOUSLY VARIABLE SURFACE PRESSURE

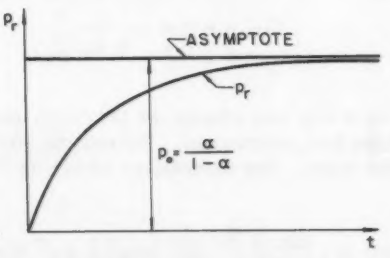

FIG. 9.—TYPICAL REFLECTION PRESSURE FUNCTION, Pr

It is of interest to note the long time solution for any case in which the surface pressure p(t) decays to zero in a finite time. In such cases, the pressure reduction p_d rises to p_o in a finite time and the reflected pressure is asymptotic to $p_o\left(\frac{\alpha}{1-\alpha}\right)$ as shown in Fig. 9. Hence,

$$\sigma(y, \infty) = 0 + p_r(\infty) - p_r(\infty) = 0 \quad \ldots\ldots\ldots\ldots (93)$$

and

$$\dot{u}(y, \infty) = \frac{1}{\rho c_1}\left[0 - \frac{2\alpha}{1-\alpha} p_o\right] + p_o\left[\frac{1}{\rho c_o} - \frac{1}{\rho c_1}\right] = 0 \quad \ldots\ldots (94)$$

Eqs. 93 and 94 indicate that the velocity and stress at every point approach zero for long times. This is to be expected a dissipative material.

LIMITING CASE, $c_1 \to \infty$

The limiting case $c_1 \to \infty$ represents a material which exhibits no recovery on unloading. The formulas for stress and particle velocity, Eqs. 91 and 92, reduce to simple forms in this case.

By use of Eqs. 88, 89 the particle velocity, Eq. 92, is in general

$$\dot{u}(y,t) = \frac{1-\alpha}{\rho c_o(t+\alpha)}\left\{p\left(t - \frac{y(1-\alpha)}{c_o(1+\alpha)}\right) - \sum_{n=1}^{\infty}\alpha^n\left[p_o - p\left\{\alpha^n\left[t + \frac{y(1-\alpha)}{c_o(1+\alpha)}\right]\right\}\right] -$$

$$- \sum_{n=1}^{\infty}\alpha^n\left[p_o - p\left\{\alpha^n\left[t - \frac{y(1-\alpha)}{c_o(1+\alpha)}\right]\right\}\right]\Bigg\} + p_o\left[\frac{1}{\rho c_o} - \frac{1-\alpha}{\rho c_o(1+\alpha)}\right] \ldots (95)$$

where c_1 has been replaced by $c_o\left(\frac{1+\alpha}{1-\alpha}\right)$ from Eq. 62.

When $c_1 \to \infty$, then $\alpha \to 1$ from below and $(1 - \alpha) \to 0$ and $(1 + \alpha) \to 2$. The terms of Eq. 95 which are not zero in the limit, are the two summations and the term $p_o/\rho c_o$. Hence

$$\lim_{\substack{c_1 \to \infty \\ \alpha \to 1}} \dot{u} = \lim_{\alpha \to 1} -\frac{1}{\rho c_o}\sum_{n=1}^{\infty}(1-\alpha)\alpha^n\left[p_o - p(\alpha^n t)\right] + \frac{p_o}{\rho c_o} \quad \ldots (96)$$

As $\alpha \to 1$, the change in the term under the summation, for each integer change in n, decreases. Therefore, the sum may be replaced by an integral in the limit. The summation involving p in Eq. 96 may then be written as

$$S = \lim_{\alpha \to 1}\sum_{n=1}^{\infty}(1-\alpha)\alpha^n p(\alpha^n t) = \lim_{\alpha \to 1}\int_0^{\infty}(1-\alpha)\alpha^n p(\alpha^n t)dn \quad \ldots (97)$$

Changing the variable of integration from n to ξ where

$$\xi = t\,\alpha^n \quad \ldots\ldots\ldots\ldots\ldots\ldots (98)$$

the sum S becomes

$$S = \lim_{\alpha \to 1} -\frac{1}{t}\int_0^t \frac{(1-\alpha)}{\log \alpha} p(\xi)\, d\xi = \frac{1}{t}\int_0^t p(\xi)\, d\xi = \frac{I(t)}{t} \quad \ldots\ldots\ldots (99)$$

where I(t) is the impulse per unit area exerted by the surface pressure during the interval zero to t. The sum containing p_o in Eq. 97 is evaluated by replacing p(t) by p_o in Eq. 99. Using Eq. 99 in Eq. 97 yields the final result:

$$\lim_{c_1 \to \infty} \dot{u} = \frac{I(t)}{\rho\, c_o t} \qquad 0 < y < c_o\, t \quad \ldots\ldots\ldots\ldots (100)$$

Eq. 100 shows that the entire mass from the surface to the wave front at $y = c_o\, t$ moves as a rigid body, since the particle velocity is independent of y.

The stress $\sigma(y, t)$ given by Eq. 91, in general, may be analyzed in a similar fashion to the particle velocity in the limiting case $c_1 \to \infty$. tThe equation analogous to Eq. 96 is:

$$\lim_{c_1 \to \infty} \sigma(y, t) = \lim_{\alpha \to 1} p(t) - \sum_{n=0}^{\infty} \alpha^n \left[p(\alpha^n t'') - p(\alpha^n t') \right] \ldots (101)$$

where

$$t' = t - \frac{y(1-\alpha)}{2\, c_o} \text{ and } t'' = t + \frac{y(1-\alpha)}{2\, c_o} \quad \ldots\ldots\ldots\ldots (102)$$

Replacing the sums by integrals and integrating in a similar manner as above, yields

$$\lim_{c_1 \to \infty} \sigma(y, t) = \lim_{\alpha \to 1} \left\{ p(t) - \frac{1}{1-\alpha} \left[\frac{I(t'')}{t''} - \frac{I(t')}{t'} \right] \right\} \ldots\ldots (103)$$

From Eq. 102

$$\frac{1}{1-\alpha} = \frac{y}{c_o (t'' - t')} \quad \ldots\ldots\ldots\ldots\ldots (104)$$

Substituting Eq. 104 into 103:

$$\lim_{c_1 \to \infty} \sigma(y, t) = \lim_{\alpha \to 1} \left\{ p(t) - \frac{y}{c_o (t'' - t')} \left[\frac{I(t'')}{t''} - \frac{I(t')}{t'} \right] \right\} \ldots (105)$$

Now as $\alpha \to 1$, the values of t'' and t' both approach t, so that Eq. 105 becomes

$$\lim_{c_1 \to \infty} \sigma(y, t) = p(t) - \frac{y}{c_o} \frac{d}{dt}\left[\frac{I(t)}{t}\right] \quad \ldots\ldots\ldots (106)$$

The result of Eq. 106 may be written in terms of the particle acceleration $\ddot{u}$ by using Eq. 100:

$$\lim_{c_1 \to \infty} \sigma(y, t) = p(t) - y \rho \ddot{u} \quad \ldots\ldots\ldots\ldots (107)$$

The stress at the surface y = 0 is

$$\sigma(0, t) = p(t) \quad \ldots\ldots\ldots\ldots\ldots (108)$$

and at the wave front:

$$\sigma(c_o t, t) = \frac{I(t)}{t} \quad \ldots\ldots\ldots\ldots\ldots (109)$$

The results given by Eqs. 100, 107 and 109 may also be derived directly by writing the equations of motion of the compacted mass which moves as a rigid body when $c_1 = \infty$.

NUMERICAL EXAMPLES

Let the surface pressure p(t) be given by

$$p(t) = p_o e^{-\theta t} \quad \ldots\ldots\ldots\ldots\ldots (110)$$

where p_o is the initial peak intensity of the pressure and θ is a time constant, with the following values.

$$p_o = 100 \text{ psi}$$

and

$$\theta = 20 \text{ sec}^{-1}$$

The properties of the medium are as follows:

$$\rho = \frac{100}{32.2} \text{ slugs/ft}^3$$

and

$$c_o = 1{,}000 \text{ fps.}$$

Particle velocities and stresses at the surface and at the wave front are calculated for the following two cases.

Case a: Propagation Velocity at Unloading, c_i = 2000 fp s (Partial Elastic Recovery).—By Eqs. 110 and 88

$$p_d(t) = p_o\left(1 - e^{-\theta t}\right). \quad \ldots\ldots\ldots\ldots\ldots\ldots \quad (111)$$

and by Eqs. 89 and 90

$$p_r(t) = p_o \sum_{n=1}^{\infty} \alpha^n \left(1 - e^{\theta\, \alpha^n\, t}\right) \quad \ldots\ldots\ldots\ldots \quad (112)$$

where α is given by Eq. 62.

Using the formulas of Eqs. 91 and 92 the stress σ and the particle velocity $\dot{u}$ can be computed at any point and time after the two functions p(t), Eq. 110, and p_r, Eq. 112, have been tabulated. Fig. 10(a) shows p(t) which is also the stress at surface and $\sigma(c_o\, t, t)$, the stress at the front. Fig. 10(b) gives the particle velocities at the surface $\dot{u}(0,t)$ and at the front, $\dot{u}(c_o\, t, t)$.

Case b: Propagation Velocity at Unloading, $c_i = \infty$ (No Elastic Recovery).—By Eqs. 110, 108 and 109 the stress at the front is given by

$$\sigma_1(c_o\, t, t) = \frac{p_o}{\theta\, t}\left(1 - e^{-\theta t}\right) \quad \ldots\ldots\ldots\ldots \quad (113)$$

and by Eq. 100 the particle velocity anywhere within the locked layers is given by

$$\dot{u}_1 = \frac{\sigma(c\, t, t)}{\rho_o\, c_o} \quad \ldots\ldots\ldots\ldots\ldots\ldots \quad (114)$$

these values are also plotted in Fig. 10

It is noted that the particle velocity $\dot{u}_1$ lies between the velocities $\dot{u}(c_o\, t, t)$ and $\dot{u}(0, t)$ and consequently $\sigma_1 < \sigma(c_o\, t, t)$, indicating that the material with no recovery gives an average value of particle velocities and a lower bound for the peak stress. In both instances particle velocities and stresses decay to zero as the time approaches infinity, while permanent strains and displacements remain.

NOMENCLATURE

The following nomenclature is used in the paper:

c_o , c_1	= acoustic velocities;
ϵ_o , ϵ_c	= elastic, locking strain (Fig. 1);
ρ_i , ρ_o , ρ_c	= initial, elastic, locked density (Fig. 1);
σ_o , σ_z	= locking stress, stress at wave front;
y, z, u	= ordinates of the locked layer (Fig. 2);
u_o , $\dot{u}_o$	= elastic particle displacement and velocity during a constant stress σ_o;

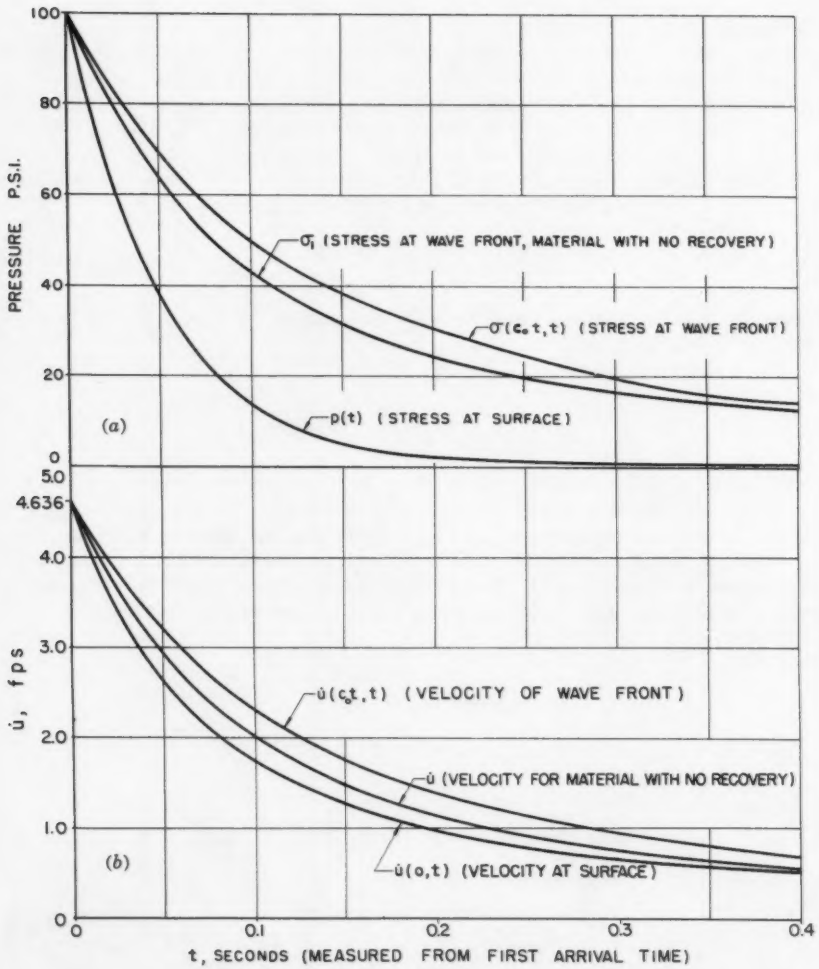

FIG. 10.—NUMERICAL RESULTS, TYPE II MEDIUM, c_o = 100 fps

z_r , u_r = ordinates relative to the medium ahead of the wave front;

t = time;

$p(t)$ = decaying pressure pulse;

p_o = initial value of $p(t)$;

p_{cr} = critical initial pressure;

P = non-dimensional pressure;

$\sum$ = non-dimensional stress;

Z, U = non-dimensional ordinates;

τ = non-dimensional time;

E_o = elastic modulus during initial loading (Fig. 5);

E_1 = elastic modulus during unloading and reloading (Fig. 5);

n = a positive integer;

I = impulse of $p(t)$;

$\alpha = \dfrac{\left(c_o/c_o\right) - 1}{\left(c_1/c_o\right) + 1}$;

$\beta = \dfrac{\left(c_1/c_o\right)}{\left(c_1/c_o\right) - 1}$; and

θ = time constant.

Journal of the
ENGINEERING MECHANICS DIVISION
Proceedings of the American Society of Civil Engineers

COMMENTARY ON PLASTIC DESIGN IN STEEL: CONNECTIONS

Progress Report No. 6 of the Joint WRC-ASCE Committee on Plasticity Related to Design

FOREWORD

This paper is the sixth in a series of reports on Plastic Design emanating from a Joint Committee of the Welding Research Council and the American Society of Civil Engineers. Reference should be made to Progress Report No. 1 (which appeared in the July, 1959 issue of the Journal of the Engineering Mechanics Division of ASCE) for such items as the Foreword, Synopsis, Definitions, and Nomenclature. For information, the complete Table of Contents appears at the beginning of this Progress Report. Chapter 8, entitled "Connections," comprises the present paper.

The Joint Committee has approved the publication of this information with the strong recommendation that it be read carefully by all structural engineers.

Note.—Discussion open until September 1, 1960. Separate Discussions should be submitted for the individual papers in this symposium. To extend the closing date one month, a written request must be filed with the Executive Secretary, ASCE. This paper is part of the copyrighted Journal of the Engineering Mechanics Division, Proceedings of the American Society of Civil Engineers, Vol. 86, No. EM 2, April, 1960.

COMMENTARY ON PLASTIC DESIGN IN STEEL

TABLE OF CONTENTS

1. INTRODUCTION
   - 1.1 Structural Design
   - 1.2 Plasticity and Design—Some Advantages and Limitations

2. BASIC PRINCIPLES
   - 2.1 Behavior of Material and Structural Elements
   - 2.2 Plastic Theory

3. ANALYSIS AND DESIGN
   - 3.1 Assumptions
   - 3.2 Statical Method of Analysis
   - 3.3 Mechanism Method of Analysis
   - 3.4 Other Methods

4. GENERAL PROVISIONS
   - 4.1 Introduction
   - 4.2 Types of Construction
   - 4.3 Material
   - 4.4 Structural Ductility
   - 4.5 Yield Stress Level
   - 4.6 Plastic Moment
   - 4.7 Loads
   - 4.8 Load Factors

5. VERIFICATION OF PLASTIC THEORY
   - 5.1 Basic Concepts
   - 5.2 Continuous Beams
   - 5.3 Frames

6. ADDITIONAL DESIGN CONSIDERATIONS
   - 6.1 Shear Force
   - 6.2 Local Buckling
   - 6.3 Lateral Buckling
   - 6.4 Variable Repeated Loading

7. COMPRESSION MEMBERS
   - 7.1 Introduction
   - 7.2 Reduction of the Plastic Moment Due to Axial Thrust
   - 7.3 Moment-Carrying Capacity of Columns
   - 7.4 Rotation Capacity
   - 7.5 The Influence of Lateral-Torsional Buckling
   - 7.6 Frame Stability

8. CONNECTIONS
   - 8.1 Straight Corner Connections
   - 8.2 Haunches
   - 8.3 Tapered Haunches
   - 8.4 Curved Haunches
   - 8.5 Beam-to-Column Connections
   - 8.6 Details with Regard to Welding
   - 8.7 Details with Regard to Bolting

9. DEFLECTIONS
   - 9.1 Introduction
   - 9.2 Deflections in the Elastic Range
   - 9.3 Deflections in the Plastic Range
   - 9.4 Deflection at Ultimate Load
   - 9.5 Step-by-Step Calculations
   - 9.6 Approximate Deflection at Working Load
   - 9.7 Deflections as a Limitation
   - 9.8 Rotation Requirements

Chapter 8

CONNECTIONS

INTRODUCTION

Connections play a key role in assuring that a structure can reach the computed ultimate load. Since connections frequently are located at points of maximum shear and moment, the details must assure the performance that is assumed in design. The principal requirements for connections are:

1. Sufficient strength.
2. Adequate rotation capacity.
3. Overall stiffness for maintaining the location of all structural units relative to each other.
4. Economical fabrication.

The various types of connections which will be discussed and which are typical of those that might be encountered in steel framed structures are designated

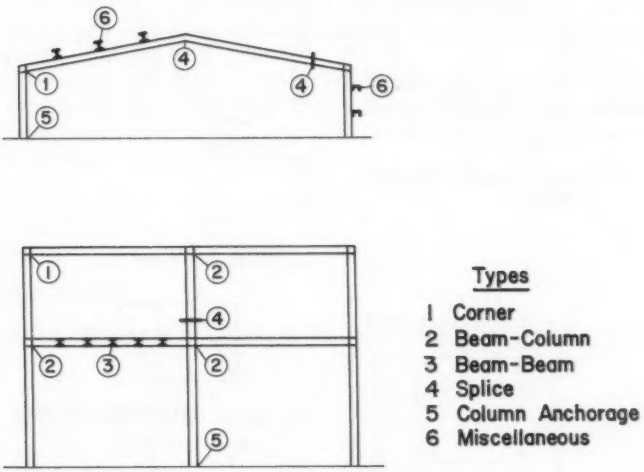

FIG. 8.1.—TYPES OF CONNECTIONS

in Fig. 8.1. These include corner connections (straight and haunched), beam-to-column connections, beam-to-beam connections, splices, column anchorages, and miscellaneous connections (purlins, girts, and bracing).

Primary attention is given herein to corner connections and beam-to-column connections. Methods of analysis are based on assumptions of stress distribution at ultimate load which satisfy equilibrium but do not violate the plasticity condition. Solutions thus constitute lower bounds to connection capacity. The same principles would be applicable, however, for the analysis of other connection types.

8.1 STRAIGHT CORNER CONNECTIONS

Straight corner connections are formed by directly joining two rolled sections. Straight corner connections in which the rolled sections are joined at right angles (as at 1 in Fig. 8.1) are sometimes called square corner connections. Studies of the theory, design, and behavior of square corner connections may be found in Refs. 8.1 to 8.6. The basic principles of the theory of connections will be illustrated by considering an unreinforced square corner connection. It is more critical than a connection in which the members do not join at right angles. Fig. 8.2(a) shows the moment diagram for a typical rectangular frame loaded with a uniformly distributed load. A typical unreinforced

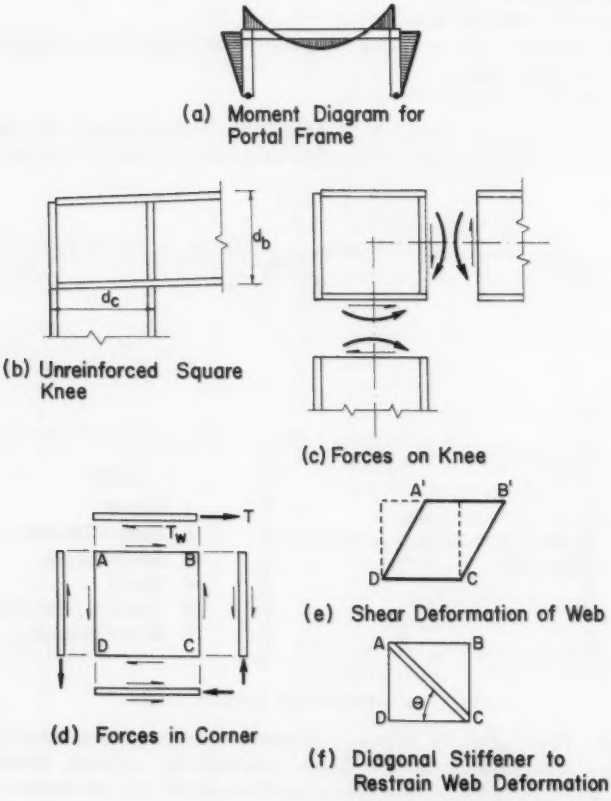

FIG. 8.2.—STRAIGHT CORNER CONNECTIONS

corner connection is sketched in Fig. 8.2(b). The moment, thrust, and shear acting on the connection are depicted in Fig. 8.2(c).

In arriving at a simple analysis of the forces in a knee it is assumed that normal stresses caused by bending moment and thrust are all carried in the flanges and that shear stresses are all carried by the web. In Fig. 8.2(d), the action of the applied forces on the parts of the corner and of the parts on each other are represented by arrows. The tensile force in the outer flange of the

beam is carried into the web in shear along line AB. In a like manner, the tensile force in the outer flange of the column is carried through the end plate into the web as a shear along line AD. In each case, the tensile stress in the flange is assumed to be linearly reduced from σ_y at the edge of the corner (B or D) to zero at the external corner (A).

The prolongation of the inner flange of the beam carries two external forces: the shear of the column and the normal force due to bending and thrust in the beam. The resultant of these two forces is carried into the corner as a shear along line DC. A similar pair of force components exerted on the vertical stiffener causes shear along line BC of the web.

In considering the effect of the forces on the equilibrium and behavior of the corner connection, it is rather obvious that an unsatisfactory condition would exist if there were insufficient material to carry the forces without buckling or general yielding. Assuming that the horizontal rolled section continues through the knee, its flanges AB and CD of Fig. 8.2(d) are sufficient to resist any forces carried in the members outside the knee and are selected to preclude local flange buckling. The end plate AD should have the same area as the flange of the column. The vertical stiffener BC must have sufficient area to carry the column compression flange force into the beam web. In all cases the welds must be sufficient to transmit the required shear or normal force. Study of the square web panel reveals that the shear forces would tend to deform the panel as shown in Fig. 8.2(e).

Consideration of the equilibrium of the horizontal forces on the portion of the outer flange between A and B in Fig. 8.2(d) will give an expression for the web thickness required to resist shear. According to the approximation stated earlier the force in the flange is given by

$$T \cong M_p/d_b$$

where

d_b = depth of beam

The maximum web shear resisting force between A and B must not exceed

$$T_w = \tau_y \, w \, d_c$$

where

w = thickness of web

d_c = depth of column

Equating the shear and flange forces gives the required web thickness w:

$$w_r = \frac{M_p}{\tau_y \, d_b \, d_c}$$

According to the Mises yield criterion the limiting shear yield stress τ_y equals $\sigma_y/\sqrt{3}$. Using this criterion, the required web thickness becomes

$$w_r = \frac{\sqrt{3} \; M_p}{\sigma_y \, d_b \, d_c} \quad \ldots\ldots\ldots\ldots\ldots\ldots (8.1)$$

This resulting expression for w_r is similar to that obtained in Ref. 8.1. It has been shown that the use of more exact analysis does not alter the results of calculations substantially (8.1).

For most wide-flange sections the web thickness will be less than w_r, in which case reinforcement is required. This may take the form of a doubler plate which increases the total thickness of the web to the required amount. However, it is nearly always more practical to provide a symmetrical pair of diagonal stiffeners. Diagonal stiffeners act somewhat like the diagonals of a truss panel in preventing shear deformation. Fig. 8.2(f) shows diagonal stiffeners between corners A and C of the web. The diagonal stiffeners are able to resist part of the normal stresses in the flanges.

By considering equilibrium of the forces on the top flange, the required area of the diagonal stiffeners may be obtained. The flange force T must be resisted by the web shear T_w and the horizontal component of the diagonal stiffener force T_s. The magnitude of the latter component is given by

$$T_s = \sigma_y A_s \cos \theta$$

where

A_s = area of a symmetrical pair of diagonal stiffeners

θ = angle of diagonal stiffeners with the horizontal ($\tan \theta = d_b/d_c$)

Noting that T must equal $T_w + T_s$ the stiffener area is found as

$$A_s = \frac{1}{\cos \theta} \left[\frac{M_p}{\sigma_y d_b} - \frac{w d_c}{\sqrt{3}} \right] \quad \ldots\ldots\ldots\ldots \quad (8.2)$$

The actual performance of straight corner connections has been studied in several tests. In Fig. 8.3 are shown the results of tests on four straight connections, A, K, L, and M made from 8B13 members [8.1]. The moment-rotation curves of the connections are compared with the moment-rotation curve for an 8B13 beam as shown by the heavy line. Of major interest are strength, stiffness, and rotation capacity. Each connection reached a maximum moment greater than that of an 8B13 beam. The rotation of each of the knees was great enough to be considered adequate to allow a structure to form a mechanism. The initial stiffness of the knees was approximately the same as that of the rolled beam, but larger rotations occurred in the knees at a lower moment because of residual stresses. However the larger rotations were not severe enough to impair the practical effectiveness of the connections.

Results of five additional tests on straight corner connections are given in Fig. 8.4. These tests were performed on knees joining several sizes of wide-flange beams [8.4]. The shaded zone at $M_h/M_y = M_p$ is so marked to depict the range of spread in shape factor of the five wide flange shapes that were tested. These tests confirm that these knees also satisfied the requirements for use in plastic design.

STRAIGHT CORNER CONNECTIONS

Web Thickness Required:

$$w_r = \sqrt{3}\, M_p / (\sigma_y\, d_b\, d_c) \quad \ldots\ldots\ldots\ldots \quad (8.1)$$

Web Stiffening:

If the web of a connection is deficient in thickness, it may be reinforced by doubler plates to meet the requirements of Eq. 8.1 or by diagonal stiffeners welded to the flanges and to the web. The area of a symmetrical pair of diagonal stiffeners should be

$$A_s = \frac{1}{\cos\theta}\left[\frac{M_p}{\sigma_y\, d_b} - \frac{w\, d_c}{\sqrt{3}}\right] \quad \ldots\ldots\ldots \quad (8.2)$$

where

θ = arc tan d_b/d_c

8.2 HAUNCHES

Haunches of either the tapered or the curved type are sometimes used to achieve a pleasing appearance. Their use in elastic design makes it possible to adapt the section of the haunch to follow more closely the shape of the moment diagram, furnishing approximately the resisting moment required at a number of given sections with resulting economies of material. Similarly, in plastic design the use of haunches also makes possible a reduction in size of the main member, which may mean the difference between using a built-up member and using a more economical rolled shape. Although the haunch will permit a reduction in main member size, it will be costly to fabricate and thus may offset some of the savings that will be realized by using the smaller main member.

Tests of haunched connections designed by methods intended primarily for elastic structures revealed that the connections exhibited good strength, but that some lacked sufficient rotation capacity. The lack of rotation capacity was attributed to premature lateral buckling [8.1]. Recently developed methods of analysis confirmed by tests show that plastic hinges can function properly in the haunch if adequate provision is made to prevent such buckling [8.7].

The effect of haunches on the analysis of a frame is to increase the number of sections at which plastic hinges may form. However, the methods of analysis are unchanged. Fig. 8.5 gives the results of a mechanism analysis of a portal frame with haunches. The correct solution depends on the loading and geometry of the structure. For the given geometry and loading the correct solution would be Mechanism 4 (Fig. 8.5(e)) and the resulting moment diagram (Fig. 8.5(g)) shows that the plasticity condition is not violated. The required plastic hinge moment M_p of the main members is smaller as a result of using the haunches. At the same time, it is necessary that the haunch be able to carry a moment M_h which is greater than this M_p-value. From the final moment diagram (Fig. 8.5(g)) the moment, thrust, and shear at any cross section of the frame may be determined for purposes of design.

8.3 TAPERED HAUNCHES

A sketch of a typical tapered haunch is given in Fig. 8.6. The forces to be considered in the design of the haunch are the moment, thrust, and shear at Section 1 where the rolled section is joined to the haunch. These would be determined from an analysis of the complete structure. (For example see Fig. 8.5).

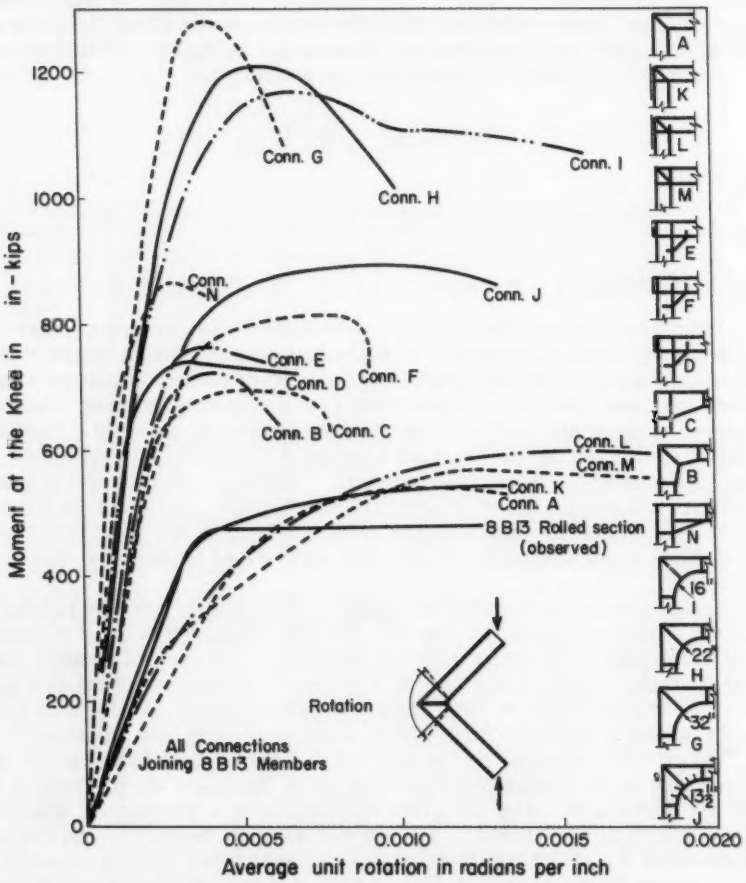

FIG. 8.3.—MOMENT-ROTATION CURVES OF CONNECTIONS

Three main problems must be considered in the design of tapered haunches. These are: (1) resistance to bending in the tapered portion of the haunch, (2) resistance to local and lateral buckling, and (3) shear stresses in the web and flange forces in and around the corner panel BDFE (Fig. 8.6).

In analyzing the tapered portion of the haunch for resistance to bending, cross sections perpendicular to the layout line of the structure may be considered. The web thickness and flange width of the haunch are usually made

equal to those of the adjoining rolled section. This insures that the web is able to carry at least as much shear and axial force as the web of the rolled section. Changes in the resistance to bending moment of the haunch may be controlled, therefore, by the thickness of the flanges and by the depth of the haunch. The outer flange is usually parallel to the layout line and the inner flange makes an angle of taper β with the layout line, thus defining the depth of the haunch at any point. At any distance x along the haunch, the moment of resistance of the cross section perpendicular to the layout line must equal or exceed the applied moment at that section determined from the plastic analysis.

The plastic moment of resistance of any cross section is given by (8.7):

$$M_{px} = \sigma_y Z_x \quad \ldots\ldots\ldots\ldots\ldots\ldots \quad (8.3)$$

where Z_x is the plastic modulus at the particular section. It has been shown that if the plastic moment of resistance is adequate at the rolled section (sec-

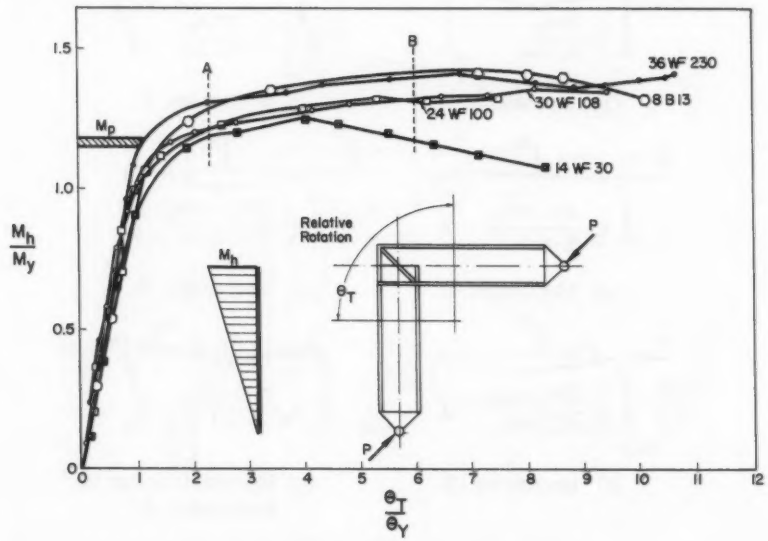

FIG. 8.4.—MOMENT-ROTATION CURVES FOR SIZE-EFFECT SERIES OF CONNECTIONS

tion 1, Fig. 8.6) and at the re-entrant corner (section 2, Fig. 8.6), there will be no necessity of checking at other sections along the haunch (8.7).

In proportioning tapered haunches, it is desirable that the flanges have the same size as the nominal dimensions of the adjoining rolled section. In this case, the flange area presented on a cross section perpendicular to the layout line would be different for a sloping flange at angle β than for a flange parallel to the layout line. The effective cross section would be unsymmetrical with respect to its major axis with resulting complexities in the calculation of the plastic modulus Z.

In Ref. 8.7, a somewhat simplified analysis is suggested to reduce the complexities of computations. As shown in Fig. 8.6, the stress in the sloping compression flange is assumed to act in the direction of the flange. To calculate the moment in the desired direction, the component of flange force parallel to

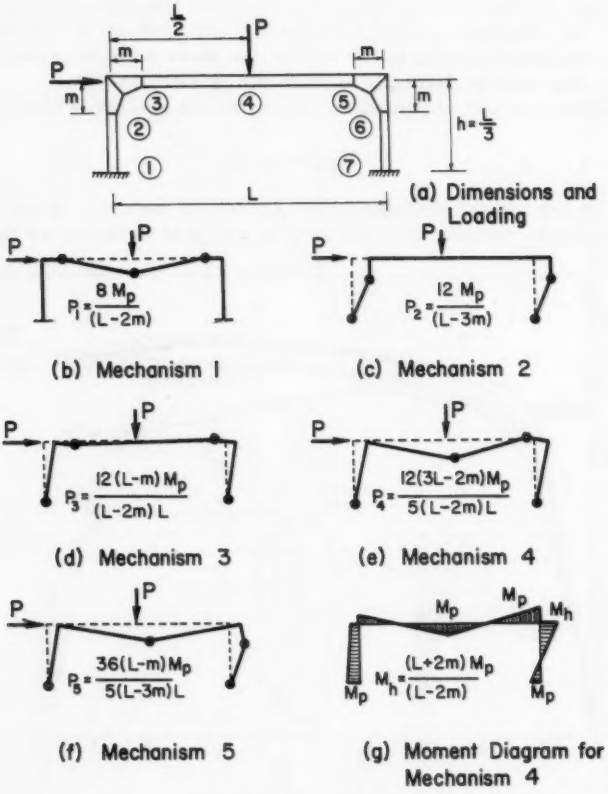

FIG. 8.5.—ILLUSTRATIVE EXAMPLE—ANALYSIS OF PORTAL FRAME WITH HAUNCHES (h = L/3)

the layout line must be obtained by multiplying the flange force by cos β. By increasing the thickness of the sloping flange, the components of flange force in each flange may be made equal, thus providing effective symmetry to the cross section. The necessary thickness of the sloping flange is

$$t_c = t_t / \cos \beta \quad \ldots\ldots\ldots\ldots\ldots\ldots \quad (8.4)$$

where

t_c = thickness of sloping (compression) flange plate

t_t = thickness of straight (tension) flange plate

β = angle of sloping flange with layout line

The plastic modulus at any section will be

$$Z_x = b\,t_t(d_x - t_t) + \frac{w}{4}\,(d_x - 2\,t_t)^2 \quad \ldots\ldots\ldots\ldots \quad (8.5)$$

where

b = width of flange

d_x = depth of haunch at any section x

w = web thickness

In cases where the angle β is less than 20°, the required increase in thickness suggested in Eq. 8.4 would not exceed 6%. Most practical design procedures would neglect such a difference. For all practical purposes, both

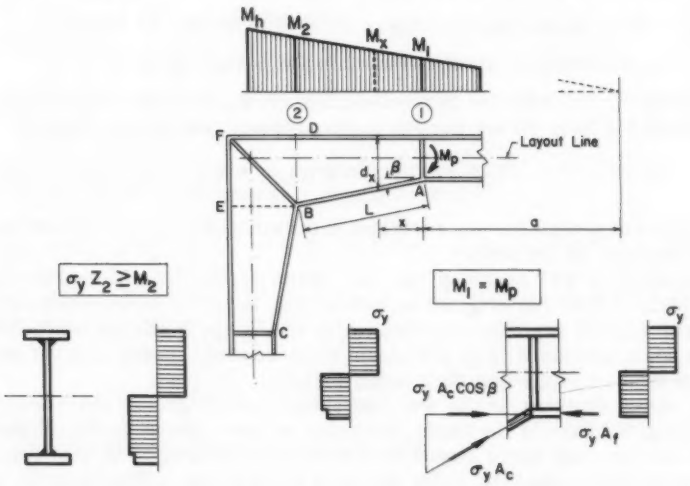

FIG. 8.6.—FORCES ON TAPERED KNEE

flanges should probably be made equal and still use the assumption that the cross section is symmetrical and that its centroid is at mid-depth.

The resistance to local buckling of the flanges of tapered haunches may be assured by adhering to the recommendations of Chapter 6.

Lateral buckling of tapered haunches depends on the slenderness of the compression flange and on the extent to which the flange is yielded and strain hardened. It is assumed that positive lateral support of the inner flange will be provided at points A, B, and C. (Fig. 8.6). Since the web provides restraint against buckling of the flange about its weak axis, the flange must buckle in its strong direction between points of support.

A conservative approximate expression for the critical buckling length of the compression flange has been obtained [8.7] by using the tangent modulus

buckling concept (8.8,8.14). It is assumed that the compression flange is uniformly stressed to σ_y, that the strain in the flange just reaches ϵ_{st}, and that the flange buckles as a pin-ended column between points of lateral bracing. These assumptions result in a critical slenderness of:

$$(L_{cr}/r_x)^2 = \pi^2 \, E_{st}/\sigma_y \quad \ldots\ldots\ldots\ldots\ldots \quad (8.6)$$

which when solved for L_{cr} gives:

$$L_{cr} = b\,\pi\sqrt{\frac{E_{st}}{12\,\sigma_y}} \quad \ldots\ldots\ldots\ldots\ldots \quad (8.7)$$

where

L_{cr} = length of flange

b = width of flange

r_x = radius of gyration of flange = $b/\sqrt{12}$

E_{st} = strain hardening modulus of steel (900 ksi for A7 steel)

σ_y = yield stress of steel assumed in the design (33 ksi)

By substituting the material properties, E_{st} and σ_y, the following critical length is obtained for fully strain-hardened compression flanges of A7 steel:

$$L_{cr} = 4.8\,b \quad \ldots\ldots\ldots\ldots\ldots \quad (8.8)$$

This expression neglects any restraint to buckling offered by adjacent portions of the flange or by the web.

Frequently it will be found that L_{cr} given by Eq. 8.8 will be less than the value obtained from the original haunch layout. In such a case, additional points of lateral support could be provided. Also the flange thickness or the depth of the haunch at Section 2 (Fig. 8.6) could be increased. Reference 8.7 suggests methods for accomplishing such modifications.

The shear stresses in the web and flange forces around the corner panel BDFE (Fig. 8.6) are of the same character as those shown in Fig. 8.2(d) for a square corner, and would result in deformation similar to that in Fig. 8.2(e) when the forces exceed the shear strength of the panel. The problem may be examined in more general form with the aid of the sketch of a haunched knee of a gable bent shown in Fig. 8.7. In this knee, the forces on the panel BDFE are to be determined. For the most severe loading, the cross sections BD and BE will be fully yielded and the total area of the flanges at these sections will be stressed to σ_y. At the re-entrant corner B, the inner flanges will have an unbalanced component of force in the direction of BF in the absence of a web stiffener. This unbalanced component of flange force would have to be carried by the web. The web could be fully yielded due to bending stresses at point B, so it is advisable to neglect the carrying capacity of the web and furnish a symmetrical pair of diagonal stiffeners along FB.

At the outer corner F, the situation is slightly different because part of the flange force could be carried by shear in the web along lines EF and DF thus reducing the components of flange force to be carried by the diagonal stiffeners at F. For this reason, the selection of diagonal stiffeners will usually be governed by equilibrium at the re-entrant corner B.

The maximum possible forces in the two flanges and in the diagonal stiffener at corner B are shown in Fig. 8.7(a). The required area of the diagonal stiffener may be determined from an equation of equilibrium of horizontal components of these forces as follows:

$$\sigma_y A_s \cos\theta - \sigma_y A_{c1} \cos\left(\beta_1 + \gamma\right) + \sigma_y A_{c2} \sin\beta_2 = 0 \quad \ldots\ldots \quad (8.9)$$

then

$$A_s = \frac{A_{c1} \cos\left(\beta_1 + \gamma\right) - A_{c2} \sin\beta_2}{\cos\theta} \quad \ldots\ldots\ldots \quad (8.10)$$

where

A_s = area of a symmetrical pair of diagonal stiffeners

A_{c1} = area of inner flange of rafter haunch

A_{c2} = area of inner flange of column haunch

γ = angle of inclination of rafter

= angle of slope of diagonal stiffener

β_1 = angle of taper of rafter haunch

β_2 = angle of taper of column haunch

In Fig. 8.7(b), the maximum possible forces at the outer corner F are shown. Equilibrium of horizontal components gives:

$$\sigma_y A_{t1} \cos\gamma - \tau_y \frac{w\, d_{ch}}{\cos\theta} \cos(\theta + \gamma) \cos\gamma - \sigma_y A_s \cos\theta = 0 \quad \ldots \quad (8.11)$$

Substituting the Mises yield criterion $\tau_y = \sigma_y / \sqrt{3}$ and solving for the required stiffener thickness gives:

$$A_s = \left[\frac{A_{t1}}{\cos\theta} - \frac{w\, d_{ch} \cos(\theta + \gamma)}{\sqrt{3}\ \cos^2\theta} \right] \cos\gamma \quad \ldots\ldots \quad (8.12)$$

A_{t1} = area of outer flange of beam haunch

w = web thickness of haunch

d_{ch} = depth of column haunch at section EB (Fig. 8.7)

If Eq. 8.12 should result in a zero or negative value for A_s, the implication is that the shear capacity of the web is adequate to transmit the outer flange force, and that diagonal stiffeners are needed only to transmit the unbalance of the inner flange force. Since in any case the web will carry some force, Eq. 8.10 based on equilibrium at the inner corner will control for ordinary haunch proportions rather than Eq. 8.12.

Transverse stiffeners at the junctions of the tapered and prismatic sections (points A and C) may be designed to carry the unbalance of the flange force due to the sudden change in direction. Since the angles β_1 and β_2 are generally quite small, the size of the stiffeners usually will be governed by minimum size requirements.

A series of tests of haunched corner connections has given experimental results agreeing very well with the concepts just outlined [8.9]. Moment-

rotation curves for these tests are shown in Fig. 8.8. Specimens 44 and 45 were made with the critical length of compression flange as given by Eq. 8.8. Specimen 44 was not braced against twisting at the inner corner while specimen 45 was braced. Specimen 45 performed satisfactorily while specimen 44 buckled before it reached the computed ultimate load although it exhibited considerable post buckling strength. Specimens 46 and 47 had compression flange lengths

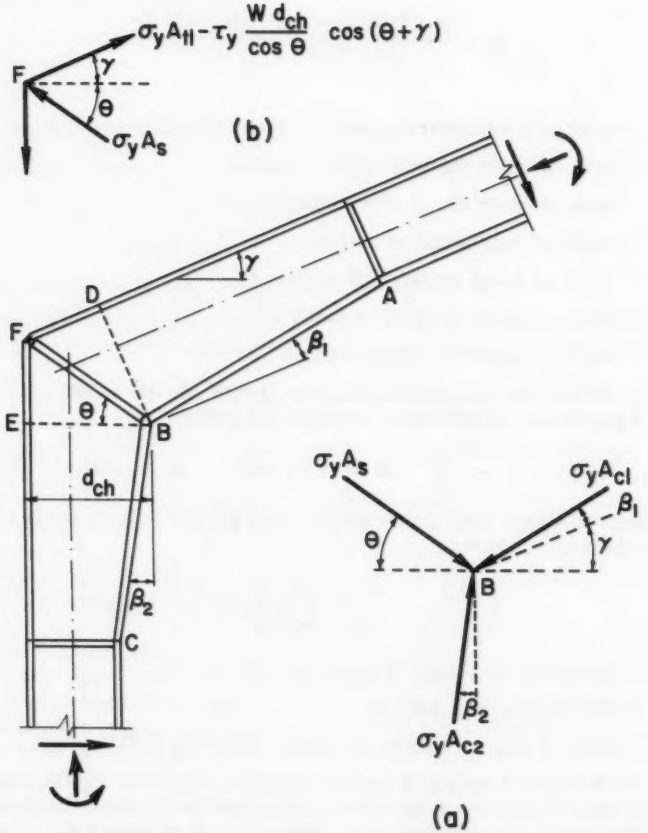

FIG. 8.7.—DIAGONAL STIFFENER FORCES IN A GABLED HAUNCHED KNEE

greater than that given by Eq. 8.8, but were modified by increasing the haunch depth and by increasing the flange thicknesses respectively. These specimens also performed satisfactorily in that they met the requirements stated earlier.

The results of these tests indicate that safe and adequate connections may be made by meeting the requirements derived by the theory. In summary, the following suggestions are made with regard to proportioning of tapered haunched connections:

TAPERED HAUNCHES

Required Plastic Modulus:

The plastic modulus should be checked for resistance to the applied moment at the deep end and the shallow end of each haunch.

Local Buckling:

The recommendations of Chapter 6 should be followed to assure that premature local buckling of flanges will not occur.

Lateral Buckling:

The critical unbraced length of a compression flange which may be strained to the point of strain-hardening throughout its entire length without premature lateral buckling is conservatively estimated as:

$$L_{cr} = 4.8\ b \quad \ldots\ldots\ldots\ldots\ldots \quad (8.8)$$

The critical unbraced length of a compression flange may be increased substantially by increasing the angle of taper β or by increasing the thickness of the flanges.

Diagonal Web Stiffeners:

To resist an unbalance of inner flange forces and reinforce the web against undue shear deformation, a symmetrical pair of diagonal stiffeners may be provided having a total area:

$$A_s = \frac{A_{c1} \cos\left(\beta_1 + \gamma\right) - A_{c2} \sin \beta_2}{\cos \theta} \quad \ldots\ldots\ldots (8.10)$$

Diagonal stiffeners should be welded to the web and to both flanges.

Transverse Stiffeners:

Transverse stiffeners at the junctions of the tapered haunch and prismatic section serve to carry the unbalance of the inner flange force due to the sudden change in direction. Minimum size requirements will usually govern the thickness.

8.4 CURVED HAUNCHES

In Fig. 8.9 are shown the layout and the applied forces for a typical curved haunch. The haunch must be designed to withstand the plastic hinge moment of the rolled section at its connection to the haunch and any larger moment which develops in the haunched portion as a result of the moment gradient.

As with tapered haunches, the three main problems to be considered in the design of curved haunches are: (1) resistance to bending in the haunch, (2) resistance to local and lateral buckling, and (3) shear stresses in the corner panel BDFE. (Fig. 8.10)

The plastic moment of resistance of any cross section x of the haunch perpendicular to the layout line is (Fig. 8.9),

$$M_{px} = \sigma_y Z_x \quad \ldots\ldots\ldots\ldots\ldots \quad (8.3)$$

As in tapered haunches, increasing the thickness of the curved flange would compensate for the reduction in effective section due to the inclination β of the flange and would make the section effectively symmetrical about its half depth. The theoretically required thickness is given by (8.7):

$$t_c = t_t / \cos \beta \quad \ldots\ldots\ldots\ldots\ldots \quad (8.4)$$

where

β = central angle between point of tangency and given section of knee

For all practical cases, the controlling angle β will be small (approximately 12°) and symmetry can be assumed without increasing the compression flange thickness. Assuming symmetry, the section modulus at any section x is

$$Z_x = b\, t_t \left(d_x - t_t\right) + \frac{w}{4} \left(d_x - 2\, t_t\right)^2 \quad \ldots\ldots\ldots\ldots \quad (8.5)$$

where

d_x = depth of haunch at any section (x)

$= d + R\ (1 - \cos \beta)$

R = radius of curvature of inner flange

$x = R \sin \beta$

This equation for Z_x may be substituted into the expression 8.3 for M_{px} and the result equated to M_x, the applied moment which must be resisted. Solving for the thickness of the tension flange gives

$$t_t = \frac{d_x - \sqrt{d_x^2 \left(\frac{b}{b-w}\right) - \frac{4\, Mx}{\sigma y\, (b-w)}}}{2} \quad \ldots\ldots\ldots \quad (8.13)$$

At some station along the haunch defined by a controlling value of the angle β, the values of d_x and M_x will require a maximum flange thickness. For values of the radius of flange curvature and distance to the inflection point that would be encountered ordinarily in practice, the controlling angle β has been found to be about 12° (8.7).

The resistance to local buckling of the flanges of curved haunches may be assured by adhering to the recommendations of Chapter 6.

Lateral stability of curved haunches is dependent upon the resistance to buckling of the compression flange perpendicular to the plane of the web. Reference 8.7 contains an approximate solution obtained by analyzing the problem as the buckling of a curved beam simply supported at the points of tangency and at the diagonal stiffener. To simplify the analysis the curved flange is conservatively assumed to have a uniform stress distribution over its whole area and length. The tangent modulus equation for the buckling of fully strain-hardened steel plates gives the following expression for the critical arc length of flange (8.7,8.8):

$$(L/r_x)_{cr} = (R\,\alpha/r_x)_{cr} = \pi\sqrt{E_{st}/\sigma_y} \quad \ldots\ldots\ldots \quad (8.14)$$

where

L = arc length of flange = $R\,\alpha$.

α = central angle of curved flange between points of lateral support. It is equal to the angle $(45^\circ - (\gamma/2))$ in Fig. 8.10 unless there are additional points of lateral support between A and B.

r_x = radius of gyration of compression flange in strong direction = $b/\sqrt{12}$.

The critical arc length when expressed in terms of the flange width becomes (For A7 steel)

$$(R\,\alpha)_{cr} = L_{cr} = 4.8\,b \ldots\ldots\ldots\ldots\ldots \quad (8.8)$$

This solution assumes a pin-ended condition. Since some end restraint would be provided by the adjoining beam segment and since the stress distribution is not actually uniform along the curved inner flange, a moderate increase could be made in the critical arc length. For a 90° connection, Eq. 8.8 reduces to:

$$R = 6\,b \text{ (approx)} \ldots\ldots\ldots\ldots\ldots \quad (8.15)$$

If for some reason it is desired to increase the radius above the value given by Eq. 8.15, additional points of support may be added to decrease the critical

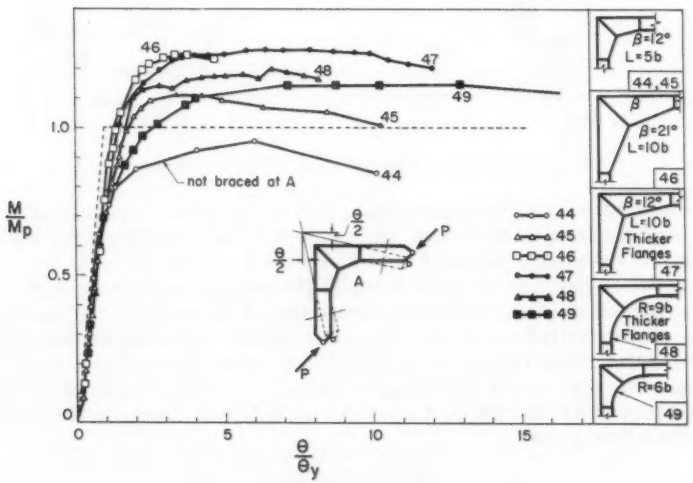

FIG. 8.8.—MOMENT-ROTATION CURVES FOR HAUNCHED CONNECTIONS

arc length according to Eq. 8.8. Other possible measures are to change the radius of gyration by increasing the flange width b or by changing the shape of the flange cross section. Also, the strains in the flange could be controlled by increasing the flange thickness.

An additional problem not encountered with tapered haunches is the cross bending of the curved flange. Cross bending is a phenomenon in which radial components of force in the curved flanges tend to bend the flange edges toward the web. It has been shown (8.7) that cross bending will have only a negligible effect on haunch behavior if the connection is proportioned so that

$$\frac{b^2}{2\,R\,t} \leq 1 \quad \ldots\ldots\ldots\ldots\ldots\ldots \quad (8.16)$$

The effect of shear force on the web will be discussed with the aid of Fig. 8.10 showing a gabled haunch. In the two segments of the haunch bounded by cross sections perpendicular to the layout lines at A and D and at E and C, the problem may be dismissed with the observation that the web area is equal to or greater than the web area of the adjacent prismatic beam which carries the

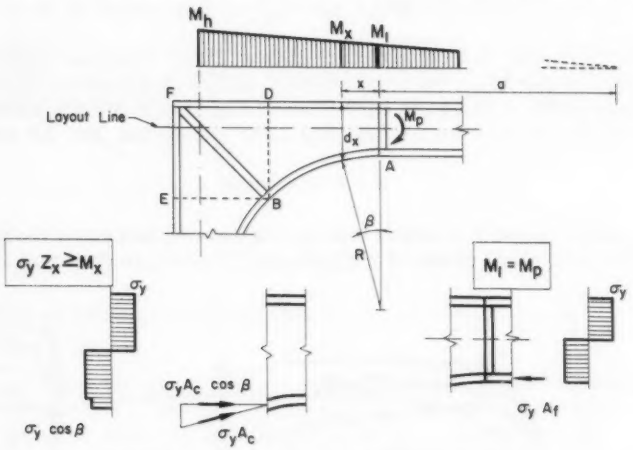

FIG. 8.9.—FORCES ON A CURVED KNEE

same shear force. In the corner panel BDFE, the forces are similar to those in the tapered haunch described in Article 8.3, and therefore Eq. 8.12 would indicate the necessary stiffener size at the outer corner F.

A second reason for using diagonal stiffeners in the corner panel is to resist web buckling due to the radial component of force from the curved inner flange. An approximation of the required stiffener size may be determined by neglecting the radial compression resistance of the web and assuming that the diagonal stiffeners resist two components of inner flange force directed along chords between AB and BC as shown in Fig. 8.10(a). Summing the forces in a radial direction gives

$$\sigma_y A_s = 2\,\sigma_y A_c \sin\left(22.5^\circ - \frac{\gamma}{4}\right) \quad \ldots\ldots\ldots\ldots \quad (8.17)$$

where

A_c = area of inner flange

Hence

$$A_s = 2\,A_c \sin\left(22.5^\circ - \frac{\gamma}{4}\right) \quad \ldots\ldots\ldots\ldots \quad (8.18)$$

Eq. 8.18 will tend to control the design of diagonal stiffeners for most curved haunches rather than Eq. 8.12. In the case of steeper gables (γ-large), it is possible that Eq. 8.12 may require larger stiffeners.

Results of tests of curved connections (8.9) are given in Fig. 8.8. Test 49 was made on a specimen which had the maximum unsupported flange length recommended by Eq. 8.8 and it performed very well. Test 48 was performed

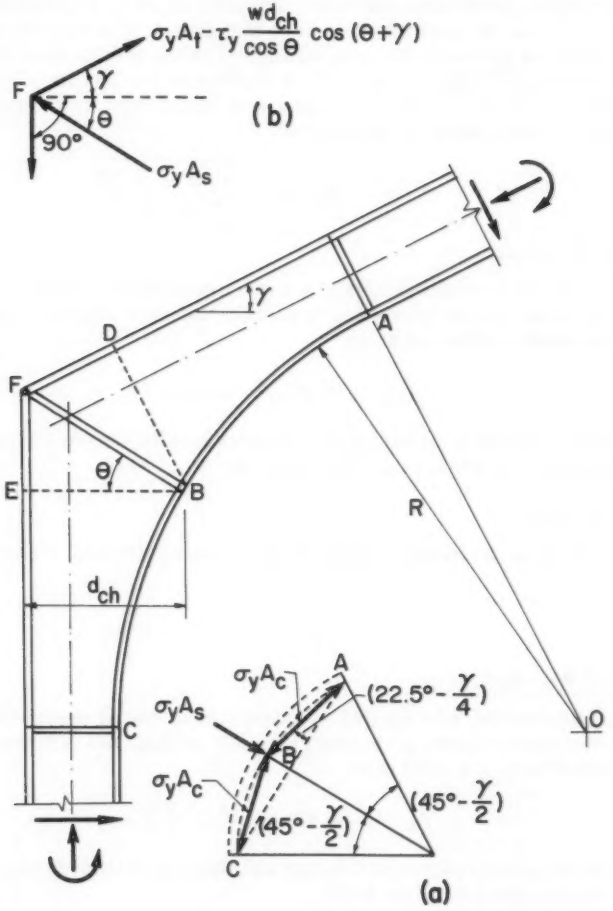

FIG. 8.10.—DIAGONAL STIFFENER FORCES IN A GABLED CURVED HAUNCH

on a specimen with a greater unsupported compression flange length, but with the flange thickness increased to reduce strains. This specimen also performed satisfactorily, but had somewhat less rotation capacity. Results of some earlier tests shown in Fig. 8.3 give an opportunity to observe the effect of radius of curvature on rotation capacity. Connection H with R - 5.5 b had somewhat less capacity. Connection G with R = 8 b had the least rotation capacity, and

might be considered inadequate. Connection J, of a slightly different design, had R = 3.4 b, and exhibited very good rotation capacity.

CURVED HAUNCHES

Required Plastic Modulus

The plastic modulus furnished at any point in the haunch must be adequate to resist the applied moment at that point. For typical values of R and moment gradient, the central angle β to the section controlling the thickness of the flange is about 12°. If the web of the haunch is no thinner than the web of the beam, the thickness of flange required to provide an adequate plastic modulus is given by

$$t_t = \frac{d_x - \sqrt{d_x^2 \left(\frac{b}{b-w}\right) - \frac{4\,Mx}{\sigma_y (b-w)}}}{2} \quad \ldots\ldots \quad (8.13)$$

Lateral Buckling

The critical unbraced length of a curved compression flange strained to the point of strain-hardening without premature lateral buckling is conservatively estimated as

$$L_{cr} = (R\,\alpha)_{cr} = 4.8\ b \quad \ldots\ldots\ldots\ldots \quad (8.8)$$

The critical unbraced length of a compression flange may be increased by increasing the thickness of the flanges.

Cross Bending

The effect of cross bending on connection behavior will be negligible if

$$\frac{b^2}{2\,R\,t} \leqq 1 \quad \ldots\ldots\ldots\ldots\ldots \quad (8.16)$$

Diagonal Web Stiffeners

To reinforce the web against buckling due to radial compression in the curved inner flange, a symmetrical pair of diagonal stiffeners may be provided having a total area

$$A_s = 2\,A_c \sin\left(22.5^\circ - \frac{\gamma}{4}\right) \quad \ldots\ldots\ldots \quad (8.18)$$

For steep gabled haunches the diagonal stiffener thickness should also be checked by means of Eq. 8.12.

8.5 BEAM-TO-COLUMN CONNECTIONS

Fig. 8.11 shows three common types of beam-to-column connections used on planar structures. The function of the "Top" and "Interior" connections is to transmit moment from one beam to another, the column carrying any unbalanced moment. The "Side" connection transmits beam moment to the upper and lower columns. The design problem is to provide sufficient stiffening material so that the connection will transmit the moment. Some columns are

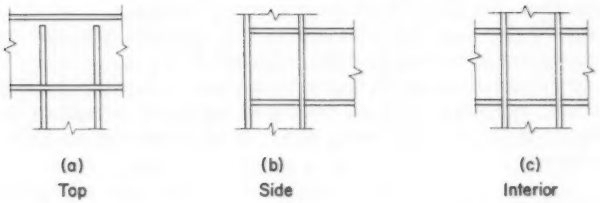

FIG. 8.11.—TYPES OF BEAM-TO-COLUMN CONNECTIONS

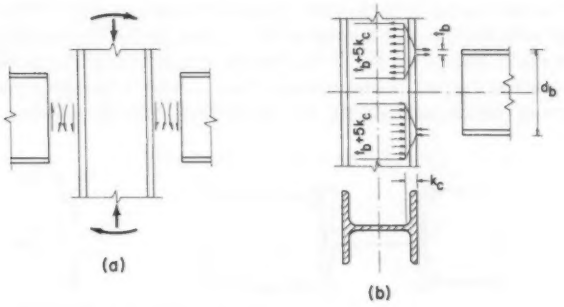

FIG. 8.12.—FORCES ON BEAM-TO-COLUMN CONNECTIONS

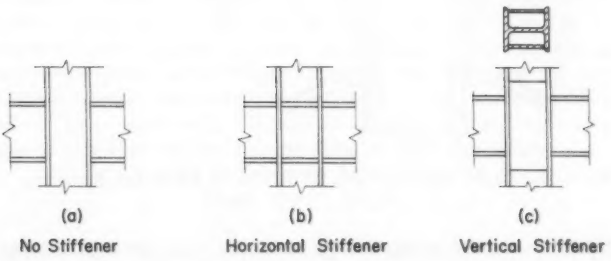

FIG. 8.13.—STIFFENING OF BEAM-TO-COLUMN CONNECTIONS

sturdy enough to carry full-moment beam connections without stiffening. Other columns require stiffening of their webs or flanges to aid in carrying the concentrated forces from the flanges of the connected beams.

Studies on the design and the behavior of full moment interior beam-to-column connections are reported in Refs. 8.10 and 8.11.

In treating problems relating to beam-to-column connections, the case of connections without stiffening will be examined as to the adequacy or inadequacy of the connections, and then some methods of providing necessary stiffening will be presented.

Columns Without Stiffeners

In Fig. 8.12(a) are shown schematically the moments and forces on a typical interior beam-to-column connection. In Fig. 8.12(b), the effect of a beam moment on a column is shown as a couple composed of the two flange forces, the beam web forces being of secondary importance. Significant effects of the beam flange forces can occur in two regions in the column. The first region is the column web where yielding may be accompanied by buckling due to the beam compression flange force or by fracture due to the beam tension flange force. The second region is the column flange where bending may contribute to the fracture of welds connecting the beam flange to the column flange.

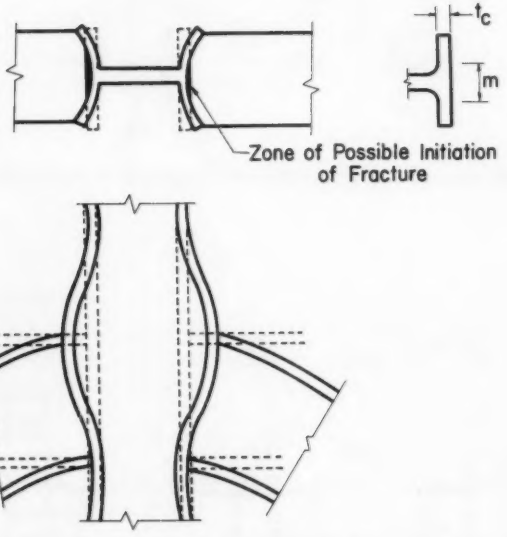

FIG. 8.14.—COLUMN FLANGE BENDING IN TENSION REGION

The tensile force in the beam flange tends to pull the outstanding column flanges as shown in Fig. 8.14. At the toes of the column flanges, flexibility allows the beam and column flanges to deform together. However, at the middle of the column flange where it is restrained by the column web, deformation is restricted and fracture is most likely to start there.

A column without stiffeners must be able to maintain static equilibrium both in regions of web yielding and flange bending. Stresses in the column caused by a concentrated beam flange force will spread out as they penetrate into the column. Because of this, the intensity of stress decreases with deeper penetration. If the spread of stresses is insufficient to reduce their intensity to the yield level at the depth of the base of the column flange fillet (k-depth), the web will not be able to provide sufficient reactive resistance to the beam flange force. This effect is most serious in the region stressed by the beam compression flange. Rational analysis of the spread of stress in a wide-flange section is difficult and is usually replaced by a linear assumption based on test results. Reference 8.11 gives the results of several tests and recommends that the stress in the column be assumed to be distributed on a 2.5:1 slope from the point of contact to the column "k-line." As shown in Fig. 8.12(b), this assumption implies that the force of a beam flange is resisted by a length of column web equal to $(t_b + 5\,k_c)$ at the column "k-line," where t_b is the beam flange thickness and k_c is the column fillet depth. For equilibrium, the resistance of the effective area of the web must equal or exceed the applied concentrated force of the beam tension or compression flange.

$$\text{Column Web Resistance} = \sigma_y\, w_c\left(t_b + 5\,k_c\right) \quad \ldots\ldots\ldots (8.19)$$

$$\text{Beam Flange Force} = \sigma_y\, A_f \quad \ldots\ldots\ldots\ldots (8.20)$$

which gives

$$\sigma_y\, w_c\left(t_b + 5\,k_c\right) \geq \sigma_y\, A_f \quad \ldots\ldots\ldots\ldots (8.21)$$

where

w_c = column web thickness

A_f = area of one flange of beam

If the column web resistance is insufficient to carry the beam flange forces, stiffeners must be provided.

Static equilibrium in cases where the column flange thickness is small involves the consideration of bending in the column flange due to the beam tension or compression flange forces. The analysis is further complicated by the fact that the flange bending occurs in two directions, both longitudinal and transverse to the axis of the member as can be visualized from Fig. 8.14. To solve the problem it is necessary to make assumptions regarding the distribution of the beam flange force on the column flange, the extent of the zone of bending in the column flange, and the effect of the central portion where the column flange joins the column web. It may be assumed that the fully yielded beam flange puts a line load on the column flange. For the beam,

$$\text{Beam flange force} = \sigma_y\, A_f \quad \ldots\ldots\ldots\ldots (8.22)$$

The thick center portion of the column flange between the ends of the fillets may be assumed to resist the beam flange force with an axial force as if it were rigid. Thus

$$\text{Column flange direct resistance} = \sigma_y\, t_b\, m \quad \ldots\ldots\ldots (8.23)$$

where

m = Distance between fillet extremities of flange of column

The remaining portion of the column flange resistance is due to bending of the projecting portion of the flange, and is affected by the projecting width of flange, thickness of flange, length of line load, length of the zone affected by bending and strength of the material. In general, the action can be looked upon as a case of plate bending, with the flange thickness being the most important geometric property. The force of resistance to the beam flange line load may be expressed by:

$$\text{Column flange bending resistance} = c_1 \sigma_y t_c^2 \quad \ldots\ldots\ldots (8.24)$$

where

c_1 is a coefficient depending on the width of column and beam flanges, extent of two-way bending, distance between column flange fillets, and boundary conditions.

To develop the full yield strength of the beam flange, the column flange resistance must be at least equal to it.

$$\sigma_y A_f = \sigma_y t_m + c_1 \sigma_y t_c^2 \quad \ldots\ldots\ldots\ldots\ldots (8.25)$$

If the column flange resistance is found to be deficient, the column flange is too thin, and stiffening is required. This effect is most serious in the region stressed by the beam tension flange.

In Ref. 8.11, Eq. 8.25 is evaluated by means of "yield line theory,"* assuming a plate bending mechanism which extends for a length of column flange equal to 12 t_c. Additional assumptions of the relative dimensions of beams and columns are made in such a way as to assure the most conservative result. From this combination of assumptions, the column flange thickness to resist a given beam flange area is obtained as follows

$$t_c \geq 0.4 \sqrt{A_f} \quad \ldots\ldots\ldots\ldots\ldots\ldots (8.26)$$

Results of tests showed that connections proportioned according to Eq. 8.26 carried the plastic moment of the beam satisfactorily. Fig. 8.15 shows the results of tests on connections designed to meet the appropriate design criteria. The "A" tests are those without stiffeners which satisfied both Eqs. 8.21 and 8.26.

Columns With Stiffeners

If the column web thickness satisfies Eq. 8.21, column stiffeners are not needed adjacent to the beam compression flange. If the column flange thickness satisfies Eq. 8.26, column stiffeners are not needed adjacent to the beam tension flange. If the column proportions fail to satisfy either of these equations, however, stiffeners should be provided. Two types of stiffeners are shown in Fig. 8.13, the horizontal stiffener and the vertical stiffener. Both types of

* Yield line theory is an upper bound plastic analysis of bending of plates in which plastic hinges are assumed to form along lines in a plate to form a mechanism.

stiffener may be proportioned by considering the additional amount of resisting force required to achieve equilibrium. The stiffeners should also be proportioned to maintain stability under their full load.

Horizontal stiffeners should preferably be furnished in symmetrical pairs opposite both beam flanges. They should be welded to the column flange and web by either groove or fillet welds. Vertical stiffeners should also be furnished in symmetrical pairs and should be deep enough to allow the beam flange force to be dispersed in the stiffener in the same manner in which it is assumed to be dispersed in the web in Eq. 8.19.

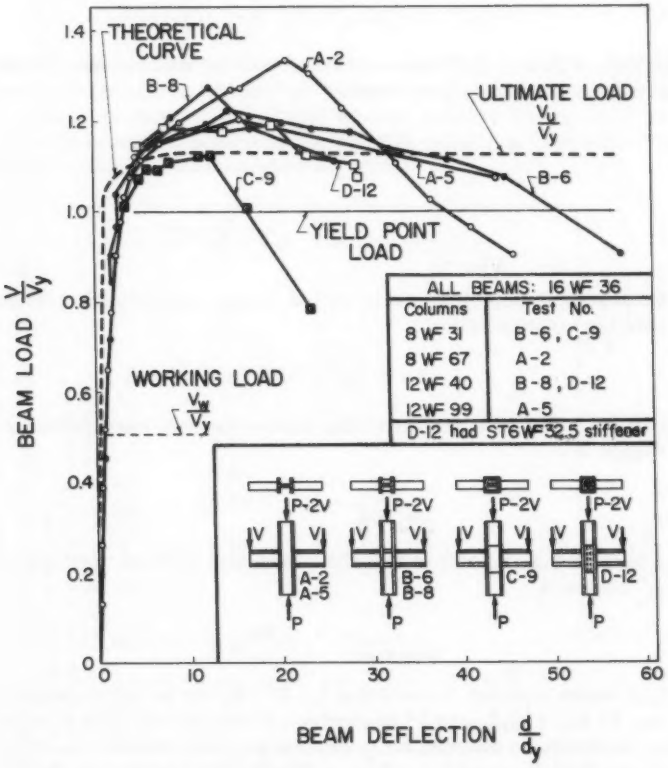

FIG. 8.15.—RESULTS OF TWO-WAY CONNECTION TESTS

Results of tests on connections using both types of stiffening are given in Ref. 8.11. Some of them are shown in Fig. 8.15. These tests and tests without stiffening were used to help establish semi-empirical methods of deciding the need for stiffeners and the proportioning of stiffeners to resist thrusts of beam flanges. If the moments applied by the beams to the columns were unsymmetrical, the same methods would be appropriate.

Critical Parts of Connections

The preceding analyses have shown that the use of stiffeners may depend either on compression in the column web (Eq. 8.21) or on tension normal to the column flange (Eq. 8.26) resulting from the end moments of the beams. For most of the rolled column sections normally only one type of failure need be checked, depending on the proportions of the column. The sections controlled by each type of failure may be tabulated, thus simplifying design.

Eq. 8.21 states that a connection will be on the verge of needing stiffeners in the compression region if

$$A_f = w_c(t_b + 5\ k_c) \quad \ldots\ldots\ldots\ldots\ldots\ldots (8.27)$$

From Eqs. 8.26 and 8.27 this connection will or will not need stiffeners in the tension region according to whether

$$t_c \lesseqgtr 0.4 \sqrt{w_c(t_b + 5\ k_c)} \quad \ldots\ldots\ldots\ldots\ldots (8.28)$$

that is

$$\frac{t_c}{\sqrt{k_c\ w_c}} \lesseqgtr 0.4 \sqrt{5 + t_b/k_c} \quad \ldots\ldots\ldots\ldots\ldots (8.29)$$

For all practical combinations of rolled beams and columns that might be used in this type of connection,

$$0.2 < t_b/k_c < 0.8 \quad \ldots\ldots\ldots\ldots\ldots\ldots (8.30)$$

By taking $t_b/k_c = 0.2$, it is seen that this connection will need stiffeners in the tension region if

$$\frac{t_c}{\sqrt{k_c\ w_c}} < 0.91 \quad \ldots\ldots\ldots\ldots\ldots\ldots (8.31)$$

By taking $t_b/k_c = 0.8$, it is seen that the connection will not need stiffeners in the tension region if

$$\frac{t_c}{\sqrt{k_c\ w_c}} > 0.96 \quad \ldots\ldots\ldots\ldots\ldots\ldots (8.32)$$

Fig. 8.16 shows a plot of the values of $t_c/\sqrt{k_c w_c}$ for all wide-flange columns in the 8 in., 10 in., 12 in., and 14 in. series. It can be seen that in most cases the column need only be checked for compression. For values of $t_c/\sqrt{k_c w_c}$ between 0.91 and 0.96 the need for column stiffening will depend on the beam, and both tension and compression should be checked.

Shear Stiffening

When the moments in the two beams at an interior connection differ by a large amount, they may cause large shears in the column web, tending to deform the web in the same manner as in a corner connection (Fig. 8.2(e)). With such an unbalance of moments, the shear in the web should be checked, and if necessary, diagonal stiffeners or a doubler plate should be added (8.12). In Fig. 8.17(a) the shears and moments acting on a typical connection are shown. Fig. 8.17(b) is a free body diagram of the forces acting on the column web just below the top flange stiffener. The forces are V, the horizontal shear present

in the column above the connection and two tensile flange forces T_1 and T_2. The flange forces are obtained approximately by dividing the moment in the respective beams by the beam depths. The net result of these forces must be resisted by a shear stress τ acting on an area of column web equal to $w_c d_c$. Thus

$$\tau\, w_c\, d_c = \frac{M_2}{d_b} - \frac{M_1}{d_b} - V \quad \ldots\ldots\ldots\ldots (8.33)$$

Assuming that $\tau_y = \sigma_y/\sqrt{3}$, the required web thickness to resist shear is

$$w_c = \frac{\sqrt{3}}{\sigma_y\, d_c} \left(\frac{M_2}{d_b} - \frac{M_1}{d_b} - V \right) \quad \ldots\ldots\ldots\ldots (8.34)$$

when the directions of moments and shears are as shown in Fig. 8.17(b). If the actual web thickness of the column is less than that in Eq. 8.34, diagonal stiffeners similar to those in Fig. 8.2(f) or web doubler plates could be used to carry the excess shearing force. The special case of a "one-sided" beam-to-column connection is obtained when M_1 equals zero.

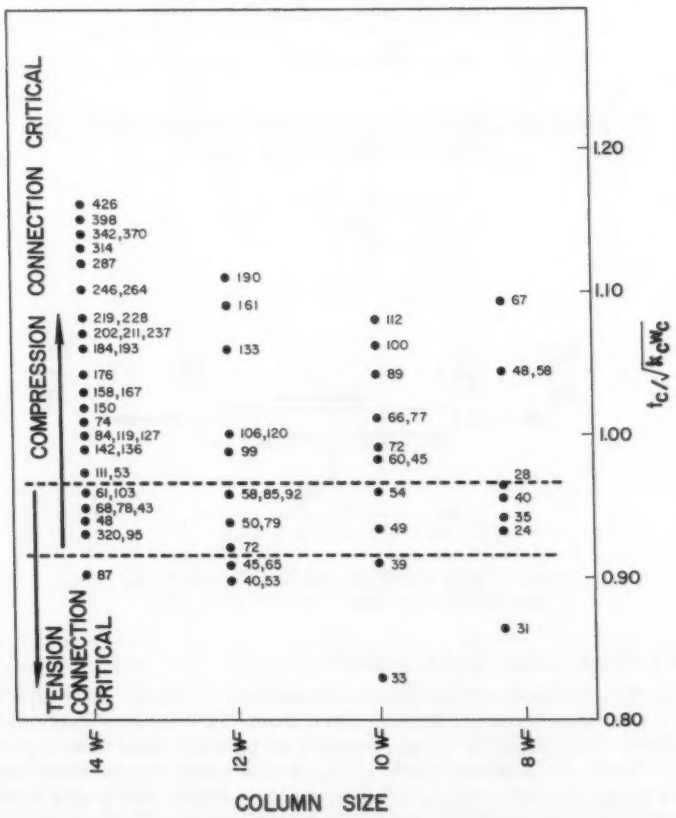

FIG. 8.16.—CRITICAL PARTS OF CONNECTIONS

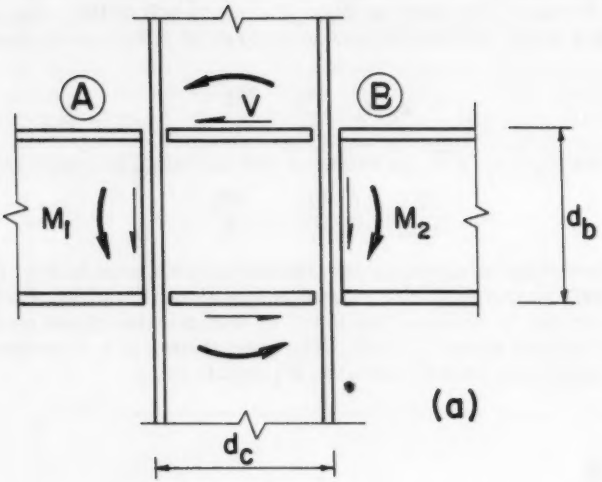

FIG. 8.17a.—SHEAR AND MOMENT ON CONNECTION WITH UNEQUAL MOMENTS ON BEAMS

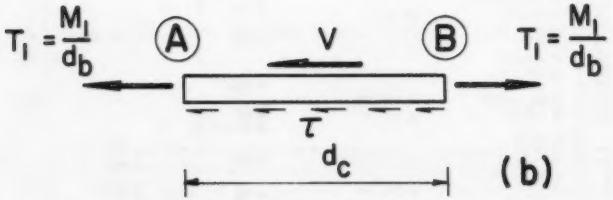

FIG. 8.17b.—FREE BODY DIAGRAM OF FORCES ACTING ON TOP STIFFENER AND COLUMN WEB

Four-Way Beam-to-Column Connections

Frequently additional beams must be framed into a single joint on a column forming a four-way beam-to-column connection. Two beams may be framed into a column web either by direct welding or by plate plus seat type of connections. When connections such as these are used, the question has been raised as to whether the triaxial stresses in the column web might cause premature failure, or on the other hand, whether a beneficial effect might be obtained through the partial stiffening action of the beams framing into the column web. A limited number of tests have been made on four-way connections. In

the specimens tested, there was no adverse effect of triaxial stresses indicated (8.11).

Sketches of the four-way connections tested are shown in Fig. 8.18. The direct-welded type, shown in Fig. 8.18(a) had a column web thickness meeting the requirement of Eq. 8.21 and hence the column web required no reinforcement to prevent crippling due to the forces applied to the column flanges by the

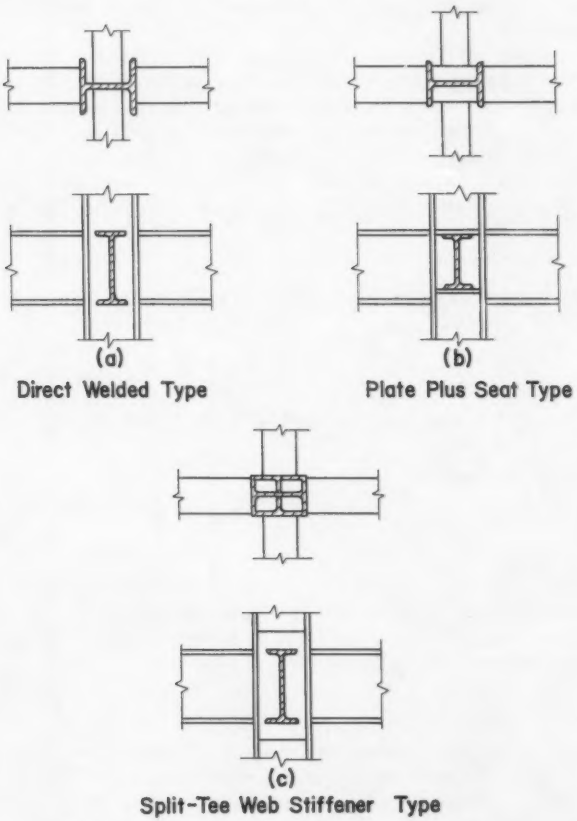

FIG. 8.18.—TYPES OF FOUR-WAY INTERIOR BEAM-TO-COLUMN CONNECTIONS

beams. The addition of two more identical beams, welded directly to the column web, appeared to stiffen the web. In the second type of connection (Fig. 8.18(b)), the horizontal plates which served as top plate and seat plate for the beams framing into the column web also served as stiffeners for the column. Because the beams framing into the web were not as deep as those welded to the column flanges, the bottom stiffener was 4 inches away from its ideal location opposite the lower flange of the deeper beam. However, the connection performed satisfactorily. The connection in Fig. 8.18(c) used split-tee sections for stiffeners in the same way that vertical plates had been used in two-way

connections. The stems of the tees served to support both the stiffeners and the column web. The flanges of the split tees served as suitable surfaces to which beams could be directly welded to complete the connection. The performance of this connection was also satisfactory. The four-way connection tests of Ref. 8.11 were performed with considerable axial load in the columns in order that the results could reflect the influence of this practical loading situation. All of these tests were performed under a symmetrical moment condition. Some special problems still remain to be solved when unequal moments are introduced.

For the design of four-way connections Ref. 8.11 recommends that the connection of the beams to the column flange be designed exactly as in a two-way connection as if the beams framing to the column web were not present. Test specimens of four-way connections designed on this assumption performed better than comparable two-way connections.

BEAM-TO-COLUMN CONNECTIONS (Beams Joined to Column Flanges)

Unstiffened Columns

Column stiffeners are not needed adjacent to the beam compression flanges if

$$w_c \geq \frac{A_f}{t_b + 5\,k_c} \quad \ldots\ldots\ldots\ldots\ldots (8.21)$$

Column stiffeners are not needed adjacent to the beam tension flanges if

$$t_c \geq 0.4\sqrt{A_f} \quad \ldots\ldots\ldots\ldots\ldots (8.26)$$

Column Stiffeners

Column stiffeners at points of bearing of beam flanges should be proportioned to carry the excess of beam flange force over that which the column web and flange are able to carry. (Stiffeners should also be proportioned so as not to buckle.)

Shear Stiffening in Column

When unbalanced moments or external forces cause shear stresses in excess of the column web capacity, stiffening should be provided for the column. Such stiffening may take the form of diagonal stiffeners or web doubler plates.

8.6 DETAILS WITH REGARD TO WELDING

In butt welds, the forces are carried in compression or tension, and are limited by the tensile or compressive resistance of the base metal or weld metal depending on which is least. Since weld metal is stronger than the base metal normally used in any joint, the strength of butt welds should be calculated on the basis of σ_y, the yield strength of the base metal.

A nominal shear stress of 22.4 ksi was selected for fillet welds. The basis for the 22.4 ksi stress was a load factor of 1.65 applied to a working stress of 13.6 ksi as presently (1960) permitted by the AWS code for building construction (8.13). Thus the calculated shear stress at maximum load exceeded the

working stress by the same ratio that a normal stress of 33 ksi exceeds a working stress of 20 ksi. Use of these stresses at ultimate load results in weld sizes for a simple beam which are usually the same as those which have proven satisfactory for years in allowable stress design.

The results of the tests in connections described in Refs. 8.4, 8.6, and 8.9 verified that the welds designed using these assumptions were adequate in that no weld failure occurred.

WELD STRESSES

Butt Welds may be assumed capable of developing on their minimum throat section the tensile yield stress of the base metal.

Fillet Welds may be assumed to be capable of developing at least the shearing yield stress of the weld metal on their minimum throat section. A safe design value may be obtained by multiplying the value presently used in allowable stress design by the ratio σ_y/σ_w, where σ_w is the allowable tensile stress of the material being used.

8.7 DETAILS WITH REGARD TO BOLTING

Bolted joints in plastic design will probably have their greatest application as field joints for erection of structures.

It could be argued that judicious selection of the locations of such joints will place them at points of low moment so that the joints will remain elastic. The design of these joints then could be handled by conventional elastic methods. However, it sometimes becomes advantageous to make field connections at points of high moment. It is thus advisable to have available methods for proportioning bolted joints to develop the full plastic moment of the connected members.

Two possible approaches available for full capacity connections are (1) to keep all parts of the joint "elastic" at maximum moment, and (2) to design parts of the joints so that fasteners and plates may yield at maximum moment along with the main members. Recent studies have emphasized the latter approach.

A limited amount of research has been performed on bolted joints designed to develop the full plastic moment of beams. References 8.15 and 8.16 give the results of tests of connections using ASTM A-325 high tensile bolts. The connections in Ref. 8.15 included both beam splices and beam-to-column connections and for each case there were examples with the bolts in shear and in tension. The connections in Ref. 8.16 were butt type connections with the bolts in tension. The results of the test programs show that it is possible to design and fabricate high tensile bolted joints which will develop the full bending strength of a member. Fig. 8.19 gives the general layout of joints which performed satisfactorily as reported in Refs. 8.15 and 8.16.

Methods of analysis and design are not discussed in detail in Ref. 8.15. Methods are discussed in Ref. 8.16, but the author suggests that better procedures based on the same fundamentals can be developed.

The essential features of any analysis of a full-moment bolted connection are the assumptions as to the load capacity of each individual bolt, the manner in which the compressive components of force are to be carried, the location of the neutral axis, and the strength of any detail material (fittings) used in forming the joint. It seems reasonable to conclude that precise solutions for the ultimate strength of joints are not necessary provided that the solutions constitute lower bounds.

An example of the assumptions that might be made in designing a high strength bolted joint is given in Ref. 8.16 as exemplified by Fig. 8.19(a), 8.19(c), and 8.19(f). The number and location of bolts in a joint were first assumed. For the bolts in tension, an "ultimate" load capacity was taken in this reference as 1.3 times the proof load of the bolts. The shear resistance provided by each bolt at ultimate load due to friction was taken at one-fourth its initial tension. All structural steel parts of the joint were assumed to be stressed to yield point. To analyze the trial design, a compression area was computed sufficient to resist the combined reaction of all the "working" bolts, that is, those on the

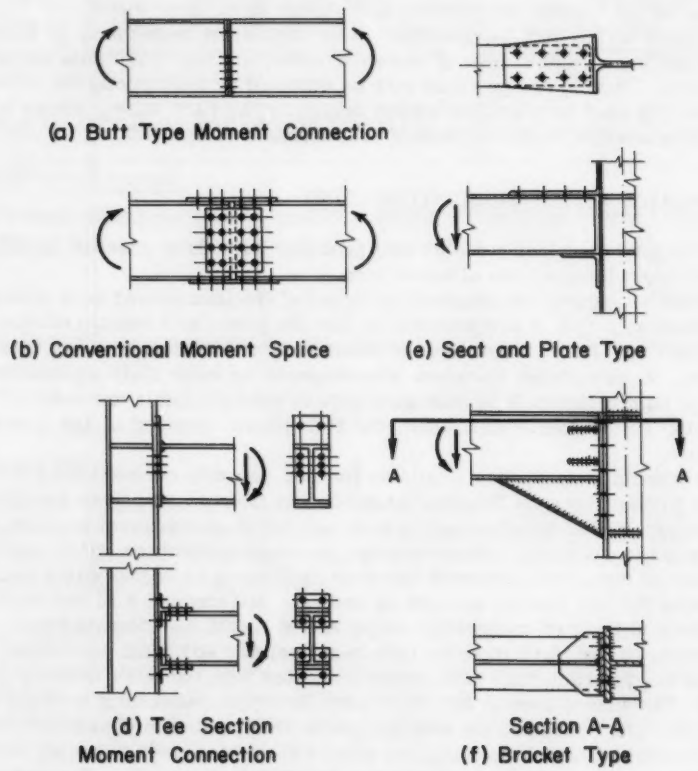

FIG. 8.19.—TYPES OF PLASTIC MOMENT CARRYING HIGH TENSILE BOLTED CONNECTIONS

tension side of the neutral axis (axis of rotation). The bending moment produced by the couple made up of the bolt tension forces and the compression force, had to equal or exceed the applied bending moment.

Reference 8.16 notes that plastically designed joints with high tensile bolts in tension require a smaller number of bolts and less fitting material than conventional moment splices which use the bolts only in shear.

Although accurate procedures leading to the most economical safe design are not yet available, the results of research show that safe bolted joints can

be designed to develop the plastic moment of the members with reasonable economy.

ACKNOWLEDGMENT

This report is based on a series of preliminary reports prepared for the Welding Research Council and the American Society of Civil Engineers by a research group at Fritz Engineering Laboratory, Department of Civil Engineering, Lehigh University. This group has been engaged through the Institute of Research in an investigation entitled "Welded Continuous Frames and Their Components"; the staff members include L. S. Beedle, G. C. Driscoll, Jr., T. V. Galambos, R. L. Ketter, T. Kusuda, G. C. Lee, T. Lee, L. W. Lu, A. Ostapenko and B. Thurlimann. The original draft was written by G. C. Driscoll, Jr. William J. Eney is Director of Fritz Laboratory and Head of the Civil Engineering Department.

The organizations that supported the Research projects out of which the basic report was prepared were the following: American Institute of Steel Construction, American Iron and Steel Institute, the Department of the Navy (Office of Naval Research, Bureau of Ships, Bureau of Yards and Docks), the Welding Research Council, and the Column Research Council.

Although much of the experimental and theoretical work reported was performed at Lehigh University, the Welding Research Council and ASCE committees have attempted to broaden this report by including the results of research at other institutions, both here and abroad. The inclusion of this information and of certain unpublished data is gratefully acknowledged.

REFERENCES

8.1 A. A. Toprac, B. G. Johnston, L. S. Beedle,
CONNECTIONS FOR WELDED CONTINUOUS PORTAL FRAMES, The Welding Journal, 30(7), 30(8) and 31(11), (1951 & 1952)

8.2 A. W. Hendry
AN INVESTIGATION OF THE STRENGTH OF WELDED PORTAL FRAME CONNECTIONS, The Structural Engineer, 28(10), (1950)

8.3 D. T. Wright
THE DESIGN OF KNEE JOINTS FOR RIGID STEEL FRAMES, BWRA No. FE 1/38, (April 1954)

8.4 J. W. Fisher, G. C. Driscoll, Jr., F. W. Schutz, Jr.,
BEHAVIOR OF WELDED CORNER CONNECTIONS, The Welding Journal, 37(5), Research Supplement, 216-s, (May 1958)

8.5 J. W. Fisher, G. C. Driscoll, Jr., L. S. Beedle,
PLASTIC ANALYSIS AND DESIGN OF SQUARE RIGID FRAME KNEES, Welding Research Council Bulletin No. 39, (April 1958)

8.6 J. W. Fisher, G. C. Driscoll, Jr.,
CORNER CONNECTIONS LOADED IN TENSION, The Welding Journal, 38(11) Research Supplement, 425-s, (November 1959)

8.7 J. W. Fisher,
PLASTIC ANALYSIS OF HAUNCHED CONNECTIONS, (Thesis), Lehigh University, (1958)

8.8 G. Haaijer, B. Thürlimann,
ON INELASTIC BUCKLING IN STEEL, Proc. ASCE, 84 (EM2), p. 1581, (April 1958)

8.9 G. C. Lee, J. W. Fisher, G. C. Driscoll, Jr.,
BEHAVIOR OF HAUNCHED CONNECTIONS, Fritz Engineering Laboratory Report 205C.27, Lehigh University (1959)

8.10 R. F. Pray, C. D. Jensen,
WELDED TOP PLATE BEAM-COLUMN CONNECTIONS, The Welding Journal, 35(7), Research Supplement, (July 1956)

8.11 J. D. Graham, A. N. Sherbourne, R. N. Khabbaz, C. D. Jensen,
WELDED INTERIOR BEAM-TO-COLUMN CONNECTIONS, AISC, New York, (1959)

8.12 L. S. Beedle,
PLASTIC DESIGN OF STEEL FRAMES, John Wiley and Sons, Inc., New York (1958)

8.13 American Welding Society
WELDING HANDBOOK, American Welding Society, New York, (1958)

8.14 F. Bleich,
BUCKLING STRENGTH OF METAL STRUCTURES, McGraw-Hill Book Company, New York (1952)

8.15 L. G. Johnson, M. A. Cannon, L. A. Spooner,
JOINTS IN HIGH TENSILE, PRELOADED BOLTS—TESTS ON JOINTS DESIGNED TO DEVELOP FULL PLASTIC MOMENTS OF CONNECTED MEMBERS, The Institute of Structural Engineers, Jubilee Symposium on High Strength Bolts, p. 52 London (June 1959)

8.16 F. W. Schutz, Jr.
STRENGTH OF MOMENT CONNECTIONS USING HIGH TENSILE BOLTS, Proc. AISC, p. 98 (April 1959)

Journal of the
ENGINEERING MECHANICS DIVISION
Proceedings of the American Society of Civil Engineers

COMMENTARY ON PLASTIC DESIGN IN STEEL: DEFLECTIONS

Progress Report No. 7 of the Joint WRC-ASCE Committee on Plasticity Related to Design

FOREWORD

This paper is the seventh in a series of reports on Plastic Design emanating from a Joint Committee of the Welding Research Council and the American Society of Civil Engineers. Reference should be made to Progress Report No. 1 (which appeared in the July 1959 issue of the Journal of the Engineering Mechanics Division of ASCE) for such items as the Foreword, Synopsis, Definitions, and Nomenclature. For information, the complete Table of Contents appears at the beginning of Progress Report No. 6 immediately preceding this paper. Chapter 9, entitled "Deflections," comprises the present paper.

The Joint Committee has approved the publication of this information with the strong recommendation that it be read carefully by all structural engineers.

Note.—Discussion open until September 1, 1960. Separate Discussions should be submitted for the individual papers in this symposium. To extend the closing date one month, a written request must be filed with the Executive Secretary, ASCE. This paper is part of the copyrighted Journal of the Engineering Mechanics Division, Proceedings of the American Society of Civil Engineers, Vol. 86, No. EM 2, April, 1960.

Chapter 9

DEFLECTIONS

9.1 INTRODUCTION

Although strength to carry the load is the primary matter of importance in most structures, certain problems related to deflections do concern the structural engineer. The deflection may exceed established limits set up by a building code or specification. Deflections may hinder the operation of moving parts or the closing of doors, or they may cause the cracking of plaster in finished ceilings. Thus, it is desirable to have methods for calculating the deflections of structures in both the elastic and plastic ranges.

This chapter will outline the basic problem of structural deflections. It will discuss briefly the calculation of deflections in the elastic range. The calculation of deflections at ultimate load will be covered in more detail. Illustrative examples will show that the deflections at working load of structures designed plastically usually are no greater than those of structures designed by elastic methods.

The calculation of the deflections of structures in the elastic range is cumbersome even after the strength analysis is complete. For this reason, it is standard procedure to dispense with the calculation of deflections when sufficient experience has been gained with a particular type of structure to indicate that deflections will not be excessive. In plastic design the same practice will be used in similar situations.

Structural deflections are in essence calculated by integration, with appropriate boundary conditions, of the differential equation:

$$\frac{d^2y}{dx^2} = \cdot \phi \qquad (9.1)$$

where

y = deflection from original straight line of member.

x = distance along member.

$\frac{d^2y}{dx^2}$ = approximate curvature of member. The approximation is valid when slope and deflection are small.

ϕ = curvature caused by bending. Thus it is a function of moment which in turn is a function of x. In the elastic range $\phi = M/E\,I$.

There are many methods of solving this equation in both the elastic and plastic ranges. The methods differ principally in the means of expressing ϕ and in the methods of handling boundary conditions. In the following sections, a number of these methods will be discussed.

9.2 CALCULATION OF DEFLECTIONS IN THE ELASTIC RANGE

Methods for calculating deflections in the elastic range are available in texts on structural theory so these methods will not be explained here. To make a precise calculation of deflections at working load of structures proportioned by plastic design it would be necessary to use one of these methods. (As will be

seen later, an upper bound to this deflection may be determined without resorting to the elastic analysis of the indeterminate structure.)

One thing elastic methods have in common is that they express the curvature ϕ, for use in Eq. 9.1, as

$$\phi = \frac{M}{E\,I} \quad \ldots\ldots\ldots\ldots\ldots\ldots \quad (9.2)$$

where

M = bending moment as a function of x.

E = Young's Modulus of elasticity.

I = moment of inertia of the cross section of the member.

A second feature of most of the elastic methods is that expressions giving the slope at all points of a deflected member are continuous functions, and that joints with other members may be fully rigid or completely free.

Certain of the methods also are adaptable for the consideration of factors contributing to deflection which ordinarily are neglected in the study of rigid frame structures. These factors are the deflections caused by axial force and shear force. In the consideration of stability problems, these additional components become important.

9.3 CALCULATION OF DEFLECTIONS IN THE PLASTIC RANGE

Several methods for calculating the deflections of structures in the plastic range are available. Five of these methods are outlined, discussed, and compared with experimental results in Ref. 9.1. In these methods, the moment-curvature relationship derived from the elastic and plastic stress-strain relationship is substituted in Eq. 9.1 and, using appropriate boundary conditions, slopes and deflections are obtained by integration. The methods differ only in the number of assumptions made in the moment-curvature relationship to simplify the computation. Table 9.1 outlines the salient features of the five methods. Fig. 9.1 shows the stress distribution associated with the assumptions for each of the methods. The simplest approach, the "plastic hinge" method, is most suitable for structural engineering applications. The additional work involved in the theoretically more "exact" methods is not justified by the accuracy gained except for special purposes.

The "plastic hinge" method assumes that the structure has only elastic regions and localized plastic hinges. This allows the use of the curvature equation in the form given as Eq. 9.2. The boundary conditions are then changed to allow for freedom of rotation at plastic hinges. As pointed out by Symonds and Neal, the controlling boundary condition is continuity at the last plastic hinge to form [9.2].* Any of the well-known methods of calculation of deflection in the elastic range may then be used with suitable handling of the boundary conditions. Methods which have shown promise are: "slope deflection," "moment area," "conjugate-beam," and the "method of work." Some advantages of the "plastic hinge" method are that it obviates the necessity of knowing the M-ϕ relationship beyond the elastic limit, and, for certain continuous beams, makes

* An exception occurs when hinge rotation has occured at one or more sections where the bending moment at ultimate load is less than the fully plastic value. For a discussion of this phenomenon see pp. 196-202 of Ref. 9.3.

TABLE 9.1—SUMMARY OF METHODS FOR CALCULATING DEFLECTIONS IN THE PLASTIC RANGE

Method	M-ϕ Relationship	Spread of Plastic Zone	Strain Hardening	Handling of Boundary Conditions	Remarks
Numerical Integration	"Exact"	Considered	Considered	Trial & Error needed to fit B. C. for redundant structure	Most Precise
Mathematical Integration	Simplified to functions expressable mathematically	Considered	Considered	Trial & Error	
ϕ - Area	Simplified	Neglected	Considered	Trial & Error	
Simple Plastic Theory	Simplified	Considered	Neglected	Trial & Error where moment is constant	
Plastic Hinge Method	$\phi = M/EI$	Neglected	Neglected	Direct	Large error in curvature for section with constant moment

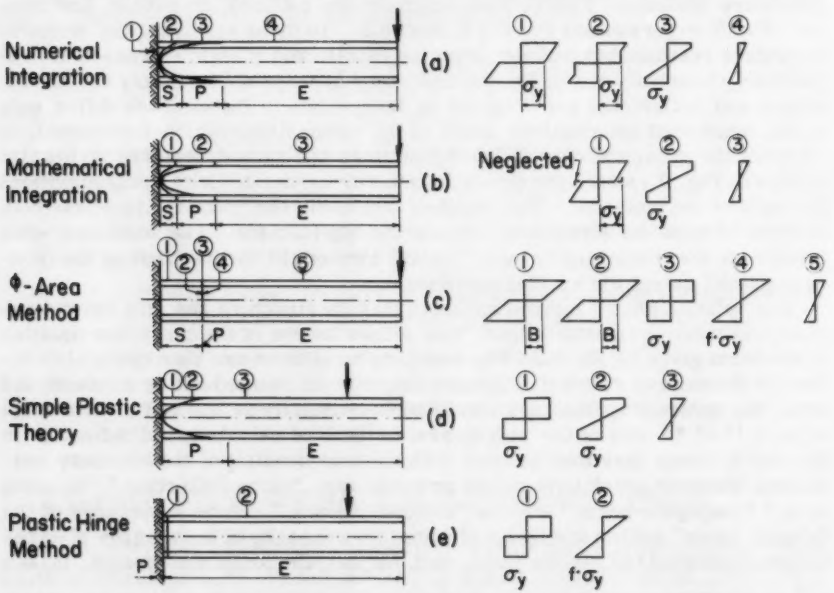

FIG. 9.1.—STRESS DISTRIBUTIONS ASSUMED FOR CALCULATING DEFLECTIONS OF BEAMS BEYOND THE ELASTIC LIMIT.

use of the deflection formulas tabulated in structural handbooks and usually available in the design office.

The other four methods discussed in Ref. 9.1 are "simple plastic theory," "ϕ Area," "mathematical integration," and "numerical integration." These methods utilize more accurate representations of the moment-curvature relationship and properties of the steel to obtain a small increase in accuracy of the calculated deflections. However, this increase in accuracy is gained at the expense of a considerable increase in complexity. A trial-and-error process must be used not only to determine the boundary conditions (last plastic hinge) but also to determine the moment and curvature. For this reason, these methods have only been used in the calculation of deflections of very simple structures such as continuous beams and rectangular portal frames (9.1, 9.4). For more complicated structures, the use of a digital computer would be required.

Deflections of more complicated structures have been calculated by the "plastic hinge" method with reasonable agreement between calculations and tests. For most practical cases, therefore, the "plastic hinge" method is recommended for deflection calculations (9.2,9.5,9.6,9.7,9.8).

9.4 SAMPLE CALCULATION OF DEFLECTION AT ULTIMATE LOAD

Slope-Deflection Method

In this section, the approximate deflection at ultimate load of the simple portal frame shown in Fig. 9.2(a) will be calculated. The assumptions used will be those given in Art. 9.3 for the "plastic hinge" method. One method of calculation is to make use of the slope-deflection equation (9.2,9.3,9.7,9.9,9.10):

$$\theta_A = \theta'_A + \frac{\Delta}{\ell} + \frac{\ell}{3\,E\,I}\left(M_{AB} - \frac{1}{2}\,M_{BA}\right) \cdots\cdots (9.3)$$

(See Fig. 9.3 for nomenclature. Clockwise M and θ are positive. When the equation is used in this form, E I must be constant in segment AB.)

The mechanism and moment diagram at ultimate load are given in Fig. 9.2(b) and 9.2(c), respectively. In Fig. 9.2(d) are given free body diagrams of the portions of the frame. To solve for the deflections δ_V and δ_H, two boundary conditions are needed. One of these is that θ_{21} equals θ_{23} because of continuity at joint 2. The second boundary condition depends on whether the last plastic hinge forms at section 3 or section 4. A trial solution of the problem will be made for each of these assumptions, and then the correct solution will be selected.

Continuity at section 2, ($\theta_{21} = \theta_{23}$)

$$\theta_A = \theta'_A + \frac{\Delta}{\ell} + \frac{\ell}{3\,E\,I}\left(M_{AB} - \frac{M_{BA}}{2}\right)$$

First, considering segment 2 - 1 and using the moments of Fig. 9.2(c)

$$\theta_{21} = 0 + \frac{\delta_H}{L/2} + \frac{L/2}{3\,E\,I}\left(\frac{7}{11}\,M_p - 0\right)$$

$$\theta_{21} = \frac{2\,\delta_H}{L} + \frac{7}{66}\,\frac{M_p\,L}{E\,I}$$

Next, considering segment 2 - 3

$$\theta_{23} = 0 + \frac{\delta V}{L/2} + \frac{L/2}{3\,E\,I}\left(-\frac{7}{11}\,M_p + \frac{1}{2}\,M_p\right)$$

$$\theta_{23} = \frac{2\,\delta V}{L} - \frac{1}{44}\,\frac{M_p\,L}{E\,I}$$

Equating θ_{21} and θ_{23}

$$\frac{2\,\delta_H}{L} + \frac{7}{66}\,\frac{M_p\,L}{E\,I} = \frac{2\,\delta V}{L} - \frac{1}{44}\,\frac{M_p\,L}{E\,I}$$

$$\delta_V = \frac{17}{264}\,\frac{M_p\,L}{E\,I} + \delta_H \quad \ldots\ldots\ldots\ldots\ldots\ldots \quad (9.4)$$

This gives one desired relationship for δ_V and δ_H which applies for either of the following trial solutions.

Trial at section 3, ($\theta_{32} = \theta_{34}$)

Considering segment 3 - 2

$$\theta_{32} = 0 + \frac{\delta_{V3}}{L/2} + \frac{L/2}{3\,E\,I}\left(-M_p + \frac{7}{22}\,M_p\right)$$

$$= \frac{2\,\delta_{V3}}{L} - \frac{5}{44}\,\frac{M_p\,L}{E\,I}$$

Considering segment 3 - 4

$$\theta_{34} = 0 - \frac{\delta_{V3}}{L/2} + \frac{L/2}{3\,E\,I}\left(M_p - \frac{1}{2}\,M_p\right)$$

$$= -\frac{2\,\delta_{V3}}{L} + \frac{1}{12}\,\frac{M_p\,L}{E\,I}$$

In the above expressions δ_{V3} is the vertical deflection with continuity assumed at section 3.

Equating θ_{32} and θ_{34}

$$\frac{2\,\delta_{V3}}{L} - \frac{5}{44}\,\frac{M_p\,L}{E\,I} = -\frac{2\,\delta_{V3}}{L} + \frac{1}{12}\,\frac{M_p\,L}{E\,I} \quad \ldots\ldots \quad (9.5)$$

Thus

$$\delta_{V3} = \frac{13}{264}\,\frac{M_p\,L^2}{E\,I}$$

And from Eq. 9.4

$$\delta_{H3} = -\frac{1}{66}\,\frac{M_p\,L^2}{E\,I} \quad \ldots\ldots\ldots\ldots\ldots \quad (9.6)$$

These values for δ_V and δ_H would be the correct values for the deflections at ultimate load if the last plastic hinge formed at point 3.

Trial at section 4, $(\theta_{43} = \theta_{45})$

Considering segment 4 - 3

$$\theta_{43} = 0 - \frac{\delta_{V4}}{L/2} + \frac{L/2}{3\,E\,I}\left(M_p - \frac{1}{2}\,M_p\right)$$

$$= -\frac{2\,\delta_{V4}}{L} + \frac{1}{12}\,\frac{M_p\,L}{E\,I}$$

Considering segment 4 - 5

$$\theta_{45} = 0 + \frac{\delta_{H4}}{L/2} + \frac{L/2}{3\,E\,I}\left(-\,M_p - 0\right)$$

$$= \frac{2\,\delta_{H4}}{L} - \frac{1}{6}\,\frac{M_p\,L}{E\,I}$$

Equating θ_{43} and θ_{45} and solving simultaneously with Eq. 9.4 gives

$$\delta_{V4} = \frac{25}{264}\,\frac{M_p\,L^2}{E\,I}$$

$$\delta_{H4} = \frac{1}{33}\,\frac{M_p\,L^2}{E\,I} \qquad \text{(9.8)}$$

The deflections calculated assuming continuity at section 4 are larger than those obtained on the basis of continuity at section 3. Consideration of the rotations at section 4 when continuity is assumed at section 3 shows that an impossible reverse "kink" would occur at section 4. Because of this reverse "kink," the assumption resulting in such a solution is discarded. Therefore, the deflections assuming continuity at section 4 are the correct deflections at ultimate load. It has been established elsewhere (9.2) that the correct set of calculated deflections will be the largest set from any series of calculations based on different assumptions of the last plastic hinge. The last plastic hinge to form will be the hinge at which continuity is assumed in calculating the largest deflection.

Dummy Load Method

Another example of the calculation of deflection at ultimate load will be given using the "dummy load" method, variations of which are called the "unit load" or "virtual work" method. This method is used in many text books on structures, for instance, Ref. 9.11.

The operations of the method are as follows: first, the moments M due to the applied loads are determined; second, a dummy unit load is applied to the

unloaded structure at the point of the desired deflection and in the direction of the desired deflection. A set of moments m in equilibrium with the unit load are then determined.

Additional special conditions used to adapt this method for the solution of deflections at ultimate load are:

(1) All members are assumed to be fully elastic between plastic hinges.
(2) Continuity is assumed at the last plastic hinge.
(3) The dummy load is applied to an auxiliary structure with frictionless hinges assumed at all but the last plastic hinge.
(4) If the location of the last plastic hinge is unknown, a solution must be made for each assumed last plastic hinge.

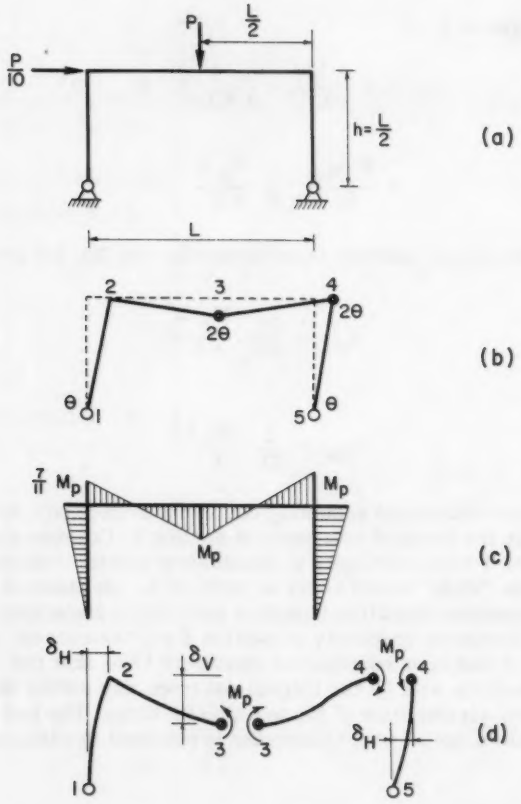

FIG. 9.2.—DEFLECTION OF PORTAL FRAME AT ULTIMATE LOAD.

After applying these conditions the deflection at the unit load due to the original applied loads is determined from a virtual work equation of the form

$$\delta\,(1k) = \int \phi\, m\, ds = \int \frac{M\, m}{E\, I}\, ds \quad \ldots\ldots\ldots\ldots \quad (9.9)$$

where

δ = Deflection in direction of unit load.

M = Moments in structure due to applied loads.

m = Moments in auxiliary structure in equilibrium with unit load.

ds = Distance along member.

E = Young's modulus of elasticity.

I = Moment inertia of member.

The equation is integrated over the whole structure, using intervals where all functions exist and are piecewise continuous. By defining limits at joints, con-

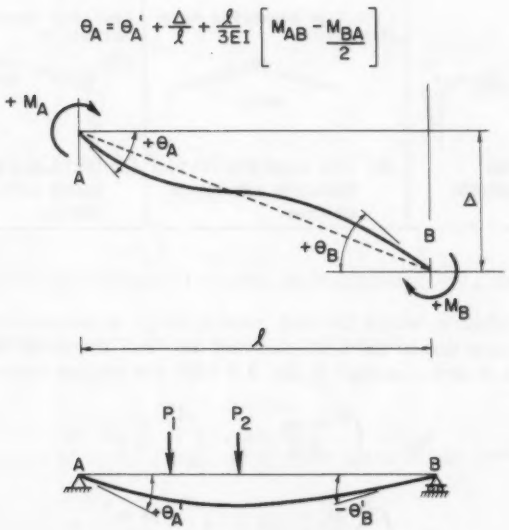

FIG. 9.3.—NOMENCLATURE FOR SLOPE-DEFLECTION EQUATION.

centrated loads and hinges, the discontinuities in the curvature functions are readily handled.

The vertical deflection at ultimate load of the ridge of the gabled frame in Fig. 9.4(a) will be calculated. The locations of the plastic hinges and the "M" moment diagram due to the applied loads are shown in Fig. 9.4(a). The necessary additional relationships from the analysis are:

$$w\, L^2 = 16.84\, M_p$$

$$\alpha = 0.355 \quad \ldots\ldots\ldots\ldots\ldots\ldots \quad (9.10)$$

The last plastic hinge may either occur at the leeward knee or in the windward rafter. By making two deflection calculations, one assuming each hinge in turn to be the last, the correct deflection will be determined.

In Fig. 9.4(b), a unit load is applied at the ridge of the structure with a frictionless hinge assumed at the knee. In other words, there is continuity in

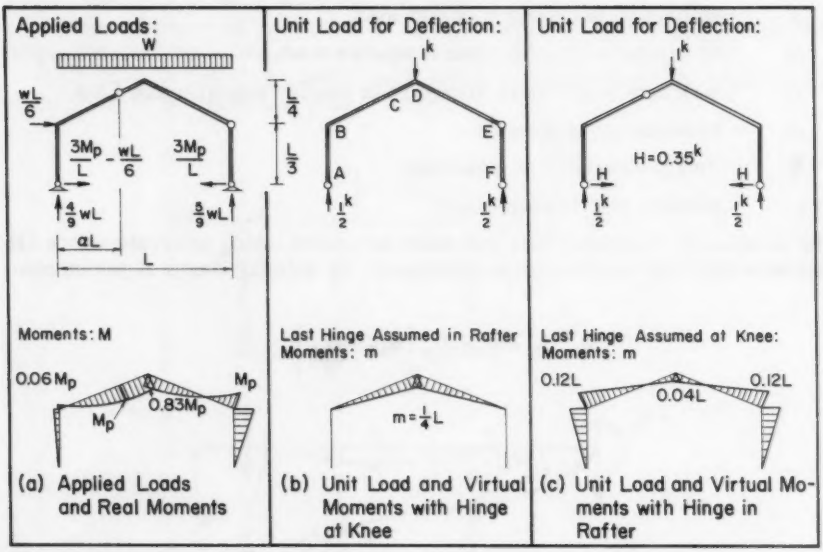

FIG. 9.4.—LOADS AND MOMENTS FOR DUMMY LOAD SOLUTION OF DEFLECTION

the windward rafter in which the last plastic hinge is assumed to occur. The resulting reactions due to the unit load and the "m" moments are also shown. Moments M and m are inserted in Eq. 9.9 with the proper expressions for ds:

$$\delta_D = \int_A^B \frac{M\,m}{E\,I}\,ds + \int_B^D \frac{M\,m}{E\,I}\,ds + \int_F^E \frac{M\,m}{E\,I}\,ds + \int_E^D \frac{M\,m}{E\,I}\,ds \quad \ldots\ldots\ldots (9.11)$$

where the limits of integration indicate the applicable points on the structure of Fig. 9.4(b):

$$\delta_D = 0 + \frac{1}{E\,I}\int_0^{L/2}\left(M_p + \frac{w\,L^2}{18} + \frac{4}{9}\,w\,L\,x - \frac{3}{2}\,\frac{M_p x}{L} - \frac{w\,x^2}{2}\right)\left(\frac{1}{2}x\right)\frac{\sqrt{5}}{2}\,dx$$

$$+ 0 + \frac{1}{E\,I}\int_0^{L/2}\left(-M_p + \frac{5}{9}\,w\,L\,x - \frac{3}{2}\,\frac{M_p x}{L} - \frac{w\,x^2}{2}\right)\left(\frac{1}{2}x\right)\frac{\sqrt{5}}{2}\,dx \quad \ldots (9.12)$$

Performing the indicated integration and substituting Eq. 9.10 results in

$$\delta_D = 0.1012 \frac{M_p L^2}{E I} \quad \ldots\ldots\ldots\ldots\ldots\ldots (9.13)$$

Instead of having a hinge at the knee, the structure with the dummy load in Fig. 9.4(c) has a hinge in the windward rafter. The structure in this condition behaves as a three-hinged arch with the "m" moments and reactions shown. Using these "m" moments with the "M" moments of Fig. 9.4(a), a second expression for deflection is obtained.

$$\delta_D = \int_A^B \frac{M\,m}{E\,I}\,ds + \int_F^E \frac{M\,m}{E\,I}\,ds + \int_B^C \frac{M\,m}{E\,I}\,ds + \int_C^D \frac{M\,m}{E\,I}\,ds + \int_E^D \frac{M\,m}{E\,I}\,ds \quad \ldots (9.14)$$

$$\delta_D = \frac{1}{E\,I}\int_0^{L/3} \left(-\frac{3\,M_p\,x}{L} + \frac{w\,L\,x}{6} \right)(-H\,x)dx + \frac{1}{E\,I}\int_0^{L/3} \left(-\frac{3M_p\,x}{L} \right)(-H\,x)dx$$

$$+ \frac{1}{E\,I}\int_0^{\alpha L} \left(-M_p + \frac{w\,L^2}{18} + \frac{4}{9}\,w\,L\,x - \frac{3}{2}\,\frac{M_p\,x}{L} - \frac{w\,x^2}{2} \right)\left(\frac{1}{2}x - \frac{H\,x}{2} - \frac{H\,L}{3} \right)\left(\frac{\sqrt{5}}{2}\,dx \right)$$

$$+ \frac{1}{E\,I}\int_0^{L/2\,-\alpha L} \left(M_p + \frac{4}{9}\,w\,L\,x - w\,\alpha\,L\,x - \frac{w\,x^2}{2} - \frac{3}{2}\,\frac{M_p\,x}{L} \right)\left(\frac{1}{2}x - \frac{H\,x}{2} \right)\left(\frac{\sqrt{5}}{2}\,dx \right)$$

$$+ \frac{1}{E\,I}\int_0^{L/2} \left(-M_p + \frac{5}{9}\,w\,L\,x - \frac{3}{2}\,\frac{M_p\,x}{L} - \frac{w\,x^2}{2} \right)\left(\frac{1}{2}x - \frac{H\,x}{2} - \frac{H\,L}{3} \right)\left(\frac{\sqrt{5}}{2}\,dx \right) \quad \ldots\ldots\ldots (9.15)$$

Integrating and substituting for w, α and H results in

$$\delta_D = 0.0159 \frac{M_p L^2}{E I} \quad \ldots\ldots\ldots\ldots\ldots\ldots (9.16)$$

Since the larger of the two calculated deflections is the correct one, then

$$\delta_D = 0.1012 \frac{M_p L^2}{E I} \quad \ldots\ldots\ldots\ldots\ldots\ldots (9.17)$$

The conclusion that the largest calculated deflection based on a given ultimate moment diagram is the correct deflection is explained on pg. 192 of Ref. 9.3. It is stated that "any incorrect solution can be found from the correct solution by superposing the displacements and hinge rotations due to a backwards motion of the collapse mechanism."

9.5 STEP-BY-STEP CALCULATIONS OF DEFLECTIONS

Occasionally, and especially for research purposes, it becomes desirable to construct the load-deflection (or load-rotation) curve for a structure. This

is done by means of a step-by-step procedure, because the load-deflection behavior is approximately linear between the formation of successive plastic hinges (9.12). The calculations to be discussed here will be based only on the plastic hinge method.

As an example, consider the deflection under load of the built-in beam in Fig. 9.5(a). In the elastic range, the load-deflection curve follows the line 0-a. The curve will cease to follow line 0-a when the moment at the left support reaches M_p. This point is designated by A on the solid curve. Thereafter the moment at the left support cannot increase, but the moments can increase at every other point in the beam. The subsequent increment of deflection of the beam will then be the same as the propped cantilever of Fig. 9.5(b). The elastic

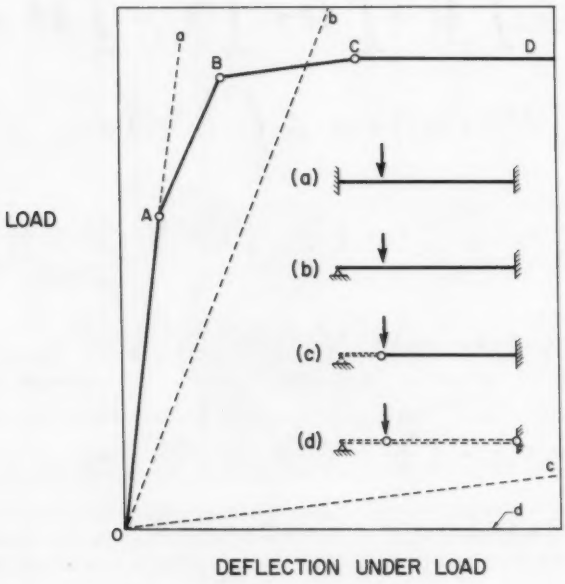

FIG. 9.5.—STEP-BY-STEP LOAD-DEFLECTION CURVE OF A BEAM.

load-deflection relationship of structure (b) when standing by itself is given by the line 0-b. The increment of deflection of the original beam is determined according to the line AB drawn parallel to 0-b. The magnitude of the increment of load corresponding to AB is determined by considering the moment under the load. A certain moment corresponding to point A exists under the load in the original structure (a). The difference between this moment and M_p is made up by the moment under the load of auxiliary structure (b). The increment of load is the amount required to raise the moment of auxiliary structure (b) from zero to the amount of the original difference from M_p, and the increment of deflection of the auxiliary structure (b) caused by this increment of load.

At this stage, there are plastic hinges both at the load and at the left support. Consequently, no increase in moment can occur at either of these points. The auxiliary structure of Fig. 9.5(c) will be used to determine the next increment of load and deflection in the same manner as was done for the first two

increments. The load at the end of the third step will be based on the moment at the right support as summed up for the three cases.

The final stage of the load-deflection curve is the horizontal portion CD representing deflection without increase of load. This can be represented schematically by structure (d) which has three hinges. Neglecting catenary effects, the load-deflection of structure (d) is represented by baseline d.

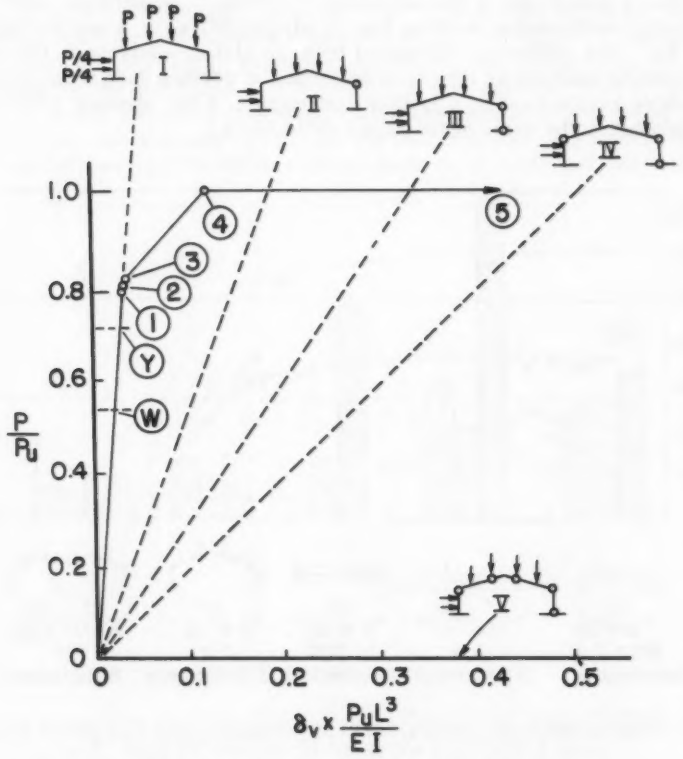

FIG. 9.6.—STEP-BY-STEP LOAD-DEFLECTION CURVE OF A PORTAL FRAME.

In summary, the load-deflection curve of a structure loaded to ultimate load may be obtained by superimposing on the elastic load-deflection curve of the primary structure, portions of the elastic load-deflection curves of auxiliary structures. The number of auxiliary structures will be the same as the number of plastic hinges.

The same procedures may be followed for rigid frame structures. Fig. 9.6 shows the load-deflection curve of a gabled portal frame and the load-deflection curves of the necessary auxiliary structures (9.7). The deflection at point (4) in Fig. 9.6 is the same as would be obtained by the methods of Art. 9.4.

9.6 APPROXIMATE DEFLECTION AT WORKING LOAD

It has been suggested (9.13) that an upper bound for the deflection at working load may be obtained by dividing the calculated deflection at ultimate load by the load factor. Calculations were made to compare this type of estimate with calculated and measured deflections at working load. Bar graphs showing these comparisons for five structures are given in Fig. 9.7. Each deflection is plotted as a percentage of the calculated deflection δ_u at ultimate load. Thus, the deflection estimated at working load is always 54% of δ_u when the load factor is 1.85. The deflection calculated from an elastic analysis at the plastic design working load and an observed deflection at working load from a test are shown where available. For a further comparison, a bar showing 1/360 of the span is plotted to the same scale as the deflections.*

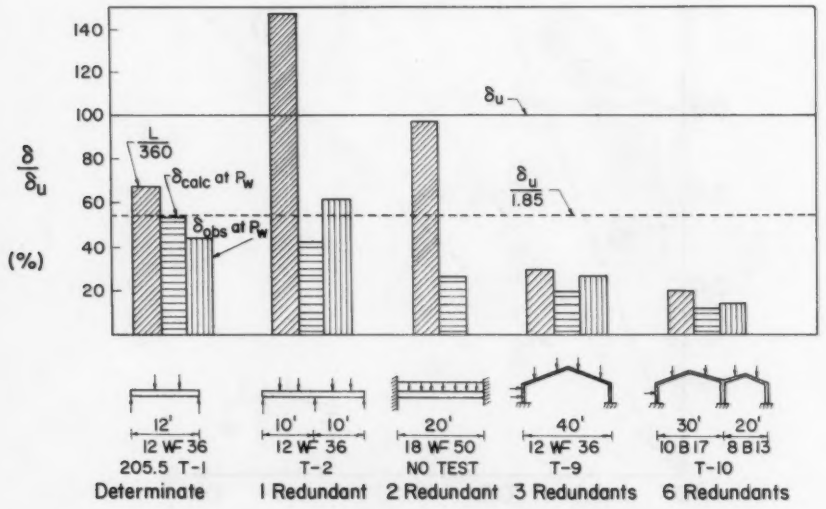

FIG. 9.7.—COMPARISON OF DEFLECTIONS AT WORKING AND ULTIMATE LOADS WITH ESTIMATED WORKING LOAD DEFLECTION.

The bar graphs show that the estimate of deflections made by dividing δ_u by the load factor is more and more in error as the number of statically indeterminate reactions increases. Whereas the approximate estimate is very good for one redundant, the estimate is four times the actual deflection at working load for the structure with six redundants. This estimate would imply excessive deflection whereas the actual deflection here was well below L/360. Unfortunately, no simple rule can be established for estimating how much in error the original calculation might be. Much depends on the order of formation of the plastic hinges. In any structure in which all plastic hinges form simultaneously, the estimate will equal the true deflection.

* L/360 is not suggested as an appropriate deflection limitation; it is shown merely because it is probably of the same order of magnitude as any practical deflection limitation.

The approximate procedure suggested is satisfactory whenever the estimated deflection calculated from this procedure does not exceed the prescribed deflection limitation. Otherwise it is necessary to resort to more accurate (and complicated) methods of calculation.

9.7 DEFLECTIONS AS A LIMITATION

One of the most important questions about deflections in plastic design is whether or not they will constitute an undue design limitation. The answer to this question on the basis of available test results and calculations is: no.

Admittedly, on the basis of the few tests and calculations for examples shown, it cannot be stated that all possible combinations have been studied. Variations in load and span do change the relationships. However, it is believed on the basis of the studies which have been made that the statements

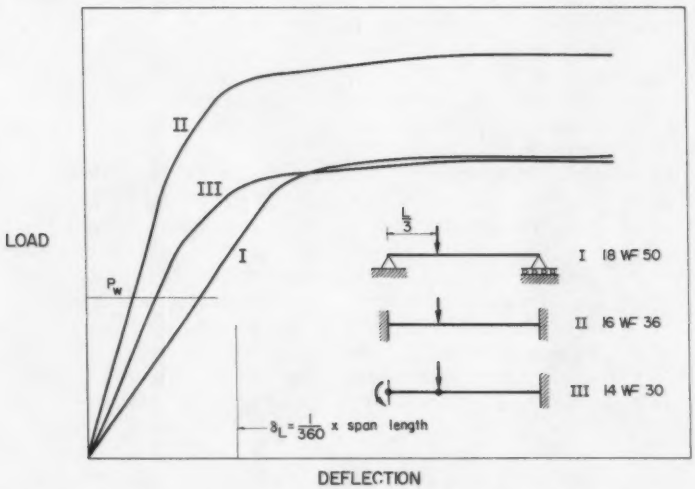

FIG. 9.8.—LOAD-DEFLECTION RELATIONSHIP FOR THREE DIFFERENT BEAM DESIGN FOR SUPPORTING THE SAME LOAD.

made here apply to typical cases and also to cases within the range of practical extremes.

Consider the case shown in Fig. 9.8 (9.10). The problem is to design a beam to carry a given load on a given span. First, picture the beam being designed as simply-supported, this being the standard with which the safety factor is compared in plastic design. The rolled section required would be an 18WF50 and the load-deflection curve would be as shown by curve I in Fig. 9.8. A horizontal mark on the graph indicates the value of the working load, and a vertical mark indicates the deflection which is equivalent to 1/360 of the span.

Next consider a fixed-ended beam designed to carry the same load on the same span according to elastic design. Because of the negative moment at the fixed ends, only a 16WF36 would be required. The load-deflection curve would be as given by curve II in Fig. 9.8. It is seen that the deflection at working load is considerably less than that of the simply-supported beam. The elastically

designed beam with fixed ends would support a much greater ultimate load than that of the simple beam. This indicates that, although both beams are designed for the same working load and both are "safe," the built-in beam has an excess margin of safety against ultimate load.

The third case in Fig. 9.8 indicates an even more economical solution by plastic design. Here only a 14WF30 is required. The load-deflection curve shows that the load capacity is equal to that of the simple beam. Though the deflection at working load for case III is greater than case II, it is considerably less than case I and would be acceptable.

9.8 ROTATION REQUIREMENTS

In addition to the problem of deflections in plastic design the rotations at plastic hinges must also be considered. For example, in the beam of Fig. 9.5, it is the inelastic rotation at the left support which allows redistribution of moments to the load point and right support of the member, thereby making possible the increase in load from points A to D. Similarly, in any continuous structure, some rotation must take place at the first plastic hinges to form, except in the case where all hinges form simultaneously. The measure of this required rotation is referred to as the hinge angle. It is of interest to determine the hinge angle that would be required in structures in order to formulate certain secondary design guides which depend upon this function.

The hinge angle may be calculated as part of the deflection calculations described in Art. 9.4. The results of numerous hinge angle calculations are presented in Ref. 9.5. Some of these results have been used in the determination of the required lateral bracing for bending members given in Art. 6.3.

In some cases, the calculated hinge angle required to form a mechanism may be quite large, implying a limitation on the design. However, practical considerations suggest that almost as good load carrying capacity may exist with a much lower hinge angle requirement. In Fig. 9.9 is plotted the theoretical load versus hinge rotation H at the first plastic hinge of a two-span frame. Seven labelled points on the curve indicate the formation of seven plastic hinges in reaching the mechanism state. Point (7) is the hinge angle that would be calculated in a rotation capacity study. Note, however, that at the formation of the next-to-last plastic hinge, point (6), the load is 98.2% of the maximum load. In order to attain this load, the required rotation is only 0.54 M_p L/(E I), or about one-third of the amount calculated for a full mechanism (1.52 M_p L/(E I)). Assurance of reaching 98% of a predicted load, along with a reasonable load factor or safety factor is generally accepted as good engineering practice. Thus, it is seen that the problem of large required rotation in highly redundant structures is not as serious as might first be suspected.

Experimental verification that a structure may behave quite satisfactorily even though it may not meet the full rotation requirement is given in Ref. 9.6. A test was performed on the two-span frame of Fig. 9.9. Although the frame did not quite attain the computed ultimate on the basis of a 40 ksi coupon stress, it reached 97.4% of this value, or well in excess of an ultimate load based upon a 33 ksi yield point (Fig. 9.10). Observations indicated that six of the seven plastic hinges were formed before lateral buckling occurred due to the instability of a lateral support which was made very flexible for test purposes. There is every reason to believe that with adequate lateral support the seventh plastic hinge would have formed, and an even greater load would have been

reached due to strain-hardening. For highly indeterminate multispan frames, large hinge angles may be required for the full development of a mechanism. However, for these same frames the load at the formation of the next-to-last hinge is almost as great as the maximum load, while the rotation at that instant is substantially less, as in the case shown in Fig. 9.9. Hence a lower

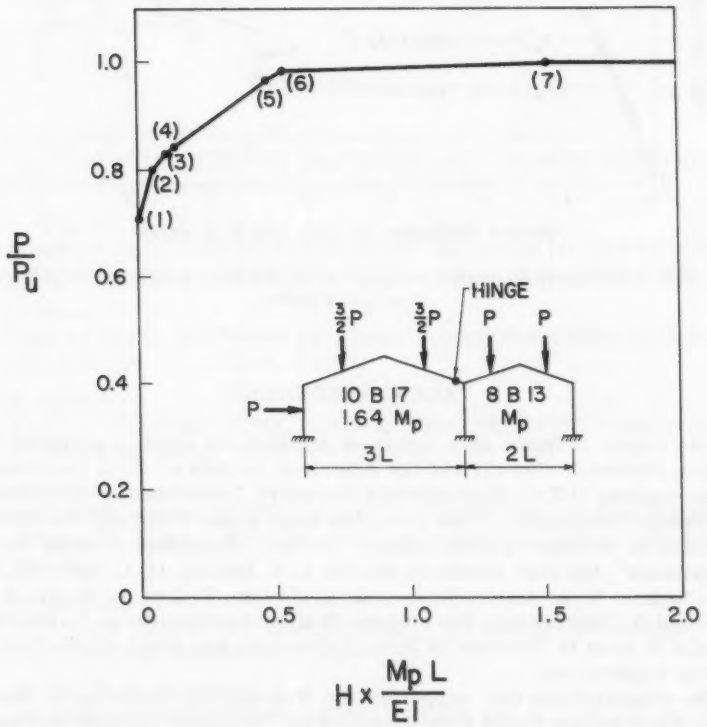

FIG. 9.9.—HINGE ANGLE REQUIRED FOR A TWO-SPAN PORTAL FRAME.

limit for rotation capacity requirement, suitable for general design purposes, need not be related to the large theoretical rotations associated with highly redundant frames.

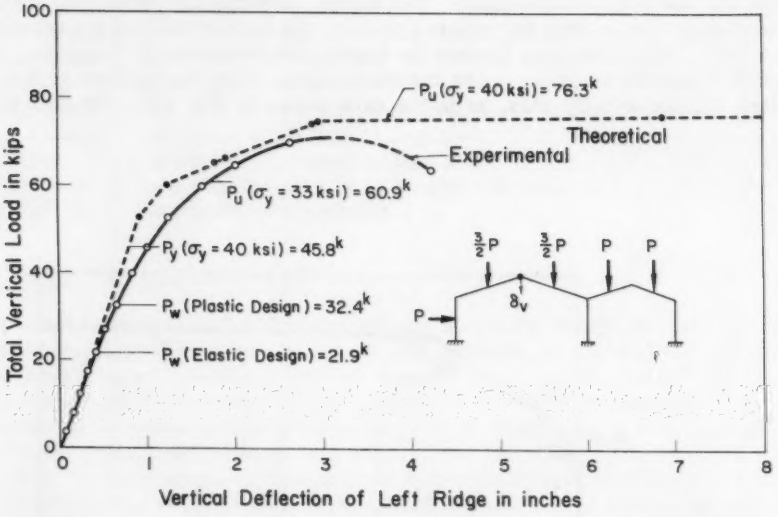

FIG. 9.10.—EXPERIMENTAL LOAD-DEFLECTION CURVE OF TWO-SPAN PORTAL FRAME.

ACKNOWLEDGMENT

This report is based on a series of preliminary reports prepared for the Welding Research Council and the American Society of Civil Engineers by a research group at Fritz Engineering Laboratory, Department of Civil Engineering, Lehigh University. This group has been engaged through the Institute of Research in an investigation entitled "Welded Continuous Frames and Their Components"; the staff members include L. S. Beedle, G. C. Driscoll, Jr., T. V. Galambos, R. L. Ketter, T. Kusuda, G. C. Lee, T. Lee, L. W. Lu, A. Ostapenko and B. Thurlimann. The original draft was written by G. C. Driscoll, Jr. William J. Eney is Director of Fritz Laboratory and Head of the Civil Engineering Department.

The organizations that supported the Research projects out of which the basic report was prepared were the following: American Institute of Steel Construction, American Iron and Steel Institute, the Department of the Navy (Office of Naval Research, Bureau of Ships, Bureau of Yards and Docks), the Welding Research Council, and the Column Research Council.

Although much of the experimental and theoretical work reported was performed at Lehigh University, the Welding Research Council and ASCE committees have attempted to broaden this report by including the results of research at other institutions, both here and abroad. The inclusion of this information and of certain unpublished data is gratefully acknowledged.

ADDITIONAL NOMENCLATURE

(See Progress Report No. 1 for basic nomenclature)

m = moments in structure in equilibrium with a unit load

s = distance along a member

α = non-dimensional parameter defining the distance to the plastic hinge in the rafter of a structure

Δ = deflection of a joint due to translation

θ'_A = rotation of joint A due to transverse loads assuming simply-supported ends of member

REFERENCES

9.1 K. E. Knudsen, C. H. Yang, B. G. Johnston, L. S. Beedle, PLASTIC STRENGTH AND DEFLECTIONS OF CONTINUOUS BEAMS, The Welding Journal, 32 (5), p. 240-s, (1953)

9.2 P. S. Symonds, B. G. Neal, RECENT PROGRESS IN THE PLASTIC METHODS OF STRUCTURAL ANALYSIS, Journal of the Franklin Institute, 252 (5 and 6), (1951)

9.3 B. G. Neal, THE PLASTIC METHODS OF STRUCTURAL ANALYSIS, John Wiley and Sons, Inc., New York, (1956)

9.4 K. H. Gerstle, DEFLECTIONS OF STRUCTURES IN THE INELASTIC RANGE, ASCE Proceedings, Paper 1290, Vol. 83 (EM3), July 1957

9.5 G. C. Driscoll, ROTATION CAPACITY REQUIREMENTS FOR BEAMS AND FRAMES OF STRUCTURAL STEEL, Ph.D. Dissertation, Lehigh University, (1958)

9.6 G. C. Driscoll, TESTS OF TWO-SPAN GABLED PORTAL FRAME, Proceedings, 1956 AISC National Engineering Conference

9.7 L. W. Lu, G. C. Driscoll, PLASTIC STRENGTH AND DEFLECTION OF A GABLED FRAME, Fritz Laboratory Report No. 205D.8, Lehigh University, June 1958

9.8 P. S. Symonds, A REVIEW OF METHODS FOR THE PLASTIC ANALYSIS OF RIGID FRAMES OF DUCTILE METAL, Techn. Report A 11-S'6/86, Brown University to Office of Naval Research, pp. 44-49, May 1950

9.9 L. S. Beedle, B. Thurlimann, R. L. Ketter, PLASTIC DESIGN IN STRUCTURAL STEEL, 1955 Summer Course Lecture Notes, Lehigh University, AISC, (1955)

9.10 L. S. Beedle, PLASTIC DESIGN OF STEEL FRAMES, John Wiley and Sons, Inc., New York, (1958)

9.11 C. K. Wang, C. L. Eckel,
ELEMENTARY THEORY OF STRUCTURES, McGraw-Hill Book Co., Inc., p. 243 ff., (1957)

9.12 C. H. Yang, L. S. Beedle, B. G. Johnston,
PLASTIC DESIGN AND THE DEFORMATION OF STRUCTURES, The Welding Journal, 30 (7), 348-s, (1951)

9.13 P. S. Symonds,
Discussion of PLASTIC DESIGN AND THE DEFORMATION OF STRUCTURES, The Welding Journal, 31 (1), 33-s-36-s, (1952)

Journal of the

ENGINEERING MECHANICS DIVISION

Proceedings of the American Society of Civil Engineers

CONTENTS

DISCUSSION

Page

Columns Under Combined Bending and Thrust, by Theodore V. Galambos and Robert L. Ketter. (April, 1959. Discussion: October, 1959. Discussion closed.)
by Theodore V. Galambos and Robert L. Ketter (closure) 163

Electrical Analog for Earthquake Yield Spectra, by G. N. Bycroft, M. J. Murphy and K. J. Brown. (October, 1959. Prior discussion: None. Discussion closed.)
by Glen V. Berg and Spiro S. Thomaides 165
by T. K. Caughey, G. W. Housner and D. E. Hudson 171
by O. A. Glogau 172

The Neutral Axis in Plastic Bending of Beams, by Aris Phillips. (October, 1959. Prior discussion: None. Discussion closed.)
by John C. Sprague 175
by H. Norman Abramson 175

Laterally Loaded Thin Flat Plates, by William A. Bradley. (October, 1959. Prior discussion: None. Discussion closed.)
by Bayliss C. McInnis, Steven Likuan Tsai and James R. Sims 179

Behavior of Structures During Earthquakes, by G. W. Housner. (October, 1959. Prior discussion: None. Discussion closed.)
by Clarence J. Derrick 183
by Glen V. Berg 185

Commentary on Plastic Design in Steel: Additional Design Considerations—I, Progress Report No. 3 of the Joint WRC-ASCE Committee on Plasticity Related to Design. (October, 1959. Prior discussion: None. Discussion closed.)
by M. N. Fialkow 187

Note.—This paper is a part of the copyrighted Journal of the Engineering Mechanics Division, Proceedings of the American Society of Civil Engineers, Vol. 86, No. EM 2, April, 1960.

COLUMNS UNDER COMBINED BENDING AND THRUST[a]

Closure by Theodore V. Galambos and Robert L. Ketter

THEODORE V. GALAMBOS,[1] A. M. ASCE, and ROBERT L. KETTER,[2] A. M. ASCE.—The writers wish to thank Mr. Winter for his enthusiastic support of their work. They wish to apologize for overlooking the fact that Reference 9 had already appeared in published form at the time this report was printed.

Further correlation between the authors' interaction curves (Figs. 6 and 7) and the "C.R.C. Interaction Equation," has been recently furnished by Charles Massonnet.[3] He has shown, in Figs. 21 and 22 of his paper, that excellent correlation exists between the writers' "exact" interaction curves and the "C.R.C. Interaction Equation," thereby proving, once more, the applicability of this latter equation.

---

[a] April, 1959, by T. V. Galambos and R. L. Ketter.

[1] Research Ass't. Prof., Dept. of Civ. Engrg., Lehigh Univ., Bethlehem, Pa.

[2] Prof. and Head, Dept. of Civ. Engrg., Univ. of Buffalo, Buffalo, N. Y.

[3] "Stability Considerations in the Design of Steel Columns," by Charles Massonnet, ASCE, Vol. 85, No. ST 7, September, 1959.

ELECTRICAL ANALOG FOR EARTHQUAKE YIELD SPECTRA[a]

Discussions by Glen V. Berg and Spiro S. Thomaides, T. K. Caughey, G. W. Housner and D. E. Hudson, and O. A. Glogau

GLEN V. BERG,[1] M. ASCE, and SPIRO S. THOMAIDES.[2]—The authors deserve commendation for having explored one of the lesser-known facets of the earthquake-engineering problem. In so doing they have contributed a little more to the fund of knowledge which ultimately leads to better building codes and more competent procedures for aseismic design.

General Discussion.—The paper suggests that a structure which survives a strong-motion earthquake in which it is distorted to such an extent that the masonry walls crack, but otherwise appears sound, has worked through a yield cycle. This may be true. However, for a steel-framed building of ordinary proportions, the distortion at which the frame members would yield is of the order of ten times the distortion at which masonry cracks would appear. The energy dissipated by the masonry walls might be substantial even if the frame never reached the yield point.

The yield-cycle concept may be useful even for such cases. Experiments have been reported[3,4] in which concrete filler panels in reinforced concrete frames have been loaded well into the inelastic region and then reverse loaded into the negative inelastic region. The load-deflection curves show a strong hysteresis loop, even for an unreinforced panel. A response curve of the elasto-plastic type would represent a rough approximation to this behavior. Shear-wall tests conducted at Stanford University,[5] as well as other experiments,[3] show response curves close to the elasto-plastic type for one-directional loading and unloading. It has been suggested[6] that reverse loadings of complete structures might produce load-deflection curves that mirror the curves for the first loading and unloading cycle, perhaps with softened features and a decaying ultimate strength. If this is so, the procedures used here may produce meaningful results for a larger class of structures than the authors claim.

The writers feel that yield excursion is the most important of the response parameters shown because it is a measure of the energy dissipated in plastic deformation. Any building code that permits plastic deformation must, in our opinion, be based on energy dissipation.

---

[a] October, 1959, by G. N. Bycroft, M. J. Murphy, and K. J. Brown.

[1] Assoc. Prof. of Civ. Engrg., Univ. of Michigan, Ann Arbor, Mich.

[2] Graduate Student, Dept. of Civ. Engrg., Univ. of Michigan, Ann Arbor, Mich.

[3] "Frictional Effects in Composite Structures Subjected to Earthquake Vibrations," by Lydik S. Jacobsen, Stanford Univ., Calif., March, 1959.

[4] "Studies of Shearing Resistance of Reinforced Concrete Plates," by M. Tomii, Report of the Inst. of Industrial Science, Univ. of Tokyo, January, 1957, (in Japanese.)

[5] "The Behavior of One-Story Brick Shear Walls," by Jack R. Benjamin and Harry A. Williams, ASCE, No. ST 4, July, 1958.

[6] Discussion of "Structural Dynamics in Earthquake Resistant Design," by Lydik S. Jacobsen, Proceedings, ASCE, No. ST 1, January, 1959.

Digital Yield Spectra.—The writers are currently engaged in research which calls for computing elasto-plastic response to earthquake by digital computer. The process used is a single-degree simplification of a method,[7] using a Runge-Kutta technique. To permit comparison of results, digital analyses have been made of the same systems reported in the paper, responding to the same earthquake component. The results are shown in Figs. B1 through B7, in which both the discussers' digital results and the authors' analog results are shown. The curves for $\lambda = 0.10$ have been omitted for clarity. A curve-by-curve comparison discloses several points worthy of comment.

The digital spectra are not as detailed as the analog spectra, so the minor fluctuations are not strictly comparable. However, the severe local fluctuations that appear in the analog curves of Fig. B1 in the period range of 3.3 to 5.0 sec are absent in the digital curves, and the points for the digital curves, which were calculated at 0.1-sec intervals of period in this region, give no hint that such local fluctuations exist. Perhaps the authors can suggest a reason for this anomaly.

The yield-displacement curves, Figs. B1 through B4, show a qualitative similarity of results, but the digital curves are lower than the analog curves for low values of yield level, and higher for high values of yield level. For $G = 0.175$ and $G = 0.24$ the digital maxima are roughly twice the corresponding analog maxima.

The yield-excursion curves, Figs. B5 through B7, also show a qualitative similarity, but the digital curves lie well above the analog curves. The digital maxima are roughly twice to three times the analog maxima, and the discrepancy tends to increase as the yield level increases. The disagreement here is especially disturbing because yield excursion is a measure of energy dissipation, which is an especially important parameter in limit design.

Possible Reasons for Differences.—There are four possible causes for the discrepancies; namely, differences in input data, errors in digital computation, errors in analog computation, or an inherent ill-condition of the problem itself.

It is presumed that the input data for the analog was obtained by photographic enlargement of the accelerogram record, and it seems reasonable to assume that the error here is small. Additional information on this point would be of value.

To produce the digital input data, the writers approximated the first 30 sec of the accelerogram closely by a piecewise linear function of time, and put the time-acceleration coordinates of the intersection points of successive line segments on punched cards. It took 562 line segments to describe the accelerogram. The axis location and initial conditions were chosen to make the mean, square computed ground displacement a minimum.[8]

Truncating the digital accelerogram at 30 sec would not have affected the results. The ground acceleration never exceeds 0.05 g after 27 sec, as compared with a peak of 0.33 g in the first few seconds. By 30 sec the oscillation would be damped sufficiently (the undamped case was not considered) to preclude a return to the yield level.

One might question whether the piecewise linear approximation used for the digital accelerogram was sufficiently accurate. But comparing the punched-

---

[7] "Dynamic Analysis of Elasto-Plastic Structures," by Glen V. Berg and Donald A. DaDeppo, to be published in Proceedings, ASCE.

[8] "Punched Card Accelerograms of Strong-Motion Earthquakes," by Glen V. Berg and S. S. Thomaides, Univ. of Michigan Research Inst., September, 1959.

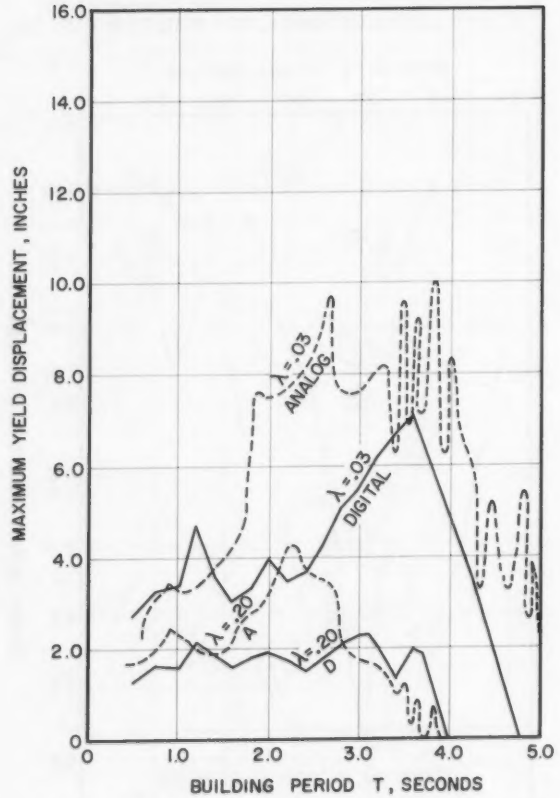

FIG. B1.—MAXIMUM YIELD DISPLACEMENT G = 0.06

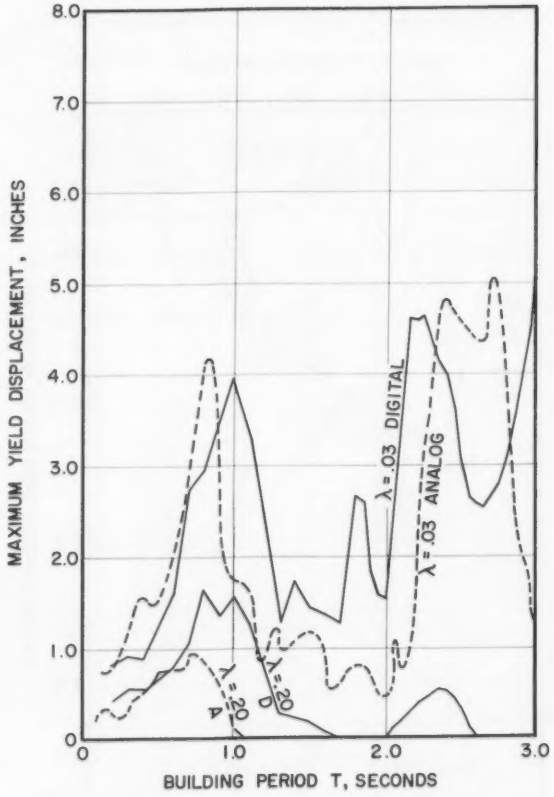

FIG. B2.—MAXIMUM YIELD DISPLACEMENT G = 0.12

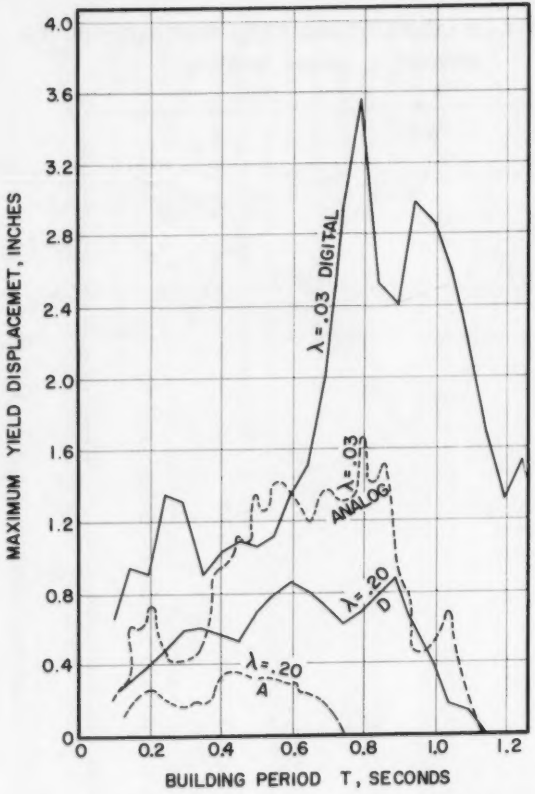

FIG. B3.—MAXIMUM YIELD DISPLACEMENT G = 0.175

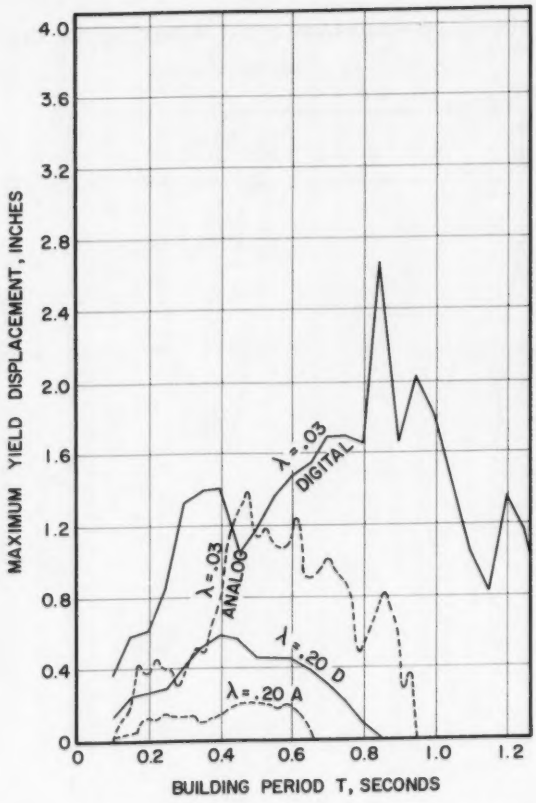

FIG. B4.—MAXIMUM YIELD DISPLACEMENT G = 0.24

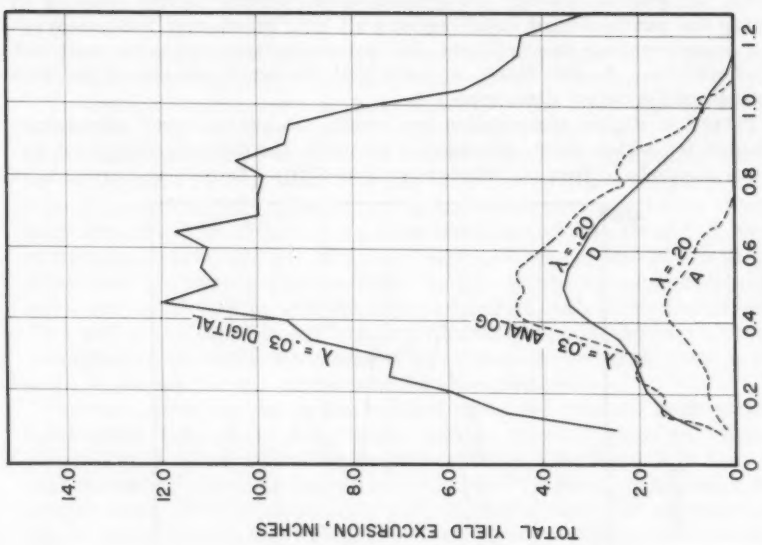

FIG. B6.—TOTAL YIELD EXCURSION G = 0.175

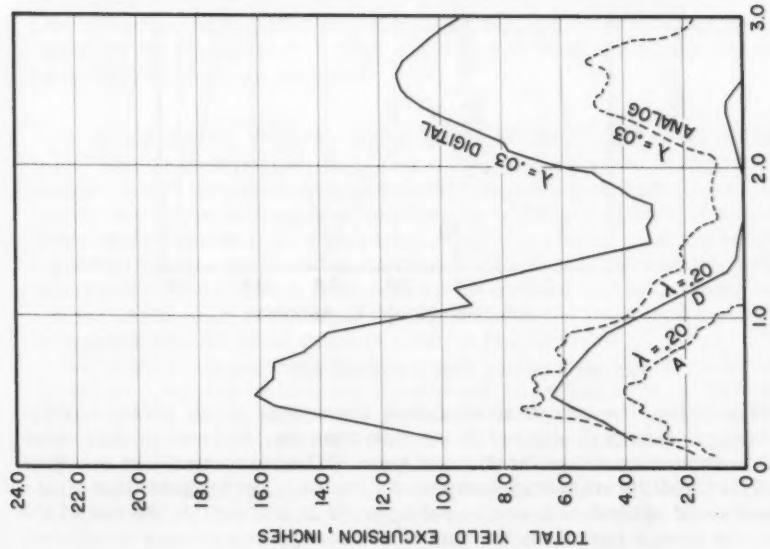

FIG. B5.—TOTAL YIELD EXCURSION G = 0.12

card accelerations with the original record reveals no significant differences. Moreover, the ground velocity and ground displacement curves obtained by integrating the punched card data[8] agree well with previously published results.[9] Linear response spectra have also been calculated and agree well with published spectra. It, therefore, appears that the input data should not be a major cause of the output discrepancies.

The errors in digital computation are small. In checks using elementary wave shapes for which exact solutions are known, the digitally computed results were accurate to four significant decimal digits. During an earthquake-

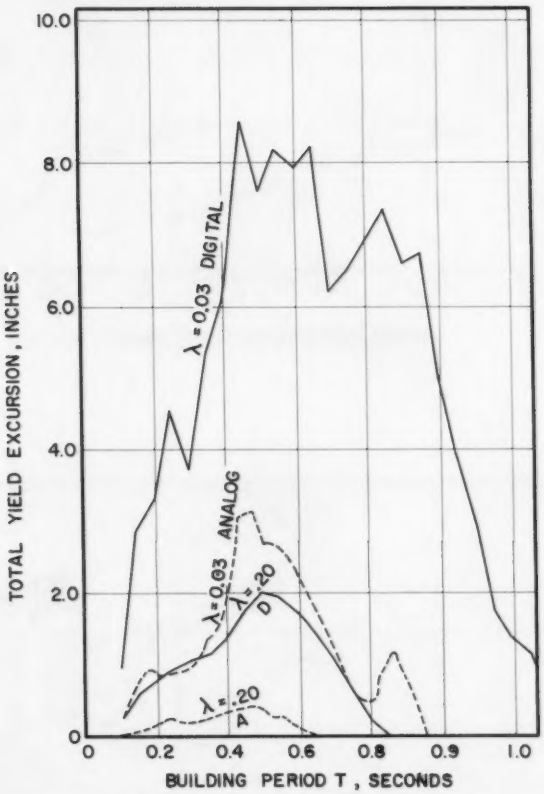

FIG. B7.—TOTAL YIELD EXCURSION G = 0.24

response solution, the computer evaluates the energy input, strain energy, kinetic energy, energy dissipated in viscous damping, and energy dissipated in plastic deformation, all as functions of time. Different computation schemes are used for the different energy components, so that an error generated in one component would not induce a compensating error in another. At the end of the solution, the energy input less the sum of the energy components is printed, to serve as an indicator of the accuracy of the solution. The total should, of

[9] "Lateral Forces of Earthquake and Wind," Joint Committee Report, Transactions, ASCE, 1952.

course, be zero. In most cases, it turns out to be substantially less than 1% of the energy input. The largest discrepancy found to date has been less than 2% of the energy input.

If the problem were inherently ill-conditioned, small differences in the input could produce large differences in the response. Although the non-linearities of the system might cause some magnification of the input differences, it seems, intuitively, that the near-random nature of the input would preclude any extreme magnification. As a rough check on this, several points for the case G = 0.175 were re-run using two perturbations of the accelerogram. In the first perturbation all acceleration readings were magnified 10%. This caused increases of 17% to 22% in total energy input, as compared with 21% for a linear system, increases of 5% to 36% in yield displacement, and 16% to 31% in yield excursion. In the second perturbation the odd-numbered acceleration ordinates were increased 0.01 g, and the even-numbered ones were decreased 0.01 g. This had the effect of superimposing a small noise on the earthquake signal. The effect of this upon the response was practically nil. In view of these results, it seems that the problem is not ill-conditioned.

Error control for the analog was not explained in detail in the paper. If the total error were of the same order as that encountered in the square wave check (Fig. 4 of the paper) the results would be adequate. It is seen in Fig. 4 that the analog response is consistently below the theoretical response for the square wave, which produces only one yield. How does this project to the case where yield occurs many times in both directions? What checks were made to insure that the yield displacement and yield excursion circuits were accurately recording all yields in such cases? Further information on the control of analog error would be desirable.

A new research area is being explored, and odd chance has made it possible to analyze the same problem by two entirely different methods. The results have an encouraging qualitative similarity but, contrary to expectations, they differ widely in magnitude. It is hoped that the authors may bring additional information to bear on the matter.

T. K. CAUGHEY,[10] G. W. HOUSNER,[11] M. ASCE, and D. E. HUDSON.[12]— It has been generally recognized that the usual earthquake response spectrum curves, which have been obtained on the assumption that structures remained linear, are far from complete descriptions of the actual state of affairs. The large energy dissipations which must come into play to limit the responses to large earthquakes must be associated with non-linear plastic action in the structure itself. The problem discussed by the authors is, thus, a most important one for earthquake-resistant design, and the extension of response-spectrum techniques into the yield range is a major step forward.

Although some calculations have been made of particular yield situations by digital computer techniques, the present investigation is the first complete application of analog methods to the problem. Some very preliminary experiments made at the California Institute of Technology, with analog circuits, indicated that the problems of obtaining force-displacement relationships with accurately defined sharp breaks was a difficult one. By using silicon diode limiter circuits the desired characteristics could be obtained over a limited

[10] Div. of Engrg., California Inst. of Tech., Pasadena, Calif.
[11] Div. of Engrg., California Inst. of Tech., Pasadena, Calif.
[12] Div. of Engrg., California Inst. of Tech., Pasadena, Calif.

range of frequencies. The problem of the variation of analog characteristics with frequency has been minimized by the scheme described in the present paper, since it is the exciting frequency that is changed rather than the analog frequency itself. It would be of interest to see the measured force-displacement characteristics as attained by the circuits used. For structural design purposes, the exact shape of the knee of this force-displacement function is perhaps of only secondary importance, in view of the fact that such relationships are usually not known for actual structures. The details of this function would likely be quite different for various types of structures, and it will require experimental studies of full-scale structures to definitely establish these patterns of behavior. It is because of these uncertainties that the linear assumption still has an important place in design calculations, although it must always be kept in mind that linear limits may give little or no information about ultimate failure conditions.

It would be expected that for the region in which the total displacements do not go far into the plastic range, the maximum yield displacements would not be very accurately determined, since small differences of large quantities would be involved. The qualitative significance of the results should not, however, be affected by these basic difficulties of analog technique.

It is evident from the conclusions reached that such yield phenomena will be of the greatest importance for earthquake resistant design problems. It is to be hoped that the authors will be able to continue these studies along the lines indicated.

O. A. GLOGAU.[13]—The authors are to be congratulated on their excellent work of bringing laboratory methods a step nearer to actual conditions. We must advance further along this line before analog results can be used directly for design code suggestions such as those in this paper. As an encouragement to further research the following comments are made:

In the following, a rigid building is meant to be a modern reinforced concrete shear wall structure and a flexible building to be a slightly damped, steel frame structure.

Earthquake resistant design is undoubtedly a dynamic problem.

On the basis of some earthquake spectra, and a number of assumptions, it has been shown that under certain foundation conditions rigid buildings develop larger base shears than flexible buildings.

As a result a suggestion is made that rigid buildings should be designed for equivalent accelerations of 50% g.

Rigid buildings when designed for only 10% g have an excellent record in severe earthquakes and would, if this suggestion was put into codes, be placed at a severe disadvantage compared to the flexible ones, about whose performance comparatively little is known at present.

It is, therefore, well to remember that there are a number of questions, with great bearing on the matter, which have not been satisfactorily answered to date. Some of these are:

1. The relationship between damping and natural period. Some researchers are of the opinion that they are inversely proportional and, thus, cancelling the advantage of the long period building (7$_1$10).[b]

---

[13] Senior Engr., Ministry of Works, Wellington, N. Z.

[b] References in parentheses refer to the 1956 Earthquake Conference.

2. The effect of various types of foundation materials on earthquake spectra, natural period and damping.

3. Probability of resonance: Is the flexible (steel frame) building more likely to become "fully" resonant in an earthquake having a coherent train of periodic motion, than a rigid building with its large variations in natural period as it becomes strained?

4. The percentage of the inherent strength of a modern, shear wall building due to the normally uncalculated effect on damping and energy absorption of partitions, stairs, etc. In the logically designed and constructed flexible building, this effect is difficult and expensive to achieve.

5. Collapse resistance to ground distortion: Rigid buildings, in particular the box-type construction, have much greater inherent collapse resistance to ground motions, in particular tilt, than flexible buildings. (The Polytechnical School in Mexico City, appears to have been a dynamic design (flexible) but collapsed in 1957, probably due to foundation failure).

Rigid buildings have been observed to rock without the existence of appreciable horizontal stress (7_1-3).

Summary.—Apart from the uncertainty as to what the actual base shear amounts to, the uncalculable effects of item (5) above have as great a bearing on the choice of a suitable load factor (and hence equivalent acceleration used in design) as the ability of a building to absorb energy. It is good engineering practice to use relatively high load factors for new and little proved constructions, and to reduce load factors for those with satisfactory performance.

THE NEUTRAL AXIS IN PLASTIC BENDING OF BEAMS[a]

Discussions by John C. Sprague and H. Norman Abramson

JOHN C. SPRAGUE,[1] F. ASCE.—Concrete is, at best, an imperfectly elastic material. Because it does not follow the rule of conventional elasticity, it is considered more correct to refer to this property in concrete as the rate of change of stress with respect to strain. Stress-strain curves are not identical for the tension and compression areas of loaded, plain concrete beams, as assumed by the author.

Since the shape of the stress diagram and the location of the neutral axis changes when the elastic limit in tension is exceeded, the stress-strain relationships in tension and compression fibers of a plain concrete beam are unequal when failure load is approached; and the compression fibers are stressed only to about 12% of potential at the instant of failure. This has been illustrated graphically for 3rd-point loading.[2] Since the compression fibers are never highly stressed, their modulus of elasticity tends to remain substantially rectilinear and constant, while that of the tension fibers is not rectilinear and decreases with increase in depth, resulting in differential ratios of compressive (E_c) to tensile (E_t) moduli of elasticity for beams of varying depth. The ratio E_c/E_t exceeds unity, for conventionally loaded beams.

Apparent "plasticity" in plain concrete subjected to loading, affords relief of elastic peak stresses in the extreme tension fibers, accompanied by local destruction of cohesion. It would be interesting to know whether or not the author considered plasticity as synonymous with inelasticity.

H. NORMAN ABRAMSON.[3]—Many of the most well-known and widely used methods of analysis of bending of beams in the plastic range involve the assumption that the neutral axis remains fixed with respect to the beam cross section. However, in many practical applications the beam section is unsymmetrical with respect to a principal axis, or else the plane of the applied loads is not parallel to a principal plane, which, in either case, leads to significant twisting (rotation of the cross section) of the beam, and resultant motion of the neutral axis, as the loading increases. In fact, this rotation of the cross section is often the primary factor in limiting the ultimate strength.

When end moments, not parallel to a principal plane of bending, are applied to beams of symmetrical cross section, the beam will bend with respect to both

---

[a] October, 1959, by Aris Phillips.

[1] Mgr., Tech. Publications, ASCE, New York.

[2] Fig. 8 of the paper "Effect of Depth of Beam Upon the Modulus of Rupture of Plain Concrete," ASTM, Vol. 55, 1955.

[a] October, 1959, by Aris Phillips.

[3] Dir., Dept. of Applied Mechanics, Southwest Research Inst., San Antonio, Tex.

principal axes, and will also twist. When the twist at the mid-span is very small and the curvature is negligible, the resisting couple must be parallel to the applied couple. However, as curvature and twist increase, the resisting couple must rotate with respect to the cross section, which in turn requires rotation of the neutral axis. Also, as bending progresses and the outer corners of the section enter the plastic condition, it can be seen that for the resisting couple to remain in the same plane, the neutral axis must rotate. This is because the "soft" corners cause the points of application of the resultant compressive and tensile forces to move toward the section centroid, and, therefore, if the plane of the couple is to remain fixed with respect to the cross section, the neutral axis must rotate in order to provide for the readjustment of the stress distribution. A similar discussion applies also for beams of unsymmetrical cross section, even if the plane of the applied couple is parallel to a principal axis.

In view of the practical importance, then, of the motion of the neutral axis in the bending of beams in the plastic range, the author's present paper dealing with analytical aspects of the problem, even though restricted to beams with cross sections having a plane of symmetry with respect to a principal axis, is most welcome.

Turning again, however, to the more complicated problems discussed above, it may be of more or less direct interest to mention, even if only very briefly, some experimental observations[4,5] relation to motions of the neutral axis when the loading is unsymmetrical and the beam cross sections are either symmetrical or unsymmetrical (rectangular, I and L-shape).

Rectangular Beam.—As one of a series of tests, a 3/8 in. by 1 in. aluminum alloy 24 S-T, rectangular beam with a length of 40 in., was subjected to bending with the plane of the applied couple at an angle of 14°-56' to the major principal axis.[4] The change in location of the neutral axis was obtained graphically from SR-4 strain readings on the beam faces. The neutral axis rotated counter-clockwise, with respect to the minor principal axis, about the same amount as the cross section, as a whole, rotated clockwise. The maximum bending moment of slightly over 2,000 in.-lb, resulted in a rotation of the neutral axis of some 10°.

I-Section Beam.—Rectangular beams of 40 in. total length with an 18 in. span at the center of I-section shape, and a value of I_x/I_y of about 10 to 1, were studied experimentally.[4] Measurements were made of flange rotation, web rotation, and horizontal and vertical components of deflection at mid-span. For loadings with the plane of the applied couple at both 15° and 30° to the major principal axis, it was found that the flanges rotated in opposite directions with respect to the web, with angles up to 3-1/2°, while the web rotated to angles up 8°, but the neutral axis showed only small rotations of a degree or two.

L-Section Beam.—Studies were also carried out with 24 S-T aluminum alloy L-section beams[5] of similar size as the I-beams (1 in. by 2 in. overall rectangular cross section) in which the plane of loading was at angles of 0°, 30°, 60°, and 76°-07' to the major principal axis. In general, the rotation of the

---

4 "Stability of Rectangular and I Section Beams in the Plastic Range," by H. A. Williams, Tech. Report No. 8, Contract AF W33-038AC-16687, Stanford Univ., June 1, 1949.

5 "An Investigation of the Bending of Angle Beams in the Plastic Range," by H. N. Abramson, Journal of the Aeronautic Sciences, Vol. 22, No. 12, pp. 818-828, December, 1955.

neutral axis was of the order of 3° to 4°. Again, the neutral axis appeared to rotate less with respect to the cross section than the cross section itself rotated with respect to its original position. The neutral axis also translated toward the compression side of the beam, by an amount on the order of 0.01 in. or 0.02 in.

These experimental results would seem to indicate that motion of the neutral axis, as well as that of the cross section as a whole, may often exhibit an important influence over the behavior of beams subjected to bending in the plastic range. Therefore, further study of these problems, in extension of the author's analysis, would be of considerable interest.

LATERALLY LOADED THIN FLAT PLATES[a]

Discussion by Bayliss C. McInnis, Stephen Likuan Tsai, and James R. Sims

BAYLISS C. McINNIS,[1] STEPHEN LIKUAN TSAI,[2] and JAMES R. SIMS,[3] F. ASCE.—The writers have been very interested in this informative paper on the experimental analysis of flat plates using the Ligtenberg method, since similar experiments have been in progress at Rice Institute. As the author points out, two methods of experimental analysis using reflected light have been developed. The one reported in this paper and developed by F. K. Ligtenberg[4] determines the surface slopes by a double exposure technique. Curvatures are then obtained graphically. An earlier technique developed by M. Dantu[5,6] obtains the image strain which is proportional to the bending strain of the plate. The method used by the Presan Corporation is essentially the same as that explained in detail by M. Dantu.[7]

Experiments have been conducted by the writers using a circular plate cut from magnesium sheet. If the surface is carefully polished to remove the slightest imperfections from the surface, good photographs of the reflections from the ruled screen can be obtained. Although somewhat better photographs have been obtained using plastic models vacuum coated with aluminum, metal models are preferred, since a constant value of the modulus of elasticity can be used for metals. As explained by Mr. Bradley, the modulus of elasticity of plastics varies.

Obtaining sufficient fringes on the photographs of the model for a reasonable interpretation of the results, and at the same time keeping the deflections small compared with the thickness of the plate so that the usual bending theory of thin plates applies, seems to be a problem in the application of the Ligtenberg method. The low modulus of elasticity of magnesium sheet, approximately 6.5×10^6 psi, makes possible the use of models 1/8 in. in thickness, with which desired deflections can be obtained with conveniently small loads.

---

[a] October 1959, by William A. Bradley.

[1] Graduate Student, Rice Institute, Houston, Tex.

[2] Graduate Student, Rice Institute, Houston, Tex.

[3] Prof. of Civ. Engrg., Rice Institute, Houston, Tex.

[4] "The Moiré Method - A New Experimental Method for the Determination of Moments in Small Slab Models," by F. K. Ligtenberg, Proceedings, Soc. for Experimental Stress Analysis, Vol. XII, No. 2, 1955, pp. 83-98.

[5] "Description d'une Méthode Nouvelle pour la Detérmination Experimental des Flexons dans une Plaque Plane," by M. Dantu, Annales des Ponts et Chaussées, No. 1, January, 1940, pp. 5-20.

[6] "Étude Expérimentals des Plaques par a Methode Optique," by M. Dantu, Annales des Ponts et Chaussees, No. 3, May-June, 1952, pp. 271-344.

[7] Ibid., p. 293.

It is interesting to compare the author's experimental results with an approximate solution which has been used by the writers for a square, uniformly loaded, clamped plate. Values for moments and deflections obtained by the author with Ligtenberg method, and values obtained by the writers using the Rayleigh-Ritz method are plotted in Fig. M2. Fig. M2 is similar to Fig. 15, except the results obtained by the Rayleigh-Ritz method are plotted in place of the author's finite difference results.

The problem of a square, uniformly loaded clamped plate was solved applying the Rayleigh-Ritz method to thin plate theory. The potential energy of the system is expressed by[8]

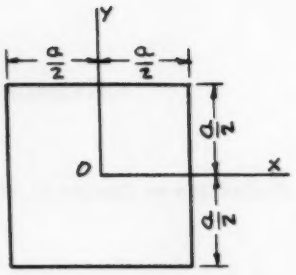

FIG. M1

$$V = \frac{D}{2} \iint \left(\frac{\partial^2 w}{\partial x^2} + \frac{\partial^2 w}{\partial y^2} \right)^2 dx\ dy - \iint_A q\ w\ dx\ dy$$

The following function, which satisfies the boundary conditions, was assumed for the normal displacement, w:

$$w = \sum_{n=1}^{\infty} A_n \left[x^{2n} - \left(\frac{a}{2} \right)^{2n} \right]^2 \left[y^{2n} - \left(\frac{a}{2} \right)^{2n} \right]^2$$

Taking only two parameters, A_1 and A_2, their values were determined by minimizing the potential energy and were found to be

$$A_1 = 0.019566 \frac{q}{D\left(\frac{a}{2}\right)^4} \qquad A_2 = 0.001855 \frac{q}{D\left(\frac{a}{2}\right)^{12}} \cdots\cdots$$

Substituting these values into the function assumed for w, yields

$$W = 0.018566 \frac{q}{D\left(\frac{a}{2}\right)^4} \left[x^2 - \left(\frac{a}{2} \right)^2 \right]^2 \left[y^2 - \left(\frac{a}{2} \right)^2 \right]^2$$

$$+ 0.001855 \frac{q}{D\left(\frac{a}{2}\right)^{12}} \left[x^4 - \left(\frac{a}{2} \right)^4 \right]^2 \left[y^4 - \left(\frac{a}{2} \right)^4 \right]^2$$

To check the accuracy of this solution, the maximum deflection of the plate, taking $\nu = 0.3$, was found to be

$$W_{max} = \frac{0.013937\ q\ a^4}{E\ h^3}$$

This answer is 1.0% greater than the value obtained by I. A. Wojtaszak.[9]

---

8 "Applied Elasticity, by Chi-Teh Wang, Mc Graw-Hill Book Co., New York, 1953, p. 288.

9 "The Calculation of Maximum Deflection, Moment, and Shear for Uniformly Loaded Rectangular Plate With Clamped Edges," by J. A. Wojtaszak, Journal of Applied Mechanics, Transactions, ASME, Vol. 59, Part I, 1937, p. A-174.

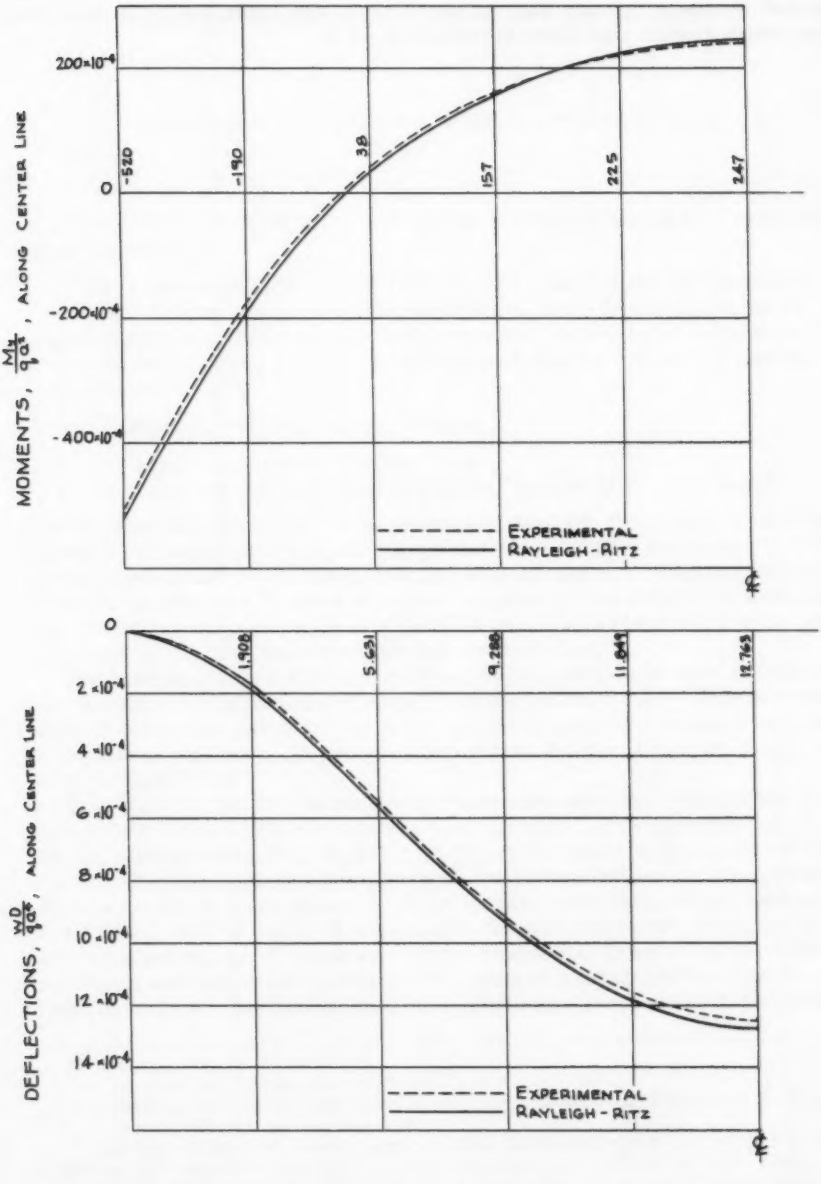

FIG. M2.—MOMENTS AND DEFLECTIONS ALONG CERTERLINE OF SQUARE, UNIFORMLY LOADED CLAMPED PLATE.

In obtaining the results to be plotted in Fig. M2, ν was assumed to equal 1/3, since this value was used by the author.

The very close agreement between the experimental results and the energy method seems to indicate that, in some cases, the experimental method may give better results than finite difference method.

BEHAVIOR OF STRUCTURES DURING EARTHQUAKES[a]

Discussions by Clarence J. Derrick and Glen V. Berg

CLARENCE J. DERRICK,[1] F. ASCE.—The author's thesis is summarized in his "Conclusions:"

> "It is more reasonable to take the point of view that the design should be such that the structures will survive the more frequent, moderate ground motions without damage but in the more rare event of very strong ground motion, damage would be tolerated so long as it was not a hazard to life and limb."

Implementation requires two definitions:

1. Of "very strong ground motion," and
2. Of the circumstances which constitute "hazard to life and limb."

It is implied that the El Centro earthquake of May 18, 1940, may be used as a standard for maximum "very strong ground motion." The station at which this earthquake was observed, instrumentally, was located on a "foundation column" of "sedimentary rock." There is reason to believe, from Gutenberg's studies,[2] that for motion at periods greater than 0.6 sec, the surface effect upon "deep alluvium" might have been considerably more violent.

The "averaged spectra" were produced by composition of records from different stations located upon different "foundation columns." This procedure tends to obliterate peculiarities of ground motion which Gutenberg attributed to foundation influence. At periods greater than 0.5 sec, these variations may be quite significant.

It is implied that the values of the "averaged spectra," multiplied by the prescribed factors will reproduce actual spectra. A comparison for the El Centro earthquake of May 18, 1940, at 20% of "critical" damping shows that a considerable discrepancy exists between the deduced values and the published spectra for the N-S component.[3] If the standard maximum is assumed as the resultant of the N-S and E-W components, the deduced values are about 2/3 of the published values. It would seem more reasonable to establish the absolute maximum, and then make allowances for increased strain, rather than to make reductions in the maximum conditions and increases in strain allowances.

---

[a] October, 1959, G. W. Housner.

[1] Cons. Structural Engr., Los Angeles, Calif.

[2] "Effects of Ground on Earthquake Motion," by B. Gutenberg, Bulletin of the Seismol. Soc. of Amer., Vol. 47, No. 3, July, 1957.

[3] "Analysis of the Taft Accelerogram of the Earthquake of 21 July 1952," by G. W. Housner, Earthquake Research Lab., California Inst. of Tech., September, 1953. ("Acceleration Spectrum" for El Centro 5/18/40, N-S, Fig. 11, p. 15; "Velocity Spectrum" for this earthquake, Fig. 14, p. 20).

Certainly, the assumptions should not be lower than the maximum component of an earthquake which actually has occurred.

The "energy" analysis proposed by Mr. Housner is a generalized solution of the problem of response by a "damped" resonator, subjected to forced stimulation. In an actual design situation, the problems are specific. The engineer is not designing an average structure for average conditions but a particular structure for maximum adverse conditions. The assumption that the distribution of mass does not influence the amount of work performed by an earthquake, is open to question.

There is, at present, no adequate "background of experience" from which the probable performance of "modern type," multi-story, framed buildings, subjected to "very strong ground motion," may be deduced. Blume's comparison of computed and observed free period, for the Alexander Building,[4] indicates that much of the rigidity of older type multi-story buildings derives from elements no longer included in modern construction. In these older type buildings, the maximum distortions apparently are not enough to over-strain the frame-work. What the San Francisco earthquake of 1906 would have done to a "modern type" multi-story building is a moot question. So far, there is no positive evidence on which to base either an analytical or an empirical solution involving "plastic action" or "damping" in "modern type," multi-story buildings.

For such situations, the case for "reasonable prudence" has been stated:

> ". . . It is also the opinion of the writers that all points of earthquake-resistant design that cannot be established on the basis of reliable empirical data or incontrovertible analysis should be treated with caution and that the design should be on the safe side."[5]

With respect to "damping," Jacobsen's opinion is illuminating: "Frictional effects in composite structures present a complicated picture, since frictional components are governed by various laws, most of which are obscure, even for limited ranges of distortion . . .," and, "It appears relatively certain that the only practical way of taking frictional forces into consideration is to use the concept of equivalent viscous damping forces, an approximation which is very satisfactory in linear and 'almost linear' cases, but in highly non-linear cases the concept gives only crude approximations."[6]

Until more is known about the performance of "modern-type," multi-story buildings, subjected to "very strong ground motion," the conservative designer has no alternative but limitation of distortions to "linear" or "almost linear" levels. Many designers are already doing this. However, in some designs, the limitation is predicated upon shears deduced from "seismic factors" prescribed by building codes. Since shears so deduced usually are only fractions—from one-fifth to one-third—of the actual maximum dynamic shears, such limitations may be unrealistic.

The assurance of public safety involves more than prevention of collapse in the structural framework and fall of debris. In a disaster, such as an earthquake developing "very strong ground motion," the hazards of fire and panic

---

[4] "Period Determinations and Other Earthquake Studies of a Fifteen-Story Building," by J. A. Blume, Proc. World Conf. on Earthquake Engrg., Berkeley, Calif., 1956.

[5] Discussions of Paper 2514, by R. R. Martel, G W. Housner and J. A. Alford, Transactions, ASCE, Vol. 117, esp. p. 771, 1952.

[6] "Frictional Effects in Composite Structures Subjected to Earthquake Vibrations," by L. S. Jacobsen, (A Technical Report Prepared under California Standard Agreement No. 1976, with Stanford University) Dept. of Mech. Engrg., Stanford Univ., March 9, 1959.

are extreme. The structural framework must be capable, not only of maintaining itself but of preventing other safety devices from becoming inoperable. Fire separation diaphragms must remain intact to prevent the spread, not only of fire but also of smoke and other asphyxiating gases. To prevent panic, elevator machinery must remain in operation, elevator doors free from jamming, and stairs and other exits unblocked. To assume that interior partitions, stairs, etc., will be wrecked, allowing the framework to distort plastically, is to beg the question.

If the building is sufficiently rigid to insure overall safety, it is probable that frame stresses will not be critical.

GLEN V. BERG,[7] F. ASCE.—On the effect of damping, Mr. Housner states that "Moderate amounts of damping will give appreciable reduction of stresses. It is also clear that large amounts of damping will give large reductions in the forces and stresses in a structure." A simple characterization of the quantitative effect of damping upon the forces and stresses can be obtained through the following crude analysis:

Some strong-motion accelerograms show a long sequence of acceleration pulses of more or less uniform magnitude, and others show a brief series of strong pulses followed by a long series of relatively weak pulses. One might idealize the former as a random function that feeds energy into a structure at a constant rate, and the latter as a single impulse. Any real earthquake should fall somewhere between these two extremes.

Responding to an earthquake of the first type, a simple structure would build up essentially a sinusoidal response tuned to its own natural frequency, and the amplitude would build up until the energy dissipated per cycle balanced the energy input. For a given rate of energy input, the maximum amplitude (and stress) attained by the structure would be proportional to $\sqrt{1/\nu}$, where ν is the fraction of critical damping.

A single impulse would cause a simple structure to respond in an exponentially decaying sinusoidal motion. For a given impulse the maximum displacement (and stress) attained by the structure would be proportional to $e^{-\nu\left(\frac{\pi}{2} - \nu\right)}$ which is, approximately, $1 - 1.57\nu + 2.23\nu^2$.

It is interesting to see how computed displacements fit between these two ideal cases. Displacement spectra have been computed by the writer for the strong-motion earthquakes of El Centro 1934, El Centro 1940, Olympia 1949, and Taft 1952. Fig. B1 shows, for typical systems selected arbitrarily from the spectrum calculations, plots of $\frac{S_d(\nu)}{S_d(0.02)}$ versus ν, where $S_d(\nu)$ is the maximum displacement of the system for damping equal to ν. The 2% of critical damping was chosen as the reference point because it represents about the least amount of damping that can exist in a real structure. (Zero was avoided because $\sqrt{1/\nu}$ becomes infinite there.) Nearly all of the displacements fit between the ideal cases, and the results are scattered over almost the entire range between them. It, therefore, appears that the two ideal cases may be considered as bracketing the quantitative effect of damping, and that trying to tie down the characterization within narrower bounds would be futile.

---

[7] Assoc. Prof. of Civ. Engrg., Univ. of Michigan, Ann Arbor, Mich.

In his discussion of limit design, the author ". . . assumes that the input energy into the overstressed structure is the same as the maximum input energy for an equivalent, elastic, undamped structure." Current earthquake research at the University of Michigan, includes an exploration of this particular point

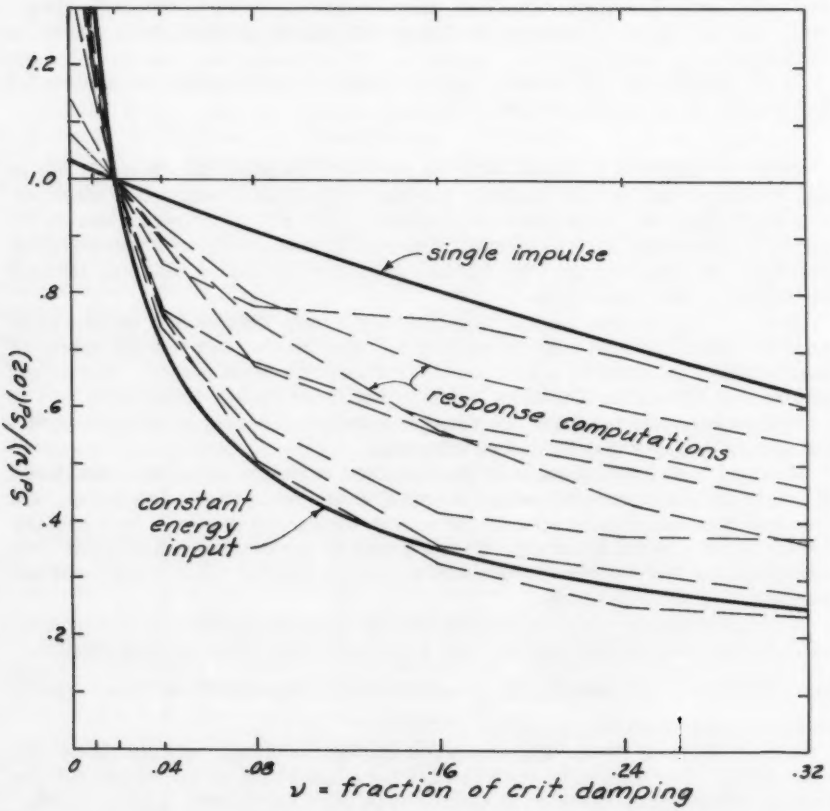

FIG. B1.—EFFECT OF DAMPING ON MAXIMUM STRESS

for elasto-plastic systems. Results to date indicate that the author's assumption is conservative on the average. However, if an attempt were made to employ the assumption for an isolated case, and the case happened to correspond to a low point in the undamped spectrum, the results could err considerably on the unsafe side.

COMMENTARY ON PLASTIC DESIGN IN STEEL: ADDITIONAL DESIGN CONSIDERATIONS—I[a]

Discussion by M. N. Fialkow

M. N. FIALKOW,[1] F. ASCE.—The expression in paragraph 6.2, of the Commentary for the maximum ratio of section depth to web thickness, which is adequate to insure against premature plastic buckling of the web for the case of combined bending and compression, warrants further consideration and discussion. This expression for depth-thickness ratio, namely,

$$\frac{d}{w} \leq 70 - 100\,\frac{P}{P_y} \qquad \left(\frac{P}{P_y} \leq 0.27\right)$$

is shown in the paper to hold for $\epsilon_{max}/\epsilon_y = 4.0$ and, consequently, furnishes a safe ratio for use when $\epsilon_{max}/\epsilon_y \leq 4.0$. The recommendation for its adoption by the Committee, therefore, implies that under "normal" circumstances, plastic collapse would occur without $\epsilon_{max}/\epsilon_y$ exceeding 4 in any of the plastic hinges. This recommendation is not concurred by the writer since, as will be shown below, this value, ($\epsilon_{max}/\epsilon_y = 4$), is frequently exceeded in normal, static, load design problems, its use imposes undue limitation on plastic deflection needed in cases of dynamic loading, and it is not consistent with the corresponding strain ratios permitted, in beam flanges during hinge rotation, by the ratio of flange width to thickness recommended by the Committee. In view of the interdependence between the maximum possible strain and the section depth-web thickness ratio, the relationship of such items as beam-shape factor and computational method to this maximum strain is also noted herein.

a. Several instances of plastic collapse under static loading, which are not considered "abnormal" but which require that $\epsilon_{max}/\epsilon_y$ exceed 4 in one or more of the plastic hinges, are cited below:

Example 1.—Fixed-End Beam with Concentrated Load at the Third Point (Fig. F1)—Beedle, in Reference 1.2, on pages 202, 203, has solved this problem and finds that, at the left support, ϕ_A, the rotation per unit length in the hinge just prior to collapse, is 8 times as great as ϕ_P, the rotation per unit length up to the elastic limit. With $\phi = \epsilon_{y0}/y_0$, it follows that $\epsilon_{max}/\epsilon_y = 8$. In this analysis, the hinge length has been taken as one eighth the distance from the point of contraflexure to the fixed end, which holds for a wide flange section with average shape factor loaded by a concentrated load.

Example 2.—Pin-supported Frame with Vertical and Lateral Loads (Fig. F2)—In Reference 1.5 on pp. 100-104, Hodge shows that the hinge rotation at joint G at collapse is 0.0135 radians consisting of rotations $\theta_{GF} = 0.0133$ and

[a] October, 1959, Progress Report No. 3 of the Joint WRC-ASCE Committee on Plasticity Related to Design.

[1] Chf., Design Branch, U. S. Army Engr. District, New York.

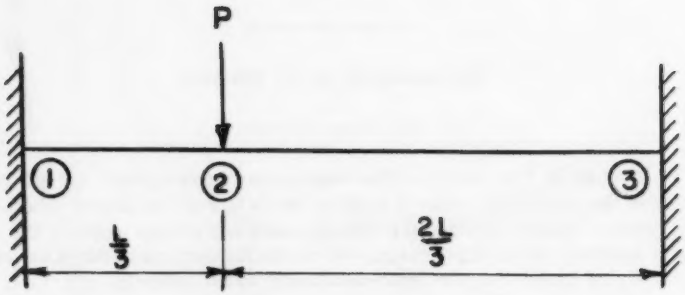
P
1
2
3
L/3
2L/3

FIG. 1

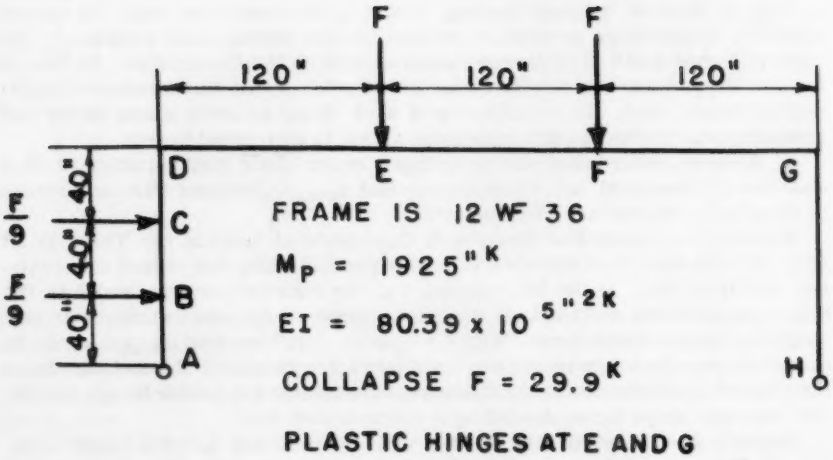
F
F
120"
120"
120"
D
E
F
G
C
B
A
H
40"
40"
40"
F/9
F/9
FRAME IS 12 WF 36
M_p = 1925"K
EI = 80.39 x 10^{5} "2K
COLLAPSE F = 29.9K
PLASTIC HINGES AT E AND G

FIG. 2

$\theta_{GH} = 0.0002$. Based on the characteristics of this frame at collapse, as shown in Fig. 1.8 of Reference 1.5, the location of the point of contraflexure in the horizontal member is computed to be 62 in. from point G; this corresponds to a hinge length of 1/8 x 62 or 7.75 in., with the hinge located on the horizontal member. For the material constants used,

$$\phi_A = \frac{\theta_G}{\Delta L} = \frac{0.0135}{7.75} = 17.4 \times 10^{-4} \text{ radians per in.}$$

and

$$\phi_P = \frac{M_P}{E\,I} = \frac{1925}{80.39} \times 10^{-5} = 2.4 \times 10^{-4} \text{ radians per in.}$$

Hence, $\epsilon_{max}/\epsilon_y = \phi_A/\phi_P = 7.25$.

b. To provide in design, for large dynamic loads of short duration, utilization of the large energy absorbing capacity of structural components when deformed into the plastic zone is often necessary to achieve practical structures. This type of design is characteristic of many "hardened" defense installations where capacity to withstand overpressures and ground shock associated with nuclear blast is essential.

(1) Keeping the value of $\epsilon_{max}/\epsilon_y$ at 4 or less in flexural members would impose a severe restriction on the amount of plastic deflection and, therefore, on the ability to absorb energy loads. Thus, in the case of either a simple or a fixed-end beam subjected to a concentrated dynamic load at the midpoint, computations indicate that the maximum deflection would be limited by this criterion to 2.5 times the elastic deflection. This contrasts with test data, for such beams, which indicate the ultimate deflection at collapse to be 26 times the maximum elastic deflection.

(2) Even if the design were developed on the basis of the above limit on $\epsilon_{max}/\epsilon_y$, the approximate nature of the assumed design overpressure and shock loading and the possibility of occurrence of loadings more severe than those assumed for design make it highly desirable that the structure be capable of deformations beyond those computed for the assumed loading.

c. The Committee recommends that for beams in bending the maximum ratio of flange width to thickness, be limited to 17. This permits the development in the flange of strains to the point of strain-hardening which corresponds to a ratio of $\epsilon_{max}/\epsilon_y$ of 12 for A7 type structural steel. Reference 6.27 reports that tests on beams with these flange dimensions confirm the theoretical rotation capacity with the further advantage of indicating no sudden drop in load capacity for strains beyond the point of strain hardening. For consistent beam design the critical web dimensions should permit maximum strains equal to those in the flange, that is, to the point of strain-hardening.

In view of the preceding, it appears to the writer that the expression cited above for maximum ratio of section depth to web thickness for beams in combined bending and compression should be revised. Adoption of an expression based on a maximum strain in the web, at its junction with the flange equal to that of strain-hardening, is believed justified; this corresponds to $\epsilon_{max}/\epsilon_y = 12$ for A7-type structural steel.

To insure proper application of the Committee's recommendations for section properties, determination of the maximum strain in the hinge is necessary. In this discussion, the method of determining ϵ_{max} has been that used by Beedle

in Reference 1.2. By this method ϕ_A is determined as the average rotation in the hinge, that is, the total hinge angle divided by the hinge length. The hinge length is taken to be the length of beam over which the moment is greater than the yield moment, and is, therefore, dependent on the beam-shape factor and the type of loading. For the case of concentrated loads, as in Examples 1 and 2 above, the hinge length varies between 0.09 and 0.15 times the distance, from the point of contraflexure to the fixed end, as the shape factor varies between 1.10 and 1.18, the usual range in shape factors for wide flange sections. Thus, in lieu of $\epsilon_{max}/\epsilon_y = 8$, as computed in Example 1 for a beam with shape factor of 1.14, this ratio would equal 11 for a beam with shape factor of 1.10. For uniform loading, the hinge length would vary between 0.3 and 0.4 of the beam length for simple spans, and between 0.05 and 0.08 times the beam length for cantilever beams. A different determination of hinge length is made in Reference 1.5 on page 103, where Hodge uses one half of the above definition of hinge length in order to compute the "average" value of the strain in the hinge. It is suggested that the Committee's further reports include recommended procedures for determination of hinge strains.

PART 2

APRIL 1960 — 12 NO. EM 2
VOLUME 86 PART 2

Your attention is invited

NEWS OF THE ENGINEERING MECHANICS DIVISION OF ASCE

JOURNAL OF THE ENGINEERING MECHANICS DIVISION
PROCEEDINGS OF THE AMERICAN SOCIETY OF CIVIL ENGINEERS

DIVISION ACTIVITIES
ENGINEERING MECHANICS DIVISION
Proceedings of the American Society of Civil Engineers

NEWS

April, 1960

PROGRAM FOR PURDUE CONFERENCE

As announced here in the January Newsletter, the EMD will hold a conference on structural mechanics at Purdue University on Thursday and Friday, May 5 and 6, 1960. The program for the three one-half day technical sessions is as follows:

May 5, Thursday Morning - Registration
May 5, Thursday Afternoon - Members and Frames

"Stability of Frames in the Presence of Primary Bending Moments", E. F. Masur, U. of Mich., and L. H. Donnell and I. C. Chang, IIT.

"Analysis of Frames with Non-Linear Behavior Subjected to Lateral Deformations", A. Ang, U. of Ill.

"Restrained Columns", M. Ojalvo, Lehigh U.

"Normal and Torsional Loading of Circular I-Beams", J. E. Goldberg and J. L. Bogdanoff, Purdue U.

May 6, Friday Morning - Plasticity

"Ultimate Strength of Over-Reinforced Beams", L. B. Kriz and S. L. Lee, Northwestern U.

"The Bearing Capacity of Floating Ice Sheets", G. G. Meyerhof, Nova Scotia Tech.

"Load Replacement in Plastic Analysis", B. C. Ringo, Mich. State.

"Traveling Loads on Rigid-Plastic Beams", P. S. Symonds, Brown U. and B. G. Neal, Univ. College of Swansea.

May 6, Friday Afternoon - Dynamics

"Electrical Energy Analogs of Vibrating Beams", F. L. Ryder, Republic Aviation Corp.

"Stress Waves and Shock in Locking Media", M. G. Salvadori and R. Skalak, Columbia U. and P. Weidlinger, engineer, N. Y.

"Energy Relations for Elasto-Plastic Systems Responding to Earthquakes," G. V. Berg and S. S. Thomaides, U. of Mich.

Note.—No. 1960-12 is part of the copyrighted Journal of the Engineering Mechanics Division, Proceedings of the American Society of Civil Engineers, Vol. 86, No. EM 2, April, 1960.
Copyright 1960 by the American Society of Civil Engineers.

May 5, Thurs. Evening - Banquet

Joint banquet with student chapters of ASCE from U. of Notre Dame, Rose P.I., Valparaiso U., Purdue U., and Ind. Section of ASCE will be held at Purdue Memorial Union Bldg. Prof. M. G. Salvadori will speak on "Mankind Faces a Technological Culture."

(D. H. Pletta, Chairman, EMD, has called a meeting of the Executive Committee for May 7 at Purdue. Members with items for the agenda should address remarks to E. Wenk, Jr., Secretary.)

PROGRAM FOR BROWN SYMPOSIUM

An advance program has been distributed for the Second Symposium on Naval Structural Mechanics at Brown University, April 5-7, 1960.

April 5, Tuesday Morning

"Problems of Plasticity in Naval Structures"

1. Static Loading—J. Vasta, Bureau of Ships.
2. Explosion and Impact Loading—A. H. Keil, David Taylor Model Basin.

"Atomic Theory of Plasticity and Fracture of Crystalline Solids"

Survey—J. J. Gilman, GE Co.
Current Research Contributions—R. S. Davis, Arthur D. Little Inc.; and C. Elbaum, Brown U.

April 5, Tuesday Afternoon

"Stress-Strain Relations and Thermoplasticity"

Survey—P. M. Naghdi, U. of Calif.
Current Research Contributions—D. C. Drucker, Brown U.; R. M. Haythornthwaite, U. of Mich.; L. W. Hu, Pa. State U.; and A. Phillips, Yale.

April 6, Wednesday Morning

"Theory of Stability and Uniqueness of Work Hardening Materials"

Survey—E. T. Onat, Brown
Current Research Contributions—B. Budiansky, Harvard; H. J. Greenberg and W. S. Dorn, IMB Corp.

April 6, Wednesday Afternoon

"Solutions of Boundary Value Problems, Plates and Shells"

Survey—P. G. Hode, Jr., IIT
Current Research Contributions—M. E. Lunchick, David Taylor Model Basin; J. H. Weiner and H. G. Landau, Columbia U.

April 6, Wednesday Evening - Banquet

"The Copernican Ptolemaic System", O. E. Neugebauer, Brown.

April 7, Thursday Morning

"Dynamic Loading and Plastic Waves"
Surveys—N. Cristescu, Rumanian Academy, N. M. Newmark, A. S.

Veletsos and S. Sutcliffe, U. of Ill.; T. H. H. Pian, MIT; E. A. Ripperger and H. J. Plass, U. of Tex.

April 7, Thursday Afternoon

"Recent Developments in Design"

Surveys—J. Heyman, Cambridge U.; and L. S. Beedle, Lehigh.
Contributions on Current Developments—W. Cohen, Bureau of Weapons, and R. T. Shield, Brown.
Concluding Remarks—W. Prager, Brown.

SECOND CONFERENCE ON ELECTRONIC COMPUTATION

As a follow-up to the initial announcement, the Committee on Electronic Computation of the Structural Division announces an enthusiastic response to the invitation for papers to be presented at the conference on September 8 and 9, 1960, at the Pittsburgh Hilton Hotel. Approximately 75 abstracts have been received from which 25 to 30 papers will be selected for the conference. Final selections will be made after receipt of the complete manuscripts, which are due April 15. The committee is anticipating an attendance in excess of 500 engineers.

SIXTH CONGRESS, IABSE

A preliminary program has been released for the Sixth Congress of the International Association for Bridge and Structural Engineering to be held June 27 through July 1, 1960, in Stockholm, Sweden.

June 27, Monday

Morning—Registration and meeting of permanent committees.
Afternoon—Opening ceremony and reception by City of Stockholm.

June 28, Tuesday

Morning—Basis of Structural Design, F. Stüssi presiding.
Afternoon—New Developments of Connections in Metal Structures, P. Dubas presiding.

June 29, Wednesday

Morning—New Developments in Bridge Building, H. Louis presiding.
Afternoon—Steel Skeleton, G. Winter presiding.

June 30, Thursday

Morning—Prefabricated Structure, G. Wästlund presiding.
Afternoon—The Design of Pile Foundations.

July 1, Friday

Morning—Important Progress in Bridge and Constructional Engineering, Composite Structures, O. A. Kerensky presiding.
Afternoon—Closing session.

TENTH INTERNATIONAL CONGRESS OF APPLIED MECHANICS

The next Congress is scheduled for August 31 through September 7, 1960, at Strsa, Italy. Apart from a number of invited general lectures, the technical sessions will be held in two sections:

Section 1—Fluid Dynamics (hydrodynamics and aerodynamics)
Section 2—Mechanics of solids (rigid-body dynamics, vibrations, elasticity, plasticity, and theory of structures).

The Proceedings of the Congress will contain the invited general lectures at full length and abstracts of papers accepted for presentation at one of the sections.

Organization of the Congress is by the Italian Organizing Committee (President: Prof. G. Colonnetti. Secretary: Dr. F. Rolla). For information on accommodations, write to: Dr. F. Rolla, Consiglio Nazionale delle Ricerche, Uffizio relazioni internationali, Piazza della Scienza 7, Rome, Italy.

BI-MONTHLY PUBLICATION OF EMD JOURNAL

The following excerpt from a letter dated January 5, 1960, to Dan H. Pletta, Chairman, EMD, from Harold Larsen, Manager, Technical Publications, should be self explanatory.

> "A review of the increased publications activity in the Engineering Mechanics Division reveals that a more frequent mailing schedule should be established for your Journal. With the present backlog of unpublished papers (19 in this office and 7 in the January issue), your Division obviously has no trouble providing us with a suitable number of papers. As a result, we would like to put you on a bi-monthly schedule beginning this April."

CORRECTIONS AND ADDITIONS

D. Pletta has called attention to two corrections and one addition to the committee lists published in the January Newsletter.

1. Chairman of the EMD Research Committee should have been R. J. Hansen of MIT rather than John S. McNown.
2. Contact member is Elmer Timby of Howard, Needles, Tammen, and Bergendoff of New York City rather than C. W. Britzius.
3. Ralph Fadum of North Carolina State is the ASCE representative to the U. S. National Committee on Theoretical and Applied Mechanics.

PLANS FOR 1961 SESSIONS

In a memorandum from M. P. White, the 1961 Program Committee (Herrmann, Suer, Cermak, Goldberg, Throop, Hall, Haltiwanger, and Gere) was asked to organize technical programs for the year beginning at the end of the 1960 Annual Convention and closing at the end of the 1961 Annual Convention, which will be in New York City.

The members were asked to consider EMD participation in three types of meetings:

1. The Annual Convention which allows EMD to hold ten to twelve half-day sessions alone or jointly with another division.
2. Regional ASCE Conventions such as the one to be held in Phoenix, Arizona, April 10-14, 1961.
3. Purely Engineering Mechanics Conferences such as the annual ASCE-ASME West Coast Mechanics Conference and the Purdue Conference to be held May 5 and 6, 1960.

ITEMS FOR JUNE LETTER

To be considered for publication in a Newsletter for circulation with the June 1960 EMD Journal, items must be on your editor's desk by April 25, 1960.

Donald L. Dean, Newsletter Editor, EMD
Department of Civil Engineering
University of Kansas
Lawrence, Kansas